INTERACTING WITH AN UNCERTAIN PHYSICAL WORLD: PROBABILISTIC MODELS OF HUMAN PERCEPTION AND ACTION

DISSERTATION VON

NILS NEUPÄRTL

TECHNISCHE UNIVERSITÄT DARMSTADT

zur Erlangung des Grades
Doktor rerum naturalium (Dr. rer. nat.)

Centre for Cognitive Science
Fachbereich Humanwissenschaften
Technische Universität Darmstadt

Darmstadt, Januar 2022

Erstgutachter: Prof. Constantin A. Rothkopf, Ph.D.
Zweitgutachterin: Prof. Dr. Katja Fiehler

Neupärtl, Nils: Interacting with an uncertain physical world: probabilistic models of human perception and action
Darmstadt, Technische Universität Darmstadt
Jahr der Veröffentlichung der Dissertation auf TUprints: 2022
Tag der mündlichen Prüfung: 13.04.2022

ACKNOWLEDGEMENTS

First of all I would like to thank my supervisor Prof. Constantin Rothkopf for giving me the opportunity to pursue my PhD in his lab, granting me the freedom to find my own topics and his support through all the difficulties that arose along the way. Next I'd like to thank our secretary Inge Galinski for her assistance in formal matters but especially for our everyday chats in the morning about family, events and hobbies accompanied by a wide selection of sweet treats.

I'm very grateful for the support of my former colleagues and friends David and Florian – and, of course, for the funny ideas and little games we came up at lunch breaks. Further I want to thank Doro, Susi, Vildan, Fabian and Niteesh for all the good times, their support und exchange about daily struggles within and outside of academia. I also want to thank my research assistants Fabian and Megan that helped me run my experiments and gather data.

The support from my family and friends was also an enormous asset for which I'm deeply grateful. And last but not least I want to thank Yuan for her loving support, endurance and cheerleading.

It would not have been possible without all of you.

ABSTRACT

Humans interact with their environment and its physical laws with ease and thereby demonstrate the ability to predict how dynamical situations unfold. Having an appropriate internal model is indispensable to do so, however, it is unclear how our brain can encompass this wealth of information and complexity of environmental states and dynamics. For instance, dropping trash into a bin while passing by is an effortless, almost unconscious process and yet a significant share of people show tremendous misconceptions when being asked about the exact same dynamics in physical reasoning tasks. This is also true for similar tasks when people are asked to make judgments about other dynamical scenes like swinging pendula or moving objects after curved trajectories. But how can this discrepancy between routine acting and deficient reasoning be explained?

An early attempt to explain this discrepancy, especially the non-rational human deviations from optimal behavior, is the reliance on rules of thumbs, often called heuristics. Based on the idea that people's internal models are likely not able to reflect the environmental complexity and thus need to rely on helpful, yet error-prone approximations of processes and dynamics, heuristics try to reveal the underlying mechanism for specific biases. However, these heuristics usually need to be individually adapted to the problem at hand and do not yield a general explanation beyond the specific task. In contrast, probabilistic models of bounded rationality have been able to quantify and explain these deviations as a consequence of human uncertainties, a priori assumptions about their environment, and internal costs such as effort. With this thesis we want to contribute to the understanding of this seeming discrepancy and reconcile these two phenomena of humans being well tuned to daily interactions and deficient in their reasoning about it using diverse tasks in controlled environments as well as computational models and algorithms describing deviations based on individual constraints.

First, we take a look at distance estimations in a judgment and a continuous action control task and the resulting deviations from optimal responses. With respect to physiological constraints, as perceptual uncertainty and action variability, and biased a priori beliefs about the size of familiar objects we describe individual deviations using probabilistic models and yet show the individual's consistency across tasks and beliefs. Since in both tasks people were constrained on viewing two-dimensional projections of distant objects and thus could only access the visual angle or apparent size they had to rely on assumptions about object sizes to infer a potential distance. The fact that the observed objects being of constant and familiar size and people likely having inaccurate and noisy beliefs can partially explain deviations in distance judgments and estimations. Size beliefs were inferred using different estimation techniques and the identified biases agreed across both techniques and were largely consistent with behavior in both distance tasks. Overall, we are showing that deviations in tasks about distance perception can be explained to a certain extent with consistent biases in human prior beliefs. Thus, we are providing evidence for human near-optimal behavior given constraints and the adequacy of probabilistic models with individual size prior for distance perception in two dimensions.

In a second experiment we extended the experimental paradigm to test human prior beliefs and internal models under conditions of varying feedback with a continuous action control task. We investigated people's belief about the non-linear dynamics of sliding objects on a surface under the effect of friction with and without visual feedback as well as their ability to transfer relevant information about mass, gained by watching collisions, to this continuous action control task. Comparison of models based on either a linear approximation or on the actual relationship described by Newtonian physics revealed that people's behavior could indeed be best described by the model prescribed by Newtonian physics, especially while feedback was available. However, even without ever having seen the object's trajectory in the feedback deprived phase people were able to accurately transfer their gained knowledge and perform extraordinary well. Not only the high Bayes factors favoring the noisy Newton model and the fact that it describes behavior well, but also the fact, that only the sheer existence of an appropriate internal model for both, sliding with and collisions without friction, can explain people correctly transferring the information to the action control task, thus strongly support the near-optimal probabilistic view on people's behavior. In summary, the results of the second experiment further highlight the superiority of probabilistic models with resource and physiological constraints over heuristics as fixed rules in explaining human behavior and apparent deviations from optimal responses.

Subsequently, we present an algorithm for the evaluation of individual cost functions to unravel an additional cause for human deviations from optimal behavior. So far only the puck sliding model considered subjective cost functions. There, the three common cost functions 0-1, hinge and squared loss were tested for by implicitly implementing different shifts of the action distribution. But here, we allowed individual parameterization of cost functions and the inclusion of effort specific costs, scaling with the magnitude of the action itself. Since action selection is finally shaped by cost functions considering these on an individual basis can be crucial to explain behavior. Using generated data we demonstrate the algorithm's capability to recover these parameters and to predict the varying influence of perceptual uncertainty and action variability on responses in production and reproduction tasks. When used on data of human behavior in diverse continuous action control tasks we were able to explain pervasively observed undershoots as interaction of asymmetric cost functions and action variability as well as identifying similarities between specific tasks. Thereby, we provide further evidence in favor of explanations for human behavior in terms of probabilistic model of decision making.

Finally, we transferred the puck sliding experiment to a VR setup enabling a naturalistic interaction with the task. Here, the assumption was that holding an actual physical puck and being able to accelerate it with a natural arm movement should facilitate the recruitment of an appropriate internal model, which is in accordance with the literature on embodied cognition. We compared data from this naturalistic task design with the previously conducted experiment on a keyboard and found that indeed individuals' behavior was significantly better described by a noisy Newton model than the next best linear approximation. This was particularly interesting since participants did not receive any feedback about the objects' trajectories and final positions. Thus the internal models governing the responses had to be a priori learned and accurately reflect the non-linearity of the environmental dynamics. These results eventually demonstrate the relevance of naturalistic interactions to investigate human

behavior and again the capability of probabilistic models to describe it.

In summary, we present several experimental designs, probabilistic models and algorithms in order to investigate people's internal beliefs about functional relationships and dynamics of their environment. By running these experiments in controlled setups on screens and in VR we were able to constrain available information and to identify relevant features supporting people in the recruitment of appropriate internal models. Our results emphasize: first, that naturalistic interaction facilitates the recruitment of realistic models in accordance with both the idea of near-optimal resource constrained models and embodied cognition. Second, people's behavior can be biased but lawfully consistent and thus pointing out the importance and generality of prior beliefs in modeling. And third, that individual cost functions incorporating an effort related term can help to quantify and explain suboptimal behavior. These results help to disentangle the mechanism behind the transition between deficient reasoning and accurate routine behavior in humans. Future research will uncover how the brain can achieve this level of performance, represent the enormous abundance of information and interlink domains of knowledge.

ZUSAMMENFASSUNG

Wir Menschen interagieren mit unserer Umwelt spielerisch leicht, was so nicht möglich wäre ohne die Fähigkeit dynamische Prozesse einschätzen zu können. Es ist unbestreitbar, dass hierzu die Existenz von passenden internen Modellen von Nöten ist, jedoch ist es unklar wie unser Gehirn es schafft mit der Komplexität und Datenfülle unserer Umwelt umzugehen. So bereitet es uns überhaupt keine Mühe etwas im Vorbeigehen in einen Papierkorb fallen zu lassen, ohne dabei auch nur ansatzweise in Verlegenheit zu geraten lange über die zugrundeliegenden Dynamiken nachdenken zu müssen, doch zeitgleich geben Versuchspersonen, die nach diskreten Schlussfolgerungen über genau diesen physikalischen Prozess befragt werden, teilweise abstrus falsche Antworten. Gleichsam grobe Fehleinschätzungen von Versuchspersonen konnten unter anderem in Experimenten mit schwingenden Pendeln und Objekten nach dem Verlassen einer erzwungenen Kreisbahn festgestellt werden. Doch wie kann diese Diskrepanz zwischen adäquatem Handeln im Alltag und groben Fehleinschätzungen in Experimenten erklärt werden?

Eine Erklärung für diese Abweichungen vom Idealverhalten wurde schon vor Jahrzehnten darin gesucht, dass sich Menschen eher auf Faustregeln bzw. Heuristiken verlassen. Dabei ist die Grundidee, dass davon auszugehen ist, dass interne Modelle im menschlichen Gehirn nicht in der Lage sind die Komplexität ihrer Umwelt abzubilden und deshalb auf fehleranfällige Vereinfachungen der zugrundeliegenden Abläufe angewiesen sind. Diese Heuristiken sind aber meist spezifisch auf das Verhalten in einzelnen Experimenten zugeschnitten und liefern dadurch auch selten allgemein gültige Erklärungen. Dem steht der Ansatz gegenüber Abweichungen im menschlichen Verhalten mit probabilistischen Modellen zu erklären, die sowohl menschliche Ungenauigkeiten als auch hilfreiche Vorannahmen berücksichtigen. In der hier vorliegenden Thesis wollen wir uns dieser Widersprüchlichkeit der weitestgehend fehlerfreien Interaktion mit unserer Umwelt und den groben Fehleinschätzungen in Entscheidungsaufgaben annehmen. Dazu werden wir im Folgenden verschiedene Experimente in kontrollierten Umgebungen ebenso wie probabilistische Modelle und Algorithmen zur Erklärung dieser Abweichungen präsentieren.

Zuerst betrachten wir die Abweichungen der Versuchspersonen vom Idealverhalten in zwei Distanz-Einschätzungs-Experimenten, eines mit binären und eines mit kontinuierlichen Antwortmöglichkeiten. Hier beschreiben wir individuelle Abweichungen, deren Beständigkeit über Experimente hinweg und Übereinstimmung mit a priori Größenvorstellungen. Das Ganze erfolgt dabei unter Berücksichtigung von physiologischen Limitierungen, wie eingeschränkter Präzision des Sehsystems und Variabilität in Handlungen, und mitunter auch Verzerrungen durch Vorannahmen, also a priori Vorstellungen. Da Versuchspersonen bei ihren Distanzentscheidungen auf zwei-dimensionale Projektionen auf einem Bildschirm und damit nur auf die scheinbare Größe beschränkt waren, mussten sie auf ihre Annahmen über Objektgrößen zurückgreifen, um überhaupt mögliche Entfernungen schätzen zu können. Durch die Verwendung von gewohnten Objekten konstanter Größe und der Tatsache, dass Menschen variable und mitunter verzerrte Größenvorstellungen über diese bekannten Objekte haben, können diese zur Erklärung der Abweichungen bei den Distanzeinschätzungen beitragen. Mithilfe zweier Inferenz Methoden wurden in-

dividuelle Größenvorstellungen bestimmt. Die so festgestellten Annahmen mitsamt der möglichen Verzerrungen waren über beide Methoden hinweg konsistent und im Einklang mit den Abweichungen bei den Distanzschätzungen. So zeigen wir, dass Abweichungen bzw. Fehleinschätzungen bei Distanzeinschätzungen in der Tat Hand in Hand mit falschen Vorstellungen über Größen und natürlicherer Variabilität in Wahrnehmungs- und Entscheidungsprozessen geht. Damit unterstützen unsere Resultate die Sicht auf menschliches Verhalten als grundsätzlich auf akkuraten Vorstellungen über die Umwelt beruhendes probabilistisches System, das optimale Entscheidungen fällt gegeben seiner Einschränkungen.

In einem weiteren Experiment zur Untersuchung von a priori Vorstellungen erweitern wir das experimentelle Design zu einer kontinuierlichen Interaktionsaufgabe unter zusätzlicher Manipulation von visuellem Feedback. Im Fokus stehen dabei die a priori Vorstellung der Versuchspersonen über die non-lineare Dynamik von unter Reibungseinwirkung schlitternden Objekten und ihre Fähigkeit, Information aus dem reinen Betrachten von Objektkollisionen auf diese kontinuierliche Interaktionsaufgabe zu übertragen. Der Vergleich von heuristisch motivierten Modellen mit realistischen, auf Newton'scher Physik basierender Modellen hat ergeben, dass das Verhalten am Besten mit realistischen statt approximativen Modellen zu beschreiben ist. Das gilt vor allem für Verhalten während visuelles Feedback vorhanden war, aber auch in anschließenden Phasen ohne Feedback. Nach dem Erlernen der Aufgabe und dem Betrachten von Objektkollisionen waren Versuchspersonen in der Lage ein Objekt im Mittel nahezu zielgenau über verschiedene Distanzen schlittern zu lassen ohne jemals zu erfahren wo dieses zum Stehen gekommen ist oder wie schnell es sich überhaupt bewegen lässt. Nicht nur sprechen die hohen Bayes Faktoren zu Gunsten der Newton'schen Modelle klar für die Sichtweise, dass interne Modelle realistischer und probabilistischer Natur sind, sondern auch die schiere Notwendigkeit dieser realistischen Modelle, um überhaupt die Information so korrekt zu erfassen und auf die Interaktion übertragen zu können. Zusammenfassend unterstreichen die Ergebnisse des zweiten Experiments noch einmal zusätzlich die höhere Passfähigkeit der probabilistischen Modelle mit realistischen Dynamiken um Abweichungen vom Idealverhalten bei Menschen zu erklären sowie ihr Nutzen bei der Beschreibung von Aufgabentransfer.

Darauffolgend gehen wir mithilfe eines neu entwickelten Algorithmus individuellen Kostenfunktionen als zusätzliche Ursache für menschliche Abweichungen vom Idealverhalten auf den Grund. Bis hierhin wurden im Modell, das das Verhalten der Versuchspersonen beim Schlittern von Objekten erklärt, nur die drei Kostenfunktionen 0-1, *hinge* und *squared loss* implizit durch eine Verschiebung der Verteilung, die die messbaren Antworten beschreibt, berücksichtigt. Bei diesem Algorithmus jedoch ermöglichen wir individualisierte Kostenfunktionen und die Integration von Kosten für den Aufwand der Aktion selbst, wie z.B. die subjektive Anstrengung. Dabei entsteht ein ganzer Parameterraum möglicher Kostenfunktionen. Da die letztendliche Wahl einer Aktion maßgeblich von den subjektiv erwarteten Kosten beeinflusst wird ist die Berücksichtigung von individuellen Kostenfunktionen entscheidend für die Erklärung menschlichen Verhaltens. Die Fähigkeit, Kostenfunktionen und auch Variabilitätsparameter aus menschlichen Antworten bei kontinuierlichen Schätzaufgaben zu inferieren, haben wir mithilfe generativer Modelle erfolgreich getestet. Angewandt auf reale Daten aus solchen kontinuierlichen Schätzaufgaben konnten wir auch die allgegenwärtige Unterschätzung von Werten durch das Zusammenspiel von indi-

viduellen, asymmetrischen Kostenfunktionen mit natürlicher Variabilität erklären und darüberhinaus noch Ähnlichkeiten zwischen einzelnen Aufgaben aufzeigen. Dadurch konnten wir weitere Evidenz für die Eignung probabilistischer Modelle zur Beschreibung menschlichen Verhaltens und Abweichungen sammeln.

Abschließend haben wir das bereits beschriebene Experiment des Objekt-Schlitterns in die virtuelle Realität übertragen, um dabei eine möglichst natürliche Interaktion zu ermöglichen. Hierbei sind wir von der Annahme ausgegangen, dass sowohl das haptische Greifen des echten Objektes als auch die natürliche Armbewegung, um es schlittern zu lassen, dazu beitragen, dass Versuchspersonen die Wahl eines passenden internen Modelles leichter fallen und sich in adäquatem Verhalten wiederfinden sollte. Diese Annahme wäre zudem dann im Einklang mit der Literatur um *embodied cognition*. Im Vergleich zum vorherigen Versuchsaufbau mit Interaktion mittels Tastatur konnte das Verhalten der Versuchspersonen signifikant besser mit dem realistischen Newton'schen Modell beschrieben werden als mit der nächstbesten linearen Approximation. Besonders interessant daran war, dass Versuchspersonen keinerlei Informationen über die Trajektorie der Objekte erhielten, d.h. das Schlittern und der Ort des Stillstandes nie zu sehen waren. Daraus lässt sich schließen, dass das interne Modell, das das Verhalten bestimmte, zuvor gelernt sein musste und korrekt die Non-Linearität der Dynamik widerspiegeln konnte. Hier zeigen unsere Ergebnisse die Relevanz von natürlicher Interaktion in Experimenten zur Untersuchung menschlichen Verhaltens auf und zugleich auch erneut die Eignung probabilistischer und realistischer Modelle dieses zu beschreiben.

Zusammengefasst präsentieren wir verschiedene Experimente, probabilistische Modelle und Algorithmen zur Untersuchung interner Vorstellungen des Menschen über funktionale Zusammenhänge und Dynamiken unserer Umwelt. Dabei identifizieren wir relevante Elemente, die die Wahl geeigneter interner Modelle beim Menschen unterstützen, indem wir Monitor- und VR-basierte Experimente unter der Kontrolle der verfügbaren Informationen durchgeführt haben. Unsere Ergebnisse zeigen dabei, dass erstens, natürliche Interaktionen die Wahl geeigneter interner Modelle fördern. Das steht dabei im Einklang sowohl mit der Idee von *embodied cognition* als auch der, menschliches Verhalten als nahezu optimal mithilfe von probabilistischen Modellen zu beschreiben. Zweitens, dass menschliches Verhalten selbst mit Verzerrungen konsistent über Aufgaben hinweg bleiben kann und dadurch nicht nur die Bedeutung sondern auch die Allgemeingültigkeit von a priori Vorstellungen bei der Modellierung von Verhalten betont. Drittens, dass individuelle Kostenfunktionen zum Einen auch Kosten für die Aktionen selbst statt nur deren Ergebnis beachten sollten und zum Anderen einen wichtigen Beitrag zum Verständnis des Auftretens von suboptimalen Verhalten leisten. Dabei helfen die Ergebnisse einen besseren Einblick in die Mechanismen des Übergangs von falschen Schlussfolgerungen über physikalische Zusammenhänge in Experimenten und dem routinierten Meistern unseres Alltages zu erlangen. Künftige Untersuchungen könnten dabei noch stärker in Richtung möglicher Erklärungen für die zugrundeliegenden neuronalen Repräsentationen unserer komplexen Umwelt und Vernetzung verschiedener Wissensdomänen gehen, die die Grundlage für diese Leistungen bilden.

CONTENTS

LIST OF FIGURES

ACRONYMS

2AFC Two-alternative forced choice

HMD Head mounted display

MCMC Markov Chain Monte Carlo

MAP Maximum a posteriori

MH Metropolis-Hastings

SEM Standard error of the mean

VR Virtual Reality

1 INTRODUCTION

The whole of science is nothing more than a refinement of every day thinking.

— Einstein, A. (1936). Physics and reality. Journal of the Franklin Institute, 221(3), 349-382.

Since the beginning of the human era one of the important and in large parts still unsolved puzzles is to understand our own mind. By searching for quantitative descriptions of behavior scientists have been trying for centuries to find fundamental mechanisms on small and large scales alike. Significant milestones on this quest were already reached in the 19th century by pioneers such as von Helmholtz in visual perception with the description of physiological optics (Von Helmholtz, 1867) and Fechner in describing both sensation in general and conscious perception with the foundation of psychophysical methods (Fechner, 1860). Nowadays, a variety of disciplines including cognitive science and neuroscience have emerged, which have devoted themselves to unraveling answers to this great question. And since the rapid increase in computational power over the last decades, computational models and analyses in these fields are becoming more important and influential. These computational models are used in cognitive science to gain insights trough inferences based on data gathered in everyday life or in specifically engineered experiments investigating human perception, cognition, and decision making. While a large number of studies have interpreted clear deviations in human judgements and behavior about the dynamics of their environment as errors and misconceptions, e.g. in reasoning about physics (Cohen, 2006; Gilden and Proffitt, 1994; McCloskey, Caramazza, and Green, 1980; Todd and Warren Jr, 1982), more recent research has begun to explain these discrepancies through natural constraints in using probabilistic models (Gershman, Horvitz, and Tenenbaum, 2015; Kersten, Mamassian, and Yuille, 2004; Kubricht, Holyoak, and Lu, 2017; Sanborn, Mansinghka, and Griffiths, 2013; Smith, Battaglia, and Vul, 2013). So, how can experimental designs and models be designed to better describe human behavior quantitatively while considering relevant constraints? What adjustments for both, experiments and analyses, should we make to gain the most insight into underlying mechanisms and potential causes for deviations from optimal behavior?

In the following chapters, we will present a sequence of experiments and associated generative probabilistic models of behavior considering natural constraints, prior beliefs, and subjective cost functions. The models are designed to explain continuous single actions in tasks while yielding inferences about otherwise unobservable variables. By taking into account physiological limitations and the inherent uncertainties of information about states of the environment, these computational analyses also provide potential explanations for human deviations from ideal behavior. Most importantly, by employing Bayesian models of behavior, we provide quantitative and interpretable models of behavior.

1.1 INFERENCES IN GENERATIVE MODELS FOR CONTINUOUS DATA

The last decades have seen a vast array of successes in modeling human behavior and inferring unobservable subjective quantities (Chater, Tenenbaum, and Yuille, 2006; Kubricht, Holyoak, and Lu, 2017; Sanborn, Mansinghka, and Griffiths, 2013; Yuille and Kersten, 2006) from describing prior expectations and their influence on human perception (Adams, Graf, and Ernst, 2004; Kersten and Yuille, 2003; Stocker and Simoncelli, 2006; Weiss, Simoncelli, and Adelson, 2002) or using MCMC sampling algorithms to study human representations of object properties (Harrison et al., 2020; Sanborn and Griffiths, 2008) to model action selection under uncertainty (Trommershäuser, Maloney, and Landy, 2003, 2008) and implict cost functions (Hoppe, Helfmann, and Rothkopf, 2018; Hoppe and Rothkopf, 2016). However, when it comes to reasoning experiments, especially in intuitive physics, so far the majority of studies investigated human reasoning based on discrete and often binary judgments. Such discrete experiments have been carried out with human subjects investigating mass ratio (Gilden and Proffitt, 1994; Sanborn, Mansinghka, and Griffiths, 2013) or stability judgments of towers of blocks (Hamrick et al., 2016), decisions about causality in collisions (Gerstenberg et al., 2017), fluid spill over when tilting containers (Kubricht et al., 2016), motion predictions for bouncing objects in contained spaces (Smith et al., 2017) or when learning in novel environments about distinct levels of mass (Ullman et al., 2018). While this restriction to discrete response options may have advantages, such as the absence of action variability, it may only be representative of a small part of daily human behavior. And since a large part of our interactions with the environment is not only based on observing and judging but also on performing actions on a continuous spectrum based on our observations, it is necessary to capture and investigate these in experiments as well. An effort in this sense already starts with investigating and formalizing discrete decisions when additionally querying participants' confidence about the decisions on a continuous scale (Gerstenberg et al., 2015). Actions on a continuous spectrum have been assessed for e.g. distance perception with auxiliary haptic cues (Battaglia, Kersten, and Schrater, 2011), when catching balls or cutting pendula (Smith, Battaglia, and Vul, 2013) or for a variety of production and reproduction tasks regarding time (Akdoğan and Balcı, 2017; Birkenbusch, Ellermeier, and Kattner, 2015), travel distance (Petzschner and Glasauer, 2011; Sun, Campos, and Chan, 2004) or force (Onneweer, Mugge, and Schouten, 2015).

1.2 OVERVIEW

In this thesis we will investigate human behavior in a variety of continuous action control tasks, showcase computational approaches to analyze behavioral patterns and relate seemingly flawed human deviations from optimal behavior to physiological and environmental constraints. In chapter 2 COMPUTATIONAL MODELING OF PERCEPTION AND ACTION we will take a look at basic computational concepts important for all subsequent models. In chapter 3 GENERALITY AND CONSISTENCY OF HUMAN SIZE PRIOR we present a first experiment about human judgments and biases in depth estimation. Here, we combine the inference of subjective beliefs about size with a physical reasoning task investigating human behavior with discrete and continuous single actions. In the following chapter 4 INTUITIVE PHYSICAL REASONING TRANSFERS TO A VISUOMOTOR TASK we will look at the human ability to transfer knowledge of physical quantities obtained through perceptual inferences

to a continuous action control task with differing levels of feedback. Moreover, we show that through learning with feedback people's behavior is accurately described by a non-linear model, a representative of the noisy Newton framework (Sanborn, Mansinghka, and Griffiths, 2013), better than by any linear heuristics approximation. In chapter 5 INFERRING PERCEPTUAL DECISION MAKING PARAMETERS FROM BEHAVIOR IN PRODUCTION AND REPRODUCTION TASKS we develop an approach in the tradition of reverse engineering to estimate several sources of uncertainty and individual cost functions from observed behavior to explain people's deviations in continuous production and reproduction tasks. Using this algorithm in chapter 6 INDIVIDUAL COSTS AS AN EXPLANATION FOR PERVASIVE UNDERSHOTS IN MOTOR TASKS we are looking at a potential explanation for pervasive undershoots in human behavior (Elliott et al., 2004; Engelbrecht, Berthier, and O'Sullivan, 2003; Onneweer, Mugge, and Schouten, 2015; Sun, Campos, and Chan, 2004; Willey and Liu, 2018b) across a broad range of continuous action control tasks. In chapter 7 NATURALISTIC INTERACTIONS ELICIT INTUITIVE PHYSICAL BEHAVIOR the influence of the action's mode on the recruitment of internal models is investigated in an virtual reality extension of the previously discussed puck sliding experiment. Finally the overall discussion and conclusion of this thesis will be presented in chapter 8 GENERAL DISCUSSION and in chapter 9 CONCLUSION.

1.3 CONTRIBUTIONS

All chapters are based on work from Neupärtl, Tatai, and Rothkopf (2020), Neupärtl, Tatai, and Rothkopf (2021) and Neupärtl and Rothkopf (2021) and may contain previously published text and figures:

- **Generality and consistency of human size prior. Chapter 3**

  In this work we investigated human depth perception in two-dimensional projections with respect to consistent prior beliefs about object sizes. In three subsequent experiments we evaluated subjective size beliefs, measured perceptual uncertainty and described individual biases in both, an two-alternative forced choice and a method of adjustment task.

  This work is currently in preparation for submission.

- **Intuitive physical reasoning transfers to a visuomotor task. Chapter 4**

  Here, we examined responses in an continuous action control task where participants were asked to propel a puck towards a target under the influence of friction. In four different phases of the experiment varying in the accessibility of relevant information hundreds of trials with differing distances were presented. Behavior was explained by and compared between two competing modeling approaches: one heuristic approach, assuming people make rough linear approximations, and one noisy Newton model, assuming that they utilize prior knowledge about the non-linearity of sliding under friction. The results show that 1) the majority of participants adapt only to the non-linearity once feedback was given, 2) they were able to transfer relevant mass information from perceiving puck collisions to the control task and 3) when given feedback human behavior was best described by the noisy Newton model approach.

This work was published in:
Neupärtl N, Tatai F, Rothkopf CA (2020) Intuitive physical reasoning about objects' masses transfers to a visuomotor decision task consistent with Newtonian physics. PLOS Computational Biology 16(10): e1007730

- **Inferring perceptual decision making parameters from behavior. Chapter 5**

  The proposed method here combines the structure of the classic Metropolis-Hastings MCMC algorithm with a deep neural network for the inference of parameters of cost functions in the spirit of amortized inference to infer perceptual uncertainty, action variability and individual cost functions for production and reproduction tasks. By assuming strictly positive distributions for inherent noise both in perception and action and costs that take into account not only the task but also the effort, we are able to present an potential explanation for systematic deviations from target values and likewise an inference approach for experimenters.

  This work was published in:
  Neupärtl, N., & Rothkopf, C. A. (2021). Inferring perceptual decision making parameters from behavior in production and reproduction tasks. arXiv:2112.15521.

- **Individual internal costs as an explanation for pervasive undershots in motor tasks. Chapter 6**

  Largely based on the method described in chapter 5 we look at a variety of experimental as well as real-world data on everyday behavior explaining potential mechanisms that lead to pervasive undershots.

  This work is currently in preparation for submission.

- **Naturalistic interactions elicit intuitive physical behavior. Chapter 7**

  In this chapter we compared human behavior when modes of interaction differed. People were asked to slide pucks either in the experiment in chapter 4 or with a puck on a table, however both without feedback about trajectories or final positions. This allowed investigating how the mode of interaction influences the recruitment of internal models for physical interaction. While no such differences may be expected in terms of a computational level explanation of physical reasoning, subjects performed more accurately in the experiment involving actual physical pucks and clearly used the mapping of distances to velocities prescribed by Newtonian physics, differently from the previous experiment. This provides evidence that subjects were able to recruit embodied representations for physical interactions with objects an that these representations were facilitated physical interactions in accordance with Newtonian physics. This result strongly suggests a role for embodied representations in physical interactions.

  This work was published in:
  Neupärtl, N., Tatai, F., & Rothkopf, C. A. (2021). Naturalistic embodied interactions elicit intuitive physical behaviour in accordance with Newtonian physics. Cognitive Neuropsychology, 1-15.

2 COMPUTATIONAL MODELING OF PERCEPTION AND ACTION

What I cannot create, I do not understand.

— Richard P. Feynman (1988). Blackboard, California Institute of Technology.

2.1 PERCEPTION AS PROBABILISTIC PROCESS

Perception is in itself a subjective process and varies from individual to individual. Even in very explicit questions without influences of context and ambiguities, clear differences in answers emerge. For example, imagine asking a dozen passers-by in the pedestrian zone about your own height. People's estimates would surely vary, however, not in an arbitrary way but likely around your actual height. The answers obtained in this way can then be visualized as a histogram or even used to approximate the probability distribution of people's potential responses $p(x)$ as shown in figure 1. Likewise, the uncertainty or variability in the perception of a single individual could be determined this way, for example, when she is asked to estimate the height of dozens of people simply assuming that she does not know that they are all of the same height.

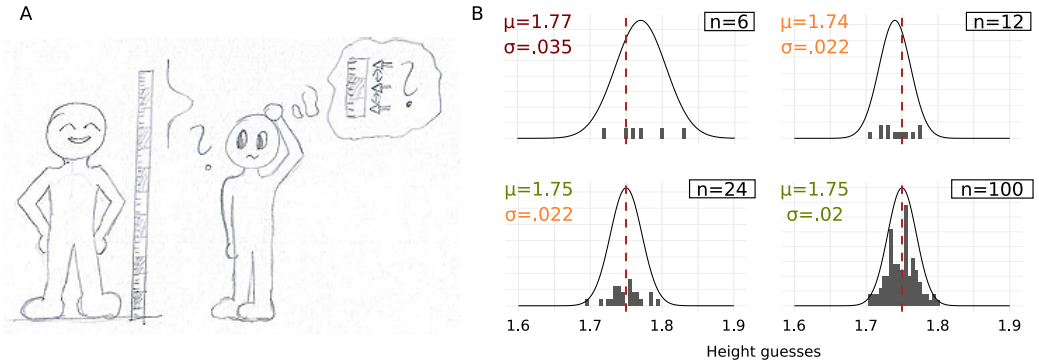

Figure 1: **Variability in continuous estimates. A) Uncertainty about the actual height.** Each individual will have uncertainty about the actual height of a passer-by. **B) Histogram and Gaussian density for sampled responses.** Potential responses of 6, 12, 24 or 100 pedestrians estimating the height of a single person. Resulting best MLE estimates are shown and colored with respect to the assumed ground-truth with $\mu = 1.75$ and $\sigma = .02$.

The quality of this approximation in turn increases with the number of answers collected as well as with background knowledge about possible functional forms. With infinite amount of possible functional forms, there are nevertheless a number of commonly used continuous probability distributions which are usually considered as good approximations to describe noisy perception. One of the most commonly used ones is the normal or Gaussian distribution $\mathcal{N}(\mu, \sigma)$ as an example for a simple and symmetric distribution that is often chosen because of its convenient mathematical

handling and shape as well as because of the implication of the central limit theorem that leads to many processes in nature to be well approximated.

$$p(x|\mu,\sigma) = \frac{1}{\sqrt{2\pi\sigma^2}} \exp -\frac{(x-\mu)^2}{2\sigma^2} \sim \mathcal{N}(\mu,\sigma) \tag{1}$$

This distribution can be described with two parameters that are additionally easy to interpret: the mean μ, determining the peak, and the standard deviation σ, specifying the variability of the data.

Parameter estimation via Maximum Likelihood Estimation

Here, the mean could be used to describe a basic bias and the standard deviation to describe uncertainty or variability of responses in the example above. Given the assumption about the normal distribution being a good functional approximation for the variability in height responses in our thought experiment, one can estimate these parameters based on the n gathered data points x_i by using maximum likelihood estimation (MLE) (Bishop, 2006):

$$\begin{aligned} p(x_1,..x_n|\Theta) = p(x_1|\Theta)..p(x_n|\Theta) = \prod_i^n p(x_i|\Theta) \;\; \text{with } \Theta = \{\mu,\sigma\} \\ \widehat{\Theta}_{MLE} = \mathrm{argmax}_\Theta \prod_i^n p(x_i|\Theta) \end{aligned} \tag{2}$$

Finding the MLE estimates for both parameters can be easily achieved by finding the zero point of the derivative of the log likelihood function. Note, using the natural logarithm turns the product into a sum and does not influence the result of the maximization but additionally yields computational advantages as avoiding quickly decreasing values for $\prod_i^n p(x_i)$ and assuring concavity in the objective function []:

$$\begin{aligned} \ln p(x_1,..x_n|\mu,\sigma) &= \sum_i^n \ln(\frac{1}{\sqrt{2\pi\sigma^2}}) - \frac{1}{2}(\frac{(x_i-\mu)^2}{\sigma^2}) = \sum_i^n -\ln(\sqrt{2}\pi\sigma^2) - \frac{1}{2}(\frac{(x_i-\mu)^2}{\sigma^2}) \\ &= -\frac{N}{2}\ln(\sqrt{2}\pi\sigma^2) - \frac{1}{2\sigma^2}\sum_i^n((x_i-\mu)^2) \end{aligned} \tag{3}$$

The best point estimate for the mean $\widehat{\mu}$ can now be calculated by differentiating with respect to μ:

$$\begin{aligned} \frac{\delta \ln p(x_1,..x_n|\mu,\sigma)}{\delta\mu} = 0 - \frac{1}{2\sigma^2}\sum_i^n 2(x_i-\mu)\cdot -1 = \frac{1}{\sigma^2}\sum_i^n (x_i-\mu) \\ 0 \stackrel{!}{=} \frac{1}{\sigma^2}\sum_i^n (x_i-\mu) \;\; \rightarrow \;\; \widehat{\mu} = \frac{\sum_i^n x_i}{N} \end{aligned} \tag{4}$$

Similarly, derivating with respect to σ and setting to zero will yield the best point estimate for the standard deviation $\widehat{\sigma}$:

$$\widehat{\sigma} = \sqrt{\frac{1}{N}\sum_{i}^{n}(x_i - \widehat{\mu})^2} = \sqrt{\frac{1}{N}\sum_{i}^{n}(x_i - \frac{\sum_i^n x_i}{N})^2} \tag{5}$$

For example, given the six sampled height responses as shown in the upper left of figure 1 B) the resulting best estimates for $\widehat{\mu}$ and $\widehat{\sigma}$ would be 1.77 and .035, respectively.

However, there are of course plenty of other distributions that model different occurrences and shapes of collected data. Especially when Gaussian distributions violate specific constraints like allowing negative values to arise due to its property of being non-zero on the entire continuous scale. These situations and the use of log-normal distributions will be discussed later, among others, in chapter 4. In the next section we will show which experiments can be used to examine and quantify behavior and what to pay attention to when setting them up and modeling data.

2.2 PSYCHOPHYSICS

In the following we briefly survey methods of psychophysics, a field concerned with quantifying sensation and conscious perception (Fechner, 1860; Hawkins, 2011; Wichmann and Jäkel, 2018), that emerged with Weber and Fechner (Fechner, 1860; Weber, 1834) and experienced a resurgence in the middle of the last century, driven largely by the work of Stevens (Stevens, 1957) and the formalization through Signal Detection Theory. In the following we will shortly address some of the indispensable foundations for the subsequent experiments from interrelationships in perception to useful experimental paradigms.

2.2.1 *Psychophysical laws*

The first classic work on postulating methods to quantify perception and its variability and trying to interpret the resulting responses lawfully was carried out in the 19th century by Weber (Weber, 1834) and shortly thereafter Fechner (Fechner, 1860). While examining human perception it was assumed that certain thresholds must be exceeded to enable people to perceive differences between stimuli. E.g. how big does a difference in height between two persons need to be to be reliably recognized by someone, to stay in the example above. These thresholds or just noticeable differences (JND) were first thoroughly examined by Weber (Weber, 1834). He found that JNDs are dependent on the type of sensation and the stimulus intensity itself. I.e. this is an early and yet no less significant finding that people's sensitivity is not independent of the stimulus intensity. Shortly afterwards, this insight was taken up by Fechner and formulated in general mathematical terms $dp = \frac{dI}{I}$, the so called Weber contrast, with dI being the JND, I the stimulus intensity and dp the perception of this difference. Fechner also stated his famous *'Maßformel'* or *Fechner-law* as a general description of perception as function of the stimuli and affected senses (Fechner, 1860):

$$p = k \ln \frac{S}{S_0} \quad \text{Fechner law or Maßformel} \tag{6}$$

with p being the perception of the stimulus, S the intensity of the stimulus, S_0 a threshold stimulus at which the stimulus is no longer perceived and k describing the

sense- and stimulus-dependent sensitivity.

This basic insight about human perception will reemerge as a relevant component in the models ahead. This is especially important since in most of the experiments in the subsequent chapters experiments were asking subjects to produce continuous responses so that data was gathered on a continuous scale and thus variability will differ in a stimulus intensity dependent way.

2.2.2 *Psychophysical methods*

Among the methods for quantitatively determining human perception and consciousness, a seemingly endless variety of experiments and designs have emerged over time. Nonetheless, they can be roughly categorized traditionally into three groups: method of limits, method of constant stimuli and method of adjustment. Here, however, we will discuss them separated into two groups to highlight the modality of possible responses: binary or discrete and continuous response tasks. For an overview see also Wichmann and Jäkel (2018), Gescheider (2013a) or Stüttgen, Schwarz, and Jäkel (2011).

2.2.2.1 *Binary response tasks: 2AFC, 2IFC and yes-no tasks*

Next, we are looking at paradigms that have been developed to measure sensation or conscious perception quantitatively. These approaches are indirect and implicit to avoid biases due to the influence of subjective a priori beliefs or action variability. I.e. participants are not explicitly asked about their percept in some arbitrary absolute scale but based on their discrete responses one can derive parameters to quantify their perception. A common feature of the three experimental designs, yes-no, two-interval forced choice (2IFC) and two-alternative force choice (2AFC), is that participants are forced to select one of their given response options regardless of their level of uncertainty. However, these paradigms differ in the presentation of stimuli and the exact nature of the response.

These differences between the experimental concepts are best explained with an example: Imagine you are a fruit seller specialized in grapefruits and you are interested in people's belief about the appearance of grapefruits as you want to avoid confusion with the oranges of the neighboring stand in a newly designed advertising space. Before committing to a specific exemplary grapefruit, you could ask one of your friends to participate in a small experiment: you are showing her several different pictures of grapefruits, varying in size and color, while asking her whether each photograph is looking like a grapefruit or not. This would be a yes-no task, since her task is to identify whether a stimulus - here the grapefruit - is present or not, see figure 2 A). This would certainly help you narrow down your selection of appropriate photographs. However, now you are interested which of the remaining ones reminds her of a grapefruit the most. In order to get an answer here, you could present her all the possible combinations of two of the chosen grapefruit-like photographs asking the question: which of the two presented fruits does look more like a grapefruit to you? This experimental design would then correspond to the 2AFC paradigm, see figure 2 B). Carrying out this procedure with a sufficient number of trials and participants may in the end yield the best choice for your advertising campaign, which is the most

frequently chosen photograph assuring a high recognition value with passers-by.

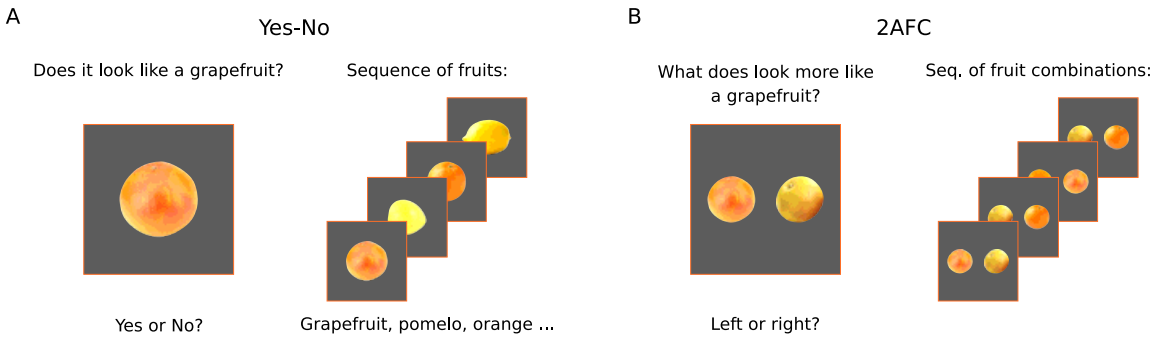

Figure 2: **Yes-No and 2AFC task for the fruit seller example. A) Yes-No task design** In the Yes-No task only one stimulus is present in each trial. The observer is asked to decide whether the stimulus searched for is present or not. Of course, this desired stimulus can also encompass an entire class, in this case a type of fruit, and not just a single specific photograph. **B) 2AFC task design.** In the 2AFC task two stimulus are presented in one trial, at the same time but spatially separated. Here, the observer is asked to decide which of the two stimuli belongs to the searched class (more likely).

The 2IFC can be seen as an extension of a 2AFC where instead of separating the stimuli spatially stimuli get separated by a time-interval into distinct frames. Similarly, both paradigms can also be extended to offering more available options in each trial, yielding nIFC and nAFC tasks - with n being the number of stimuli presented per trial.

Yes-No and forced choice tasks have been implemented in a huge variety of application fields from investigating human perception, like children's discrimination ability in their olfactory sense (Gellrich et al., 2017), testing hand devices for stiffness discrimination in VR (Maereg et al., 2017) or examining the learning of auxiliary haptic cues and interaction with visual cues in judging bulginess (Adams, Kerrigan, and Graf, 2010), or physical reasoning tasks, like judging the stability of towers of blocks (Hamrick et al., 2016), fluid spill over when tilting containers (Kubricht et al., 2016) or causality in collisions (Gerstenberg et al., 2017), up to investigating monkeys' neuronal responses in neuroscience with random-dot kinetograms (Britten et al., 1992; Gold and Shadlen, 2003), with vibrotactile stimuli (Luna et al., 2005), measuring human representations based on MCMC sampling logic (Harrison et al., 2020; Sanborn and Griffiths, 2008) or examining human planning in visual search (Hoppe and Rothkopf, 2019).

2.2.2.2 *Continuous response tasks: MoA, production and reproduction tasks*

Instead of allowing only discrete responses and thus restricting behavior usually to less natural scenarios, continuous response tasks offer a more complex alternative. More complex as they contain additional elements that are a natural part of our actions and significantly affect people's behavior: action variability and cost functions.

Action variability comprises several sources, but the most prominent is motor variability as studied and quantified in motor control (Todorov and Jordan, 2002), here a variable involuntarily influence on the movements of the participants in experiments, as shown for pointing tasks (Trommershäuser, Maloney, and Landy, 2003,

2008), tracing curves or hitting balls in a table tennis environment (Todorov and Jordan, 1998; Todorov, Shadmehr, and Bizzi, 1997) or [...]. At least as significant is the influence of individual cost functions on behavior (Körding and Wolpert, 2004b; Wolpert and Landy, 2012) that depends not only on the task (Trommershäuser, Maloney, and Landy, 2008) but the effort itself to perform the appropriate action (Hoppe, Helfmann, and Rothkopf, 2018).

Both, action variability and cost function, affect these continuous response tasks, however here the Method of Adjustment (MoA) clearly differs from the production and reproduction tasks: in a MoA task participants are asked to adjust a stimulus or more precisely a certain property of the stimulus to meet a given specification. This can be, for example, the length of a bar that is to be adjusted so that it matches the length of a second object. And since, in general, the participants are allowed to perform their adjustment in any number of steps the final property may be less affected by individual action variability. Still, with costs for each action and thus accumulating costs for continuing to adjust, the action variability will influence responses made in a MoA as well. In production and reproduction tasks, on the other hand, actions can be performed only once in a trial and cannot be corrected afterwards. While in reproduction tasks a certain sensory stimulus is shown or an action is carried out and the instruction is to subsequently generate a response of equal magnitude, in production tasks participants are asked to produce such a response or action without having seen or executed it before. For example, a classic production task would be either a task to walk a certain distance or to throw an object at a target (Willey and Liu, 2018b). When producing an initial reference for the action to be executed subsequently, like walking or cycling a certain marked distance and then repeating it without markers (Petzschner and Glasauer, 2011; Sun, Campos, and Chan, 2004), participants face a reproduction paradigm.

2.3 BAYESIAN MODELING FRAMEWORK OF PERCEPTION

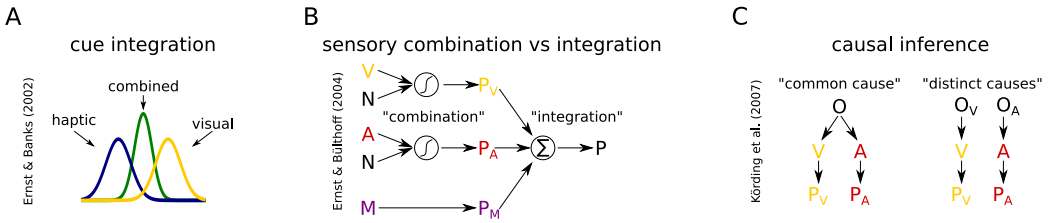

Figure 3: **Concepts for modeling perception. A) Cue integration.** Cue integration describes the optimal fusion of different information sources based on their reliability into one percept of the stimulus, i.e. the relevant property of the underlying cause. **B) Sensory combination vs integration.** The distinction between sensory combination and integration covers the fact that different cues might appear in differing coordinates or units and thus need to be transformed before being integrated into one percept. **C) Causal inference.** In causal inference the observer may decide whether two sensations do or do not have a common cause or they might combine the estimates according to the relative uncertainties of the respective causal scenario.

Based on the probabilistic description of human perception several significant concepts have been derived for its modeling. In the following sections we will briefly outline some of the key concepts and their fundamentals: how to combine different sources of cues optimally? Which intermediate steps might be necessary for success-

ful integration of multiple sensory cues? How to find solutions when multiple causes are conceivable?

2.3.1 *Cue integration*

It is not surprising that in many situations of daily life we can rely on several of our senses to guide us in making decisions: whether we want to cross a road, both noticing engine sounds and approaching vehicles, or at sensing the first drops on our skin assure ourselves of the weather condition by looking upwards to spot clouds. While we are accustomed to assuring ourselves when assessing the state of our environment , the question is whether we are doing this in an optimal way.

We start with the assumption that n cues x_i about a certain state need to be integrated into one percept. Now we further assume that all cues can be described as independent and stemming from Gaussian distributions with the same mean μ but with differing standard deviations σ_i. An approach to get the minimal variance unbiased estimator $\widehat{X}$ would be to use the weighted average here (Cochran, 1937; Jacobs, 2002; Kersten and Yuille, 2003; Landy, Banks, and Knill, 2011; Landy et al., 1995):

$$\widehat{X} = \sum_{i}^{N} x_i w_i \quad , \quad \textit{weighted average} \tag{7}$$

Note, the weighted average automatically becomes the sample mean if all samples or cues come from the same distribution, i.e. have the same variance σ_i^2 and thus the same reliability r_i:

$$\text{with} \quad w_i = \frac{r_i}{\sum_i^N r_i} \quad \& \quad r_i = \frac{1}{\sigma_i^2} \tag{8}$$

However, this is only the simplest approach to arrive at an estimate with minimum variance. So far the model assumes samples or cues x_i that arise from a single Gaussian distribution or several but with the same mean μ. That is a rather unrealistic assumption in natural conditions were cues might have different reliabilities. Even presumable influences of people's prior knowledge about likely states of X on their perception is not considered yet. However, this can be elegantly solved by taking a Bayesian point of view on the problem in order to extend the model.

In the Bayesian approach uncertainty about the state S of a variable of interest is described as a probability distribution called *posterior* $p(S|D)$. This posterior reflects the individual belief about the true state S, unknown to the individual, dependent on the data D, which can and was observed by the individual, i.e. their sensory measurement. This belief is shaped by the individual's *prior belief* about potential states of the world $p(S)$ and the *likelihood* $p(D|S)$ or $L(D;S)$, a function describing the probability of states S giving rise to the actually observed data D. Thus the posterior is proportional to the product of the prior belief and the likelihood:

$$p(S|D) \propto p(S)p(D|S) \tag{9}$$

Since the likelihood function is not a probability distribution and thereby the product does not need to integrate to 1, a factor for normalization is necessary to end up

with a normalized probability distribution again. This denominator $p(D)$ is called the *marginal likelihood* or *evidence*, since it is the distribution marginalized over all states S and an indicator of the model's plausibility. This evidence term can for example directly be utilized for model comparison (Pooley and Marion, 2018).

$$p(S|D) = \frac{p(S)p(D|S)}{p(D)} = \frac{p(S)p(D|S)}{\int p(S)p(D|S)dS} = \frac{\text{prior} \cdot \text{likelihood}}{\text{evidence}} \quad \textit{Bayes formula} \tag{10}$$

Bayes formula can be simply remembered and derived using the chain rule [] for joint probability and restructuring, like:

$$p(S, D) = p(S)p(D|S) = p(D)p(S|D) \tag{11}$$

Now we can use the Bayesian framework and equations 9 & 10 to rephrase the original problem of cue integration. Given n cues for an estimate we can describe the likelihood of the data as the product of each cue's probability distribution:

$$p(D|S) = \prod_{i}^{n} p(D_i|S) \tag{12}$$

With both cues being conditionally independent and Gaussian distributed the resulting likelihood will again be Gaussian distributed with reduced variance. For an example with two cues assume we want to estimate the position of a bird in a tree. We hear the bird chirp and we see slight movements in the densely leafed tree crown. It is also known that human visual sensory precision usually exceed that of audition (Alais and Burr, 2004; Körding et al., 2007) and hence $\sigma_A > \sigma_V$. With an uninformative uniform prior we again end up with the MLE estimate as minimum-variance estimator like in equation 7 and 8, as e.g. shown for the combination of haptic and visual cues in Ernst and Banks (2002).

$$\sigma^2_{VA} = \frac{\sigma^2_V \sigma^2_A}{\sigma^2_V + \sigma^2_A} \quad \text{since} \quad r_{VA} = \sum r_i \tag{13}$$

For our example this means that the final percept will be somewhere between the position of the sound and the movements in the tree crown, however shifted to the more reliable visual cue. However, given the shape of a tree an informative prior is likely. Then the posterior belief about potential states $p(S|D)$ is proportional to the product of the likelihood and prior belief $p(S)$.

$$p(S|D) \propto p(S) \prod_{i}^{n} p(D_i|S) \tag{14}$$

With an almost bell-shaped tree crown, see figure 4 B), we could assume for $p(S)$ a Gaussian distribution again to end up with a Gaussian distribution for the posterior belief.

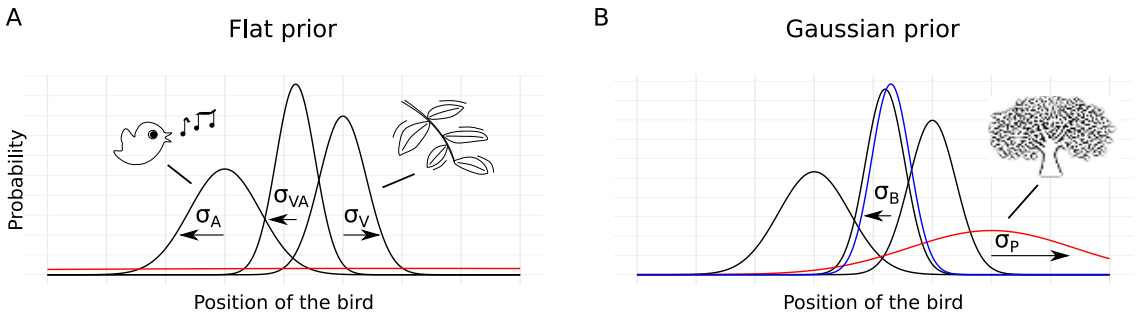

Figure 4: **Cue integration of visual and auditory cue based on cue reliability. A) Flat prior.** Prior knowledge about potential bird positions is absent or extremely uncertain - high σ_P - and does not influence posterior belief significantly. Hence, maximum-a-posteriori coincides with MLE estimate based on both cues. **B) Gaussian prior.** Prior knowledge - smaller σ_p - additionally influences belief. Could be based on e.g. position of the tree and the knowledge that birds are more likely in the dense parts of the crown.

The idea of integrating cues optimally based on their reliability has been tested among others in auditory localization (Searle et al., 1976), in ventriloquist auditory-visual localization (Alais and Burr, 2004), depth estimation (Landy et al., 1995), surface slant estimation via texture and stereo cues (Knill and Saunders, 2003) and prior assumptions about isotropy (Knill, 1998), edge localization via texture orientation and spatial frequancies (Landy and Kojima, 2001) or object height estimation via visual and haptic cues (Ernst and Banks, 2002).

2.3.2 *Binding and causal inference*

Now that we have reviewed the theory of optimal Bayesian integration of cues, the question arises at which point one should integrate different cues anyway. In doing so, we dive into an even larger and more general question about the 'binding problem' (Burwick, 2014; Von Der Malsburg, 1999) spanning fields from psychology to neuroscience: how and when are several feature bound to a single object or percept? Influential ideas about the 'how' and 'when' are the feature integration theory (FIT) (Treisman and Gelade, 1980), arguing that focused attention is necessary to bind stimuli into a single object, and the temporal correlation hypothesis (TCH) (Von Der Malsburg, 1994), proposing that neuronal signals that are correlated in time explain binding (Burwick, 2014; Von Der Malsburg, 1999). In synaesthetic binding, as an example for abnormal binding, digits might evoke colors or words the perception of taste (Robertson, 2003; Sagiv and Robertson, 2005; Ward and Mattingley, 2006) and even the visual perception can be affected by this color-photism (Smilek et al., 2001).

But at which discrepancy or dissonance does binding or cue integration break down in regular cases? This dissonance between different cues has among others been investigated for the ventriloquism effect, where temporal and spatial timing maintain the illusion (Munhall et al., 1996; Slutsky and Recanzone, 2001). When people are told that visual and auditory cues have a common cause, cue reliability is optimally considered in stimulus localization estimates (Alais and Burr, 2004). However, when they report that cues are not perceptually unified, i.e. have distinct causes, cue integration breaks down and estimates are not longer influenced by the additional cue (Körding et al., 2007; Wallace et al., 2004).

2.3.3 *Explaining away for multiple causes*

In daily life we encounter common situations in which one does not find several cues with a clear allocation to one cause, but that an individual cue or percept can have competing explanations, i.e. different underlying causes. This creates the need to explain away potential causes in order to fin the most likely cause (Kersten, Mamassian, and Yuille, 2004; Kersten and Yuille, 2003; Murray, Schrater, and Kersten, 2004; Neupärtl and Rothkopf, 2018).

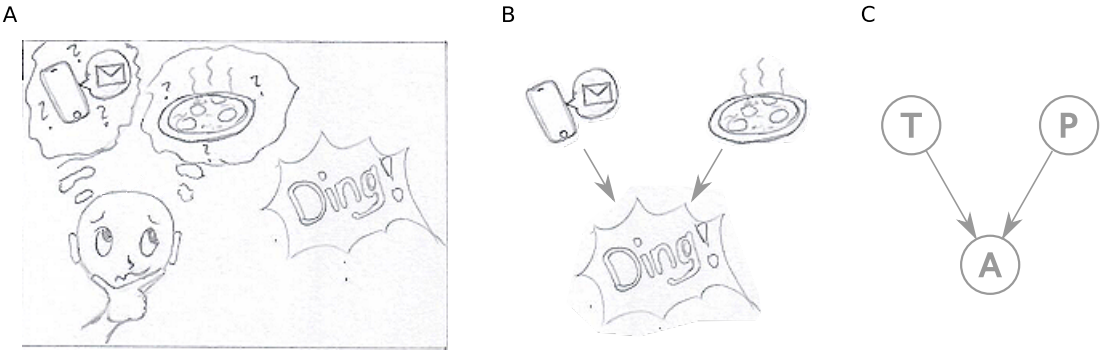

Figure 5: **Two competing causes for auditory stimulus. A) Ambiguity about cause.** Auditory signal 'Ding' can be caused by either the telephone or the micro-grill. **B) Pictorial graph presentation.** Either of the two events may have triggered the sound. **C) Graph.** Nodes representing causes and stimuli and edges show their dependency.

Imagine you are an undergraduate student (again) and still with poorly developed cooking skills while lacking the money to frequently visit restaurants. But therefore, you've developed a preference for simple frozen food suitable for your own microwave grill. However, the notification sound of the microwave when the grill program has finished is very similar to that of the messenger app on your smartphone when receiving messages, as shown in figure 5 A). Having waited for your pizza for quite a while and receiving many messages all day makes both causes seem similarly likely to you.

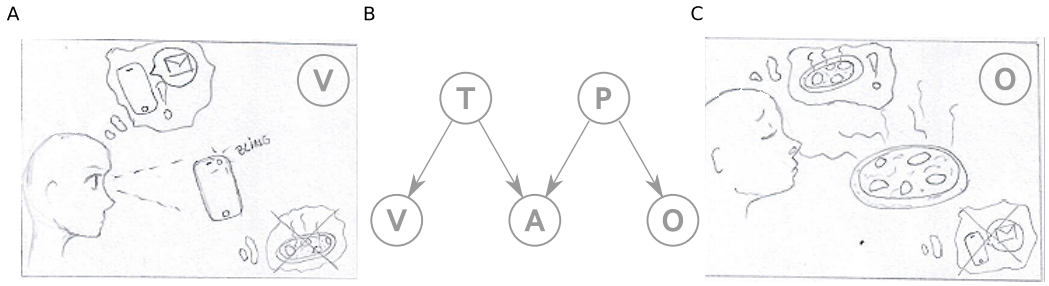

Figure 6: **Explaining away the ambiguity using additional available sensory measurements. A) Auxiliary visual measurement.** Using the visual sense to check whether the telephone's light is flashing helps to disambiguate the cause. **B) Graph with both auxiliary cues.** Both, the visual and olfactory cue, can help to find the actual cause. **C) Auxiliary olfactory measurement.** Using the olfactory sense to check whether the pizza has already developed its distinctive scent.

However, rather than walking to either your grill or to your phone on the desk you can use your other senses, too. You could try to peek from some distance if your cell phone light is blinking, see figure 6 A). If it is blinking you gathered evidence from

your smartphone for receiving a message in your app as being the more likely cause for the sound. Since you just have a binary decision to make - walking to the grill or the phone - you'd decide to go to the phone based on its now higher likelihood of being the cause. Likewise, you could use your olfactory sense. During the exam phase of the last semester you have trained this sense abundantly and recognize quite well whether a pizza could be almost done. Here, a distinctive scent would in turn lead you to consider the grill as a probable cause and to approach it, see figure 6 C). Importantly, in both cases, the posterior probability for the competing cause of hearing a sound decreases based on the increased posterior probability for the cause, for which you gathered evidence.

2.4 BAYESIAN DECISION THEORY

So far we have described several concepts trying to explain perceptual processes: from simple estimation of latent variables, the integration of cues into a single percept up to disambiguating multiple causes for a single cue. But which action is optimal given the perception and how can this process be described?

Here the Bayesian decision theory (BDT) (Gelman et al., 2013; Maloney and Mamassian, 2009) provides a normative probabilistic framework for solving this problem. Based on the prior belief $p(S)$ about the environmental state of interest and the likelihood of the observed data $p(D|S)$, the so-far observer wants to perform an optimal action a_{opt}. I.e. the action that maximizes her expected gain or, alternatively, minimizes her expected costs $\mathcal{L}(a, S)$.

$$a_{opt} = \arg\min_{a} E[\mathcal{L}(a, S)] \tag{15}$$

Usually this cost function depends on the presented task (Körding and Wolpert, 2004b; Trommershäuser et al., 2005) but it may include costs for the effort producing the action itself, since people are sensitive to motor costs (Hagura, Haggard, and Diedrichsen, 2017) or costs for withholding an action such as blinking (Hoppe, Helfmann, and Rothkopf, 2018). When combining the subject's prior belief $p(S)$, the likelihood $p(D|S)$ and the fact that the action output $p(a_{var}|a)$ is subject to noise as well, the equation 15 can be written as (Landy, Banks, and Knill, 2011):

$$a_{opt} = \arg\min_{a} \iiint \mathcal{L}(a_{var}, S)\; p(a_{var}|a(D))\; p(S)\; p(D|S)\; da\, dD\, dS \tag{16}$$

In an estimation task state S can be a certain duration of an auditory stimulus. The subject has a prior belief $p(S)$ about the state, assuming she is used to this kind of task. Hearing the stimulus in a single trial generates data D and its likelihood $p(D|S)$ which reflects her internal model, here simply assuming some probability distribution like a Gaussian or log-normal distribution. Based on her task, reproducing this perceived stimulus as precisely as possible, we can assume that the cost function will be zero at the actual and correct value and symmetrically increasing around it. Thereby, penalizing erroneous deviations as a function of distance to the actual value. The action distribution $p(a_{var}|a)$ describes the motor variability of the subject when she is reproducing the interval by e.g. a key press duration on a keyboard. Finally,

integrating over all possible states, the data points obtained and potential actions and minimizing the outcome for action a yields the optimal action a_{opt} to choose.

In the subsequent chapters we will revisit the idea of cost functions shaping behavior: a comparison between models with different potential cost functions is done in chapter 4 for a puck sliding task and in chapter 5 we will propose an algorithm estimating individual generic cost functions for estimation tasks with variability constraints.

3

GENERALITY AND CONSISTENCY OF HUMAN SIZE PRIOR

Love truth, but pardon error.
Aime la vérité, mais pardonne à l'erreur.

— Voltaire, "Deuxième discours: de la liberté," Sept Discours en Vers sur l'Homme (1738)

3.1 INTRODUCTION

3.1.1 *Environmental prior beliefs*

When interacting with the environment we need to include prior knowledge and expectations about the benefit of certain outcomes associated with the actions we take. Both, prior beliefs as well as expected utilities are learned either by experience from perception (Adams, Graf, and Ernst, 2004; Hoppe, Helfmann, and Rothkopf, 2018; Seitz, Kim, and Watanabe, 2009), sensorimotor feedback (Körding and Wolpert, 2004a), interactions like path integration (Petzschner and Glasauer, 2011), or by explicit description (Hertwig et al., 2004; Trommershäuser et al., 2005; Weber, Shafir, and Blais, 2004). Even systematic errors or illusions can be well explained when taking potential prior biases into account (Girshick, Landy, and Simoncelli, 2011; Weiss, Simoncelli, and Adelson, 2002). But there are however situations where prior knowledge about specific variables in our environment enables us to draw conclusions in the first place.

3.1.2 *Ambiguity of two-dimensional scenes*

One of these situations is the decoding of the ambiguity of apparent size, which is the visual angle, into the size of an object and its distance to an observer (Kilpatrick and Ittelson, 1953). Especially, when seeing a two-dimensional projection of a scene and only having information about the visual angle of an object, prior knowledge or additional cues about the size help us to infer potential distances correctly (Battaglia, Kersten, and Schrater, 2011).

3.1.3 *Inference of subjective beliefs*

Thus, in order to understand and describe human behavior precisely inference of potentially underlying prior beliefs is vital. Such inferences have been investigated in synthetic cases, where participants were trained on specific distributions, (Sanborn and Griffiths, 2008) or on familiarity tasks with transfer of priors between separate tasks (Houlsby et al., 2013). Here, we want to combine the approach shown in (Sanborn and Griffiths, 2008) to infer size prior of three commonly known sports balls for each participant with a distance estimation and judgment task for familiar objects in two-dimensional projections.

Here, each subject participated in three subsequent experiments: i) a two-alternative forced choice task (S-2AFC) measuring subjective beliefs about sizes of familiar objects (size prior) in a virtual environment, ii) a continuous distance estimation task using the method of adjustment (MoA) and a iii) binary distance judgment task (D-2AFC). With this design we can independently measure individual size priors using the S-2AFC experiment and perceptual uncertainty regarding the visual angle using the D-2AFC. Both variables are crucial to explain behavior and potential biases in the MoA and D-2AFC task and thus can be measured beforehand rather than need to be inferred. Based on the data from these three experiments we can compare participants' consistency across the two distance judgment and estimation tasks, estimate subjective prior and perceptual uncertainty and investigate people's posterior belief with a Bayesian model.

3.2 MATERIALS AND METHODS

3.2.1 *Participants*

Five subjects ($f = 2, m = 3, \mu_{age} = 25.0$) took part in the experiment. All participants were undergraduate or graduate students recruited at the Technical University of Darmstadt, who received course credit or payment (10 euro/hr) for participation. All experimental procedures were carried out in accordance with the guidelines of the German Psychological Society and approved by the ethics committee of the Technical University of Darmstadt. Informed consent was obtained from all participants prior to carrying out the experiment.

3.2.2 *Apparatus*

All participants had normal or corrected to normal vision and were seated approximately 45 cm away from the computer screen in the two-dimensional part of the experiment. The screen subtended 61.5 cm or 93.3° in visual angle horizontally and 36.5 cm or 49.2° visual degree vertically. In the VR setup participants wore an Oculus Rift head-mounted display (HMD) with 1080 x 1200 resolution and a horizontal field of view of 88°. Additionally, participants were asked to demonstrate how they would hold an imaginary ball with their hands in front of an Intel Realsense Depth Camera D435.

3.2.3 *Task procedure*

In the following we will describe the experimental procedure for each of the three subsequent tasks. Each subject participated in these experiments in the same order. In figure 7 an overview for the three experiments is shown.

Experiment 1: familiarity choice task (S-2AFC): In the first experiment we measure subject's subjective prior belief about the size of three sports balls in VR, see first column of figure 7. We utilized the approach to run MCMCs with humans acting as acceptance function (Sanborn and Griffiths, 2008). To this end, participants were asked to select in a two-alternative forced choice task which of two objects presented looked more familiar or realistic to them with respect to their size while being able to move and look freely in VR, see figure 8 C). These simultaneously shown objects only differed in their size but were identical otherwise. Object sizes in the

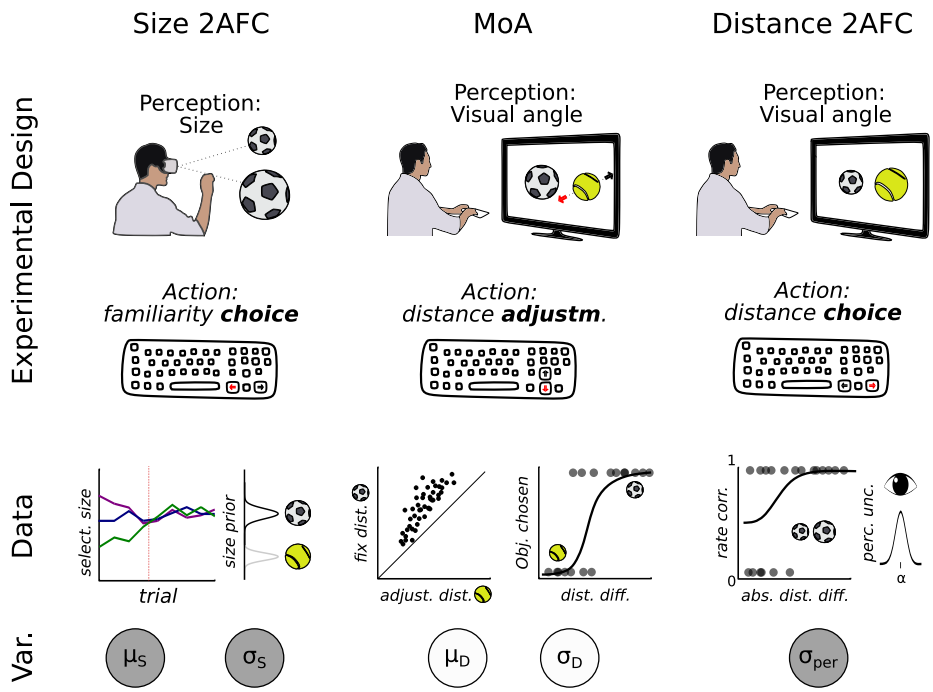

Figure 7: **Experimental design.** Subjects participated in three subsequent tasks. In the S-2AFC task subjects were asked to perform a familiarity judgment task. Seeing two different sized spheres with the same surface texture (sport balls) they should pick the more realistic one. In each following trial the rejected sphere is replaced by a new size sample drawn from a proposal distribution. Based on the accepted samples from multiple runs (chains) with differing starting points with regard to the initial sphere sizes, subjective distributions for sphere sizes can be derived for each participant. In the MoA task subjects were asked to adjust the position of one sphere to the same distance of a second immobile sphere from another type, which means that they only encountered combinations of different sport balls. Thus, their belief about the object size, especially when differing from the actual sizes, should strongly influence their responses in this method of adjustment task. In the last D-2AFC task participants were asked to judge which of the shown objects was closer to them as observer.

subsequent trials were then sampled with respect to previous decisions: the previously selected size is used as the mean of a proposal distribution. This distribution is then used in turn to sample a new and differently sized object as an alternative to present to the participant. In order to achieve both, a precise measure of which decisions already correspond to the subjective belief and as little influence as possible from initially chosen variables, using multiple chains with differing starting points is essential. Since not all values correspond to the actual beliefs at the beginning, a choice has to be made from when on the decisions are representative for the actual belief. This position in the chain will be called burn-in from here on, analogously to standard MCMC algorithms. By using multiple chains this burn-in can be obtained as the index beyond which all chains have intersected at least once, see the red line exemplarily sketched in figure 7 *'Experiment 1 - Results'*. Preceding size values of the accepted proposals are not taken into account for estimating the prior distributions.

Three different common sport balls were displayed: a tennis, base and soccer ball. Each participant was supposed to complete 450 trials for each distinct object divided over three initialized chains. Chains of the same object were never shown in successive trials. However, which of the other two sport objects was shown was random.

Figure 8: **VR setup.** A) VR replica of the room. B) Participant's front view of the desk. C) Single trial of the familiarity choice task (S-2AFC).

It was also always switched between the chains within the sport objects. I.e. participants could not see the same chain again until the fourth run after they saw it at the earliest and that, as well, only with a probability $p = .125$. This approach ensured that participants could not remember previously selected samples and only selected objects based on the conformity of the size with their own subjective belief. Initial values of the three chains were uniformly drawn from three non-overlapping ranges $3-7$, $11-15$ and $19-23$cm. New samples were drawn from a Gaussian proposal distribution with its mean at the previously selected size $\mu_{prop} = s_{sel}$ and a standard deviation σ_{prop} at 1 for tennis and base ball and 1.5 for the soccer ball. These values were adjusted to achieve an appropriate convergence speed while ensuring that even subtle deviations that are still visible to the participant appear and thus can be distinguished. For the same reason of detectability, proposals were discarded and resampled that would make jumps much too large, from twice the standard deviation, or much too small, that is below 0.1 times the standard deviation. Between each trial a 100ms black screen was shown as transition. In each trial the position of the new sample, right or left, was randomly drawn. The objects were placed 20cm apart on a table that replicated the actual table in the lab in front of which the participants were sitting in VR. The table served both, the immersion in VR and as an additional relative reference size for estimating samples, and thereby helped to measure the actual subjective belief more precisely, see figure 8 C). Similarly, to improve the precision of the measurement, participants spent one minute in a replica of the room in VR, see figure 8 A) before the start of the experiment to adjust to VR and the environment.

Experiment 2: distance estimation task (MoA): In the second experiment, see the second column of figure 7, participants were asked to match the distance of two distinct sport objects on a two-dimensional computer screen via method of adjustment (Gescheider, 2013b). Objects were randomly placed left or right again. One of them could be moved via button presses on a regular keyboard in order to match the other object's perceived distance. In contrast to the first experiment, the sizes of the objects were kept constant based on official specifications: tennis ball with 6.6cm, base ball with 7.45cm and soccer ball with 22cm diameter.

Each object combination with two different sports objects was shown 160 times, with each object being mobile in 80 trials, leading to overall 480 trials for every participant. No same-object combinations were shown in the method of adjustment task. Initial distances of both objects were drawn uniformly in a range between .7 and 2m. The lower limit of this distribution was chosen to strike a balance between preventing overlap between the objects or the observer, i.e. the camera, and keeping the object positions as close as possible. This is useful since close positions make it easier for the participants to determine the individual distances and thus provide less noisy

data. Objects were spawned and could be moved on lines originating at the observer at a 30 degree angle to each other.

Experiment 3: distance judgment task (D-2AFC): In the third and last experiment participants were asked to judge which of two presented sport balls was closer to them in a distance two-alternative forced choice task (D-2AFC) on a two-dimensional computer screen as shown in the last column of figure 7. Again, objects were randomly placed left or right again and object specific sizes were kept constant across the experiment at the same levels as in the MoA task before.

Here, participants judged 100 trials in each object combination, here also including combinations with identical objects, leading to 600 trials per participant. These identical object combinations can then be utilized to estimate the perceptual uncertainties of participants regarding visual angles on a computer screen, since there were no more size influences to consider. In order to avoid many trials with too easy decisions objects' decisions within a trial were kept close. This was achieved by sampling the distance of one object dependent on the other. Thereby getting more data points in the range where clear decisions were difficult to make and thus improving the precision and significance of the psychometric functions. The first object was randomly chosen at one of two distances, close at $0.9\mathrm{m}$ or distant at $1.2\mathrm{m}$ and randomly placed left or right. Then the distance of the second object was sampled with a Gaussian distribution with its mean being the first object's distance. The standard deviation was slightly different for close and distant positions since more distant positions yield increasingly small visual angles and thus distance differences need to get bigger for participants to sense them. Similarly standard deviations differed for object combinations with identical and different objects, since the former is easier as it is reduced to a purely perceptual task in which only the object with the larger visual angle has to be selected. Both considerations lead to following values: $\sigma^{\mathrm{id}}_{\mathrm{close}} = .15$, $\sigma^{\mathrm{id}}_{\mathrm{dist}} = .2$, $\sigma^{\mathrm{diff}}_{\mathrm{close}} = .24$ and $\sigma^{\mathrm{diff}}_{\mathrm{dist}} = .35$. Sampled distances that deviated less than $1\mathrm{cm}$ or more than two times the standard deviation from the mean, i.e. the distance of the other object, were discarded and re-sampled.

3.3 BAYESIAN NETWORK MODEL OF PERCEPTUAL INFERENCE

Here we will describe the probabilistic generative model that describes how latent quantities like individual a priori beliefs about size and distance of sport objects influence people's perception of distances of objects given their visual angle. Using the subject's size beliefs already inferred from the S-2AFC task and perceptual uncertainty estimated from D-2AFC task as observed variables (see last row *"Variables"* in fig. 7) we can now infer the actual belief about each object's distance for every subject. First model shown in fig. 9 A) is used to infer parameters for the size belief for each object and participant based on people's choices in the first S-2AFC experiment. Using these inferred size beliefs we can describe people's posterior belief about object distances for each actual visual angle while inferring their a priori belief (μ_D, σ_D) about distances with the Bayesian net shown in fig. 9 B).

The first model is used to come up with the most appropriate parameters for the size beliefs measured in the S-2AFC. For each participant and object the unknown mean μ_S and standard deviation σ_S parameter of a log-normal distribution is in-

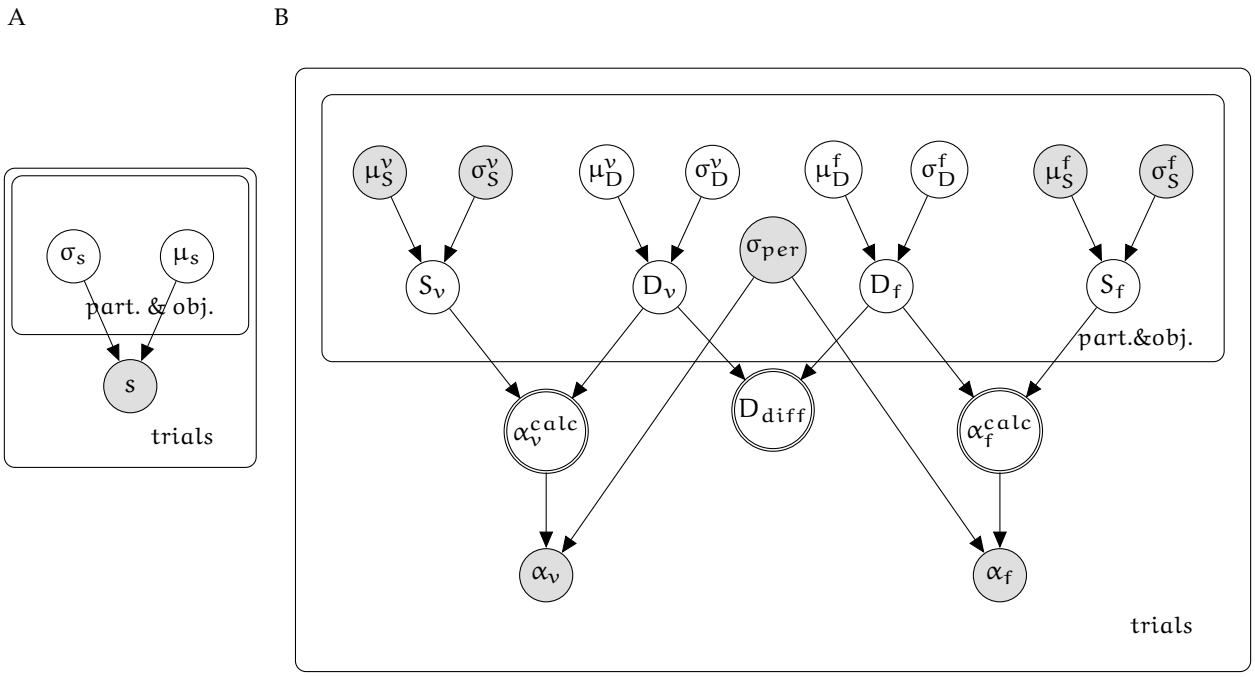

Figure 9: **Bayesian graphical models for S-2AFC and MoA experiments. A) S-2AFC.** Simple mean μ_S and sigma σ_S inference for log-normal size distributions. Yielding one parameter pair for each participant and object describing the size belief. **B) MoA.** Model describing the belief about objects' distances in the method of adjustment task based on the previously determined size beliefs, i.e. the size belief parameters μ_S^v, μ_S^f and σ_S^v, σ_S^f. Perceptual uncertainty σ_{per} about the actual visual angle α can be inferred from D-2AFC data with same object combinations for each participant.

ferred based on the proposed samples accepted by the participant. However since chains are deliberately initialized along a broad spectrum, early trials are not yet representative for the actual internal belief and need to be discarded before the inference process. For a reliable burn-in specification the index at which all chains have intersected at least once was chosen, see column 1 of figure 7 *'Data'* for a simplistic visualization or figure 10 A).

The parameters μ_S and σ_S inferred in this manner represent each individual's a priori size belief about each object as log-normal distribution and can now in turn be used to describe participants' a priori and posterior beliefs about object distances in the MoA task, as shown in figure 9 B) as grey-colored observed nodes in the upper row. In the MoA experiment, the task was to move objects to the same perceived distance, so that one could imagine to stretch the arm equally far to be able to touch both objects.

Here the subjective belief about the size of the objects plays a prominent role, because only the two-dimensional projection in visual angle could be seen on the monitor. And since the two-dimensional projection is a direct interaction of size and distance, one should be able to attribute deviations from ideal behavior here to a-priori differences in size beliefs and uncertainty in perception. The connection of the quantities is as follows:

$$\alpha = 2\tan(\frac{S}{2D}) \quad \text{with} \quad \alpha \text{ as visual angle, S as object size \& D as distance} \tag{17}$$

Having inferred the individual size beliefs for each object together with knowing the visual angle of the object on screen allows statements about the distance perceived by the participant to be made. Nevertheless, there are two other sources of variability: the uncertainty in the perception of the visual angle σ_{per} and the a priori belief about the distance of certain object types D. The latter will be considered by using participant and object specific distance prior with unknown hyper parameters μ_D and σ_D.

In addition to the parameters of the size prior and the actual visual angle, the perceptual uncertainty σ_{per} is known and displayed as a gray node in the model, since it can be estimated based on same object combination trials of the last D-2AFC experiment, see section 3.4.2. Following the model graph the joint posterior probability of the observed data d and the model parameters Θ can thus be stated simplistically for one object as:

$$p(d, \Theta) = p(S)p(\mu_D)p(\sigma_D)p(D|\mu_D, \sigma_D)p(\alpha|S, D, \sigma_{per}) \tag{18}$$

3.4 RESULTS

3.4.1 *Individual size beliefs*

First, we will examine the raw data from the S-2AFC experiment. Each participant had to choose the more appropriate object size out of two samples in three chains per object. The resulting chains are shown in figure 10 A) separated in rows by participant and in columns and through color by object affiliation. One can see that initial points of these chains are randomly scattered along the y-axis and that the burn-in indices, marked by the red dotted lines, emerge after all chains have intersected, as both previously described in section *'Task procedure'* in more detail.

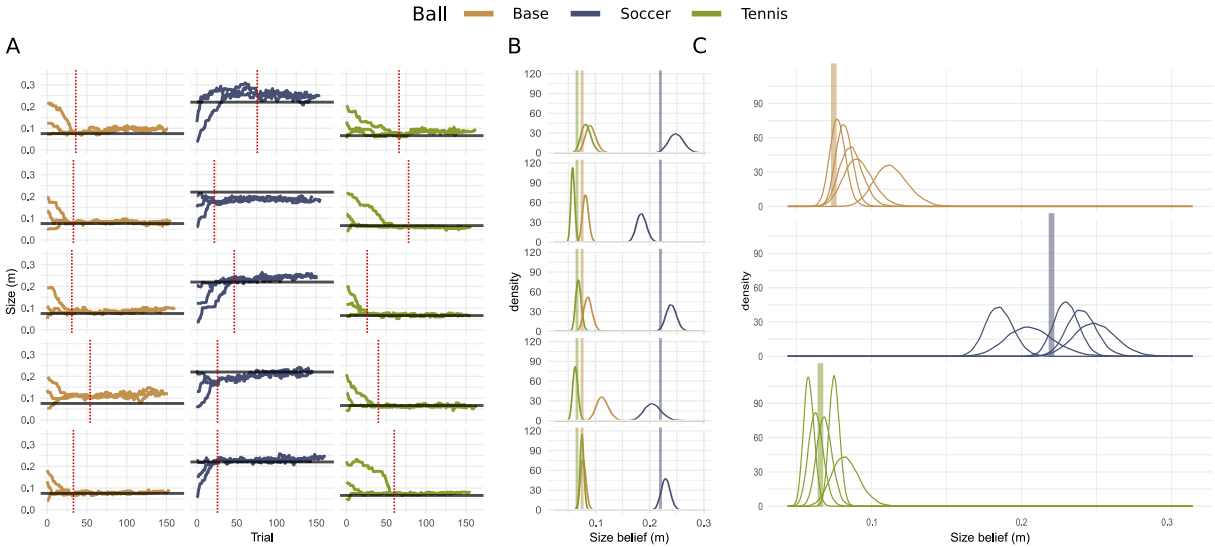

Figure 10: **Resulting sampling chains of experiment 'S-2AFC' with burn-in.** A) Chains from human sample rejection task. For each chain the chosen size in each trial is depicted. Vertical lines indicate burn-in positions where all chains have intersected. B) Posterior predictive values for sizes based on log-normal distributions of Bayesian size prior model, see figure 9A). C) Overview of resulting prior size beliefs.

Based on the raw data and choice of burn-in indices we used the minimal model for parameter inference, shown in figure 9 A), to come up with suitable log-normal distributions that describe each individual's size beliefs. These resulting beliefs about object sizes or size prior are shown in figure 10 B) for all objects separated by participant. Actual object sizes, based on official guidelines and used for experiments 2 and 3, are marked by colored horizontal lines, making individual deviations apparent. So are e.g. all participants significantly deviating in their size belief about soccerballs from the actual value at .22m in diameter (multiple Wilcoxon signed rank test with continuity correction, $p < .001$). However, if we look at the whole population based on the distribution of the mean values of the log-normal soccer size prior, we see that they do not deviate significantly from the actual value (One Sample t-test, $t = 0.1765$, $p = .8685$). I.e. each participant has a more or less large bias in her size belief but the total population does not. This unbiasedness is also true for the tennis (One Sample t-test, $t = 0.8521$, $p = .4422$) and baseball (One Sample t-test, $t = 2.3666$, $p = .0771$). Interestingly, however, the baseball is the only object that was overestimated by all participants, whether only slightly or clearly, which also shows in the mean deviation of the size prior mean values from the actual size being almost one order of magnitude bigger ($\mu^{\mu}_{err,T} = .0037m$, $\mu^{\mu}_{err,B} = .0148m$ and $\mu^{\mu}_{err,S} = .0021m$). As expected, the mean values of the participants' size prior again vary across all three different objects (Kruskal-Wallis rank sum test, $chi - squared = 11.58$, $p = 0.0031$) for each object comparison (Pairwise comparisons using Wilcoxon rank sum test, Benjamini-Hochberg adjusted, $p_{SB} = .012$, $p_{TB} = .032$ and $p_{TS} = .012$). I.e. people did know that these objects differed in size.

3.4.2 *Estimating perceptual uncertainty*

As previously mentioned, data from the D-2AFC can be used to estimate individual's perceptual uncertainty about displayed two-dimensional visual angles, since responses do not incorporate action variability and can be free from any influence of subjective size beliefs. For this purpose, the same object combinations of the D-2AFC are helpful as they can be viewed as being reduced to a simple perceptual discrimination task: 'which of the two identical sport objects is closer?' thus becomes 'which of the two objects is bigger on the screen?'. That means these trials remain free from the influence of subjective size beliefs and action variability and thereby help to measure the perceptual uncertainty unbiased.

In figure 11 the resulting psychometric curves for each participant are shown. Responses of individual trials were plotted on the x-axis according to the difference in visual angle of the two objects shown and on the y-axis according to the correctness of the participant's decision. In addition the best fits of the cumulative log-normal distributions are displayed with their recognition threshold at .75 probability highlighted with a red dashed line. These thresholds are at a low level for all participants, suggesting high visual precision, in a range of $\sigma_{per} = .0021$ to .003 in visual degree. This inference can then be utilized to determine the perceptual uncertainty node σ_{per} in the model describing participants' sensations in the MoA task.

3.4.3 *Consistency across tasks*

Before proceeding to the different analyses on the consistency of subjects in their decisions, we will first take a look at raw data and explain their interrelationship and the estimated parameters for a single subject as an example. We do this using visual-

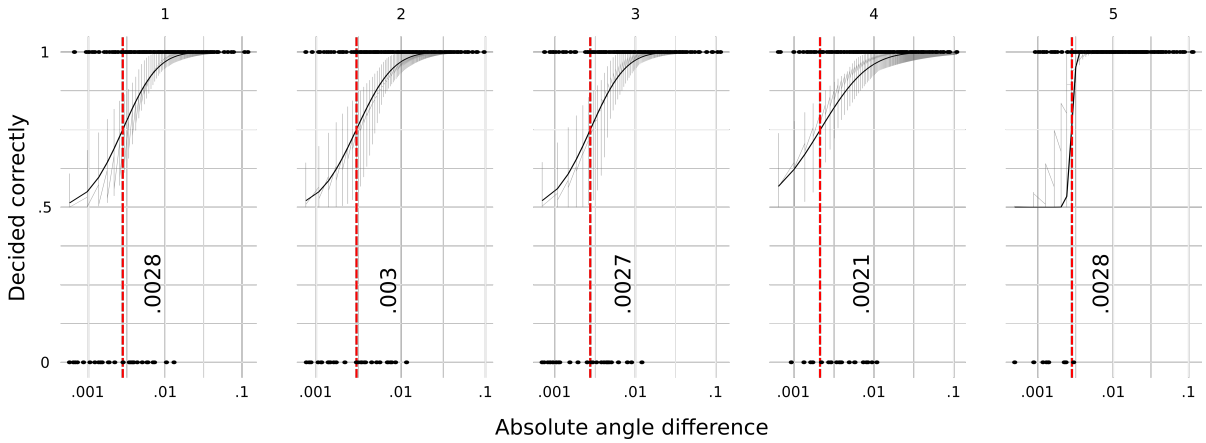

Figure 11: **Cumulative log-normal fits as psychometric curves.** Psychometric curves for same object combinations in the D-2AFC experiment for each participant showing the thresholds for visual perception in absolute difference of visual angles. Raw data points show whether a participant decided correctly and the estimated line approximates participant's probability of recognizing a difference in visual angle size correctly. Red line indicates the threshold at $p = .75$.

izations of estimated parameters like size prior and ratios, the psychometric curves from the D-2AFC and the raw data from the MoA task - see figure 12.

In the first panel A) of figure 12 in the upper left, the size prior estimated based on the data from the S-2AFC task for participant #4 are shown. The resulting distributions and the actual size ot the objects are correspondingly colored. Deviations in meter from the actual size are additionally noted next to the distributions. For a better assessment of the effect of these subjective size beliefs, the size ratio beliefs of each possible combination are shown in the middle panel B) of figure 12. Here, the actual size ratios are again marked by vertical lines showing the relative biases. Ratios are formed by dividing the size of the actually bigger object and result in values greater than 1. As one can see , especially the base- and tennisball combination as well as the soccer- and baseball combination deviate clearly from the actual size ratio, since the baseball's size was strongly overestimated by the subject, as shown in A).

Data from the MoA and the D-2AFC task are shown in panel C) exemplary for trials with soccer- and baseball combinations. The distance of the fixed and adjustable object in the MoA task are shown on the y- and x-axis of the left plot, respectively. Decisions in the MoA task can be split for each combination in two groups depending on which object was at a fixed distance and which was free to adjust. Each trial is color coded based on the adjustable object: here, in trials with orange data points the baseball and with blue ones the soccerball was to adjust. Correct responses, where the adjustable object is pushed exactly to the same distance, will fall on the black diagonal line. Given the subject's clearly shifted belief about the size of the baseball and thus compromised belief about the size ratio, we expect to see a bias in the MoA data. This bias should have two different directions depending on which of the two objects was free to move. We can see that the participant relatively overestimates the size of the baseball in the orange colored trials when moving it, as she does not correctly move it far enough. I.e. with a still too large visual angle of the baseball she already has the impression of a further distance. Vice versa, when moving the soccerball she overestimates the actual distance of the baseball and therefore also puts the soccerball too far, which can be seen in the blue data points' deviation from the optimal line. This bias should then in turn be reflected in the data of the D-2AFC, too. Here,

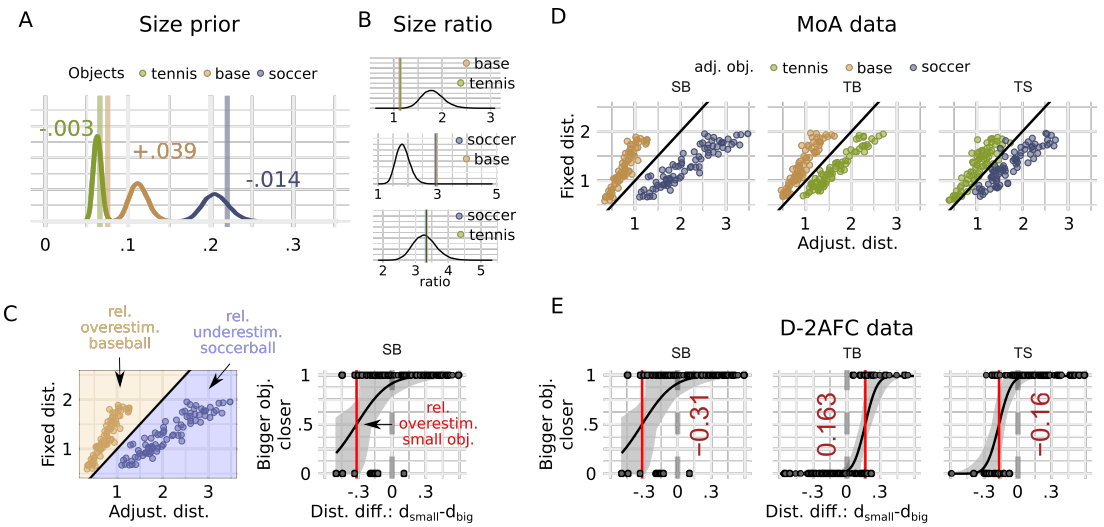

Figure 12: **Single participant data (#4): size beliefs, MoA and D-2AFC decisions. A) Size prior.** Subjective size beliefs as distributions, correct sizes marked by accordingly colored lines and mean shift in meter. **B) Size ratio beliefs.** Showing the deviation of the ratio belief from the actual ratio. **C) Data structure explanation.** MoA and D-2AFC data for base- and soccerball comparison. **MoA:** Actual distance of fixed object on the y-axis as function of the final distance of adjustable object. Trials are colored conditioned on the adjustable object type. Baseballs were placed to close, since the subject is overstimating the baseball relatively to the soccerball, and thus deviating in the light orange area. Vice versa when the soccerball was adjustable. **D-2AFC:** Subject's decision in each trial whether the actual bigger object is closer as function of the distance difference. Negative shifts of the threshold are expected if the smaller object is relatively overestimated. **D) MoA data for all object combinations.** Relative overestimation of the baseball strongly influences decisions for SB and TB combinations. **E) D-2AFC data for all object combinations.** In SB combination soccerball is chosen too early and in TB combination tennisball is chosen too long as function of the distance difference - both signs of the overestimation of the baseball.

the decision whether the soccerball, as the bigger object, is closer to the participant is shown as function of the difference in distance of the both objects to the observer. At negative values on the x-axis the baseball is closer to the observer, since the difference is calculated from the distance of the small object minus the large object, and at positive values the soccerball is closer. Based on the participant's decisions in this 2AFC we can estimate a psychometric function yielding a threshold estimate that indicates potential biases. As expected, the participant perceives the baseball in all trials to be further away than it is, resulting in a negative threshold reflecting this bias.

In figure 13 further data and biases for two participants in MoA and D-2AFC tasks are shown. One can see that e.g. one object combination per participant is almost unbiased in both experiments as a sign of consistency across the two tasks: in case of participant #2 the SB (soccer-baseball) and of participant #5 the TB (tennis-baseball) combination. Likewise, consistent but this time strongly biased are combinations TB and SB for participants #2 and 4, respectively.

However, rather than just describing the consistent directionality (or consistent absence) of bias in both experimental tasks for each participant and combination, we can quantify the magnitude of these biases using the estimated thresholds of the psychometric fits for the D-2AFC data and the difference between the slopes for both

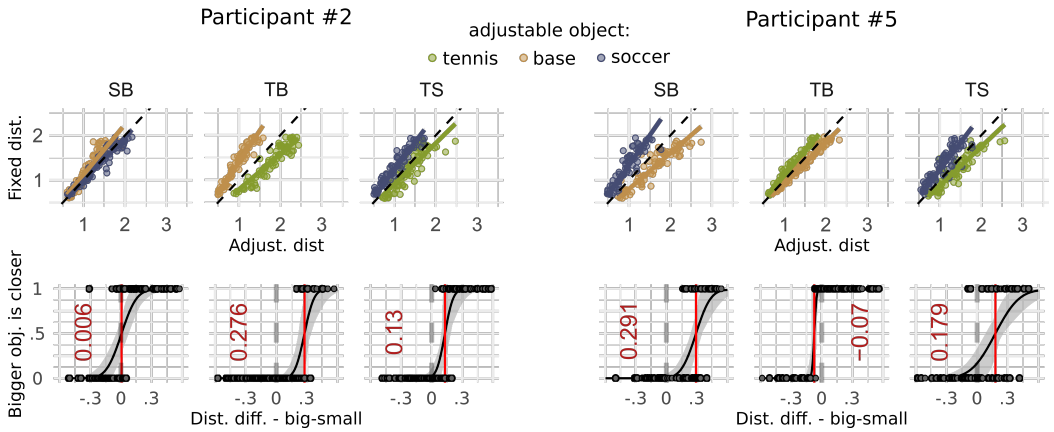

Figure 13: **MoA and D-2AFC data consistency for two participants.** Absence or the directionality of biases are consistent for each participant within each object combination.

conditions in the MoA data. The correlation of these two variables for all participants and object pairs $\rho_{t,s} = .8819$ is highly significant (Pearson's product-moment correlation, $t = 6.7432$, $p < .001$). Further, we can visualize participants' consistency by plotting thresholds and slope differences on the y- and x-axis as scatter plot and calculate the linear regression, see figure 14 A). This calculated regression is likewise highly significant ($F = 45.47$, $p < .001$, adj. $R^2 = .7606$) with an estimated intercept of .0173 that does not differ significantly from zero ($t = .594$, $p = .563$), both showing the participants' overall high consistency across both tasks.

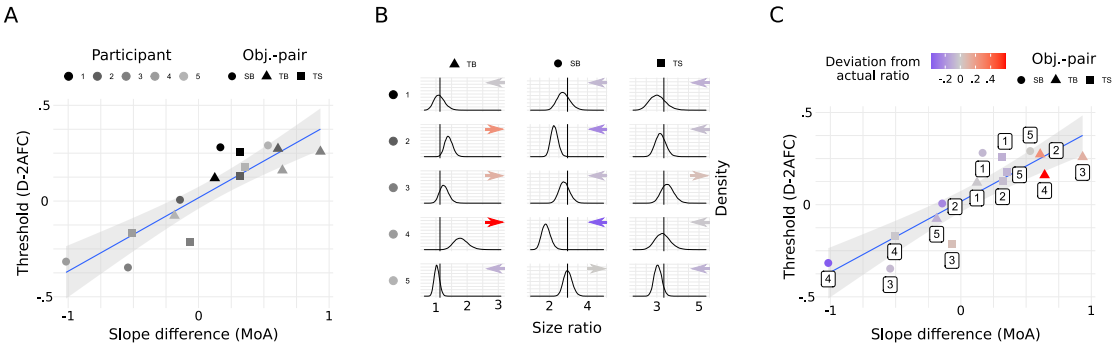

Figure 14: **Consistency of thresholds, slope differences and biases in size ratio beliefs.** A) Threshold values of the psychometric functions as function of the slope differences between MoA regressions for each participant and object combination. Regression shows the systematic consistency across both tasks. B) Size ratio beliefs for each participant and combination. Vertical lines indicate actual size ratio and colored arrows the direction and degree of the deviation. C) Again thresholds as function of slope differences with regression and now with data points colored by the relative deviation of the size ratio belief from the actual ratio shown in B).

In a next step we can extend this comparison of consistency with respect to the inferred size and size ratio beliefs of the participants. Size ratio beliefs for all participants and combinations are shown in figure 14 B) with vertical lines indicating the actual size ratios. Deviations of the mean values of the inferred size ratio beliefs from these actual ratios are visualized via arrows: their orientation depicts the direction of the deviation and their color its relative percentage amount. These colors are then used to investigate and highlight the consistency of size ratio beliefs with behavior in both, the MoA and D-2AFC, tasks, as shown in figure 14 C). Here, data points further down in the bottom left should become increasingly more blue, corresponding to a

relative overestimation of the smaller object and thus reduced ratio belief, while data points on the upper right should turn increasingly red, corresponding to a relative underestimation of the smaller object and thus increased ratio belief. This turns out to be true for participants' object pairs with strongly biased size ratio belief, especially for participants #$2-4$ in object combinations TB and SB, see rows 2-4 and columns 1-2 in B) and blue circles and red triangles for 2-4 in C). However, some data points deviate from this overall pattern, like 3-TS, showing slight biases with inverse orientation in size ratio belief and tasks, or 5-SB showing an mostly unbiased size ratio in B), however in both tasks the participant #5 overestimates the soccer-baseball ratio. When calculating a linear regression like for figure 14 A) but this time for the relative percentage deviation of the size ratio beliefs as function of the MoA slope differences, we can obtain again a significant result ($F = 9.648$, $p = .008$, adj. $R^2 = .3819$) with an estimated intercept of $-.0298$ that does not differ significantly from zero ($t = -.659$, $p = .521$). This can be considered as a sign of an overall consistency between behavior in the MoA task and the inferred size prior. Looking at the same regression for the deviation of the size ratio beliefs as function of D-2AFC thresholds, however, does not yield a significant result ($F = 2.392$, $p = .155$, adj. $R^2 = .0904$). This might be caused by clear outlier like 3-TS (participant with bias in D-2AFC but no bias in size ratio belief) or 2-SB (participant with no bias in D-2AFC but with relevant bias in size ratio belief), see figure 14 C).

So far, we can state that participants' behavior is 1) highly consistent across the MoA and D-2AFC tasks and that 2) size ratio beliefs match the MoA data but 3) cannot significantly explain the behavior in the D-2AFC.

Finally, we can use the Bayesian graphical model shown in figure 9 B) to investigate participants' posterior beliefs about the object distances in the MoA trials. Based on the inferred subjective prior beliefs about object sizes, the estimated perceptual uncertainty based on decisions in the D-2AFC task and the final positions and visual angles of the objects in the MoA task we can infer participants' belief about each object's distance in a trial. And since the task was to move the adjustable object to the same distance, we can check whether their decisions were optimal given their subjective beliefs. We can do this by calculating the mean values for participants' posterior belief for both objects in every trial. These mean values are shown in figure 15 for the fixed and adjustable object in green. Actual distances are colored orange and ideal responses are indicated by the blue dashed line.

Here, six object pairs have been selected as examples for differing model results: in figure 15 A) and B) participants' object pairs are shown whose MoA data can be well explained using the inferred size prior and the Bayesian model, C) data where no changes are expected due to the unbiased size ratio beliefs and D) overcompensation caused by stronger biased size ratio belief than MoA data suggests.

Especially, in A) the strong deviation of the participant's orange colored responses from the dashed optimal line is obvious and can be completely corrected with the inferred subjective size prior. The high consistency of MoA data and size prior can be also found in the regression's slope parameters, with raw data slopes β_D from left to right of .6067 and 1.623 turning to model posterior slopes β_M of .9914 and .9940. Thereby, the model also significantly reduces the error (Wilcoxon signed rank, $V = 12792$, $p < .001$) with mean error values μ_{err} dropping from $-.84$ and $.48m$ to

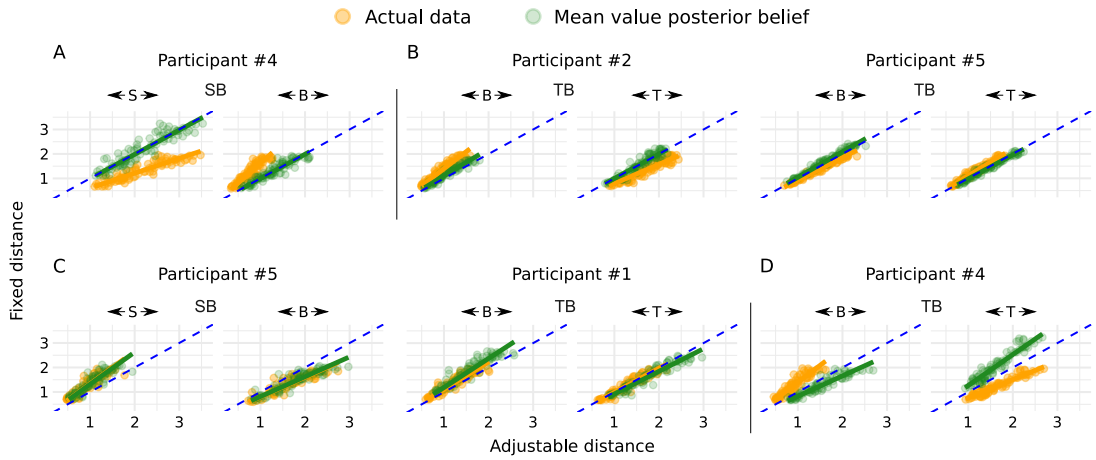

Figure 15: **MoA decisions and model's mean posterior belief.** A) Large deviation of optimal behavior in MoA task can be well explained using the inferred subjective size beliefs. B) Model based on the slightly deviating size beliefs explains slight deviation. C) Bias in model posterior remains since size ratio belief is not (clearly) deviating from actual value. D) Model overcompensation due to strong deviation in size ratio belief.

$-.01$ and $0m$, respectively. With less intense deviation in size beliefs participants #2 and 5 posterior beliefs are improved for the TB pair: raw data slopes β_D from left to right of 1.397 and .7894 turn to posterior slopes β_M of 1.1034 and .9994 for participant #2, and raw data slopes β_D again from left to right of .9220 and 1.107 turn to posterior slopes β_M of 1.042 and .9798 for participant #5. Given the subjective size beliefs participant #2's mean error changes from .39 and $-.38m$ to .11 and $.01m$ and participant #5's mean error changes from $-.11$ and $.13m$ to .07 and $-.03m$. Mean error values for each are trial are likewise significantly smaller for the model compared with the raw data for participant #2 (Wilcoxon signed rank, $V = 12700$, $p < .001$) and #5 (Wilcoxon signed rank, $V = 9450$, $p < .001$). For all regression slopes and changes see table 1.

3.4.4 *Size prior: measurement and reliability*

As size prior are latent and unobserved quantities that have tremendous impact on distance estimation, precision in their determination is essential. Yet it is often difficult to measure these beliefs explicitly or estimate them implicitly in models. Especially since inference with probabilistic models will always yield values that explain the data given the model. But how to be certain these values are meaningful and general? Up to this point, we have used the estimated prior beliefs in a first step to describe and explain behavior in two separate experiments at once. However, we chose another additional method to assure ourselves about the fit and correctness of the measured prior: We utilized people's imagination and muscle memory by asking them to pose with their hands in front of a depth camera indicating the size of the three objects.

In figure 16 A) a resulting depth matrix of a participant sitting in front of the camera can be seen in a three-dimensional view. Participants were then asked to place their hands so that they are parallel and with the edge of their hands facing the camera while trying to imagine holding a specific object between their palms, see figure

	Part. + obj. pair	β_D T adj.	β_M T adj.	β_D B adj.	β_M B adj.	β_D S adj.	β_M S adj.
1	1 TB	0.99	0.92	1.11	1.19		
2	1 TS	0.89	0.80			1.20	1.34
4	1 SB			0.95	0.91	1.11	1.16
7	2 TB	0.79	1.00	1.40	1.10		
8	2 TS	0.91	0.90			1.23	1.25
10	2 SB			1.12	0.87	0.98	1.26
13	3 TB	0.71	0.77	1.64	1.50		
14	3 TS	1.01	1.06			0.94	0.90
16	3 SB			1.31	1.26	0.77	0.80
19	4 TB	0.75	1.27	1.40	0.83		
20	4 TS	1.25	1.29			0.75	0.73
22	4 SB			1.62	0.99	0.61	0.99
25	5 TB	1.11	0.98	0.92	1.04		
26	5 TS	0.87	0.78			1.22	1.36
28	5 SB			0.80	0.81	1.33	1.31

Table 1: **Regression slope parameter β for data und model posterior of the MoA task.** Values separated in rows by participant and object pair and in columns by adjustable object and data β_D and model β_M. The megnitude of deviation from 1 as a sign for the strength of bias in the MoA raw or modeled data.

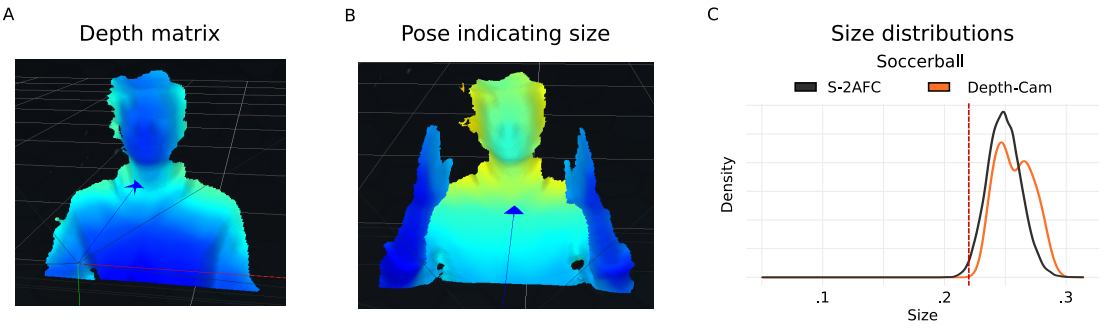

Figure 16: **Size belief measurements via depth camera.** A) Participants were placed in front of a camera measuring a depth profile. B) Meanwhile they were asked to pose with their hands parallel to the camera indicating their belief about. C) Measuring the closest distance between two opposing points in their palm forty times across several frames yields an a priori size belief distribution (orange) which can be compared to the inference of the S-2AFC task.

16 B). These specific objects were again the three sport objects in a random order.

Size prior estimated via S-2AFC and via depth camera are shown for all participants and objects in figure 17 A) in black and orange, respectively. To obtain the samples for the depth camera condition forty measurements of distances between the palms were taken across multiple frames of the recorded videos. The estimated mean μ_{Cam} and standard deviation σ_{Cam} for these samples are compared with values μ_{AFC} and σ_{AFC} from the S-2AFC data in panel B) and C) of figure 17. There is no significant difference found when comparing these mean size values between the

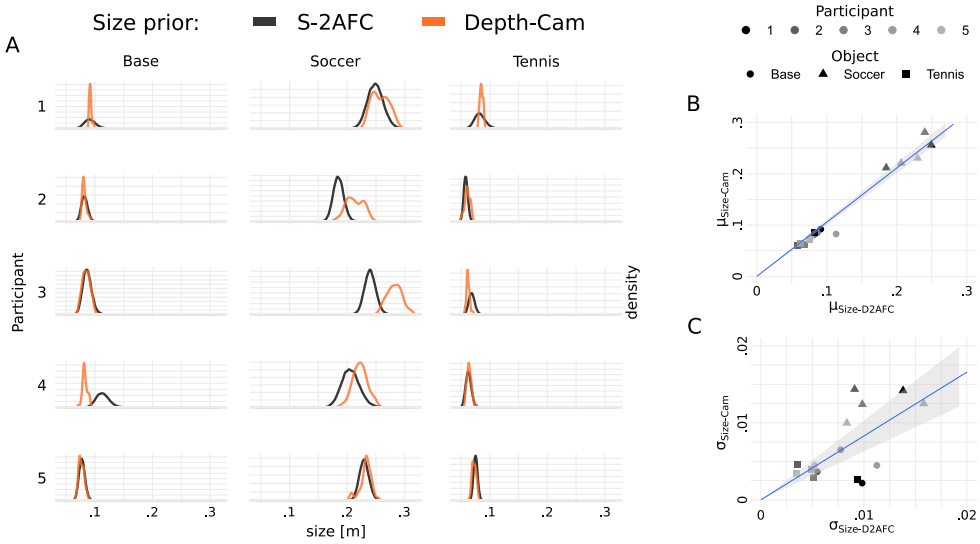

Figure 17: **Comparison size prior from S-2AFC and depth camera.** A) Size prior distributions for each participant and object. Type of measurement separated by color: S-2AFC in black and depth camera data in orange. B) Mean value of size prior estimated by depth camera as function of values from S-2AFC. C) Standard deviation of measured values for depth camera data as function of S-2AFC.

S-2AFC and the depth camera condition (Wilcoxon signed rank test for paired samples, $V = 41$, $p = .3028$). Likewise there is so significant difference for the standard deviation (Wilcoxon signed rank test for paired samples, $V = 84$, $p = .1876$). That means the inferred values using the human MCMC approach seem to be meaningful and not biased by the type of measurement.

3.5 DISCUSSION

Here, we were interested in measuring prior beliefs specifically about familiar objects and investigate whether people's behavior was in accordance with them. Since these beliefs about familiar size are useful cues for distance estimation (Gogel, 1963; Hochberg and Hochberg, 1952; Kilpatrick and Ittelson, 1953) and can even be essential especially in a two-dimensional projection without stereo or auxiliary cues, we ran two experiments limited to two-dimensional projections testing people's perception of distance. In both experiments people's perception of distance was investigated, differing in the type of available responses: discrete answers in a 2AFC and continuous adjustments in a MoA task. Individual responses across the tasks were highly consistent and yet able to demonstrate varying biases between participants. Likewise, inferred beliefs about familiar sizes were also largely in agreement across both methods of measuring, however, do not necessarily concur with each individual's behavior in all conditions.

As unobserved subjective prior beliefs about environmental variables usually influence behavior strongly (Adams, Graf, and Ernst, 2004; Petzschner and Glasauer, 2011; Stocker and Simoncelli, 2006; Trommershäuser et al., 2005; Wolpert and Landy, 2012) and sometimes are even pivotal to explain behavior at all (Hochberg and Hochberg, 1952; Kilpatrick and Ittelson, 1953) it is crucial to consider their influence in modeling. Identifying these beliefs about familiar size is especially important, since real sizes of familiar objects have been reported to be automatically recognized by participants leading to a stroop effect (Konkle and Oliva, 2012), potentially even before

the objects are correctly identified (Long and Konkle, 2017). Prior beliefs about size as well as cues that are able to influence the perception of size and thus distance - or vice versa - have been investigated among others for haptic cues improving distance perception in an interception task (Battaglia, Kersten, and Schrater, 2011), prior beliefs about familiar size in time-to-contact judgments (Hosking and Crassini, 2010) or when reaching for and trying to grasp objects (McIntosh and Lashley, 2008). Yet it can be difficult to measure these prior beliefs in a rather direct way than just to fit them to data. There have been various approaches to measure and infer these subjective beliefs e.g. for stimuli lengths and animal categories (Sanborn and Griffiths, 2008), matching of colors to words, indicating the pleasantness of musical chords, assigning emotions to face expressions (Harrison et al., 2020) or face familiarity (Houlsby et al., 2013). Here, we have taken up the approach of Sanborn and Griffiths, 2008 but without the need to train participants to an arbitrary and artificial distribution since we were interested in the already established subjective beliefs about the size of familiar objects. We were able to show that the participants were overall unbiased in their mean size beliefs with respect to actual object sizes, while individual beliefs about single objects of course could differ from the actual size, as well. Furthermore, we tested whether the prior determined this way were meaningful and correct by asking participants to indicate the diameter of the objects with their hands in front of a depth camera. Using this visuomotoric task yields an additional advantage of using an embodied action. This could be useful since embodied cognition states inter alia that the body and its various forms of interaction can translate to differences in cognitive processing (Foglia and Wilson, 2013). It was shown that e.g. body postures can facilitate the retrieval of memories (Dijkstra, Kaschak, and Zwaan, 2007). This might mean that people can benefit from such a visuomotoric recollection to retrieve beliefs with an improved precision or less bias. We found that samples from the depth camera were in accordance with the data from the size MCMC experiment. This means, since there was no significant difference found, that size prior correctly reflected the subjective belief or at least that both methods used to measure these prior yield the same individual biases.

In order to check participants' consistency we can compare both distance perception tasks as well as the conformity of biases with subjective size prior beliefs. All participants exhibited highly consistent behavior across both distance estimation tasks, the MoA and D-2AFC, as shown with the highly significant correlation $\rho_{t,s} = .8819$ ($p < .001$) of biased thresholds in the D-2AFC and the deviations from optimal line in MoA. Meaning, the direction and degree of biases scaled comparably in both experiments, see again figure 14 A). However, when considering the biases in the subjective beliefs the Bayesian model did not necessarily explain deviations well for all participants and object pairs. These inconsistencies might arise from imprecise and biased measurements of their size beliefs. Yet this is less likely since we have employed two different methods to measure these beliefs which yielded similar results. Another cause for the inconsistency between size beliefs and judgments might arise from participants using heuristics to simplify their tasks. Describing behavior as arising from heuristics, approximations and combinations or so called rules-of-thumb, as an idea to break down computationally highly demanding tasks in easier approximations, is common e.g. in object interception (Belousov et al., 2016; Zago et al., 2009), in judgments about probability (Tversky and Kahneman, 1974) or physical properties (Cohen, 2006; Gilden and Proffitt, 1994). Here, a potential approximation could be the usage of a fixed ratio of visual angles as a decision threshold in both experiments. It

is also conceivable that participants, given their degree of uncertainty, were biased by their first choice and stick to it for the sake of consistency, whether it reflected their size prior well or not. However, with the small number of participants up to this point, this question cannot be conclusively resolved and more data will be gathered.

In summary, the results confirm the value of the human MCMC approach (Sanborn and Griffiths, 2008) to access individual and subjective a priori beliefs as well as demonstrate the consistency of human behavior in distance estimation tasks. However, so far not all behavioral biases can be explained by a Bayesian model considering the individual perceptual uncertainty and shifted subjective beliefs.

4

INTUITIVE PHYSICAL REASONING TRANSFERS TO A VISUOMOTOR TASK

Every thing of nature works according to laws.
Ein jedes Ding der Natur wirkt nach Gesetzen.

— Kant, I. (1791). Grundlegung zur metaphysik der Sitten.

4.1 INTRODUCTION

4.1.1 *Human predictions in physics - heuristic or realistic*

Whether sliding a glass containing a beverage on a counter top in your kitchen or shooting a stone on a sheet of ice in curling, acting successfully in the world needs to take physical relationships into account. While humans intuitively sense an understanding of the lawful relationships governing our surroundings, research has disputed that this is indeed the case (McCloskey, Caramazza, and Green, 1980; Todd and Warren Jr, 1982). Instead, human judgements and predictions about the dynamics of objects deviate systematically from the laws of Newtonian mechanics. Past research has interpreted these misjudgments as evidence that human judgements violate the laws of physics and that they instead use context specific rules of thumb, so called heuristics (Cohen, 2006; Gilden and Proffitt, 1994; Todd and Warren Jr, 1982). E.g., when judging relative masses of objects such as billiard balls based on observed collisions, people seem to use different features of motion in different contexts and end up with erroneous predictions (Todd and Warren Jr, 1982).

But recent research has provided a different explanation of human misjudgments on the basis of the fact that inferences in general involve sensory uncertainties and ambiguities, both in perceptual judgements (Kersten, Mamassian, and Yuille, 2004; Knill and Richards, 1996) as well as in reasoning and decision making (Gershman, Horvitz, and Tenenbaum, 2015; Griffiths et al., 2010). Therefore, physical reasoning needs to combine uncertain sensory evidence with prior beliefs about physical relationships to reach predictions or judgements (Hamrick et al., 2016; Sanborn, Mansinghka, and Griffiths, 2013; Smith, Battaglia, and Vul, 2013; Smith and Vul, 2013; Ullman et al., 2018). By probabilistically combining prior beliefs and uncertain observations, a posterior probability about the unobserved physical quantities is obtained. Judgements and predictions are then modeled as based on these probabilistic inferences. Thus, deviations from the predictions of Newtonian physics in this framework are attributed to perceptual and model uncertainties.

4.1.2 *Noisy Newton framework*

This framework of explaining reasoning about physical systems on the basis of Newtonian mechanics and perceptual uncertainties has been referred to as the noisy Newton framework (see e.g. (Kubricht, Holyoak, and Lu, 2017) for a review). It has been quite successful at explaining a range of discrepancies between predictions of Newtonian physics and human predictions for various perceptual inference tasks, including

subjects' biases in judgements of mass ratios when observing simulated collisions of objects, if perceptual uncertainties are taken into account (Sanborn, Mansinghka, and Griffiths, 2013; Smith et al., 2013). Additionally, the noisy Newton framework can also explain why human judgements depend on experimental paradigms, because tasks differ in the availability of knowledge about objects' properties (Smith, Battaglia, and Vul, 2018). As an example, this suggests an explanation for the fact that judgements about physical situations based on a static image representing a situation at a single timepoint have usually been reported to deviate more from physical ground truth compared to richly animated stimuli (Kaiser et al., 1992), which additionally allow to estimate objects' velocities. Nevertheless, some persistent failures of intuitive physical reasoning have been suggested to be caused by distinct systems of reasoning compared to the more calibrated physical reasoning underlying visuomotor tasks (Smith, Battaglia, and Vul, 2018).

4.1.3 *From reasoning and discrete actions to continuous visuomotor control*

While physical reasoning has been studied predominantly using tasks in which subjects needed to judge physical quantities or predict how objects continue to move, much less is known about how intuitive physical reasoning guides actions. Commonly, experimental paradigms have asked subjects to judge physical properties in forced choice paradigms such as relative masses in two-body collisions (Gilden and Proffitt, 1994; Hamrick et al., 2016; Sanborn, Mansinghka, and Griffiths, 2013; Smith and Vul, 2013), predict the future trajectory of an object when no action is taken based on an image of a situation at a single timepoint, such as a pendulum (Smith, Battaglia, and Vul, 2018), a falling object (Kaiser, Proffitt, and McCloskey, 1985), or whether an arrangement of blocks is stable (Hamrick et al., 2016). Other experiments have asked subjects to predict a trajectory of objects (McCloskey and Kohl, 1983) or their landing position (Smith, Battaglia, and Vul, 2013) after seeing an image sequence, but again without subjects interacting with the objects in the scene. Recent studies have also investigated more complex inference problems in which subjects needed to learn multiple physical quantities by observing objects' dynamics (Ullman et al., 2018) or quantified how much entropy reduction for forced choice questions about physical properties of objects was achieved by interactions with objects in a scene (Bramley et al., 2018). By contrast, the literature on visuomotor decisions and control (Körding and Wolpert, 2004a, 2006; Todorov, 2004; Trommershäuser, Maloney, and Landy, 2003) has seldom investigated the relationship between visuomotor decisions, actions, and control and physical reasoning. Notable exceptions are studies, which have investigated how humans use internal models of gravity in the interception of moving targets (Zago et al., 2004) and how exposure to 0-gravity environments (McIntyre et al., 2001) changes this internal model. Nevertheless, these studies did not investigate the inference and reasoning of unobservable physical quantities. Other studies have investigated how perceptual judgements and visuomotor control in picking up and holding objects in the size-weight and material-weight illusions can be dissociated (Baugh et al., 2012; Flanagan, Bittner, and Johansson, 2008). Nevertheless, these studies did not investigate the relationship of intuitive physical reasoning and visuomotor actions.

Here we investigate how human subjects guide their actions based on their beliefs about physical quantities given prior assumptions and perceptual observations. Thus, we combine work on intuitive physics (Hamrick et al., 2016; Sanborn, Mans-

inghka, and Griffiths, 2013; Smith and Vul, 2013) and visuomotor control (Flanagan, Bittner, and Johansson, 2008; Körding and Wolpert, 2006; Trommershäuser, Maloney, and Landy, 2003; Zago et al., 2004). First, do humans use the functional relationships between physical quantities as prescribed by Newtonian mechanics in new task situations? Specifically, when sliding an object on a surface the velocity with which the object needs to be released needs to scale linearly with the object's mass but with the square-root of the distance the object needs to travel. Second, when interacting with simulated physical objects, do humans interpret differences in objects' behavior in accordance with physical laws? Specifically, when two objects slide according to two different non-linear relationships, subjects may attribute these differences to the lawful influences of unobserved physical quantities such as mass. Third, after having observed collisions between objects do humans adjust their actions consistent with the inferred relative masses of those objects? Specifically, while it is known that subjects can judge mass ratios of two objects when observing their collisions, it is unclear whether they subsequently use this knowledge when sliding those objects. To address these questions, subjects were asked to shoot objects gliding on a surface under the influence of friction to hit a target's bullseye in a simulated virtual environment. The simulated puck was accelerated by subjects' button presses such that the duration of a button press was proportional to the puck's release velocity. A succession of four phases investigated, what prior assumptions subjects had about the relationships between their actions and physical quantities, whether they could learn to adjust their actions to different objects when visual feedback about their actions was available, whether they would interpret the differences in objects' behavior in accordance with physical laws, and whether they could transfer mass ratios inferred from observing collisions to adjust their actions accordingly.

Analysis of the data shows that subjects adjusted their press-times depending on the distance the pucks had to travel. Furthermore, subjects adjusted the button press-times to get closer to the target within a few trials when visual feedback about the puck's motion was available. Because perceptual uncertainties and motor variability can vary substantially across subjects and to take Weber-Fechner scaling into account, we subsequently analyzed the data with a hierarchical Bayesian interaction model under the assumption that subjects used a Newtonian physics based model and compared it to the prediction of a linear heuristics model. Importantly, because subjects needed to adjust their button press-times, the model needs to account for perceptual judgements and the selection of appropriate actions. We include a comparison of three cost functions to investigate subjects' selection of press-times. Based on this model of the sliding task, we find evidence that subjects used the functional relationship between mass and distance of pucks as prescribed by Newtonian physics and readily interpreted differences between two pucks' dynamics as stemming from their unobserved mass. Moreover, biases in subjects' press-times can be explained as stemming from costs for not hitting the target, which grow quadratically with the distance of the puck to the target's bullseye. After observing 24 collisions between an unknown puck and two pucks with which subjects had previously interacted, we found evidence that participants transferred the inferred relative masses to subsequent sliding actions. The mass beliefs from observing the collisions were inferred by a hierarchical Bayesian observation model. Thus, intuitive physical reasoning transfers from perceptual judgements to control tasks and deviations from the predictions of Newtonian physics are not only attributable to perceptual and model uncertainties but also to subjects' implicit costs for behavioral errors.

4.2 MATERIALS AND METHODS

4.2.1 *Participants*

Twenty subjects took part in the experiment. All participants were undergraduate or graduate students recruited at the Technical University of Darmstadt, who received course credit for participation. All experimental procedures were carried out in accordance with the guidelines of the German Psychological Society and approved by the ethics committee of the Technical University of Darmstadt. Informed consent was obtained from all participants prior to carrying out the experiment. All subjects had normal or corrected to normal vision and were seated so that their eyes were approximately 40 cm away from the display and the monitor subtended 66 degrees of visual angle horizontally and 41 degrees vertically. In the vertical direction the monitor had a resolution of 1080 pixels, which corresponded to a distance of approximately 11.5m in the simulation. Four participants have been excluded from the analysis (three due to incorrect task execution and one due to incomplete data; f=9, m=11, age=[18,27], median=22.5, mean=22.25).

4.2.2 *Task procedure and physics*

Participants were instructed to shoot a puck in a virtual environment into the bullseye of a target, similar to an athlete in curling. The shot was controlled by the duration of pressing a button on a keyboard. Participants were told that they were able to adjust the force, which initially was going to accelerate the puck and thus the initial velocity of the puck, by the duration of their press. Additionally, participants were told that realistic friction was going to slow down the puck while sliding on the simulated surface. The general objective of the experimental design was to investigate whether subjects adjusted their shooting of the pucks in a way that was in line with the physical laws governing motion under friction. Specifically, the magnitude of the initial impulse exerted on the puck determines how far the puck slides on the surface. Thus, subjects needed to adjust the duration of a button press according to the distance between the randomly chosen initial position of the puck and the target on each trial. The different experimental phases allowed investigating subjects' prior beliefs about the puck's dynamics, their adjustments of button presses when these beliefs were updated given visual feedback of the puck's motion, and the potential transfer of knowledge about relevant object properties to the control of the puck from perceiving object collisions. Therefore we designed a task with two conditions and four consecutive experimental phases, which differed in the availability of previous knowledge and feedback.

Laws of motion governing the puck's motion. At the beginning of each trial, subjects saw the fixed target and a puck resting at a distance chosen uniformly at random between one and five meters from the target's bullseye. To propel the puck toward the target, subjects needed to press a button. To model the relationship between the button press and the puck's motion, we reasoned as follows. Human subjects have been shown to be able to reason accurately about the mass ratio of two objects when observing elastic collisions between them (Sanborn, Mansinghka, and Griffiths, 2013). In elastic collisions, according to Newtonian laws, the impulse transferred by the collision is proportional to the interaction duration with a constant force. In other words,

the duration of the interaction with a constant force leads to a linearly scaled impulse. Given a constant mass m of a puck and assuming a constant surface friction coefficient μ, Newtonian physics allows deriving the button press-time T_{press} required to propel the puck to the target at a distance Δx:

$$T_{press} = \sqrt{\frac{2\mu g m^2}{F^2}\Delta x} \propto m \cdot \sqrt{\Delta x} \tag{19}$$

with gravitational acceleration g and a constant force F. Here, the constant force F is being applied by the interaction, i.e. the button press of duration T_{press}, which is physically equivalent to an elastic collision with an object. Note that this formulation of the interaction has the additionally intuitive consequence that the release velocity of the puck scales linearly with the duration of the button press (see S1 Appendix "Puck Movement"). The second expression clarifies, that the press-time scales linearly with the mass of the puck, while it scales with the square-root of the distance to the target. Obviously, this relationship assumes perfect knowledge of all involved

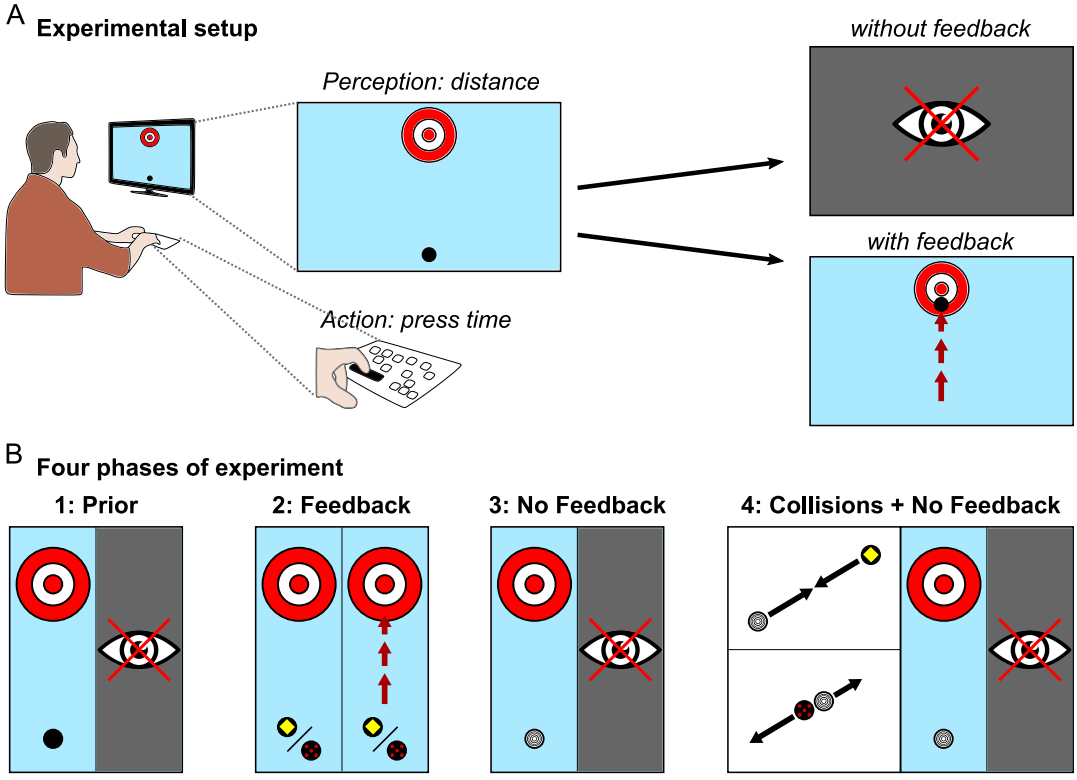

Figure 18: **Task design. (A)** Single trial illustration. Target area and puck are presented on a monitor from bird's-eye perspective. Releasing the pressed button accelerates the puck by applying a force, which is proportional to the press-time. In trials without feedback the screen turned black after button release, while in feedback trials participants were able to see the puck moving according to simulated physics. **(B)** Four phases of the experiment. In the 'prior' phase, no feedback about puck motion was available, whereas in the 'feedback' phase subjects obtained visual feedback about the pucks' motion. Two pucks with different colors and correspondingly different masses were simulated. In the 'no feedback' phase subjects obtained a new puck as indicated by a new color and obtained no feedback. In the last phase, subjects first watched 24 collisions between the new puck and the pucks they had interacted with in the 'feedback' phase before interacting again with the puck. Note that the puck of the 'no feedback' and 'collisions + no feedback' phase are identical.

quantities. The movement of the puck was implemented by simulating the equivalent difference equations for each frame given the friction and the velocity of the preceding frame:

$$x_{t+\delta t} = x_t + v_t \delta t \tag{20}$$

$$v_{t+\delta t} = v_t - a_{fr} \delta t. \tag{21}$$

4.2.3 *Phases of the experiment*

Phase 1: Prior beliefs. In the first phase, we wanted to investigate, which functional relationship subjects would use a priori to select the duration of button presses depending on the perceived distance between the puck and the target. A black puck with unknown mass m was placed at a distance to the target drawn uniformly at random. Participants received no further information about the puck or the environment. Participants were instructed to press the button in a way so as to bring the puck into the target area, but after pressing the button for a duration t^{pre} and releasing it the screen turned black to mask the resulting movement of the puck. This screen lasted for at least half a second until the participant started the next trial by button press. All participants carried out fifty trials. Thus, the collected data allowed relating different initial puck distances to the press-times subjects selected based on their prior beliefs.

Phase 2: Visual feedback. The second phase was designed to investigate, how participants adjusted their button press-times in relation to the simulated masses of pucks and their initial distances to the target when visual feedback about the pucks' motion was available. To this end, participants carried out the same puck-shooting task but with two different pucks, as indicated by distinct surface textures (yellow diamond versus five red dots, see figure 18 b, *Feedback*). The two pucks were alternating every four trials with a total number of two-hundred trials. The two different pucks were simulated with having differing masses, resulting in different gliding dynamics. In this condition, participants received visual feedback about their actions as the pucks were shown gliding on the surface from the initial position to the final position depending on the exerted impulse. Thus, because the distances traveled by the two pucks for different initial positions as a function of the button press-times t^{pre} could be observed, participants could potentially use this feedback to adjust their press-times on subsequent trials. Note, that the two pucks were only distinguished by a color cue and no cue about mass was given apart from the different dynamics. Half the participants were randomly assigned to the 'light-to-heavy' condition, in which the two pucks had masses of 1.5 kg and 2.0 kg, and the other half of the participants were assigned to the 'heavy-to-light' condition, in which the pucks had masses of 2.0 kg and 2.5 kg.

Phase 3: No feedback. In phase three, we wanted to investigate how having observed the sliding of the pucks in phase two influenced participants' press-times with an unknown puck. Subjects were asked to shoot a new puck they had not seen before to the target without visual feedback, as in the first experimental phase, for one-hundred trials (figure 18 B, *No Feedback*). The texture of the puck consisted of five

concentric rings. For participants in the 'light-to-heavy' condition, the new puck had a mass of 2.5 kg whereas for participants in the 'heavy-to-light' condition the new puck had a mass of 1.5 kg. However, different from phase one, in which subjects had not obtained feedback about the pucks' motion, by phase three participants had already interacted with three pucks and obtained visual feedback about the motion of two pucks. Importantly, participants had received feedback about the non-linear nature of gliding under friction in phase two, albeit scaled differently for the two pucks. Thus, this experimental phase allowed investigating, whether subjects use the functional mapping from puck distances to press-times prescribed by Newtonian physics and what assumptions about the mass of an unknown puck they used.

Phase 4: Collisions & no feedback. With the final experimental phase we wanted to investigate, whether participants can use the relative mass ratios inferred from observing collisions between two pucks to adjust their subsequent actions with one of those pucks. At the beginning of phase four, participants watched a movie of twenty-four collisions between two pucks. One was always the puck with unknown mass used in phase three (without feedback; five rings) (see figure 18 B, *Collisions No Feedback*), while the second puck was one of the two pucks presented in phase two (see figure 18 B, *Feedback*). Each collision thus showed one of the two previously seen pucks from phase two selected at random colliding with the puck from phase three with a total of twelve collision with each of the two known puck. By observing these elastic collisions participants were expected to learn the mass ratios between pucks, as shown in previous research (Sanborn, Mansinghka, and Griffiths, 2013; Smith et al., 2013). Note that the pucks were simulated without the influence of friction in these collisions, ensuring that participants only obtained a cue about relative masses and not about the dynamics under friction for the puck from phase 3. After watching these collisions, subjects were asked to shoot the puck from phase three again without obtaining visual feedback, as in phases one and three, for one-hundred trials. Thus, subjects interacted with the same puck as in phase three but had now seen the collisions of this puck with the two pucks they had interacted with. This experimental phase therefore allowed investigating, whether subjects used the learned mass ratios and transferred them to the control task to adjust their press-times. Importantly, having learned the mass ratios between pucks needs to be transferred to the press-times, which differ in a physically lawful way depending on the initial distance of the pucks to the target. As the two pucks from phase two of the experiment were only distinguished by color, such a transfer indicates that subjects had attributed the different dynamics to their masses consistent with Newtonian physics. Thus, if subjects used an internal model of physical relationships, they should be able to adjust their press-times for the new puck without ever having seen it glide.

4.3 RESULTS

4.3.1 *Behavioral results*

As subjects did not receive visual feedback about the consequences of their button presses in the first phase of the experiment, the button press-times reflect the prior assumptions they brought to the experiment. Indeed, subjects' press-times t^{pre} grew with the initial distance between the puck and the target. The button press times for all phases of the experiment are shown in figure 19. The correlation between t^{pre}

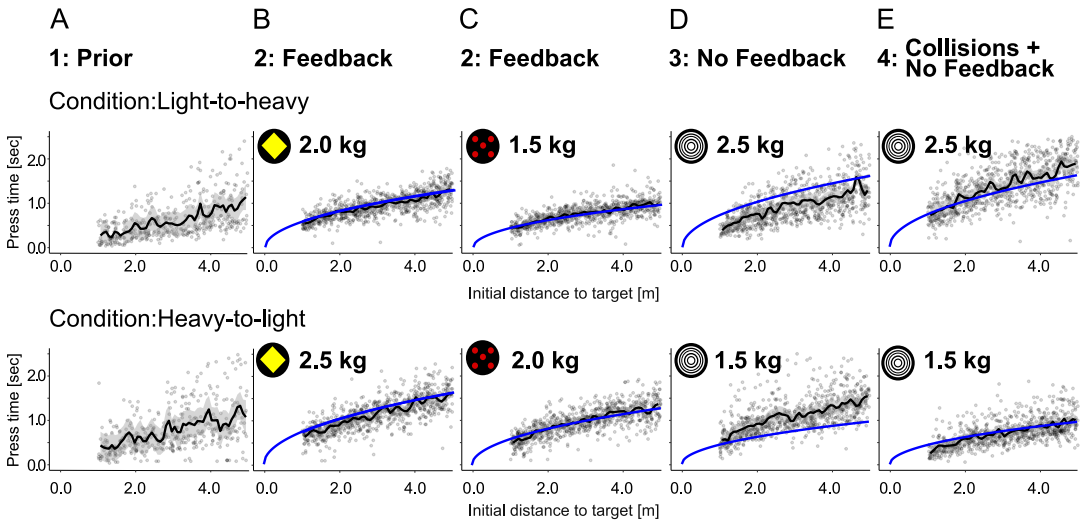

Figure 19: **Press-times as function of initial distance to target.** Press-times for all participants by condition and experimental phase are shown with data points in black and Newtonian relationship with perfect knowledge about the involved parameters in blue. The top row shows the data of subjects in the light-to-heavy condition and the bottom row shows the data of subjects in the heavy-to-light condition. **(A)** Press-times of participants in the first phase ("prior"), **(B)** second phase ("feedback") for the yellow puck, **(C)** second phase ("feedback") for the red puck, **(D)** third phase ("no feedback"), and **(E)** last phase ("collisions and no feedback") after having seen 24 collisions.

and the initial distance was 0.482 ($p < 0.001$). However, the functional relationship according to Newtonian physics prescribes a scaling of the press-time according to the square-root of the distance as specified in eq. 19. The correlation between press-times t^{pre} and the square-root of the initial distance was 0.478 ($p < 0.001$). We expected the standard deviation of press-times to scale with the the mean of press-times in accordance with the Weber-Fechner scaling. This was confirmed by subdividing the range of distances into three intervals of the same size, i.e. $[1, 2.33]m$, $(2.33, 3.66]m$, and $(3.66, 5]m$ and computing the standard deviation of press-times within these three intervals resulting $2.97 \times 10^{-1}s$, $4.19 \times 10^{-1}s$, and $5.69 \times 10^{-1}s$.

In phase two, participants adjusted their press-times based on observing the gliding of the pucks after button presses. Performance was evaluated by calculating the mean absolute distance of pucks to the target after sliding. The mean absolute error over the entire phase was $0.928m$ ($0.0177m$ SEM), see figure 20. Accordingly, the correlation between t^{pre} and the initial distance was 0.644 ($p < 0.001$) and with the square-root of distance 0.646 ($p < 0.001$). The performance improved between the first eight trials at the beginning of the phase (mean absolute error $1.76m$) and the last eight trials at the end of the phase (mean absolute error $0.89m$). The adjustment of pressing times was achieved on average after only a few trials, as revealed by a change-point analysis (Lee and Wagenmakers, 2014), which showed that after six trials the average endpoint error of the puck was stable (see figure 21). Note that this includes four trials with one puck of the same mass and two trials of the second puck with a different mass.

Phase three involved shooting a new puck, which subjects had previously not interacted with, without visual feedback. Note that the puck was identical to the puck subjects later interacted with in phase four after seeing the collisions. This phase there-

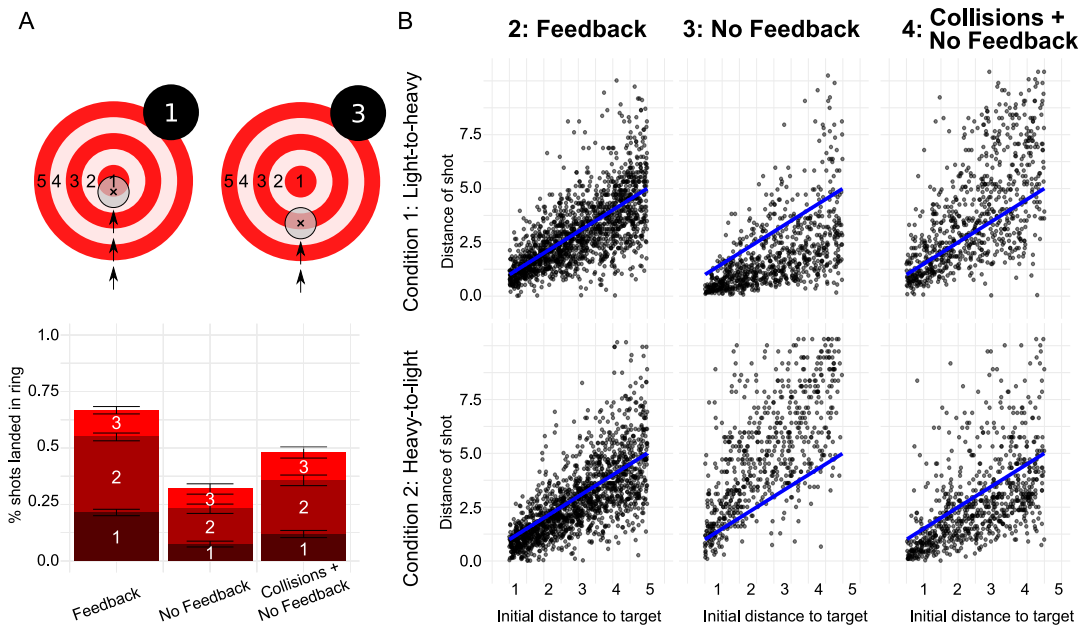

Figure 20: **Task performance and pucks' traveled distance for three phases of experiment.** **(A)** Participants' performance by experimental phase as quantified by pucks' average absolute error in final position. The number of the ring at which the center of the puck stopped was used for coding performance, e.g. 1 and 3 in the shown cases. **(B)** Aggregated final positions of pucks versus initial distance of pucks to target. Phases of the experiment are separated by columns and conditions are separated by rows. The line of equality representing final positions prescribed by the Newtonian model with perfect knowledge of all parameters is shown in blue.

fore allowed testing whether subjects used the non-linear scaling of the press-times depending on initial distance of the puck after having observed the pucks' motion in phase two. As expected, performance was significantly lower with the new puck without obtaining visual feedback. Mean absolute error was 2.87m (0.104m SEM), see figure 20. The correlation between t^{pre} and the initial distance was 0.599 ($p < 0.001$) while the correlation between t^{pre} and the square-root of the initial distance was 0.603 ($p < 0.001$). Given that subjects had already obtained feedback about two pucks in phase two but did not obtain feedback in this phase, their press-time distribution could potentially be the mixture of the two press-time distributions of the two previous pucks, which were different in the conditions 'light-to-heavy' and 'heavy-to-light'. We compared the combined press-time distributions of phase two with the press-time distribution of phase three for each condition with the Kolmogorov-Smirnov test. Press-times in phase three reflected the behavior of both previous pucks combined for condition 'heavy-to-light'(Kolmogorov-Smirnov, D = 0.0538, p = 0.092, see figure 22 B, "Kolmogorov tests - press-times in phase two & phase three") and approximately for condition 'light-to-heavy' (Kolmogorov-Smirnov, D = 0.156, $p < 0.001$, see figure 22 A).

At the beginning of phase four subjects watched a movie showing 24 collisions between the pucks from phase two, for which visual feedback of the gliding had been available, and the unknown puck from phase three. Thus, this condition allowed testing whether observation of the collisions was used to infer the mass ratios of pucks and to subsequently adjust the pressing times for that puck from phase three. Performance was significantly higher than in phase three (see figure 20) with a mean absolute error of 1.63m (0.0440m SEM), although the puck was the same as in phase three and although subjects did not obtain visual feedback. This effect was significant

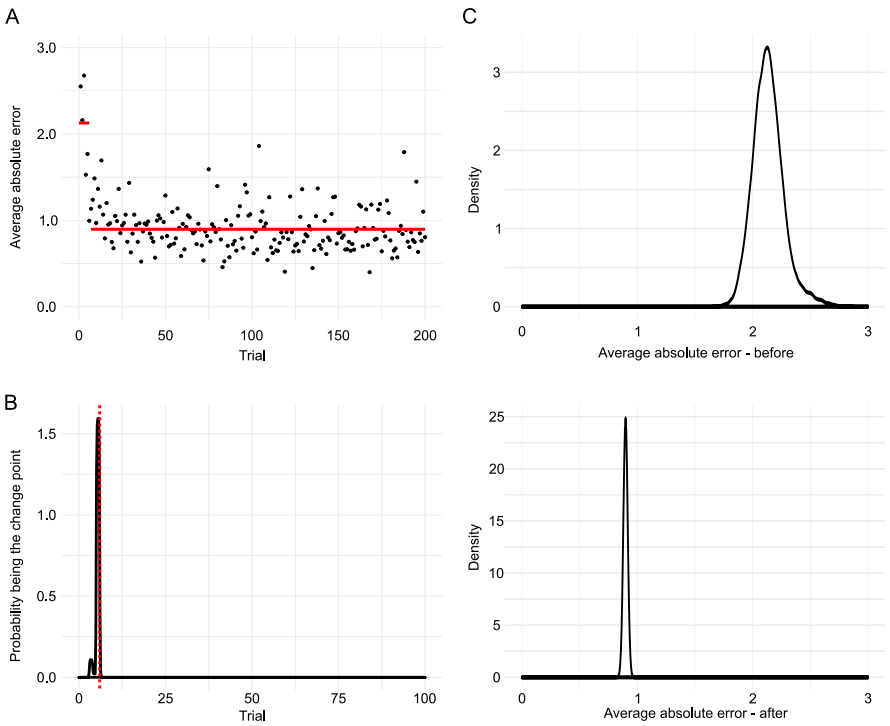

Figure 21: **Change point detection.** Average absolute error as function of trials and posterior of mean average error derived using the change point detection model. **(A)** Average absolute error over participants as function of trial number. **(B)** Posterior over change point τ. Red dotted line marks trial six. **(C)** Posterior of mean error before and after change point.

for both conditions as tested with Wilcoxon Signed Rank test for the absolute error (light-to-heavy: W = 339300, p = 0.018; heavy-to-light: W = 441330, $p < 0.001$). This shift towards longer and shorter press-times in the light-to-heavy and heavy-to-light condition respectively is depicted in figure 24. The shift was statistically significant by testing with a Wilcoxon Signed Rank test for shorter and longer press-times for both conditions respectively (light-to-heavy: W = 158580, $p < 0.001$; heavy-to-light: W = 490620, $p < 0.001$). For more detail of the error distributions across phases two to four see figure 23.

Taken together, these analyses suggest, that subjects adjusted their press-times both depending on the distance of the pucks to the target and depending on the pucks' masses used in the simulation. Furthermore, the analyses provide a very weak initial hint, that subjects may have scaled their press-times with respect to mass and with a non-linear function of initial distance after having obtained visual feedback about the pucks' motion. Finally, observing collisions between pucks lead subjects to adjust their press-times even without obtaining visual feedback. In the following section we provide two computational generative models, one for the sliding task and one for the collision observation task to quantitatively analyze participants' press-times in terms of perceptual, physical, and behavioral quantities.

4.3.2 *Interaction model results*

The above analyses give only a weak indication that our participants were able to adjust their press-times consistent with Newtonian physics and that they transferred

the inferences about relative mass ratios from observing collisions to the press-times, and are limited in several ways. First, perceptual variables such as the initial distance of the puck to the target were uncertain for our subjects, which is not quantitatively entering the correlation analyses of press times with physical predictions under the assumption of perfect knowledge of all parameters. Secondly, our participants had to press a button to propel the puck. For longer press-times, subjects are known to demonstrate variability in pressing times, which scales linearly with its mean and which may vary considerably between subjects. Thirdly, while subjects pressed a button and observed the simulated motion of the pucks from a bird's eye view on a monitor, it would be desirable to be able to estimate subjects' belief about the masses of the different pucks implicit in their press-times. Therefore, we devised a hierarchical Bayesian model of the full visuomotor decision task to provide a computational account of our subject's behavior.

The Bayesian network model in figure 25 expresses the relationship between variables on a subject-by-subject and trial-by-trial basis. While as experimenters we have access to the true initial distance x used in the simulation of the puck and displayed on the monitor as well as the measured press-time t^{pre} chosen by the subject on a particular trial i, subjects themselves do not know these values. Instead, each participant j has some uncertain percept of the puck's distance $x^{per}_{i,j}$ and, potentially, some belief about the mass $m_{j,k}$ of the puck, which depends on its color and the phase of the experiment k. This structure of the graphical model from the experimenter's view leads to the following joint distribution $p(d, l)$ with observed data $d = \{x, t^{pre}\}$ and latent variables $l = \{x^{per}, \sigma^x, m, \sigma^t\}$, where trial, puck and participant subscripts were omitted for clarity:

$$p(d, l) = p(x)\ \ p(\sigma^x)\ \ p(x^{per}|x, \sigma^x)\ \ p(m)\ \ p(\sigma^t)\ \ p(t^{pre}|x^{per}, m, \sigma^t, \theta) \tag{22}$$

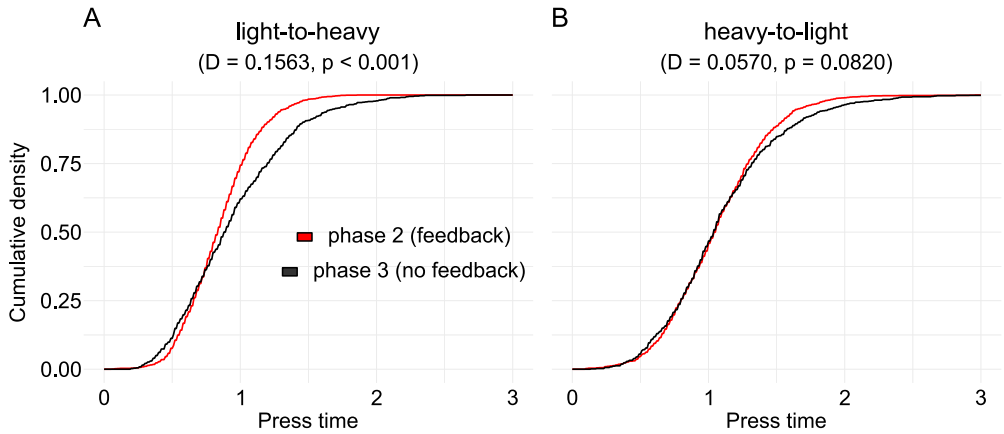

Figure 22: **Kolmogorov tests - press-times in phase 2 & phase 3.** In the light-to-heavy condition both distributions of press times when seeing pucks and without feedback in phase 3 differ significantly. However, considering the asymmetry within the task response - press-times and potential masses are only constrained single-sided towards lower values with a minimum at zero - this difference in press-time distributions is surprisingly small. **(B)** In the heavy-to-light condition there was no significant difference between the distribution of press-times of both combined feedback pucks and the unknown puck before observing the collisions as revealed by the Kolmogorov-Smirnov test. This suggests that participants adhere to their previous adjusted strategies when facing decisions in great uncertainty.

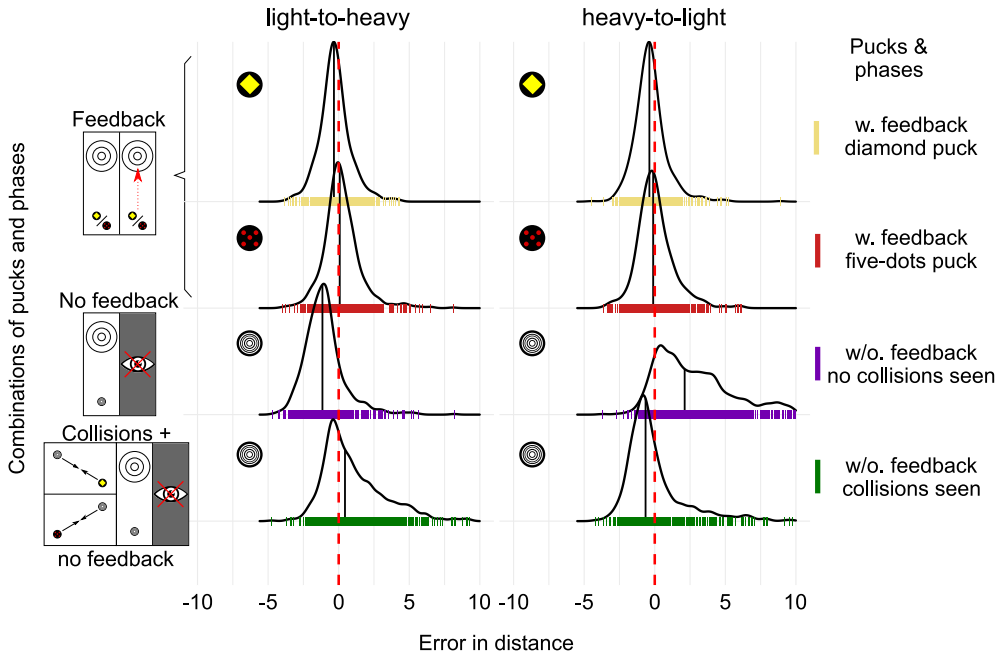

Figure 23: **Distance error distributions.** Final discrepancy between target and puck pooled for all participants. Pucks being shot too short are shown with negative values, pucks with a positive deviation were shot too far. Columns showing the the data for both conditions and rows divide into puck and phase combinations. The first two rows (in gold and red) showing the error distributions for both pucks with feedback in phase 2. The error distribution for the unknown puck in phase 3 before seeing the collisions is shown in the second last row (in purple) with greater deviation, with a clear bias and bigger spread. In the last row the error distributions are depicted for the unknown puck after having seen the collisions with the previous learned pucks, showing a reduced bias.

Here, $p(x)$ is known to the experimenter as the actual distribution of distances to target used in the simulations. By contrast, the distribution of perceived distances $p(x^{per}|x, \sigma^x)$ is the noisy perceptual measurement by our participants described as a log-normal distributed variable, ensuring that samples are strictly positive and including uncertainty scaling according to Weber-Fechner (Battaglia, Kersten, and Schrater, 2011). $p(\sigma_x)$ describes the prior distribution over possible values of this perceptual uncertainty. Participants' prior beliefs about the masses of the different pucks $p(m)$ are described by gamma distributions, which entail the constraint that masses have to be strictly positive. The log-normal distribution of actually measured press-times $p(t^{pre}|x^{per}, m, \sigma^t)$ depends on the noisy perception of the distance to target x^{per}, the belief about the mass of the object and the variability in acting, which is the press-time variability σ^t with its gamma distribution $p(\sigma^t)$. We additionally summarize all constant factors, i.e the surface friction coefficient, the gravitational acceleration, the constant interaction force in the parameter θ.

The potential functional relationship between the perceived distance of the puck to the target and the required press-time is expressed in the deterministic node representing t^{int} in the Bayesian network. We consider two possible functional relationships between the press-time and the distance to be covered: subjects may use a linear relationship between press-time and initial distance as a simple heuristic approach:

$$H_1 : \quad t^{int} \propto x^{per} \tag{23}$$

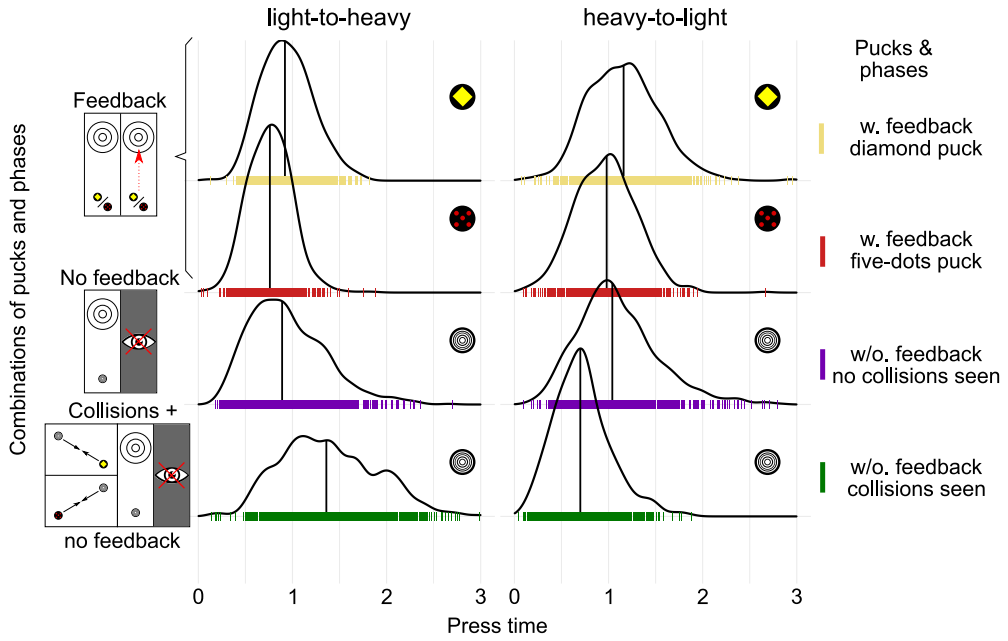

Figure 24: **Press-time distributions.** Pooled press-time distributions for all participants. Columns showing the the data for both conditions and rows divide into puck and phase combinations. First two rows showing the press-times for the pucks with feedback. Press-time distributions in phase 3 without feedback are shown in row three in blue. Without further information participants' behavior in phase 3 is strongly influenced by the previous phase and its press-time distribution: press-time distributions for the unknown puck in phase 3 reflect roughly the combined distributions of press-times of the previous pucks in phase 2 (Kolmogorov $D = 0.0538$; $p = 0.092$ for heavy-to-light, $D = 0.156$; $p = 9.8 \times 10^{-12}$ for light-to-heavy).

or may use the square-root relationship as prescribed by Newtonian physics according to Eq. 19:

$$H_2 : \; t^{int} \propto \sqrt{x^{per}} \tag{24}$$

As experimenters, we only have access to the observed data d, i.e. the actual distances given the experimental setup and the measured press-times. We use Bayesian inference employing Markov-Chain Monte-Carlo to invert the generative model and infer the latent variables describing subjects' internal beliefs given the observed data d:

$$p(l|d) = \frac{p(d,l)}{p(d)} = \frac{p(\sigma^x)\;\; p(x^{per}|x,\sigma^x)\;\; p(m)\;\; p(\sigma^t)\;\; p(t|x^{per},m,\sigma^t,\theta)}{p(t|x)} \tag{25}$$

However, modeling perception as inference may not be sufficient to describe our participants' behavior and their selection of actions. Given a posterior over mass and distance describing the perceptual belief of a subject on a particular trial, a specific press-time needs to be selected. In order to model this selection process we take action variability and potential cost functions into account. Cost functions govern which action, here the press-time, should be chosen given a posterior belief and a cost function, which quantifies how the decision process penalizes errors on the task.

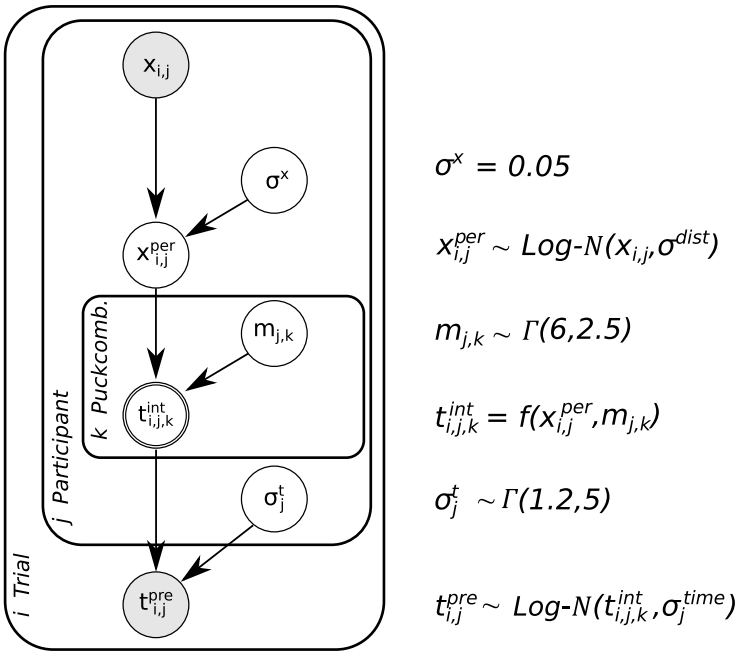

Figure 25: **Hierarchical Bayesian network for the Newtonian interaction model.** The model expresses the generative process of observed press-times $t^{pre}_{i,j}$ across trials i, participants j, and pucks k including Weber-Fechner scaling given perceptual uncertainties of distance $x_{i,j}$ and mass $m_{j,k}$ of the pucks and subjects' press-time variability. The parameter values refer to the prior probability distributions. See the text for details.

This means that it is assumed that participants select an action that minimizes potential costs associated with missing the target. Loss functions, describing the rewards or costs for every action in the action space, can have any arbitrary form, nonetheless we chose a set of three standard loss functions and compare their predictions: 0-1, absolute and quadratic loss functions. These three canonical loss functions express subjects' implicit preferences for reaching a decision about press-times based on a putative perceptual posterior: the 0-1 loss corresponds to penalizing equally all deviations between the chosen value and the correct value, the absolute loss corresponds to penalizing deviations from the true value linearly, and the quadratic loss penalizes the deviations quadratically. It can be shown that these loss functions lead to different decisions for a continuous variable with a non-symmetric distribution (Gelman et al., 2013). Thus, assuming that humans do have costs for missing the target and associated policies to minimize these costs, leads to three different model versions for each model class (see figure 26).

In order to evaluate participants' behavior computationally we first utilized subjects' data from phase two of the experiment to estimate their perceptual uncertainty and behavioral variability. We chose to start with analyzing phase two for two reasons: first, if participants are able to use visual feedback about the pucks' dynamics to adjust their press-times, predictions of the model with the correct physical relationships should capture the behavior better than the linear heuristics model. Secondly, inferred values for latent variables describing visual uncertainty in distance estimation and variability in press-times are less prone to be assigned additional uncertainty. Additional uncertainty arising in all other phases of the experiment due to the lack of visual feedback should be assigned to the uncertainty about the mass or the linear scaling rather than to the variability of press-times in general. Therefore, by evalu-

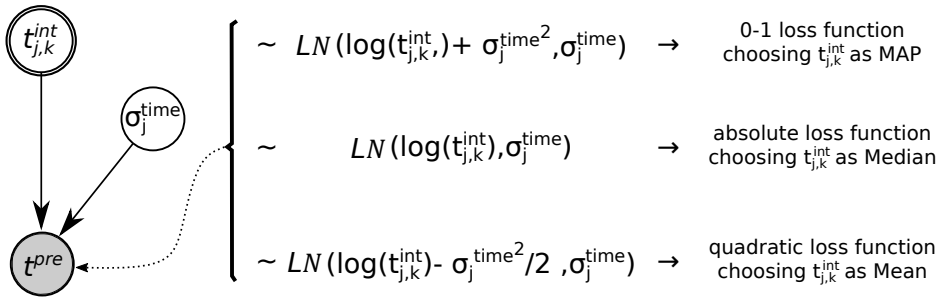

Figure 26: **Implementation of cost functions.** Derivation of the three cost function models based on the expressions for the measures of the central tendency of the log-normal distribution with its mode $exp(\mu - \sigma^2)$, median $exp(\mu)$ and mean $exp(\mu + \frac{\sigma^2}{2})$. Setting the intended press-time to one of these measures for the press-time distribution is equivalent with choosing the 0-1, absolute or quadratic loss function.

ating data from phase two "feedback" first, values for the press-time variability and uncertainty in the perception of distances can be estimated for each participant.

First, we used the data of phase two "feedback" to investigate, which of the three loss functions best describes our participants' data. In order to choose the appropriate cost function explaining participants' actions most accurately, we computed the press-times predicted by the linear heuristics and the Newtonian model and applied the three cost functions to both models. This was achieved by using the inferred maximum a posteriori (MAP) values for the latent variables in both model classes, i.e. the mass m in the Newtonian and a linear factor in the heuristic linear model class. This allowed calculating the residuals, i.e. the difference between subjects' actual press-times and the predicted press-times for all six combinations of two models and three cost functions. The residuals are shown as a function of the distance to the target in figure27. The strong correlation of residuals and distance to target indicates a systematic bias of the linear heuristics model, whereas the weak correlation of the Newtonian model demonstrates its superiority in explaining the measured data. These relationships were tested with Spearman correlation tests for each model and cost function. The data show highly significant correlations for all models ($p < 0.001$ in all cases; 0-1 loss function: $\rho_{New} = 0.167$, $\rho_{lin} = -0.550$; abs. loss function: $\rho_{New} = 0.124$, $\rho_{lin} = -0.643$; quadratic loss function: $\rho_{New} = 0.0976$, $\rho_{lin} = -0.686$) and higher correlation in the linear model for each cost function ($p < 0.001$ in each case, with Bonferroni corrected $\alpha_{crit} = .017$).

Secondly, the posterior predictive distributions for press-times estimated from data in phase two (see S1 Appendix, "Posterior predictive checks for press-times") match the actual behavior of the participants more closely compared to the linear heuristics model. Kullback-Leibler divergence for each pair support this with divergence values at 0.0558 and 0.0851 for the Newtonian and linear model, respectively. Not only did the Newtonian model capture participants' press-times in phase two better than the linear heuristics model, but this also affected the inferred variabilities. While perceptual uncertainty only varied marginally (see figure 28 (A)), the posterior distributions of the press-time variability σ^t_j show higher values for the linear model (see figure 28 (B)) compared to the Newtonian model. This was confirmed by calculating a repeated measure ANOVA on the posterior distributions of press-time variability for both models, showing that the difference was highly significant ($F = 39.2$, $p < 0.001$).

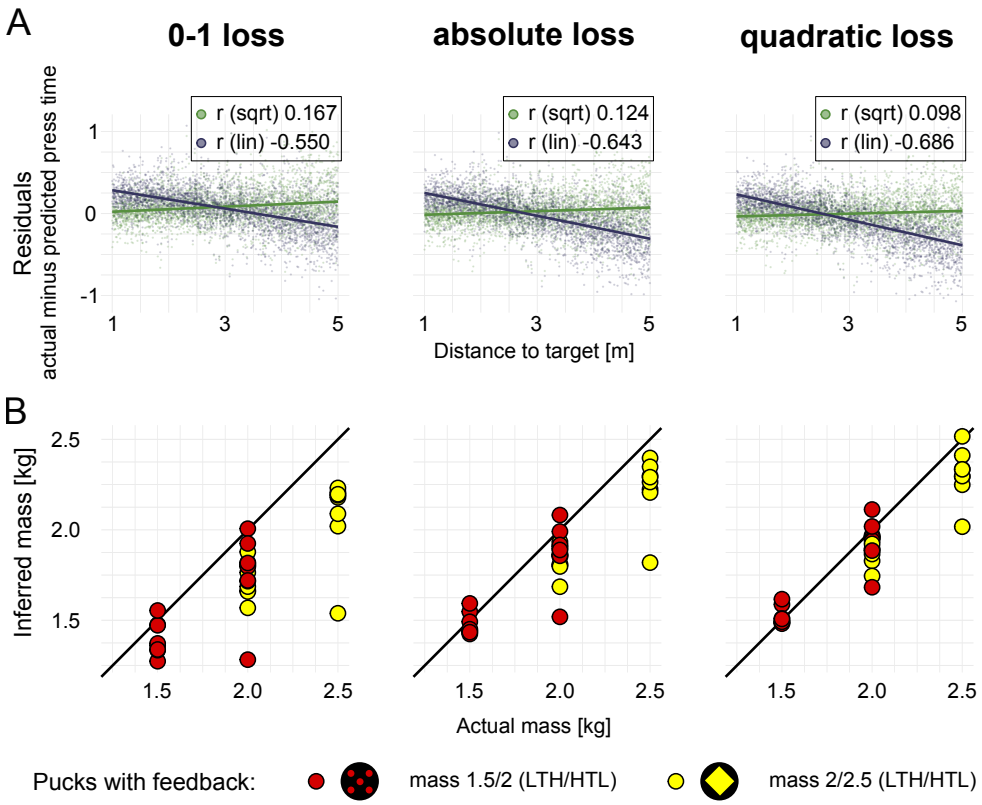

Figure 27: **Residuals of estimated press times and inferred masses in phase two for three cost functions. (A)**Residuals were calculated for each participant and each puck in phase two ("feedback") given the actual press-times and the best fits for the linear heuristics and the Newtonian model. Residuals for both models were calculated for all three cost functions. **(B)** MAP estimates of the masses used by individual subjects inferred according to the Newtonian model for the the three cost functions. Red and yellow pucks had different masses for subjects in the two conditions "heavy-to-light" and "light-to-heavy".

This elevated level of uncertainty is necessary for the linear heuristics model to compensate for the diminished ability to capture the relationship of initial distances and participants' press-times. Therefore, in the following we used the Newtonian model with quadratic cost, because it shows the lowest residual correlation, smallest divergence in posterior predictive distributions of press-times, and smallest press-time variability.

A consequence of selecting the quadratic cost function on the basis of the analyses of press-time residuals and posterior predictive distribution of press-times allows comparing the masses inferred on the basis of participants' behavior. Remarkably, posterior distributions inferred with data aggregated over participants only from phase two match actual masses implemented in the physical simulations better for the quadratic cost function (see figure 27 (B) and figure 29). In both conditions inferred beliefs about the masses are closer to the actual masses implemented in the simulations when presuming that participants use a quadratic loss function. This was confirmed by testing for the absolute differences between the posterior belief and the actual mass for each condition, puck and cost function. An ANOVA revealed highly significant differences ($F = 486$, $p < 0.001$) and post-hoc tests showed that the posterior belief when using the quadratic cost function is the closest fit for all pucks ($p < 0.001$ condition light-to-heavy, yellow diamond puck; $p = 0.002$ red dots

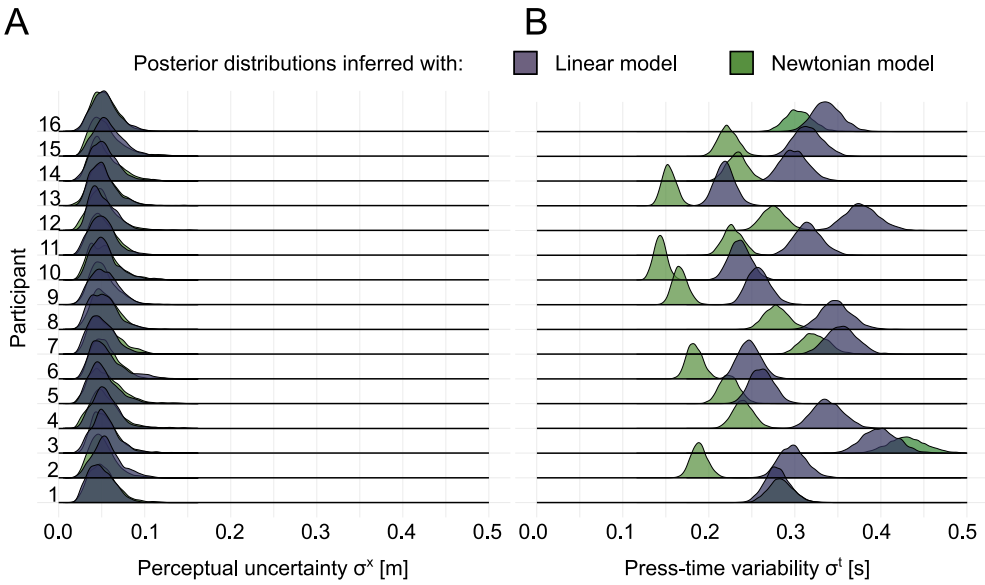

Figure 28: **Posterior estimates of perceptual uncertainty and press-time variability inferred with data from phase two "feedback". (A)** Inferred posterior distributions of perceptual uncertainty for the linear heuristics model and the Newtonian physics model. Dark green distributions display posterior distributions for the Newtonian model class, dark blue ones for the linear model class. A separation into cost functions is not included since the different cost functions did not lead to significant differences. **(B)** Inferred posteriors for individual press-time variability varied significantly between subjects between the two models. All but one participant show lower or equal values of variability regarding the press-time for the Newtonian model class.

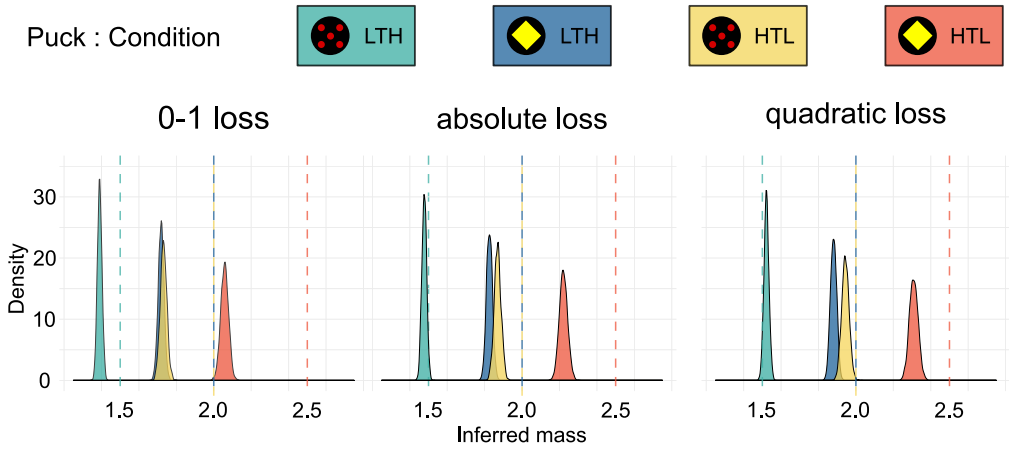

Figure 29: **Latent masses by cost function: aggregated data from phase 2.** Inferred latent mass beliefs with aggregated data from phase 'feedback' for each cost function. Posterior distributions for mass belief aggregated over all participants for each cost function. Colored, vertical lines indicate actual mass of pucks. In comparison the quadratic loss function leads to posterior distributions that fit closest to the actual masses in the experiment.

puck; $p < 0.001$ condition heavy-to-light, yellow diamond puck; $p < 0.001$ red dots puck). This result also held at the individual participant levels as illustrated in figure 27 (B)). Thus, the quadratic cost function, which best described participants' press times, revealed that participants' mass beliefs were more accurate compared to assuming other cost functions.

Subsequently, we used the MAP values of the inferred press-time variabilities $\hat{\sigma}^{t}_{MAP}$ for each subject as fixed values for the analyses of data of all experimental phases. The same applied for the MAP values of the inferred perceptual uncertainties $\hat{\sigma}^{x}_{MAP}$ which did not differ across subjects or models (see figure 28 (A)) and therefore were set to one fixed value for all subjects. Note that the mean was 0.05m in simulation space, which, given the current setup corresponded to approximately 4.7 pixels on the monitor. Using the hierarchical Bayesian interaction model, samples of the posterior predictive distributions of press-times and of the perceptual uncertainty are used to infer latent variables for both the linear and the Newtonian models. The posterior predictive distributions of press-times are shown in figure 38. Evidence was in favor of the Newtonian model compared to the heuristics model across all phases of the experiment with the exception of the *Prior* phase. The largest differences in prediction power appears in the *Feedback* phase with the Newtonian model being the considerably better choice to describe the actual press-times. This superiority of the Newtonian model over the linear heuristic one remains in the subsequent phases even without any visual feedback. This was again tested by running two-sample Kolmogorov-Smirnov tests for posterior predictive distributions of phase three of both models and the actual data, as well as calculating the Kullback-Leibler divergence for each pair, resulting in lower K-S statistic values for the Newtonian model (D = 0.0436, p = 0.00521) compared to the linear one (D = 0.0851, $p < 0.001$). KL divergence values are 0.0582 and 0.0599 for the Newtonian and linear model, respectively.

Finally, to confirm that the behavioral data of our subjects was best described by the Newtonian model with quadratic cost function we carried out model selection using the *product space method* (Lodewyckx et al., 2011). In this approach, a mixture model combines both the linear and the Newtonian model to account for the data. An index variable indicates, which of the two models is selected at each iteration to explain the data. Given that both models have the same a priori probability to be chosen, the Bayes factor equates to the posterior odds of the index variable. Resulting Bayes factors are shown in figure 30. Given the complete data set from all phases there is small support for the Newtonian model (Bayes factor K of 2.33). When only considering data from the *Prior* phase there is weak support for the linear model (K = 1.88). Instead, when considering all phases but the first phase there is substantial support for the Newtonian model (K = 3.71) and strong evidence for the square-root model in the feedback phase (K = 9.71).

The hierarchical Bayesian interaction model also allows inferring the masses best describing our subjects' internal beliefs given the Newtonian model and the measured press-times. Not surprisingly, mean mass beliefs vary strongly across subjects in the *Prior* phase, where participants had to make decisions without any observations of the pucks, only relying on their prior beliefs about the potentially underlying dynamics and environmental conditions. Nevertheless, the variances of mass beliefs within the first phase were surprisingly small for individual subjects with a mean of 0.0023 kg, potentially indicating that each subject consistently used a belief about the mass of the puck. Inferred values for these prior mass beliefs are displayed in figure 32 for each participant.

When obtaining visual feedback in the *Feedback* phase of the experiment, subjects only needed on average six trials to adjust their press-times so that mass beliefs were

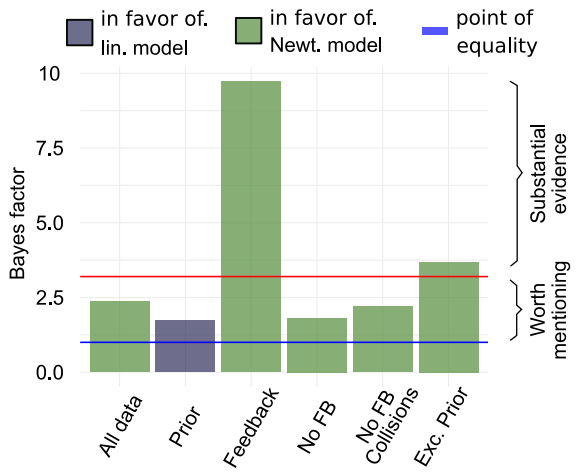

Figure 30: **Bayes factors calculated from posterior odds sampled using the product space method.** Bayes factors are displayed for different phases and combinations of phases. Blue line at 1 marks the point where neither model is stronger supported by evidence. Red line at 3.2 marks the transition from Bayes factors being only worth mentioning to substantial evidence in favor of one the models. Colors of bars indicate the model favored by the Bayes factors.

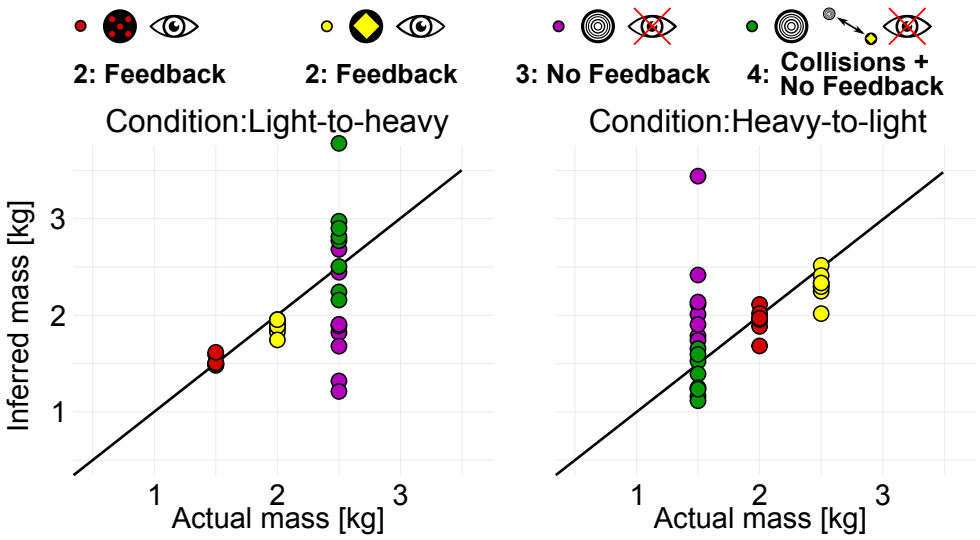

Figure 31: **MAP values of inferred latent mass in Newtonian model class with quadratic loss function for each participant and condition.**

stable thereafter. Implicit mass beliefs were quite accurate with the mean of inferred MAP values at 1.5218 and 1.8818 kg in the condition light-to-heavy (1.5 and 2.0 kg) and 1.9415 and 2.3068 kg in condition heavy-to-light (2.0 and 2.5 kg). figure 31 shows the MAP estimates of the masses for both conditions and phases two to four for all subjects.

In phase three *No Feedback* participants faced an unknown puck without any visual feedback but with the acquired knowledge about the relationship of press-time and distance. Note however, that participants had learned two different mappings from distances to press-times in phase two, one for the red puck and one for the yellow puck. Thus, participants had to select press-times without knowing the mass of the unknown puck. As reported above, the press-time distributions in this phase of the experiment were close to the combined press-times that subjects had used for the two pucks in the previous phase two of the experiment. The corresponding MAP

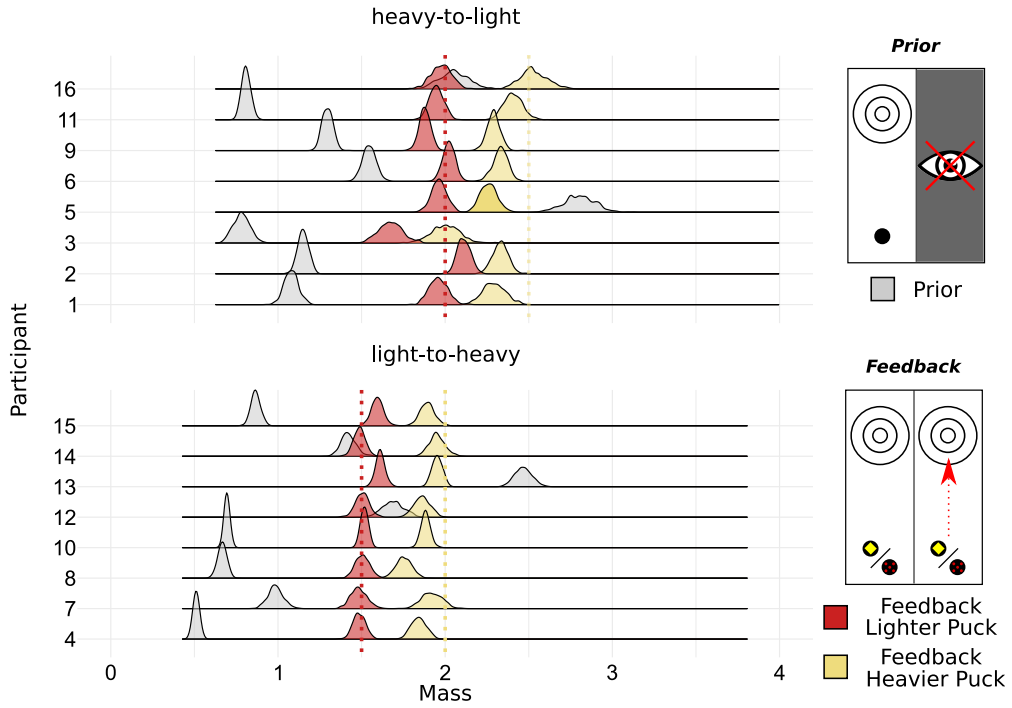

Figure 32: **Latent masses: phase 'prior' and 'feedback'.** Inferred latent mass in Newtonian model class with quadratic loss function for each participant and with data from *Prior* and *Feedback* phase. Posterior mass distributions for each participant in *Prior* and *Feedback* phase. Gray distributions show the inferred mass distribution for an unknown puck before participants have encountered the task dynamics. Resulting mass distributions for both pucks in feedback trials in red (light puck) and yellow (heavy puck). Dotted lines indicate actually implemented mass for each of the feedback pucks.

mass beliefs were accordingly approximately the average of the two previous pucks' masses with 1.87 and 2.19kg and corresponding mass distributions differed significantly for the two conditions light-to-heavy and heavy-to-light (ANOVA: $F = 1060$, $p < 0.001$; see also figure 33). But after observing the 24 collisions in phase *Collisions + No Feedback* of the two known pucks with the unknown puck participants were able to adjust their press-times so that the estimated mass beliefs were significantly closer to the true values used in the simulations than in the previous phase. This was quantified by running a repeated measures ANOVA of the deviations from the actual mass ($F = 7.103$, $p = 0.0176$). Thus, the mass beliefs implicit in our participants' press-times reflected the inferred mass ratios and transferred from having observed the pucks' collisions to the subsequent visuomotor control task. Note that this implies that subjects must have interpreted the dynamics of the red and yellow pucks in the second phase as stemming from objects' masses, as otherwise a physically consistent transfer to a new puck would be very difficult to explain.

4.3.3 *Observation model result*

Participants in our experiment were apparently able to make appropriate inferences in phases with feedback, altering their beliefs about unknown objects based on previous inferences and new observations, and to transfer this knowledge to an action-control task. But how were they able to make these adjustments after observing

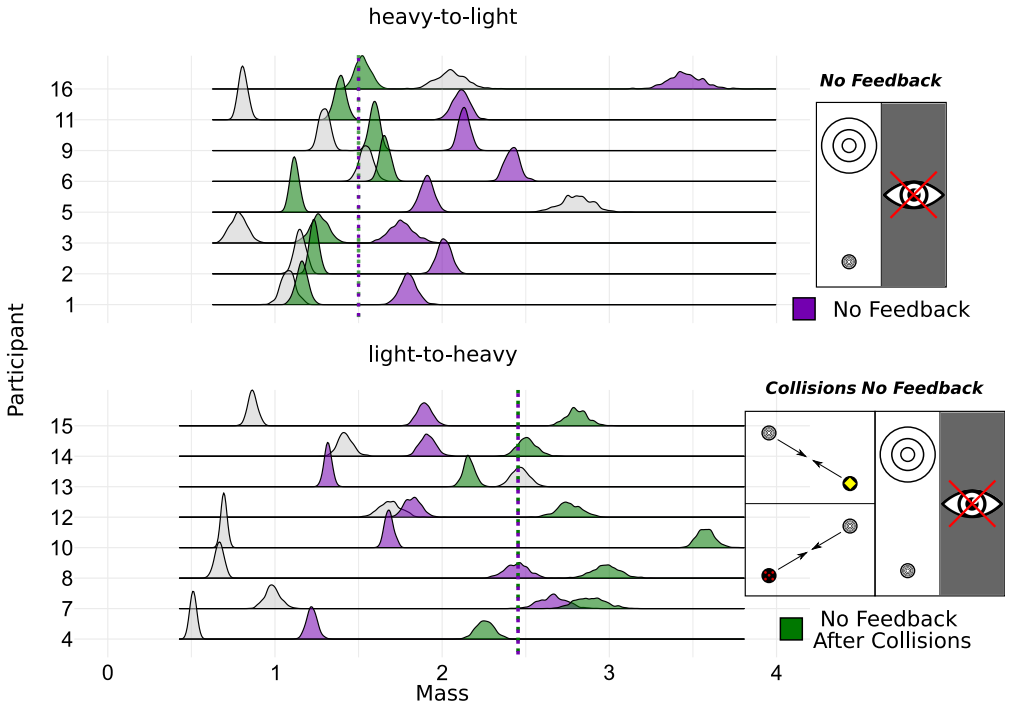

Figure 33: **Latent masses: phase 'no feedback' and 'collision and no feedback'.** Inferred latent mass in Newtonian model class with quadratic loss function for each participant with data from *Prior* and both *No Feedback* phases. Posterior mass distributions for each participant in *Prior* and *Feedback* phase. Gray distributions show again the inferred mass distribution for an unknown puck before participants have encountered the task dynamics. Distributions in violet and green are the posterior mass distributions of the unknown puck without feedback before and after the participants saw collision with known pucks. Dotted line marks the actual mass of the unknown puck.

collisions and perform well with a continuous range of responses? Here, we want to look at another Bayesian model capturing the learning process through observations. To this end, we adapted a hierarchical Bayesian observation model similar to (Sanborn, Mansinghka, and Griffiths, 2013; Smith and Vul, 2013), which describes how subjects could infer the relative mass ratios of two pucks from observing their elastic collisions. But, here we used the mass beliefs inferred from phase two of the experiment with the interaction model as initial prior mass beliefs in the observation model for phase four of the experiment on-a-subject-by-subject basis. This allows comparing how subjects' uncertainty decreases on the basis of perceptual observations compared to visuomotor interaction.

The Bayesian network model for the observation task in figure 34 expresses the relationship between variables on a subject-by-subject basis for observing 12 collisions for each of the two pucks. The model incorporates the generative physical relationship of velocities and masses in elastic collisions as shown in (Sanborn, Mansinghka, and Griffiths, 2013). The grey nodes are known to the experimenter: the initial velocities v_F of the known feedback puck and v_{NF} of the unknown no-feedback puck, the resulting velocities u_F and u_{NF}. Individual subjects' posterior mass beliefs at the end of phase two inferred with the interaction model, shown on the left panel of figure 34, were used as prior mass beliefs of the yellow and red pucks in the observation model for each participant. Unknown parameters are depicted as white nodes and were inferred with MCMC. Subjects' uncertain beliefs about the pucks' velocities are

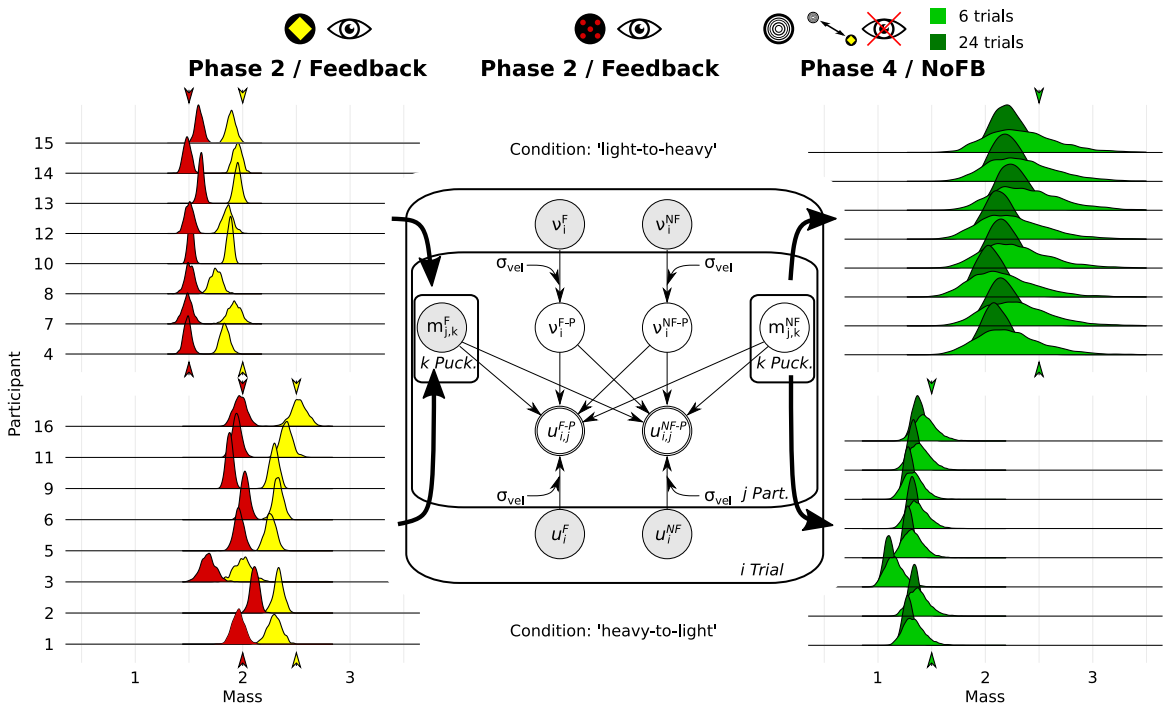

Figure 34: **Bayesian model for learning through observing collisions with prior and posterior mass beliefs.** The left panel shows inferred posterior mass beliefs for the pucks from feedback phase 2 for each participant. All 100 trials were used to infer the mass beliefs. These posteriors were used as priors for the inference from observations. The graphical model for learning by observing collision is shown in the middle panel. Uncertainty about the pucks' velocities is introduced for the initial velocities v_F and v_{NF} as well as for the resulting velocities u_F and u_{NF} after the elastic collision. Utilizing the physical relationship of velocities and masses in an elastic collision enables inferring beliefs about the unknown puck based on previous mass beliefs of pucks in phase 2. Resulting posterior mass beliefs are shown in the right panel for inferences based on 6 and 24 observations of collisions.

incorporated for the initial velocities v_F and v_{NF} as well as for the resulting velocities u_F and u_{NF} after the elastic collision. To describe the perceptual uncertainty of velocities we used a log-normal distribution with σ_{vel} fixed at 0.2 and its mode at the actual velocity (see figure 6 in (Sanborn, Mansinghka, and Griffiths, 2013) or section "Subject Performance" in (Smith and Vul, 2013) for comparison). Inferred posterior mass beliefs for the new puck are shown in the right panel. This structure leads to the following joint distribution $p(d, l)$ with observed data $d = \{v_F, v_{NF}, u_F, u_{NF}, m_F\}$ and latent variables $l = \{v_F^{per}, v_{NF}^{per}, u_F^{per}, u_{NF}^{per}, m_{NF}\}$, where actual and perceived velocities are summarized for both pucks using an index i to v_i and u_i for abbreviation purposes:

$$p(d, l) = p(v_i)\ p(u_i)\ p(m_F)\ p(v_i^{per}|v_i, \sigma_{vel})\ p(m_{NF})\ p(u_i^{per}|u_i, v_i^{per}, m_F, m_{NF}, \sigma_{vel}) \quad (26)$$

The observation model allows inferring participant's mass beliefs for the puck, which they had first interacted with in phase three of the experiment. Importantly, the two Bayesian models allow inferring the uncertainty in participants' mass beliefs after only six and after 24 trials, both for the interaction phase two and the observation of the collision movies, see figure 35. These results quantify, how uncertainty in mass beliefs decreased over trials and the difference in uncertainty reduction due to

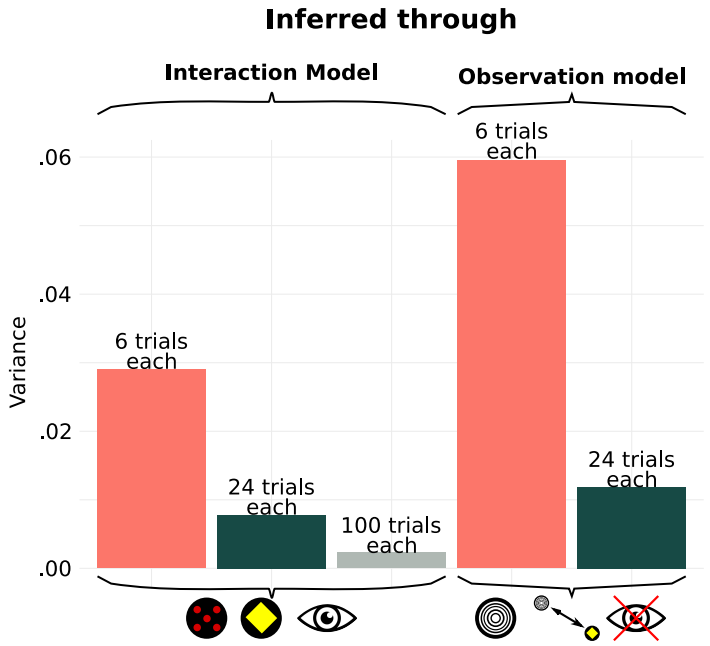

Figure 35: **Learning progress of mass beliefs during interaction and observation.** Barplot of averaged variance for both models and a given number of observations. First three columns show the average variance in posterior mass beliefs for inferences with 6, 24 and 100 trials per puck and participant. Two last columns show the average variance of mass beliefs of the unknown puck resulting from inference using the collision model for 6 and 24 trials, while using the posterior mass belief of the known pucks from the interaction model with 100 trials each.

interactions versus observations. More specifically, as expected, subjects' variance in inferred posterior mass beliefs for each puck decreased with the progression of trials when using the interaction model with data from phase 2 (Friedman chi-squared = 62.06, p-value < 0.001 & Conover's PostHoc $p < 0.001$ for all comparisons) and, as well, when using the observation model with mass beliefs from phase 2 with the highest precision after 100 trials (Wilcoxon signed rank test, $V = 136$, $p < 0.001$). Additionally, the variance in resulting inferences about the mass in the observation model is significantly higher than the variance of the mass beliefs used as input, as we compared variances on subject basis for columns three, four and five (Kruskal-Wallis chi-squared = 37.43, p-value < 0.001 & Dunn PostHoc for grey compared to red and green, each $p < 0.001$, see figure 35). Thus, the larger variance in participant's mass estimates after observing the pucks' collisions compared to interacting with them, see e.g. figure 31, stems from the fact that subjects needed to use the uncertain mass beliefs of the red and yellow pucks when observing the collisions and had additional uncertainty stemming from inferring pucks' velocities. Furthermore, the predictions of the idealized observation model deviate quantitatively from mass beliefs inferred using the interaction model for two reasons: 1) participants would need to remember their belief about the mass of feedback pucks perfectly while performing in phase 3 and 4, whereas these beliefs may well suffer from memory effects, and 2) they will be biased from initial, uninformed guesses in phase 3 before they have seen any collisions and thus probably show recency effects, as well (see e.g. participant 7 & 8 in figure33).

4.4 DISCUSSION

Although people are able to interact with the physical world successfully in everyday activities, classic research has contended that human physical reasoning is fundamentally flawed (Cohen, 2006; Gilden and Proffitt, 1994; McCloskey, Caramazza, and Green, 1980; Todd and Warren Jr, 1982). Recent studies instead have shown that biased human behavior in a range of perceptual judgement tasks involving physical scenarios can be well described when taking prior beliefs and perceptual uncertainties into account (Hamrick et al., 2016; Sanborn, Mansinghka, and Griffiths, 2013; Smith, Battaglia, and Vul, 2013; Smith and Vul, 2013). The reason is that, inferences in general need to integrate uncertain and ambiguous sensory data and partial information about object properties with prior beliefs (Gershman, Horvitz, and Tenenbaum, 2015; Griffiths et al., 2010; Kersten, Mamassian, and Yuille, 2004; Knill and Richards, 1996). Much less is known about how intuitive physical reasoning guides actions. Here, we used a perceptual inference task involving reasoning about relative masses of objects from the intuitive physics literature and integrated it with a visuomotor task. Subjects had to propel a simulated puck into a target area with a button press whose duration was proportional to the puck's release velocity. The goal was to investigate how people utilize relative masses inferred from watching object collisions to guide subsequent actions.

Specifically, we devised an experiment consisting of four phases, which differed in the available sensory feedback and prior knowledge about objects' masses available to participants. The physical relationship underlying the task requires subjects to press a button for a duration that is proportional to the mass of the puck and proportional to the square-root of the initial distance. This allowed examining peoples' prior assumptions about the underlying dynamics of pucks' gliding, their ability to adjust to the pucks' initial distances to the target and to the varying masses of pucks, and the transfer of knowledge about relevant properties gained by observing collisions between pucks. A hierarchical Bayesian generative model of the control task and one of the collision observation task accommodating individual differences between subjects and trial by trial variability allowed analyzing subjects' press-times quantitatively. Importantly, we also tested, which of three cost functions best describe our subjects' choices of press-times.

In the prior phase without visual feedback, subjects adjusted their press-times with the initial distance of the puck to the target. Not surprisingly, because subjects did not obtain any feedback about their actions and therefore the degree of friction, the magnitude of the applied force, and the scale of the visual scene, could only hit the target by chance. Nevertheless, model selection slightly favored the linear heuristics model compared to the square-root model, i.e. subjects approximately scaled the press-times linearly with the initial distance to target. Thus, subjects came to the experiment with the prior belief that longer press-times would result in longer sliding distances but did not scale their press-times according to the square-root of the initial distance of the pucks as prescribed by Newtonian physics. As subjects did not sense the weight of the pucks and did not obtain any visual feedback about the pucks' motion, the observed behavior in this phase of the experiment may be dominated by the uncertainty about the underlying mapping between the duration of button presses and the pucks' release velocities, the effects of friction, and the visual scale of the simulation. Remarkably, while no feedback was available, each participants' scaling

of press-times was consistent as indicated by individuals' variance in posterior mass estimates being of the same order of magnitude as in feedback trials, see figure 32.

When visual feedback about the pucks' motion during the feedback phase was available, subjects needed on average only six trials to reach stable performance. This is particularly remarkable, because it corresponds to adjusting the press-times to a single puck's mass over the four initial trials and then adjusting the press-times within only two subsequent trials to a new puck with a different mass. Thus, the observation of the pucks' dynamics over six trials was sufficient to adjust the press-times with the square-root of initial distance, but differently for the two pucks, see figure 19. Note that in phase two, subjects only had a contextual color cue distinguishing the two pucks. Therefore, subjects needed to learn two different functions relating the pucks' initial distances to the required press-times, one for each puck, without any explicit reference to mass. Data from this phase of the experiment were utilized to infer parameters describing individual subjects' perceptual uncertainty and motor variability. Perceptual variability was consistent across subjects and varied only marginally so that a constant value of $\sigma^x = 0.05m$ was used across subjects and models for all other phases of the experiment. Remarkably, this corresponds to a distance of 4.7 pixels in the vertical direction on the display monitor with a resolution of 1080 pixels. By contrast, the variability of press-times σ^t varied substantially across subjects with almost all subjects lying between $0.15s$ and $0.33s$, so that individuals' parameters were used in all subsequent models.

Given that the variability of peoples' press-times scales with the mean of the duration, longer press-times can lead to larger deviations from the targeted press-time. This can result in larger errors by overshooting the target. To reduce possible overshoots, participants may implicitly aim at a shorter distance, which can be quantified through a cost function incorporating the relative desirability of the pucks' final distance to the target. Therefore, we tested which of three commonly used cost functions best described subjects' press-times: the 0-1 cost function, the quadratic cost function, and the absolute value cost function. Model selection using the product space method showed that the press-times were best explained by the Newtonian physics model when taking into account perceptual uncertainty, motor variability and the quadratic cost function. Similarly, this was confirmed through posterior predictive checks of press-times and the analysis of the correlation of the residuals between predicted and observed press-times with the initial distance to target.

Thus, participants adjusted the press-times with the square-root of the initial distance to the target and used the contextual color cue of the pucks to adjust the press-times. Subjects only had the contextual cue of different colors between the two pucks but adjusted the press-times in such a way that this was interpretable in terms of the two different masses used in the puck's simulations. Therefore, just on the basis of these adjustments alone, one might argue that subjects may have adjusted their press-times based on the available visual feedback about the pucks' motion without any recurrence to a the concept of physical mass. That this is unlikely, is due to the following two phases of the experiment.

Previous research has demonstrated, that people can infer the mass ratios of objects from observing their collisions (Hamrick et al., 2016; Sanborn, Mansinghka, and Griffiths, 2013; Smith and Vul, 2013; Ullman et al., 2018). Here, subjects were asked

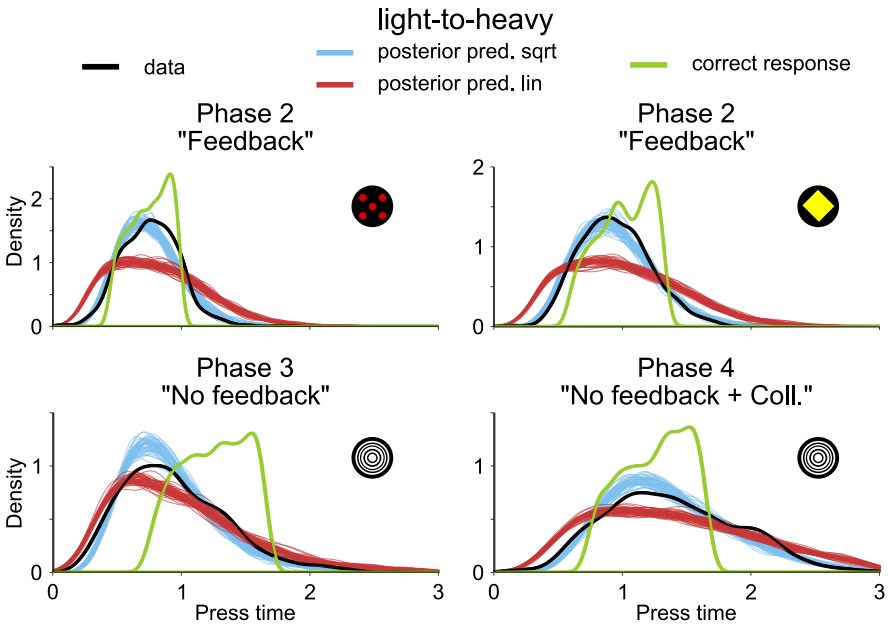

Figure 36: **Deviations from fully-observed Newtonian physics and model predictions (light to heavy).** Posterior predictive for press times, actual press times and ideal responses for phases two to four and condition light-to-heavy. Black distributions show the actual data, red and blue ones display samples from posterior predictive distributions of both, the linear and Newtonian model, and green ones show the correct responses given perfect knowledge about the underlying physics and all parameters. Visualizing the enhanced suitability of this noisy Newtonian model framework compared to Newtonian models excluding prior preferences and uncertainties in describing human behavior.

to propel one particular puck before and after seeing 24 collisions between this puck and the two pucks for which they had previously obtained visual feedback. Note that the two pucks in phase two were only distinguished by a color cue and that subjects might have only learned two different mapping from initial distances to press-times, as no explicit cues about mass were available. But subjects readily utilized the inferred mass ratios to adjust their press-times to reach the target more accurately in phase four of the experiment. That the different dynamics were to attribute to different masses and that relative masses from observing the collisions could be transferred to press-times entirely relied on subjects intuitive physical reasoning. This is strong evidence that participants in our experiment interpreted the dynamics of the red and yellow pucks from phase two to be caused by their respective masses. Model selection provided evidence, that subjects continued to use the square-root relationship of initial distance and scaled their press-times consistent with Newtonian physics to successfully propel the puck to the target.

Different from tasks requiring a forced choice response (Cohen, 2006; Gilden and Proffitt, 1994; Hamrick et al., 2016; McCloskey, Caramazza, and Green, 1980; Sanborn, Mansinghka, and Griffiths, 2013; Smith and Vul, 2013; Todd and Warren Jr, 1982; Ullman et al., 2018), participants in the current experiments provided a continuous action by pressing a button for variable durations. Therefore, it is not sufficient to model our participants' actions as in an inference task, e.g. by assuming that subjects choose a press-time on the basis of the mass belief with highest probability, i.e. the MAP. Instead, modeling continuous actions requires a cost function, which additionally incorporates people's variability in press-times. This is evident when comparing

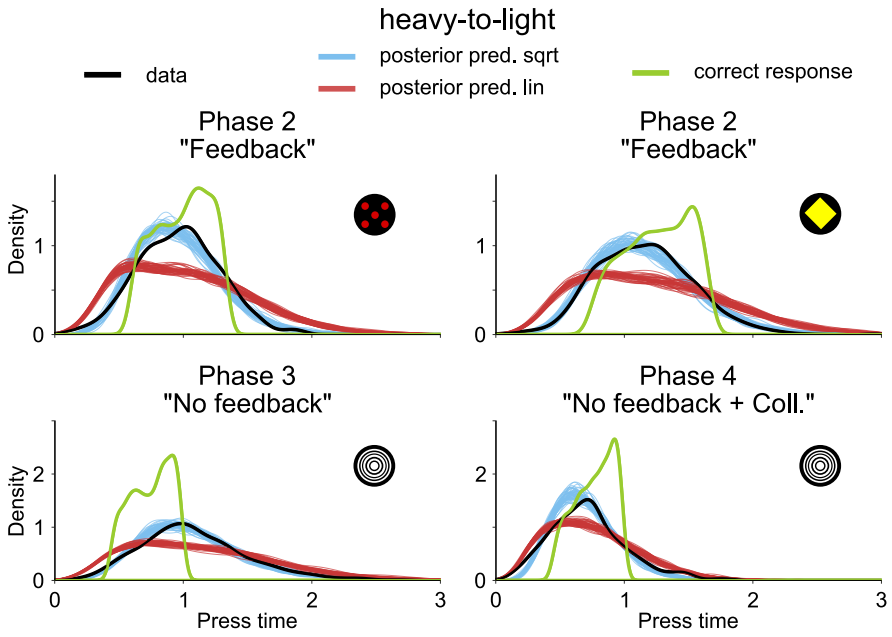

Figure 37: **Deviations from fully-observed Newtonian physics and model predictions (heavy to light).** Posterior predictive for press times, actual press times and ideal responses for phases two to four and condition heavy-to-light. Black distributions show the actual data, red and blue ones display samples from posterior predictive distributions of both, the linear and Newtonian model, and green ones show the correct responses given perfect knowledge about the underlying physics and all parameters. Visualizing the enhanced suitability of this noisy Newtonian model framework compared to Newtonian models excluding prior preferences and uncertainties in describing human behavior.

the press-times according to the different models considered here, see figure 36 & 37. Remarkably, posterior means of masses best explaining our participants' press-times were closer to the true masses used in the pucks' simulations for the quadratic cost function compared to the other cost functions. Thus, the current study establishes that people's deviations from the predictions of Newtonian physics are not only attributable to prior beliefs and perceptual uncertainties but also to implicit cost functions, which quantify internal costs for errors due to participants' action variability.

Taken together, the present study is in accordance with previous studies on intuitive physics within the noisy Newton framework (Kubricht, Holyoak, and Lu, 2017). The systematic deviations in our subjects' press-times from the those prescribed by Newtonian physics under full knowledge of all parameters were explained quantitatively as stemming from perceptual uncertainties interacting with prior beliefs according to probabilistic reasoning. Previous studies had also shown, that people are able to infer relative masses of objects from their collisions (Hamrick et al., 2016; Sanborn, Mansinghka, and Griffiths, 2013; Smith and Vul, 2013). The present study additionally shows, that subjects can utilize such inferences and transfer them to a subsequent visuomotor task. This establishes a connection between reasoning in intuitive physics (Hamrick et al., 2016; Sanborn, Mansinghka, and Griffiths, 2013; Smith, Battaglia, and Vul, 2013; Smith and Vul, 2013) and visuomotor tasks (Flanagan, Bittner, and Johansson, 2008; Körding and Wolpert, 2006; Trommershäuser, Maloney, and Landy, 2003; Zago et al., 2004). Crucial in the quantitative description of participants' behavior was the inclusion of a cost function. Commonly, cost functions in

visuomotor behavior are employed to account for explicit external rewards imposed by the experimental design, e.g. through monetary rewards (Dayan and Daw, 2008; Trommershäuser, Maloney, and Landy, 2003) or account for costs associated with the biomechanics or accuracy of movements (Körding and Wolpert, 2006; Todorov, 2004). The present model used a cost function to account for the costs and benefits implicit in our participants visuomotor behavior and may encompass external and internal cost related to different task components, perceptual, cognitive, biomechanical costs and preferences. Inferring such costs and benefits has been shown to be crucial for the understanding of visuomotor behavior (Hoppe and Rothkopf, 2016, 2019; Zhang et al., 2018).

The results of the present study furthermore support the notion of structured internal causal models comprising physical object representations and their dynamics. Although our participants never sensed the weight of pucks, they readily transferred their visual experiences by interpreting them in terms of the physical quantity of mass. A recent study (Schwettmann, Tenenbaum, and Kanwisher, 2019) found support at the implementational level for representations of mass in parietal and frontal brain regions that generalized across variations in scenario, material, and friction. While our results do not provide direct evidence for the notion of internal simulations of a physics engine (Battaglia, Hamrick, and Tenenbaum, 2013), they also do not contradict them. While it could be argued that structured recognition models may be sufficient for the inference of object properties such as mass, in our experiment subjects had to act upon such inferences, which strongly suggest the availability of representations of mass.

Finally, the present study also shows the importance of using structured probabilistic generative models that contain interpretable variables when attempting to quantitatively reverse engineer human cognition (Zednik and Jäkel, 2016). Previous research has demonstrated pervasive and systematic deviations of human reasoning from probabilistic accounts (Tversky and Kahneman, 1974). Similarly, systematic deviations in physical reasoning (Cohen, 2006; Gilden and Proffitt, 1994; McCloskey, Caramazza, and Green, 1980; Todd and Warren Jr, 1982) have been interpreted as failures of physical reasoning. It is only more recently, that a number of these deviations have been explained through computational models (Battaglia, Hamrick, and Tenenbaum, 2013; Hamrick et al., 2016; Sanborn, Mansinghka, and Griffiths, 2013; Smith, Battaglia, and Vul, 2013; Smith and Vul, 2013) involving structured generative models relating observed and latent variables probabilistically. These models involve the explicit modeling of prior beliefs and perceptual uncertainties (Kersten, Mamassian, and Yuille, 2004; Knill and Richards, 1996) as well as uncertainties in visuomotor behavior (Körding and Wolpert, 2004a, 2006; Trommershäuser, Maloney, and Landy, 2003), which have been modeled successfully in a probabilistic framework. As such, the present study is in line with efforts of understanding perception and action under uncertainty through computational models, which use structured probabilistic generative models and external as well as internal costs (Gershman, Horvitz, and Tenenbaum, 2015).

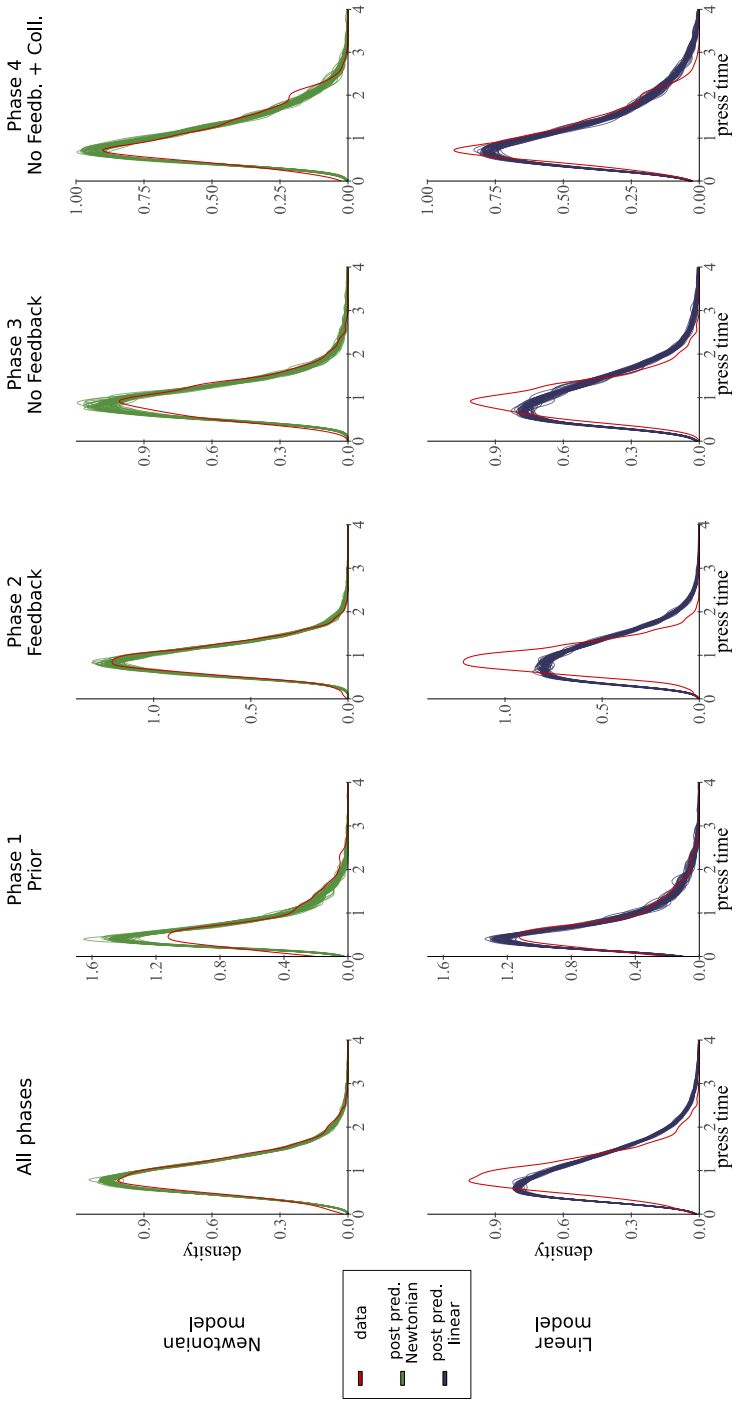

Figure 38: **Posterior predictive checks for press-times in both models.** Posterior press-time predictions for both, the linear and the Newtonian model with quadratic cost function, and separately for every phase. Actual data is shown as red line. Model predictions in dark green (50 iterations) of the fitted Newtonian model match the data closely and surpass the fitted linear model in dark blue for the complete data set and in almost every phase individually.

5

INFERRING PERCEPTUAL DECISION MAKING PARAMETERS FROM BEHAVIOR IN PRODUCTION AND REPRODUCTION TASKS

5.1 INTRODUCTION

Psychophysics has developed a variety of experimental paradigms to measure human decision making under perceptual uncertainty. Different experimental paradigms can be distinguished by the specifics of how stimuli are generated, presented, and which responses are required by participants. One of the most common paradigms is the two-alternative forced choice task (2AFC) (Gescheider, 2013a; Stevens, 1958; Stüttgen, Schwarz, and Jäkel, 2011; Wichmann and Jäkel, 2018), which confronts the subject with a binary decision regarding the property of a stimulus and thereby allows the experimenter to draw conclusions about the subject's perceptual sensitivity given the stimulus and the task conditions. Other experimental paradigms include the two-interval forced choice task (2IFC), where stimuli are presented sequentially, and the yes-no task, in which the subject needs to detect a stimulus, which is either present or absent (Gescheider, 2013a; Stevens, 1958; Stüttgen, Schwarz, and Jäkel, 2011; Wichmann and Jäkel, 2018).

Because all these tasks involve binary responses, they differ fundamentally from other psychophysical paradigms such as production and reproduction task. While production tasks ask subjects to generate a graded response with a target magnitude, in reproduction tasks subjects first sense a stimulus magnitude and are then instructed to reproduce the sensed stimulus magnitude. The distinguishing factor here is that actions can be taken on a continuous scale and thus, in addition to the purely perceptual uncertainty, action variability is introduced into the overall noise manifested in decisions. Classic examples of a production task include walking to targets using visual cues (Harris, Jenkin, and Zikovitz, 2000; Mittelstaedt and Mittelstaedt, 2001) and time estimation tasks after stimuli onset (Miltner, Braun, and Coles, 1997; Wild-Wall, Willemssen, and Falkenstein, 2009) and of a reproduction task are path length reproduction (Berthoz et al., 1995; McNaughton et al., 2006; Petzschner and Glasauer, 2011), time interval reproduction (Buhusi and Meck, 2005; Fraisse, 1984) and force reproduction (Onneweer, Mugge, and Schouten, 2015; Shergill et al., 2003; Walsh, Taylor, and Gandevia, 2011).

Bayesian models combining prior beliefs with sensory measurements have been successfully applied to provide computational level explanations of human behavior in perceptual decision tasks (Knill and Richards, 1996). Very often, these studies employ a particular psychophysical paradigm, to measure perceptual uncertainties. Exemplary studies on human cue integration such as Ernst and Banks (2002) and Knill and Saunders (2003) first measured the uncertainties of individual cues with classic psychophysical tasks. In both cases, the models assumed Gaussian distributions describing perceptual noise or more generally, perceptual uncertainties. Similarly, experimental paradigms involving continuous actions in visuomotor behavior have often also used Gaussian distributions to capture response variability. Exem-

plary studies such as Körding and Wolpert (Körding and Wolpert, 2004a) and Trommershäuser, Maloney, and Landy (2003) represented spatial distributions of manual response variability with normal distributions.

According to Bayesian decision theory, the optimal decision depends not only on the combination of prior beliefs about unobserved environmental parameters with the likelihood of these parameters given sensory measurements as represented by the inferred posterior, but additionally takes the response variability introduced by the necessary action into account. The loss function encompasses the costs and benefits for deviating from the true target value, which is the consequence of response variability. Broad experimental evidence suggests, that the nervous system takes this variability into account when carrying out movements (Harris and Wolpert, 1998; Körding, 2007; O'Sullivan, Burdet, and Diedrichsen, 2009). If the involved uncertainties are normally distributed and the cost function is symmetric, then selecting the optimal response leads to an action that corresponds to the mean of the posterior distribution, which coincides with the mode and the median in case of normal distributions. But in case of asymmetric cost functions and skewed probability distributions describing perceptual uncertainties and action variability, these quantities may interact in non-trivial ways resulting in optimal responses, which can be systematically biased. Importantly, while human cost functions in psychophysical tasks have been measured, they are often conveniently assumed to be symmetric (Körding and Wolpert, 2004b).

Here we introduce a computational approach to infer the parameters in Bayesian decision models of production and reproduction tasks in the spirit of rational analysis (Griffiths, Lieder, and Goodman, 2015; Simon, 1955). The model employs log-normal distributions both for the perceptual uncertainty, as this accommodates well known perceptual Weber-Fechner phenomena (Battaglia, Kersten, and Schrater, 2011; Dehaene, 2003) , and for the response variability observed in humans (Hamilton, Jones, and Wolpert, 2004; Harris and Wolpert, 1998; Van Beers, Haggard, and Wolpert, 2004).

Specifically, we infer individual's perceptual uncertainty, response variability, and their subjective cost function based on the responses in production and reproduction tasks. Importantly, these types of tasks require a graded response with different magnitudes. Thus, behavior balances the trade-off between task fulfillment and effort, leading to possibly non-trivial response distributions of undershoots and overshoots, which are ubiquitous in human psychophysical experiments. We show that this framework is able not only to recover the parameters in Bayesian decision models for diverse cost functions but additionally can be utilized to guide designing psychophysical experiments.

5.2 METHODS

5.2.1 *Continuous Cost Optimized Parameter Inference for decision making tasks*

Here we present a method to infer parameters from subject's behavior in decision making tasks involving a continuous response, which includes production and reproduction tasks. We employ Markov Chain Monte Carlo (MCMC) and optimization based on a neural network approximation to infer posterior distributions describing perceptual uncertainty, action variability and parameterized cost functions, including

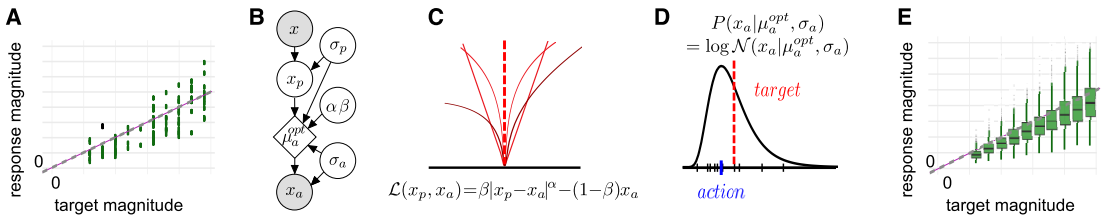

Figure 39: **Inference model**. **A** Typical behavioral data in a production or reproduction task. **B** Bayesian network of response generation from the perspective of the researcher. **C** Examples of parameterized costfunctions including effort. **D** Log-normal response distribution. **E** Simulated responses using inferred model parameters.

costs for action outcomes and response efforts. These parameters can be inferred on an individual-by-individual basis for for a wide range of continuous response tasks and data. By using log-normal distributions for perceptual uncertianty and action variability we constrain values to a strictly positive range and importantly reproduce Weber-Fechner like phenomena, i.e. variability that increases with stimulus magnitude.

5.2.2 *Bayesian observer model*

We first assume that the experimenter's stimulus is a continuous random variable $x \in \mathbb{R}^+$. Perception leads to an internal variable x_p, which we model as having a log-normal distribution with variance σ_p resulting in the distribution $P(x_p|\mu_p, \sigma_p)$:

$$P(x_p|\mu_p, \sigma_p) = \log \mathcal{N}(x_p|\mu_p, \sigma_p) \quad \text{with} \quad \mu_p = \log(x) + \sigma_p^2 \tag{27}$$

where $\log \mathcal{N}(x_p|\mu_p, \sigma_p)$ is a log-normal distribution with its mode at the actual target x. This modeling choice accommodates the known scaling of uncertainty in the human sensory system, commonly referred to as Weber-Fechner scaling (Battaglia, Kersten, and Schrater, 2011; Neupärtl, Tatai, and Rothkopf, 2020). The perceptual uncertainty can either be measured independently through experimental means (Wichmann and Jäkel, 2018) or it can be inferred given behavioral data. In the former case its value is fixed and in the latter case a hyperprior incorporating prior knowledge about the possible range of its magnitude can be used with $\sigma_p \sim \log \mathcal{N}(\mu, \sigma^2)$.

In order to act optimally given a task and the perceived magnitude of the stimulus, human subjects are assumed to try to minimize their costs as described by Bayesian decision theory (BDT). In production and reproduction tasks, subjects aim at getting as close as possible to a target magnitude with their response. Therefore, in these tasks costs depend on how close the action leads to the actual target. It is commonly assumed that subjects evaluate outcomes based on a function of their absolute error (Körding and Wolpert, 2004b; Wolpert and Landy, 2012), i.e. that they assess the value of an action on a continuous scale based on the absolute distance from the target, regardless of whether they fall above or below the desired value. Such cost functions are symmetrical around the target value and can be formalized as:

$$\mathcal{L}'(x_p, x_a) = |x_p - x_a|^\alpha \tag{28}$$

with the target value x, the value of a single action outcome x_a and an exponent α describing the shape of the cost function, e.g. with values of α at 1 or 2 cost functions correspond to the L_1 or hinge-loss and L_2 or quadratic cost functions, respectively.

However, production and reproduction experiments require subjects to produce a response that increases in magnitude with the sensed magnitude of the stimulus. Thus, the task-dependent description of costs does not yet suffice, since actions

themselves are already associated with effort and thus costs. These costs can now be included in the cost function term relative to the costs for the outcome of the action:

$$\mathcal{L}(x_p, x_a) = \beta\,|x_p - x_a|^{\alpha} + (1-\beta)\,x_a \tag{29}$$

with β governing the trade-off between task costs and production effort. That is, if β is close to 1, actions are dominated by the costs due to the expected errors whereas if β is close to 0, actions are instead dominated by the effort cost due to the response action. Accordingly the factor $1-\beta$ describes the raye of effort increase for responses at higher magnitudes. A suitable prior over the parameter β can be obtained using the beta distribution $\beta \sim \text{Beta}(a_1, a_0)$. The parameter α again determines the shape of the task dependent costs and its hyperprior is chosen as a log-normal distribution with $\alpha \sim \log \mathcal{N}(\mu, \sigma^2)$.

The actions themselves are in turn affected by variability, which is also known to be signal dependent and the nervous system takes this variability into account when carrying out movements. Therefore, the optimal action takes into account the perceptual uncertainty, the expected action variability and applies the costs stemming from the task's goals and the effort in producing the response. This can be expressed as the solution to the minimization of the overall expected loss:

$$\mu_a^{opt} = \min_{\mu_a \in \mathcal{R}_+^*} \int_0^\infty \int_0^\infty \mathcal{L}(x_p, x_a|\alpha, \beta)\, p(x_a|\mu_a, \sigma_a)\, p(x_p|\mu_p, \sigma_p)\, dx_p\, dx_a. \tag{30}$$

Algorithmically, we use amortized inference to approximate response distribution using a regression neural network trained with numerically solved samples. The action variability is already included in the optimization problem to obtain the optimal action while considering and compensating for motor noise as well. This leads to log-normal response distribution with a mode that reflects individual task and action specific costs while including perceptual and action associated variability:

$$P(x_a|\mu_a^{opt}, \sigma_a) = \log \mathcal{N}(x_a|\mu_a^{opt}, \sigma_a) \tag{31}$$

Due to the non-symmetrical form of $p(x_p)$ and $p(x_a)$ together with non-trivial cost functions, optimal responses do not necessarily have to aim for the actual target. Thus, the interplay of perceptual uncertainties, response variability, and complex asymmetric cost functions can explain biases and systematic deviations in subjects' responses. Inference of these parameters given observed behavior can therefore quantitatively ascribe seemingly suboptimal behavior to objective task parameters and subjective costs and benefits. The whole process is The pseudo algorithm for the complete inference process is shown The complete inference process is summarized as pseudo algorithm 1 and additionally visualized in figure 40.

5.2.3 *MCMC with neural network approximated optimization*

To infer the aforementioned parameters we utilize Markov Chain Monte Carlo (MCMC) sampling together with a neural network, which approximates the parameters of the optimal response distribution given the sampled parameter values. Similar techniques for likelihood or posterior approximations via neural networks are also increasingly popular across various fields from reinforcement learning (Hamrick et al., 2020; Wulfmeier, Ondruska, and Posner, 2015) and cognitive neuroscience (Fengler et al., 2021) to population genetics (Beaumont, Zhang, and Balding, 2002). We start

Algorithm 1 Inference algorithm for production and reproduction tasks

Draw chain startvalues $\Theta_0 = [\alpha_0, \beta_0, \sigma_0^p, \sigma_0^a]$ from priors and MH-stepsize s
for iterations i from 1 to N **do**
    Draw new proposal $\Theta_p \sim N(\Theta_{i-1}, s)$
    Approximate optimal action distribution parameter μ_a^{opt} via neural network
    $\Longrightarrow$ find μ given α, β, σ_p, σ_a according to eq.30
    Calculate posterior probability of actual responses $P(x_a^{act}|\mu_a^{opt}, \sigma_a)$
    if $\frac{p(proposal)}{p(previous)} > r \sim U[0,1]$ **then**
        Accept proposal $\Theta_i \Leftarrow \Theta_p$
    else
        Reject proposal $\Theta_i \Leftarrow \Theta_{i-1}$
    end if
end for

the Metropolis-Hastings algorithm by drawing samples from symmetrical proposal distributions for each parameter. Given the resulting cost function, magnitude of the variability and the target one can calculate the optimal parameter of the response distribution μ_a^{opt}, i.e. the optimal aiming point for the response. Given the asymmetry of a log-normal distribution, its mode does not have to coincide with the target. Accordingly, a subject could intentionally aim for values deviating from the target in an attempt to minimize her own costs. For example, in a task requiring responses involving large effort, it may be more suitable to undershoot the target in order to obtain a good task-effort trade-off.

5.2.4 *Network structure and training*

The optimization needs to be done for each data point in each MCMC iteration, which is costly for large data sets originating from experiments with continuous response variables. Therefore, we trained a neural network approximating this optimization, allowing to infer behavioral parameters on large data sets more efficiently. With the neural network yielding the ideal shift of the log-normal distribution's mode for each data point and the previously drawn action variability σ_a one can calculate the likelihood of the data given the model and its parameters.

For inference of the optimization, we utilized a regression neural network (see figure 40 step 4 *'Optimization'*) with four hidden layers approximating the optimal position of the response distribution's mode given the perceptual uncertainty σ_p, the action variability σ_a, both cost function parameters α, β and the actual target x. The six layers are as follows: an input layer with, depending whether σ_p is known or not, 4 or 5 units, layer one with 16 units and leaky ReLu activation (alpha at .1), layer two with 64 units and leaky ReLu activation (alpha at .05), layer three with 16 units and ReLu activation, layer four with 4 or 5 units and sigmoid activation, and layer five as a single unit output layer.

We trained several networks depending on whether the perceptual uncertainty was assumed to be known and thus could be fixed to a specific value or whether it was assumed to be unknown and therefore needed to be inferred, too. Training used 200 epochs for each neural network with fixed σ_p, only differing in the magnitude of perceptual uncertainty (σ_p at .05 and .2 for the puck and beanbag task, see figure 44

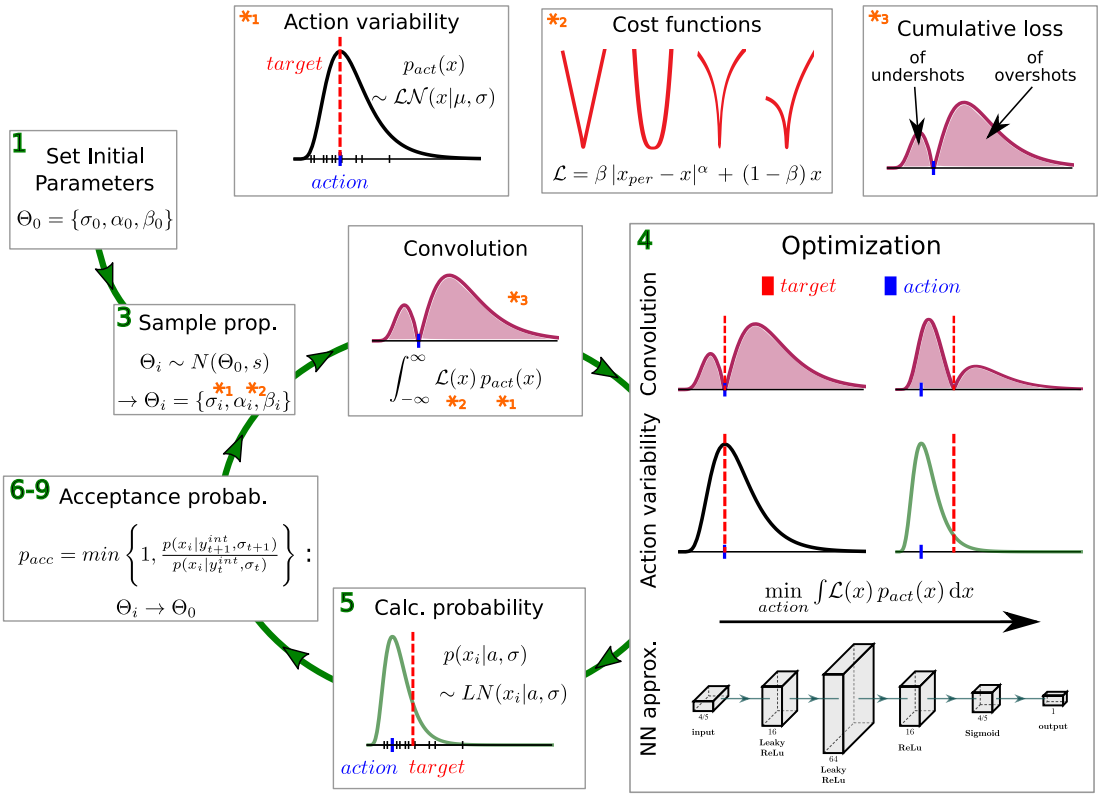

Figure 40: **Visualization of cost inference algorithm.** Numbers reflect the steps in Algorithm 1 while red arrows indicate the process direction. The chain starts at 1) with the initial parameter for action variability and cost function. In 3) based on these parameters and their associated stepsizes a first new proposal is drawn from a Gaussian distribution. These values lead to a response distribution, a cost function and the result of their product the weighted distribution. This distribution has its mode initially at the target position - that e.g. is the value to be reproduced in a reproduction task. However, depending on the value of alpha and beta, this choice may not necessarily have the lowest cumulative cost and therefore is optimized in 4) with respect to the position of the mode of the response distribution y_{int}. The optimization process of finding the best action given the constraints is approximated with a neural network shown in the bottom row for both known and unknown perceptual uncertainty. Input values are action variability σ_a, cost function coefficients α and β, the actual target x and - if unknown - the perceptual uncertainty σ_p. Networks had six layers: an input layer with 4 or 5 units, layer one with 16 units and leaky ReLu activation (alpha at .1), layer two with 64 units and leaky ReLu activation (alpha at .05), layer three with 16 units and ReLu activation, layer four with 4 or 5 units and sigmoid activation, and layer 5 as a single unit output layer. In step 5) the likelihood of the data given σ and y_{int} is calculated as well as the prior probability of σ, α and β for the initial parameters. MH acceptance rule in steps 6-9).

& 45) and 600 epochs for the neural network with variable σ_p (see figure 41). In both cases we used the mean-squared-error loss for training, early stop callbacks based on validation loss, and a validation split of 0.2. The training data consisted of 18,910 samples for networks with known and 123,752 samples for the network with unknown σ_p. To obtain training data, we sampled parameter values for α, β, σ_p, σ_a and target positions (4-par network: σ_a .01 to 1, α .01 to 4, β .5 to .99 and target .2 to 5; 5-par network: σ_a .01 to 1, σ_p .005 to 1, α .01 to 8, β .5 to .99 and target .2 to 5). For each resulting parameter set, we calculated the mode of the optimal action distribution, i.e. the distribution yielding the lowest costs, by solving equation 30 numerically with Brent's method. Training was stable with a mean absolute error of 0.05. It should be pointed out, that using this network is predominantly a tool to speed up the optimization shown in equation 30. Evaluation of each iteration's proposals is again performed via rejection sampling as in the traditional Metropolis-Hastings algorithm.

5.3 EXPERIMENTS

In the experimental evaluations we first show how the proposed method can be used to investigate how behavioral responses such as undershoots and overshoots in potential experiments depend on both the experimental parameters and parameters describing a subject's uncertainty and cost function. This can be utilized to adjust experimental parameters to facilitate inference of the model's parameters given observed behavior. We proceed to show how the proposed method can be utilized to obtain posterior distributions over parameters describing behavior in production and reproduction tasks. Specifically, we evaluate the inference algorithm on synthetic data showing that it is possible to recover individual posterior probabilities for the parameters governing perceptual uncertainties and parameter of the cost function based on empirical data. Finally, we apply our method to experimental data from two production tasks (Neupärtl, Tatai, and Rothkopf, 2020; Willey and Liu, 2018b), showing that the cost functions and action variability parameters can be recovered.

5.3.1 *Investigating the feasibility of task designs*

To investigate the expected behavior in an experiment, we simulate the responses arising from the Bayesian decision model for parametrically changing perceptual uncertainty and response variability. By assuming different cost functions including those that explicitly implement subjective costs for effort, we can investigate the resulting parameter ranges with associated undershoots and overshoots. The corresponding parameter spaces can be visualized, as in figure 41. These plots show the optimal aiming point for each combination of action variability (x-axis) and perceptual uncertainty (y-axis). The optimal aiming point corresponds to the mode of the resulting response distribution and accordingly undershoots are colored in blue while overshoots are colored in red. The combination of parameters resulting in an optimal aiming point coinciding with the perceived position of the target, i.e. an unbiased aiming point from the perspective of the experimenter, is marked in green. Each column shows the relative position of optimal aiming points for different types of exemplary cost function: from symmetric cost functions (column 1-3) to asymmetric ones involving higher effort costs (column 4,5).

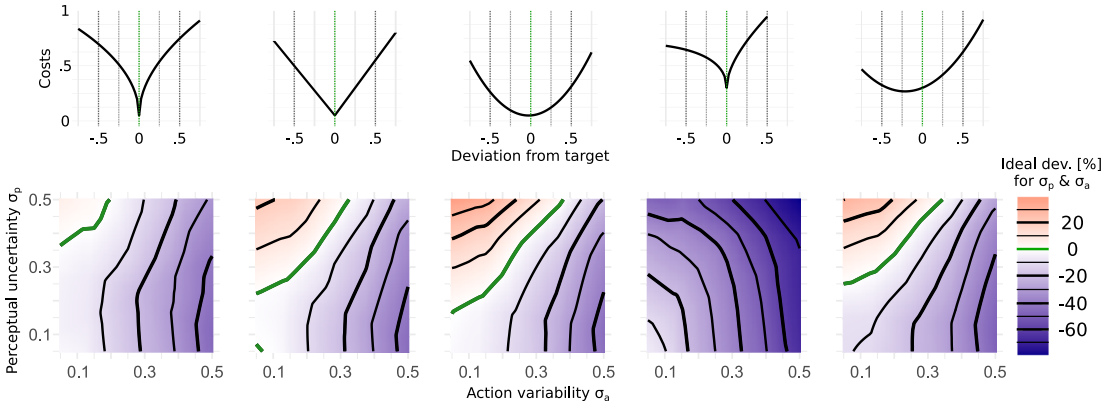

Figure 41: Tile plot showing the influence of perceptual uncertainty σ_p and action variability σ_a on the intentional target, i.e. mode of the log-normal() response distribution, for five different cost functions. Both axes range from .05 to .5 to display realistic values. Color code describes whether actions are expected to match the target (green line), undershoot it (blue regions) or overshoot it (red regions). Deviations are presented on a percentage scale of the actual target.

This allows basic conclusions about the influences of different magnitudes of the individual parameters: i) increasing action variability result in an increasing tendency to undershoot the target (see x-axis in figure 41), the consequence of avoiding costly overshoots arising from the heavy-tailed log-normal response distribution, ii) high values of perceptual uncertainty, on the other hand, can lead to overshoots (see y-axis), especially when action variability is low and α coefficients are high, see first three columns in figure 41. Consider for example the case of high perceptual uncertainty about the actual target and no action variability. Then, the responses falls exactly on the mean of the perceptual distribution for the squared loss. Thus, the experimenter would observe overshoots, since the actual target is the mode of this perceptual distribution. This effect is further enhanced by stronger subjective penalties on the response errors, i.e. larger values of alpha, see figure 41 columns 1-3.

These theoretical implications give experimenters the opportunity to consider in advance effects of certain parameter adjustments. When designing an experiment, experimenters always set up a cost function, even if it is only implicit in the task description. By changing the task demands or by directly including an explicit cost function they can influence the potential parameter space for participants. Similarly, it can be useful to measure the perceptual uncertainty of subjects in advance or to manipulate it in certain task conditions in order to guide behavior in predictable ways.

5.3.2 *Inferring behavioral parameters from synthetic data*

We proceed to validate the proposed inference algorithm by showing numerical evaluations on synthetic data sets allowing to compare recovered parameters with ground truth. In all simulations we used the priors $\beta \sim \text{Beta}(10, 2)$ and $\alpha \sim \log \mathcal{N}(3.5, 2)$, initialized eight chains to explore the parameter space with 5,000 samples each, used the results to start a chain with 20,000 samples and optimized initial parameters and stepsize. First, we demonstrate the ability of the algorithm to recover parameters from synthetic data and use the framework to generate predictions based on the best parameter setting. To do so we generated 200 data points, uniformly distributed on

a continuous range (from 1.2 to 4.8, see generic responses as green data points in figure 42 (C)). This allows a test under realistic conditions, as they occur e.g. in psychophysics tasks as time reproduction (Birkenbusch, Ellermeier, and Kattner, 2015), throwing (Willey and Liu, 2018a,b), lifting or walking tasks (Petzschner and Glasauer, 2011; Sun, Campos, and Chan, 2004). These values can now be thought of as target values that a subject tries to achieve with her actions and can be interpreted on trial by trial and subject by subject level. Here, we chose three different sets of data, which vary in their cost function parameters but neither in their range nor their uncertainties (all with $\sigma_p = .05$ and $\sigma_a = .3$). Thus, besides investigating the ability to recover values, influences of different cost functions on behavioral response patterns become more conspicuous.

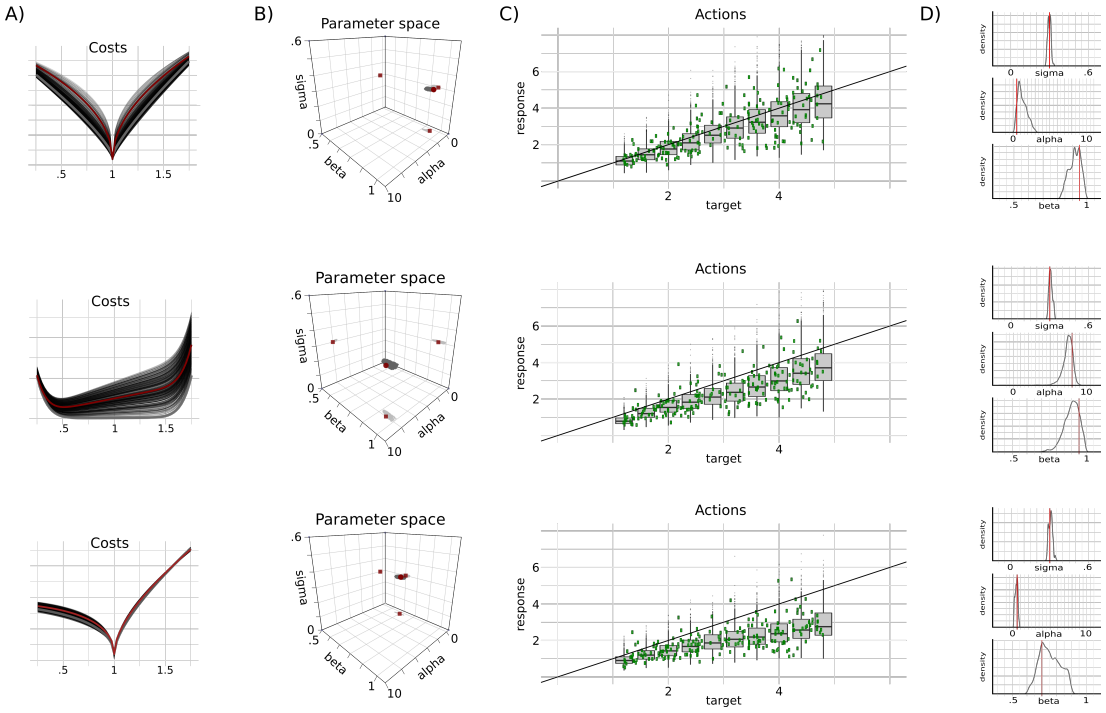

Figure 42: Response pattern of a generic reproduction task and its recovery for three different cost parameter settings. (A) Recovered cost functions and ground truth cost function (dark red). (B) Three-dimensional space with the most likely recovered parameters in dark grey and ground truth values in dark red. (C) Generated responses based on ground truth parameters as green dots and predictions as box plots based on the most likely sample. (D) Posterior distributions for α, β and σ_a parameters and ground truth marked by red vertical lines.

Each row in figure 42 shows one simulation of a particular subject with a particular cost function, the recovered parameters and resulting predictions. With clear prioritization of the task, i.e. a high task motivation (here, $\beta = .95$), and a concave functional dependence of the cost on the absolute distance ($\alpha = .5$), we can observe a cost function, almost symmetric around the target value, in the first row. Together with an intermediate action variability ($\sigma_a = .3$) and a low perceptual uncertainty ($\sigma_p = .05$), this nearly symmetric cost function leads to the largely unbiased behavior in (C) as green data points, which differ from the ideal line only through the increased action variability. Given the data it is now possible to reverse engineer the underlying parameters: (D) depicts the complete posterior distributions for σ_a, α and β, of which the five percent data points with the highest likelihood are additionally represented in the three-dimensional parameter space (B). In (A), the ground truth

cost function (in darkred) and the cost functions belonging to the inferred parameters are plotted. The cost function belonging to the recovered parameter setting with the highest likelihood is used to generate synthetic responses shown as grey boxplot in (C) (10,000 data points distributed over ten targets). The same procedure is followed in the second and third row with modified cost functions: second row shows a flatter cost increase around the target ($\alpha = 8$) and thus a slightly increased influence of the action cost, despite unchanged β, resulting in the expected slight deviation of the behavior from the ideal line in data and prediction. In the third row however, α is again at 0.5 as in the first row, only this time with a decreased value of 0.7 for β and thus creating higher costs for longer or greater actions. Deviations of the inferences were extremely small for the action variability σ_a with modes at 0.3053, 0.3034 and 0.3091 and RMS errors of 0.0124, 0.0149 and 0.0164 for the three data sets, respectively, given the actual value of 0.3. Inferred values for the α parameter show higher variability with modes at 0.8209, 7.5105 and 0.4910 given their actual values at 0.5, 8 and 0.5 and with RMS errors of 0.9928, 0.8846 and 0.2136. Inferences for β yield modes at 0.9161, 0.9101 and 0.7047 with actual values at 0.95, 0.95 and 0.7 and RMS errors of 0.0510, 0.0706 and 0.0885. This validates the overall high precision in recovering the parameters under variability for a set of just 200 sampled data points.

For a more profound explanation and visualization of the resulting samples of cost function parameters we can display, besides the one-dimensional cost functions for a specified target (e.g. at 1 as in figure 42), costs as a function of both, potential targets and actions. Figure 43 shows targets and actions in a range from 0 to 5 with corresponding costs as colored tile plots for samples of the two generic data sets in the second and third row of figure 42. We visualized two-dimensional cost profiles of three samples of cost function parameters for each example. The upper row shows cost functions of three high posterior probability samples when recovering the cost function from simulated behavioral response data, from left to right: the sample with the highest likelihood and, in order to portray the entire diversity and range of inferred cost functions, showing the sample with the highest and lowest inferred α value. Low costs are shown in green while high costs increasingly fade into orange and white.

This two-dimensional visualization is especially useful since the one-dimensional visualization of the recovered shape of the cost functions in the second row of figure 42 can be misleading and suggests a wider variety of potential cost functions despite the previously presented accurate parameter recovery. However this can be explained as an interplay of two factors: First, the high ground truth value of the α coefficient of 8 causing a cost landscape which is very flat close to the target and has an extremely steep increase of costs for further deviations. Thus, differences in the β parameter become more noticeable within close proximity to the target, but show only a small overall influence due to the cost function being dominated by alpha at larger distances. With the second factor, the action variability σ_a of .3, these small differences in costs at small deviations in A-C) of figure 43 become irrelevant. Since especially the cost functions in A-C) have high α parameters, cost values increase rapidly with larger deviations, leading to a difficult interpretability of short deviations relative to each other, see upper left and lower right of the two-dimensional cost tile plots in the middle row where deviations of actions from the target are maximal. In order to solve this and make it visually more accessible we also depicted the resulting tile plots with logarithmized values of cost in the last row. There the high functional sim-

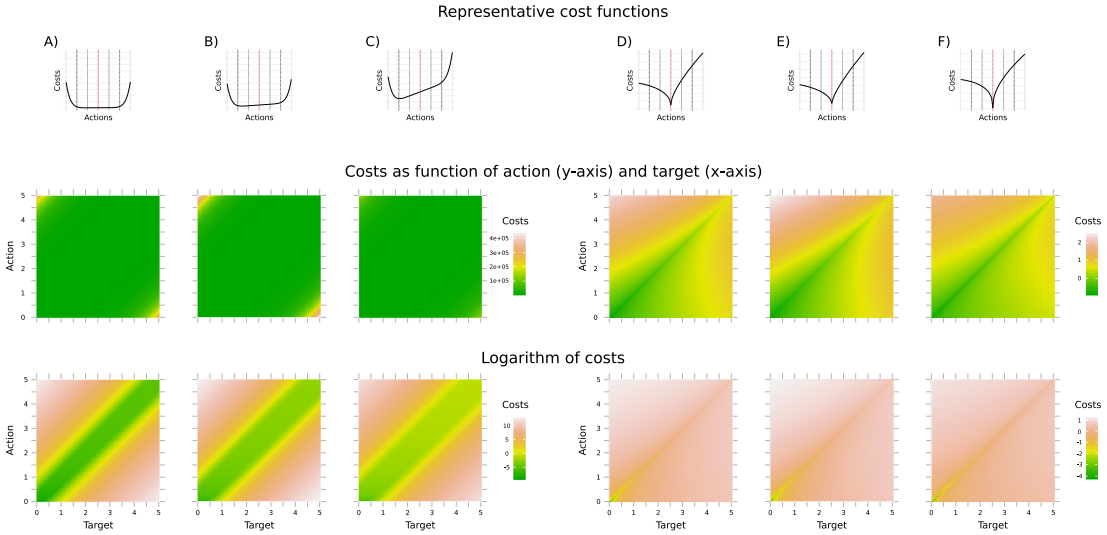

Figure 43: Comparison of three sampled cost functions with high posterior probability for each of the two simulated data sets in the second and third row in figure 42. Bottom row depicts the log value of costs to better visualize the steep gradients, especially for the left example. Left panel A-C): three exemplary cost functions with associated costs for the second case in figure 42. Right panel D-F): three exemplary cost functions with associated costs for the third case in figure 42.

ilarity of these cost functions becomes apparent again. When in the end the action variability σ_a of .3 is additionally considered even the slight differences in costs for small deviations are no longer a relevant factor.

5.3.3 *Inference for continuous action control tasks*

In addition to generic data and theoretical statements, we will analyze anonymized data from two different continuous action-control tasks in the following. For this purpose, we infer the sensory and motor descriptive parameters and the cost functions on an individual level for two exemplary subjects each. In one task participants were asked to propel a puck pressing a key on a keyboard into gliding towards a target (Neupärtl, Tatai, and Rothkopf, 2020) and in the other they were asked to throw a bean bag with their hands to a target (Willey and Liu, 2018b). Both tasks are characterized by actions being on a continuum and both perception and the action itself being subject to variability. In the puck task however people could control the initial velocity of the object by the duration of a key press with uniformly drawn distances to the target to cover whereas in the beanbag task the object was directly controlled via muscle power for five different distances.

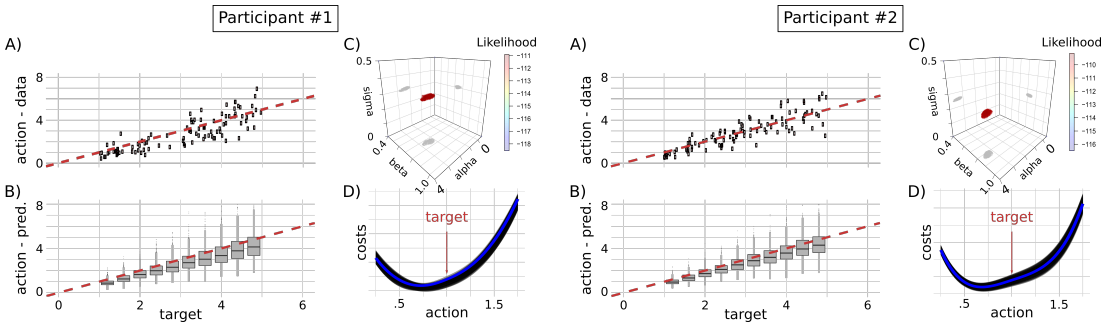

Figure 44: Puck sliding as action control task. Both targets and actions are on a continuous scale. (A) actual responses (y-axis) given the targets (x-axis). (B) predictions based on best inferred parameter setting as boxplots for exemplary targets (1,000 data points each). (C) most likely 5% of posterior distribution for α, β and σ_a in 3D parameter space. (D) cost functions corresponding to parameters in (C). Best sample highlighted in blue.

Inferred parameters for two participants of the puck task are shown in figure 44: (A) showing the actual responses as a function of the target stimulus, (B) model predictions based on the most likely parameter combination of α, β and σ_a (values for σ_p were adopted from the original study), (C) the five percent sampled parameters with the highest likelihood in 3D space for better visibility and (D) the corresponding cost functions. Clearly, inferences for both subjects are similar. Participant one exhibits slightly higher variability in her responses (A) as inferred in (C). In both cases the convex shape of the cost function increasingly penalizes larger deviations.

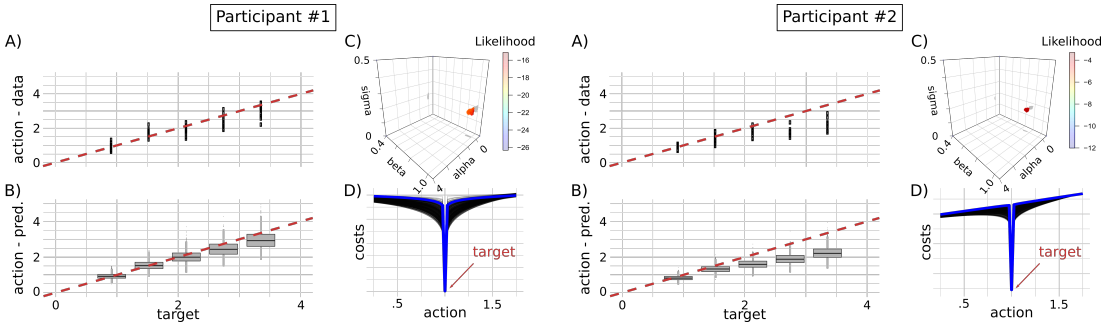

Figure 45: Beanbag throwing as action control task. Targets on five discrete positions and actions on a continuous scale. (A) actual responses (y-axis) given the targets (x-axis). (B) predictions based on best inferred parameter setting as boxplots for these targets (1,000 data points each). (C) most likely 5% of posterior distribution for α, β and σ_a in 3D parameter space. (D) cost functions corresponding to parameters in (C). Best sample highlighted in blue.

Figure 45 depicts responses and inferences for two participants of the beanbag throwing task: (A) showing the actual responses for each of the five target distances, (B) model predictions based on the most likely parameter combination of α, β and σ_a (σ_p again adopted from the original study), (C) the five percent sampled parameters with the highest likelihood in 3D space and (D) the corresponding cost functions. Again, we find strong similarities between subjects with respect to their action variability and shape of their cost function. Thereby participants in different tasks are potentially forming clusters in the 3D parameter space, and yet showing differences on the individual level. So that slight deviations in a parameter can lead to clear distinction in behavior, e.g. in figure 45 the lower value for β in participant 2 causes a

more asymmetric cost function and a stronger tendency to undershoot target values with increasing distance. However, here we showed only two examples as representatives for all participants from two action control tasks. Even though with them being the best individual representatives for the population they still do not reflect the whole diversity of parameters and thus cost functions and behavioral patterns.

5.4 DISCUSSION

Production and reproduction tasks are a popular tool in psychophysics and yet also a complex computational problem, since people's behavior is influenced by diverse factors, for not only the perception but also the response in these continuous tasks are subject to variability while their behavior is additionally shaped by internally and externally motivated cost functions. Here we present an inference algorithm as a useful tool to investigate human behavior in these continuous decision making situations by inferring posterior beliefs about meaningful parameters describing the complete process from perception to final response. Using this framework we can explain seemingly suboptimal behavior, quantify responses in terms of meaningful parameters. In our framework we use logarithmic representation of perception and actions, naturally accommodating Weber-Fechner phenomena in human behavior (Battaglia, Kersten, and Schrater, 2011; Neupärtl, Tatai, and Rothkopf, 2020). Additional support for the presence of such representations comes from recent studies that have indicated e.g. that intuitive representation of numbers in humans (Dehaene et al., 2008; Siegler and Opfer, 2003) or time in animals (Roberts, 2006; Yi, 2009) may be of logarithmic nature.

Similar work on a priori identifiability of probabilistic models in estimation tasks was done by Acerbi, Ma, and Vijayakumar (2014). They developed a probabilistic framework to recover prior beliefs in estimation tasks and to investigate candidate experimental designs a priori by comparing and ranking their identifiability. Here, we focus on inference of parameters that can describe perception, action, and multiple individual cost functions without the influence of strong priors over distributions in experiments. This can be particularly useful when distributions are complex, the experiment is too short to learn them, or there is no feedback on the actions at all. In doing so, we infer not only task specific costs but also, unlike Acerbi, Ma, and Vijayakumar (2014), the cost of performing the action itself. This part of the costs can be especially important for continuous tasks like production and reproduction tasks with increasing magnitude of the target stimulus, which can exemplary be seen for participant two in figure 45 with her increasing tendency to undershoot the target values.

Important prerequisites for our framework are the ability of subjects to assess their own uncertainty and variability and to adjust their behavior optimally given their uncertainty and cost functions. The high degree of the former capability was shown in studies investigating human movement planning and interval timing (Balcı et al., 2011; Hudson, Maloney, and Landy, 2008; Sims and Gray, 2008) and likewise for animals from rats (Foote and Crystal, 2007) to macaque monkeys (Hampton, 2001). The fact that subjects can adapt to external cost functions and the influence of costs, inherent in the execution of the action itself, has been shown in e.g. visuo-motor experiments where subjects explicitly adapt to external cost functions when pointing on a screen while also optimally include their own uncertainty (Trommershäuser,

Maloney, and Landy, 2008). However, here we additionally include costs for efforts. For example, it has been shown that people are sensitive to these costs in 2AFC tasks when the necessary force is manipulated (Hagura, Haggard, and Diedrichsen, 2017). These effort costs also need to be considered in computational models in line with bounded rationality to accurately describe human behavior as e.g. done for the suppression of blinking in an event detection task (Hoppe, Helfmann, and Rothkopf, 2018).

Given its trial by trial nature our proposed algorithm can be susceptible to outlier and inconsistent behavior. These data points can strongly alter inferred parameters, changing conclusions about perceptual uncertainty, action variability and cost functions. However, this vulnerability can be as well used to detect even subtle changes in behavior in sequential data. Taken together we introduced an useful inference tool to quantify behavior in continuous decision tasks and to a priori investigate appropriate experimental settings.n previous studies addressing differences in physical reasoning between tasks (Smith, Battaglia, and Vul, 2018) and quantifying different sources of uncertainty in physical reasoning (Smith and Vul, 2013) by adding the mode of physical interaction as an additional factor. This may also reconcile some previous result on intuitive physics, which reported strong deviations from Newtonian physics, but utilized very abstract depictions of scenes and no possibility for interaction (Caramazza, McCloskey, and Green, 1981; Todd and Warren Jr, 1982).

The present results are additionally relevant for the question of how the brain may implement physical reasoning. Previous studies have found evidence for the representation of abstract physical factors in parietal and frontal regions, when physics students thought about verbally presented physics terms (Mason and Just, 2016). Similarly, recent studies involving physical reasoning about objects' dynamics on the basis of short movies also identified frontal and parietal regions representing abstract physical quantities such as mass (Schwettmann, Tenenbaum, and Kanwisher, 2019) and involved in judging physical interactions (Fischer et al., 2016). These results give credence to the notion of causal generative models of physical objects and their interactions compared to model-free pattern recognition approaches, such as those based on deep neural networks. Nevertheless, the involvement of overlapping parietal regions in the representation of physical quantities such as mass when planning visuomotor interactions (Gallivan et al., 2014) and the additional involvement of motor related regions in such tasks (Chouinard, Leonard, and Paus, 2005) speak for a crucial role of embodied representations (Anderson, 2003; Foglia and Wilson, 2013; Wilson, 2002) in physical reasoning at the implementational level.

6

INDIVIDUAL COSTS AS AN EXPLANATION FOR PERVASIVE UNDERSHOTS IN MOTOR TASKS

6.1 INTRODUCTION

6.1.1 *Undershots in various actions*

Whether when moving to a target, moving their arms, grabbing objects, estimate time intervals or even when making saccades to new fixation points animals and people constantly show patterns of movements that end up to be too short (Becker and Fuchs, 1969; Bergmann et al., 2011; Elliott et al., 2010, 2004; Engelbrecht, Berthier, and O'Sullivan, 2003; Harris, 1995; Lejeune and Jasselette, 1986; Lejeune and Richelle, 1982; Lowe, Harzem, and Spencer, 1979; Sun et al., 2004; Weber and Daroff, 1971; Zeiler and Hoyert, 1989). These underestimations or undershots have been observed among others in pigeons during perching and treadle pressing (Lejeune and Jasselette, 1986; Lejeune and Richelle, 1982), in rats and pigeons for time estimation in fixed-interval schedules (Lowe, Harzem, and Spencer, 1979) and for time reproduction in pigeons (Zeiler and Hoyert, 1989). People on the other hand show underestimations e.g. when placing objects relative to a target point (Elliott et al., 2004), when reaching and aiming, especially for initial movements (Elliott et al., 2010), when covering distances by walking or bicycle (Bergmann et al., 2011; Sun, Campos, and Chan, 2004; Sun et al., 2004) or when moving an object on a computer screen under uncertainty (Engelbrecht, Berthier, and O'Sullivan, 2003). Even for saccades to target points, general initial undershots have been reported that underestimate the distance to the fixation point by up to ten percent (Becker and Fuchs, 1969; Harris, 1995; Weber and Daroff, 1971).

6.1.2 *Reasons for undershots*

But why do these undershots occur? Especially when it has often been argued that people can act close to optimally given their limitations and constraints (Hoppe and Rothkopf, 2016, 2019; Todorov, 2004), usually having accurate beliefs about their accustomed environment and its statistics (Girshick, Landy, and Simoncelli, 2011; Mamassian and Goutcher, 2001; Stocker and Simoncelli, 2006), utilizing appropriate models of their environment (Neupärtl, Tatai, and Rothkopf, 2020; Sanborn, Mansinghka, and Griffiths, 2013; Smith and Vul, 2013), and being able to precisely learn and act upon new environmental statistics (Hoppe, Helfmann, and Rothkopf, 2018; Hoppe and Rothkopf, 2016). Even after learning, the tendency to underestimate distances seems not to change but rather to manifest itself (Elliott et al., 2010, 2004; Engelbrecht, Berthier, and O'Sullivan, 2003). Reasons for these undershots were sought in costs for the duration of saccades (Harris, 1995) or in the attempt to minimize costs for energy-costly overshots in limb movements (Elliott et al., 2010; Lyons et al., 2006; Oliveira, Elliott, and Goodman, 2005). Here we suggest however that this behavior can be explained consistently across this variety of scenarios with three underlying assumptions: i) uncertainty in perception and variability in action execution as log-

normal distributed entities, ii) cost functions describing the desirability of an outcome and the effort necessary to produce it and iii) the interaction of uncertainty and cost functions based on individual's endogenous knowledge about their own uncertainty.

There are several reasons to consider a logarithmic representation of perception and action execution. Properties of log-normal distributions naturally take Weber-Fechner phenomena, variability that scales with the intensity of the stimulus, into account and further lead to strictly positive values for both perception and action variables. These strictly positive values should be considered as more realistic than Gaussian distributed ones, as used before in (Battaglia, Kersten, and Schrater, 2011; Neupärtl, Tatai, and Rothkopf, 2020). A log-normal distributed representation of perception is indeed controversial (Brannon et al., 2001; Cantlon et al., 2009), however more recent studies discuss and indicate that such an assumption seems to fit, e.g. for number representations for different age groups and socialization (Cantlon et al., 2009; Dehaene et al., 2008; Siegler and Opfer, 2003). For animal behavior it was likewise argued that subjective time is consistent with the linear Scalar Timing theory (Gibbon and Church, 1981) whereas more recent research with pigeons (Roberts, 2006) or rats (Yi, 2009) showed evidence that speaks for a logarithmic representation of time rather than a linear one as well. For a review about scalar properties in animal timing see (Lejeune and Wearden, 2006).

The second assumption of the framework proposed here is that human decisions are influenced by cost functions. Whether in economic decisions (Tversky and Kahneman, 1974), in pointing tasks (Trommershäuser, Maloney, and Landy, 2008) or virtual curling (Neupärtl, Tatai, and Rothkopf, 2020), it is known that goals and their associated evaluations of single trials, i.e. cost functions, fundamentally influence human behavior. Further, it was shown that subjects' decisions are not only influenced by the outcome alone but as well by the cost of the action itself (Elliott et al., 2010; Hagura, Haggard, and Diedrichsen, 2017; Hoppe, Helfmann, and Rothkopf, 2018; Lyons et al., 2006; Oliveira, Elliott, and Goodman, 2005). This is why cost functions integrated in this framework not only consider the outcome but also the effort to achieve it. In order to explain the interaction between uncertainty and cost functions, the knowledge of the individual about his own uncertainty is required. More recent research showed that people and animals can take their endogenous uncertainty into account in order to maximize reward or conversely minimize costs (Akdoğan and Balcı, 2017; Balcı et al., 2011; Hudson, Maloney, and Landy, 2008; Sims and Gray, 2008).

The impact of these asymmetrical distributions, cost functions and the endogenous knowledge about uncertainty on continuous visuomotor tasks is discussed in the following and visualized exemplarily in figure 46. Cost functions used in this framework consider the cost of the outcome and action itself and can take an unlimited number of shapes enabled by a continuous parameter space. Using this framework we can quantitatively reverse engineer human cognition (Zednik and Jäkel, 2016) and determine various influencing factors for individual subjects in continuous tasks, from uncertainties to individual cost functions. Eventually, we show how the resulting variability of log-normal distributed variables can additionally be transformed into weberfractions for comparability reasons.

6.2 MCMC WITH INTERMEDIATE OPTIMIZATION

6.2.1 *Optimizing responses under uncertainty and costs*

Actions are not only subject to uncertainties in the perception on which they are based on, but also to variability in their execution. Both sources of variability are considered here in the form of log-normal distributed variables (see figure 46). Crucial however, apart from these sources of variability, are the costs $\mathcal{L}$ associated with possible outcomes. In general, there would be an unlimited number of possible forms of cost functions. But there are obvious assumptions about potential forms of these cost functions. E.g. subjects will likely evaluate values based on a function of their absolute error, that means regardless of whether they are slightly above or below the desired value. Hence we assume at the beginning costs for potential outcomes of actions to be symmetrical around the target:

$$\mathcal{L} = |x_t - x|^{\alpha}$$

With x_t being the target value, x the value of a single outcome and α a coefficient describing the form of the cost function - e.g. values of α at 1 or 2 correspond to the hinge loss and quadratic cost function, respectively.

A further adjustment of the cost functions was applied by including basic costs for the execution of actions. I.e. a term of the costs, which adapts to the magnitude of the action x_a itself. The variable x_a and x can be identical for e.g. a press-time reproduction task with action costs increasing with the press duration but can be distinct for e.g. a curling task were x correspond to the distance covered and x_a could correspond to the necessary power to accelerate the puck (Neupärtl, Tatai, and Rothkopf, 2020). These costs can now be included in the general cost function term relative to the costs for the outcome of the action:

$$\mathcal{L} = \beta\,|x_t - x|^{\alpha} + (1-\beta)\,x_a$$

With x_a being the effort to achieve the value of x and β a coefficient describing the trade-off between task and effort. High values for β make the task the determining factor whereas low values strongly emphasize the effort to reach certain values.

Both the fact that subjects can adapt to external cost functions and the influence of costs, inherent in the execution of the action itself, has been shown in studies. In a visuo-motor experiment, for example, (Trommershäuser, Maloney, and Landy, 2008) have shown that subjects explicitly adapt to external cost functions when pointing on a screen while also optimally include their own uncertainty in the execution. (Hagura, Haggard, and Diedrichsen, 2017) have shown that subjects in a 2AFC experiment are sensitive to the force required for an action and show a bias towards less demanding actions. With parameters for the uncertainty in the perception and execution and for the form and weighting of the cost functions one can calculate the expected cost given that the response distribution peaks at the target , see figure 46 *action variability* and *convolution*. However, the question arises whether this positioning is ideal, i.e. yields the minimal expected cost, for given values of σ, α and β. In figure 46 *optimization*,

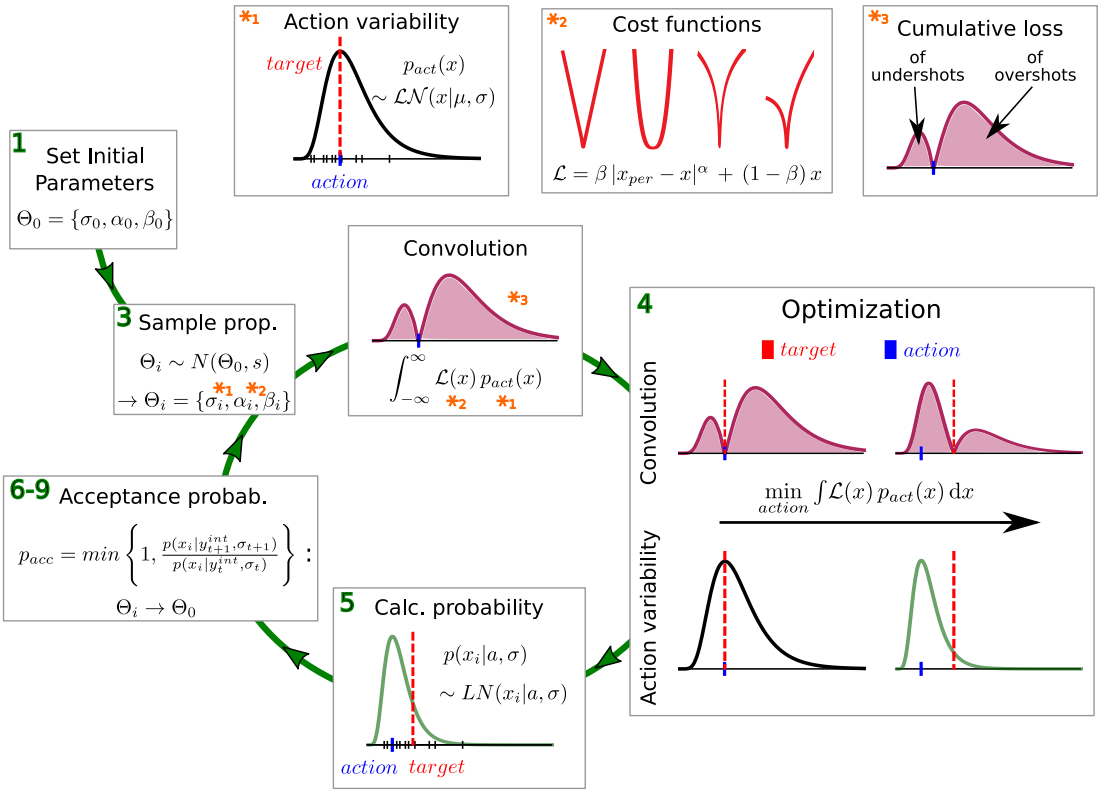

Figure 46: **Recap-visualization of cost inference algorithm.** Numbers reflect the steps in Algorithm 1 while red arrows indicate the process direction. The chain starts at 1) with the initial parameter for action variability and cost function. In 3) based on these parameters and their associated stepsizes a first new proposal is drawn from a Gaussian distribution. These values lead to a response distribution, a cost function and the result of their product the weighted distribution. This distribution has its mode initially at the target position - that e.g. is the value to be reproduced in a reproduction task. However, depending on the value of alpha and beta, this choice may not necessarily have the lowest cumulative cost and therefore is optimized in 4) with respect to the position of the mode of the response distribution y_{int}. In step 5) the likelihood of the data given σ and y_{int} is calculated as well as the prior probability of σ, α and β for the initial parameters. MH acceptance rule in steps 6-9).

an ideal shift of the response distribution for a given set of parameters is shown, minimizing the overall expected cost. Based on these principles we built an MCMC algorithm, sampling potential values, optimizing the relative peak position of the response distribution to the target and calculating posterior probabilities for these parameters given the data.

6.2.2 *Metropolis Hastings and Simulated Annealing*

As a starting point for developing our algorithm we used Metropolis-Hastings. Metropolis-Hastings algorithms usually show a decreasing acceptance rate with the model complexity. However, it was shown that there is an ideal acceptance rate for any higher dimensional models (Roberts, Gelman, Gilks, et al., 1997). We addressed this problem with an approach based on Simulated Annealing (Kirkpatrick, Gelatt, and Vecchi, 1983). With two adjustments it is possible to cover a larger search space for potentially adequate variable combinations: i) using a reasonably large step size to be able to explore faster and broader and ii) an exponentially increasing acceptance-threshold,

starting at a very low level and eventually ending at a threshold value identical with common Metropolis-Hastings. This means that the majority of the proposed samples are accepted, large areas of the search-space are evaluated, and nonetheless allows the chain to finally end up in an area that provides the highest probabilities. Based on these samples we can determine an improved step size and initial parameters for a classic MH-MCMC run (see 1 & 3 in figure 46). By adjusting the step size we can assure an appropriate acceptance rate with simultaneous assurance that the chain is not stuck in local minima. With the resulting posterior we can not only determine the uncertainty of the subjects but also draw conclusions about the underlying cost function. This in turn gives us information about the individual evaluation of single outcomes and about the relative weighting of the task and intrinsic costs, i.e. the effort required for the execution.

6.2.3 *Neural Network Approximation of the Likelihood*

The optimization shown in figure 46 has to be done for every target value in the data set and for every set of sampled parameters in each iteration. Thus, running this MCMC based algorithm takes time, especially for continuous data with varying target distances. However, by approximating this optimization using a neural network this process can be accelerated. After training the model with 300,000 sampled combinations of target values, model parameters and the corresponding ideal action, i.e. the ideal shift of the log-normal distribution's mode, we can quickly pull the ideal action based on the samples for action variability σ_a, cost parameters α and β as well as the target value x from the network.

We utilized a regression neural network with six layers: an input layer with 4 units, layer one with 16, layer two with 32, layer three with 64, layer four with 32 units, all with Hyperbolic tangent activation function, and layer five as a single unit output layer with ReLu activation function. The network was trained for 1,000 epochs. Rather than running the time costly optimization we can now utilize the network in each iteration for a multitude of individual target values.

6.2.4 *Predictions from the Generative Model*

Using this framework we are not only able to infer individual probability distributions for uncertainties and parameter of the cost function based on empirical data, but also to make predictions about the impact of changes in uncertainty or cost functions and to visualize these theoretical expectations a priori. Some of these predictions are shown in figure 47 for different levels of action uncertainty σ and cost function parameters α and β. Resulting optimal behavior given uncertainty and cost constraints is depicted with box-plots of action responses as function of binned target values. One can simply imagine a time reproduction task with multiple trials per target time binned over a range from .5 to 3 seconds. Red lines indicate the correct response for each bin. However, it becomes evident that given the constraints, the behavior that results in the lowest cost will result in more or less pronounced undershots on average, depending on the cost function and the level of uncertainty. Basically, the greater the variability or uncertainty and the stronger the gradient in costs between small and large errors, the more pronounced the undershots in behavior will be.

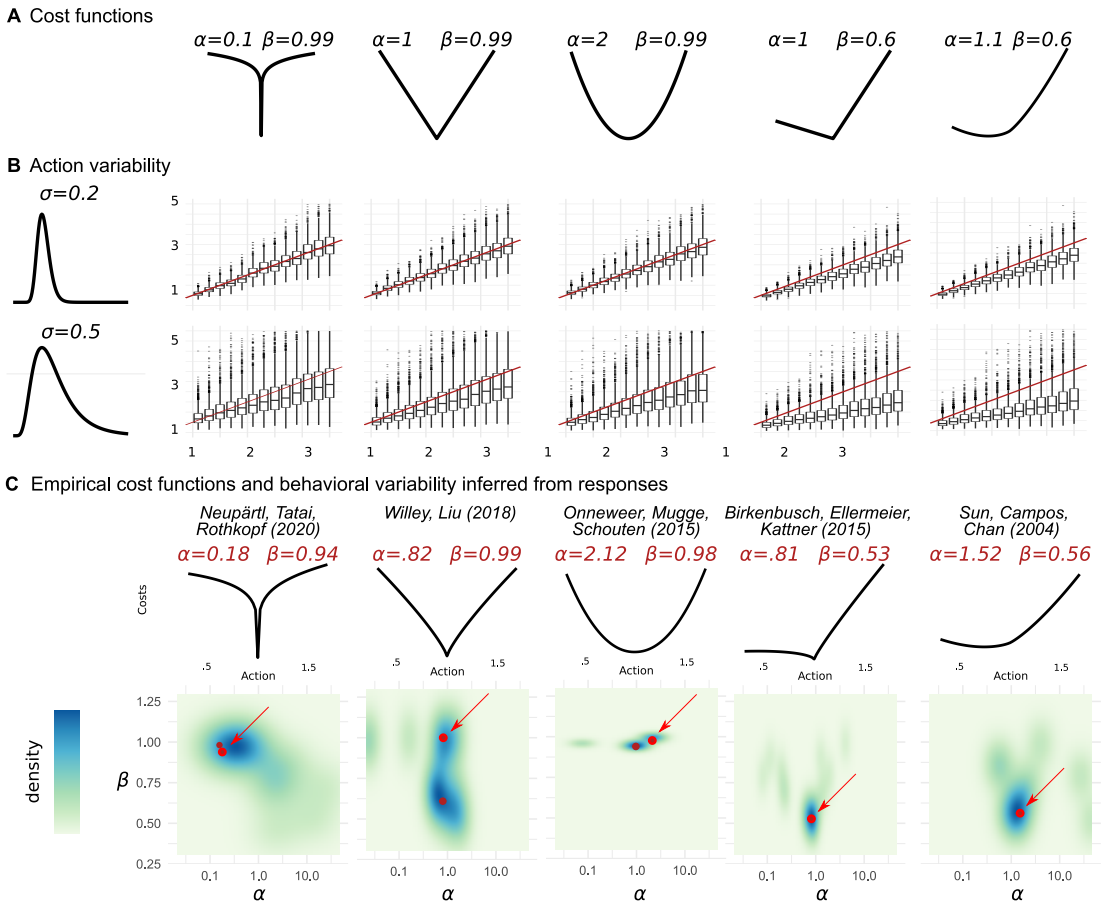

Figure 47: **A) Exemplary cost functions.** Five different generic cost functions from concave to convex and low effort to high effort. Parameters shown on top. **B) A priori model predictions**. Predictions using the generative model shown in figure 46 for different values of σ, α and β. Box-plots show the optimal distribution of responses for different target positions given log-normal perceptual uncertainty, action variability and cost functions. **C) Task specific cluster of cost functions**. Two dimensional density plot of cost function parameters α and β of each individual's best sample. Cluster show similar and consistent behavior across participants and differences between different experiments. Participants used for the upcoming task specific visualizations of inferences in figures 48-52 are highlighted as red dots. One cost function, participant additionally marked by an red arrow, for each task is depicted in the upper row.

6.3 EXAMPLES OF UNDERSHOTS IN VISUOMOTOR BEHAVIOR

Using this inference approach we analyzed 69 participants across five different motor tasks, from sliding pucks on a screen and reproducing time intervals via button press to throwing bags and reproducing force levels by hand. In figure 47 C) one can see an overview for each task's density plot of participants' most likely cost function parameter α and β, highlighting the high level of uniformity within and differences across tasks. More detailed description of each task and its associated inferences for exemplary participants are shown in the following sections from '*Undershots in virtual curling*' to '*Undershots in distance reproduction*'.

Values arising from these actions are depicted as function of the actual target in the upper part of figures 48-52 A) for one or two exemplary participant. Ideal responses would be located on the red dashed line. The lower part shows predictions of the

generative model using the most likely parameter combination found by the MCMC run. Predictions are here shown as box plots for several illustrative target positions in the range of the original. For each target 1,000 responses were sampled from the model. In column B) the five percent sampled parameter combinations with the highest likelihood are depicted with σ_a, α and β spanning the three dimensional space. For a better overview, additional projections on the two-dimensional planes are visualised as grey shadows, and for the purpose of comparing the different data sets, the boundaries of the three dimensional space are constant across all subjects and experiments. The cost functions associated with these parameter combinations are shown in column C) for a chosen action. The cost function of the most likely parameters, α and β, is highlighted in blue. Two dimensional visualizations of costs as function of both, the action and the target, are shown in column D) and E), showing the absolute costs and their logarithm respectively.

Undershots in virtual curling

The first data set we are looking at deals with everyday interactions of humans in their environment governed by physical laws (Kubricht, Holyoak, and Lu, 2017; Neupärtl, Tatai, and Rothkopf, 2020; Sanborn, Mansinghka, and Griffiths, 2013).

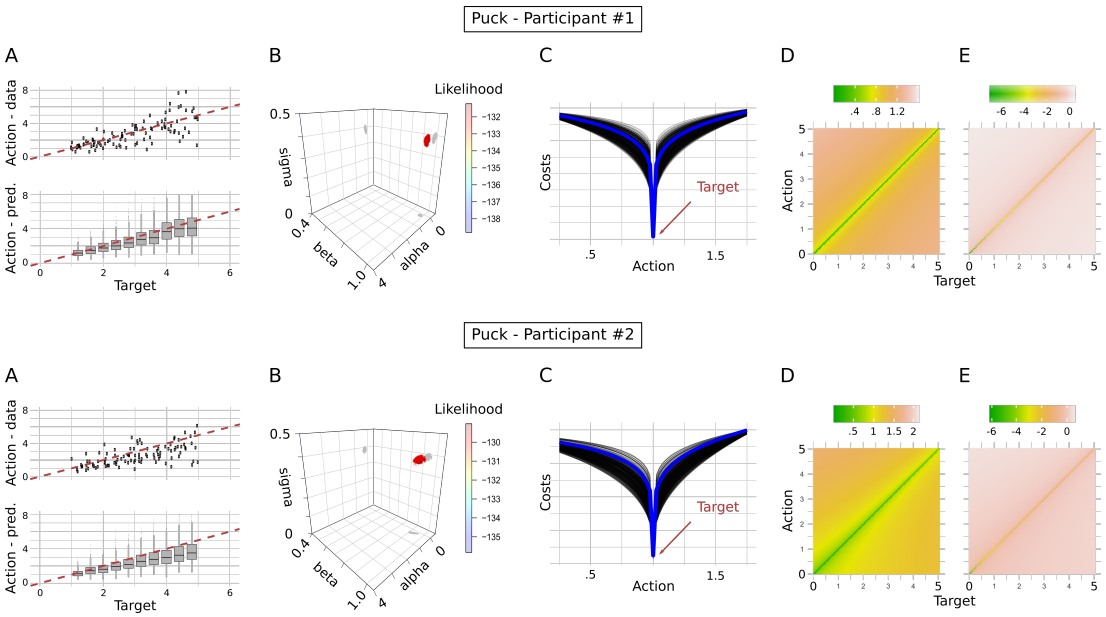

Figure 48: **Puck curling data (Neupärtl, Tatai, and Rothkopf, 2020). A** Participant's actual responses (scatter plot) and model predictions (box plot) as function of the target magnitude. **B** 3D scatter plot of the five percent samples with the highest likelihood from iterations with adjusted step size and initial values. **C** 1D visualization of cost functions corresponding to each α-β pair shown in B) for a target magnitude of 1. Cost function of the sample with the highest likelihood, also used to generate predictions in A), highlighted in blue. **D,E)** 2D visualization of cost functions with action values here on the y-axis and target values on the x-axis - D) shows the absolute costs and E) their logarithm, useful for steep gradients.

Actions in this continuous visuomotor task are shaped by participants' intuitive understanding of physics. Participants were asked to propel a puck on a surface aiming for a target's bulls eye while realistic friction was acting on the gliding puck

(Neupärtl, Tatai, and Rothkopf, 2020). The acceleration of the puck to an initial speed was adjusted by the participants via the duration of a key-press.

With 14 out of 16 participants, almost every participant showed a mean undershoot with the heavy puck in the experiment's feedback phase when participants were able to learn the correct scaling, ranging from an average undershot of 0.02 to 0.78m. The density plot of inferred cost function parameter α and β in figure 47 C) shows the distribution of the best model parameters of all participants in the first column 'Puck'. Obviously, a cluster is formed with mean values at $\alpha = .37$, $\beta = .97$, containing 9 participants and thereby bundling more than half of all participants. We picked two participants from the cluster, highlighted as dark red points: a first participant with a slightly pronounced and a second one with a stronger tendency to undershoot. Inferences and model predictions for both, participant #1 ($\alpha_1 = .16$, $\beta_1 = .98$) who showed just a weak tendency to undershoot the target with a mean error of $\mu_{err,1} = .16$m and #2 ($\alpha_2 = .18$, $\beta_2 = .94$) with a mean undershot of $\mu_{err,2} = .48$m, are shown in the upper and bottom row of figure 48, respectively.

Undershots in beanbag throwing

In the second data set we examine the performance of participants in a beanbag throwing experiment of Willey and Liu, 2018b.

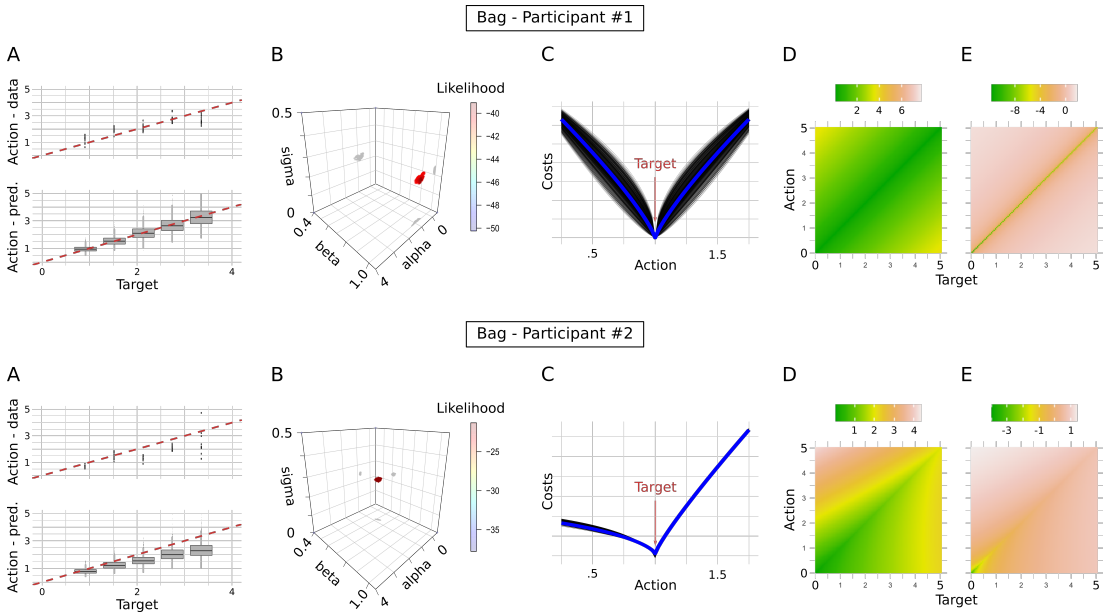

Figure 49: **Beanbag throwing data (Willey and Liu, 2018b).** Responses of two exemplary participants from the beanbag throwing experiment and the corresponding parameter inference.

Participants were asked to throw a beanbag twelve times at a target. Targets were placed at five different distances from 3 to 11 feet with 2 feet increments (.9144 to 3.3528 in meter). In the pretest condition participants viewed the distance once and then threw a beanbag twelve times in a row at the target. They did not receive any visual or verbal feedback between the trials. Due to the lack of feedback, subjects were unable to learn and form some prior about the statistics of the experiment in

this condition and had to rely on their internal model.

With 16 of the 20 analyzed participants the majority showed a mean undershot across the five different distances in a range of .03 to .61m. Figure 47 C) visualizes the emergence of two cost function clusters. Both show very similar α parameters ($\alpha_A = .98$ and $\alpha_B = 1.04$) but differ with high and low β values ($\beta_A = .98$ and $\beta_B = .6$). Indicating that people in the second cluster B with stronger pronounced asymmetric cost function showed a potential higher influence of action effort on behavior. I.e. some participants probably had a harder time to handle the beanbag's weight with respect to the target distances. Participant #1 ($\mu_{err,1} = 0m$, $\alpha_1 = .82$, $\beta_1 = .99$) and #2 ($\mu_{err,2} = .54m$, $\alpha_2 = .8$, $\beta_2 = .61$) are depicted in figure 49 as representatives for cluster A and B, respectively.

Undershots in force reproduction

The third data set contains data from a force reproduction task conducted by Onneweer, Mugge, and Schouten, 2015.

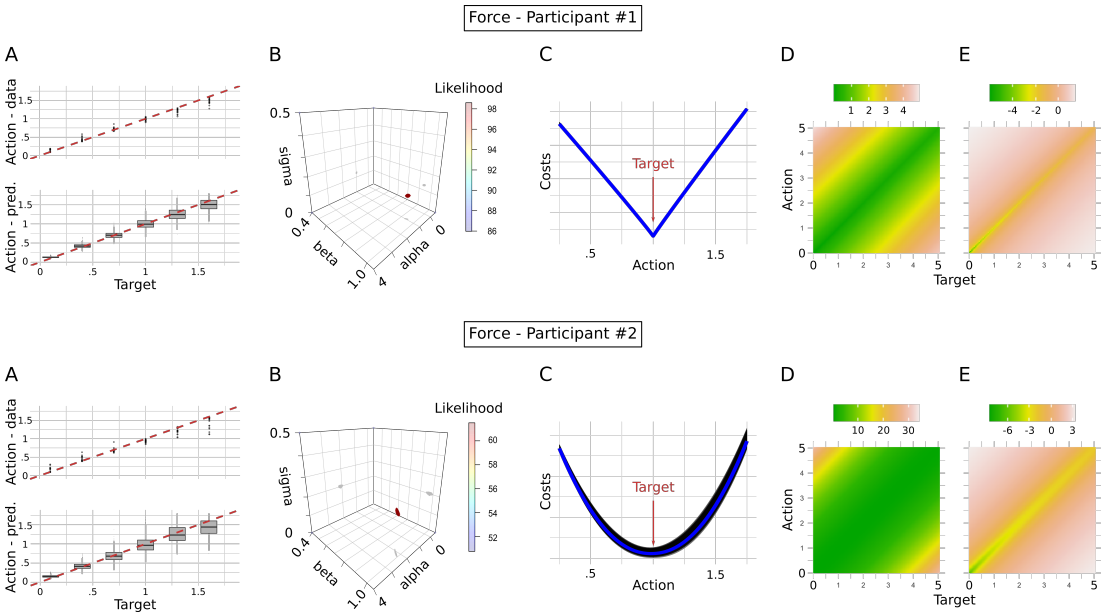

Figure 50: **Force reproduction data (Onneweer, Mugge, and Schouten, 2015).** Responses of two exemplary participants from the force reproduction experiment and the corresponding parameter inference. Note that target and response values are shown here as hundredths of Newton.

Here, participants were asked to reproduce six different force levels (10, 40, 70, 100, 130, 160 N) eight times in a randomly presented order. This range of action magnitude was normalized to a range of .1 to 1.6 for comparison purposes and since the network was trained with data in a range up to 5 in target values.

In this force reproduction task 9 out of 10 participants showed an overall mean undershot, ranging from 2.3 to 9.7N. They showed small but consistent undershooting, increasing with the force magnitude. Figure 50 shows two participants, again each one representative for one of the two cluster. In both clusters high values of the β parameter ($\beta_A = .94$ and $\beta_B = .99$) lead to largely symmetrical cost functions. With

mean α values of $\alpha_A = .95$ and $\alpha_B = 2.17$ clusters are extremely close to the common hinge and squared loss functions. These almost symmetric cost functions together with the low action variability ($\sigma_{a,1} = .11$ & $\sigma_{a,2} = .20$) are the cause for the low extent of undershots for both, participant #1 ($\mu_{err,1} = 4.1N$, $\alpha_1 = .96$, $\beta_1 = .93$) and #2 ($\mu_{err,2} = 2.3N$, $\alpha_2 = 2.12$, $\beta_2 = .98$), in figure 50.

Undershots in time reproduction

In the fourth data set we can examine responses from an auditory time reproduction task carried out by Birkenbusch, Ellermeier, and Kattner, 2015.

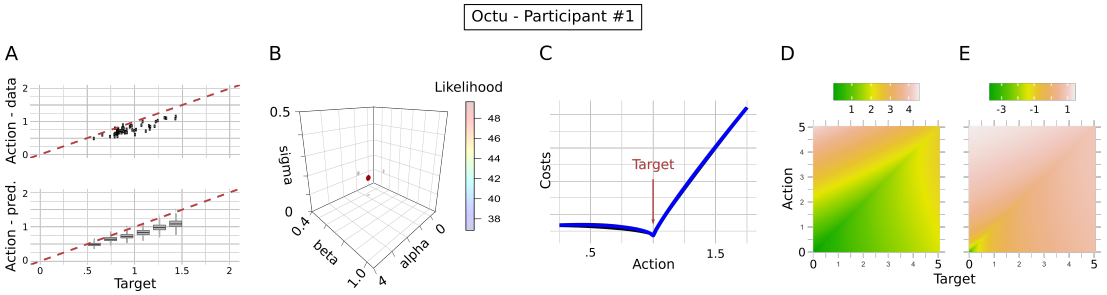

Figure 51: **Time reproduction data (Birkenbusch, Ellermeier, and Kattner, 2015).** Responses of one examplary participant from the time reproduction experiment and the corresponding parameter inference.

In this time reproduction task all 11 participants showed an overall mean undershot, ranging from .03 to .4s. One apparent cluster in figure 47 C) is formed at $\alpha = .83$ and $\beta = .54$, describing the ubiquitous undershots across all subjects. Despite her low action variability ($\sigma_{a,1} = .11$) a strongly pronounced undershot can be seen exemplary for the cluster in participant #1 ($\mu_{err,1} = .19s$, $\alpha_1 = .81$, $\beta_1 = .53$), in figure 51. Here this asymmetry in cost functions however might more likely to be linked to a lack of patience in reproducing the asked time intervals than to a physiological effort as in the force reproduction task.

Undershots in distance reproduction

In the fifth data set we investigate undershots in a walking distance reproduction task of Sun et al., 2004.

All 12 participants undershot their target on average in a range from .04 to 5.09m. In figure 47 C) one clear cluster can be found at $\alpha = 1.5$ and $\beta = .6$ and its asymmetry in costs can explain participants' tendency to undershoot the target even with the low average action variability in the cluster ($\sigma_a = .14$). In figure 52 one representative participant's responses and inferred parameters are shown ($\mu_{err,1} = 3.59m$, $\alpha_1 = 1.52$, $\beta_1 = .56$).

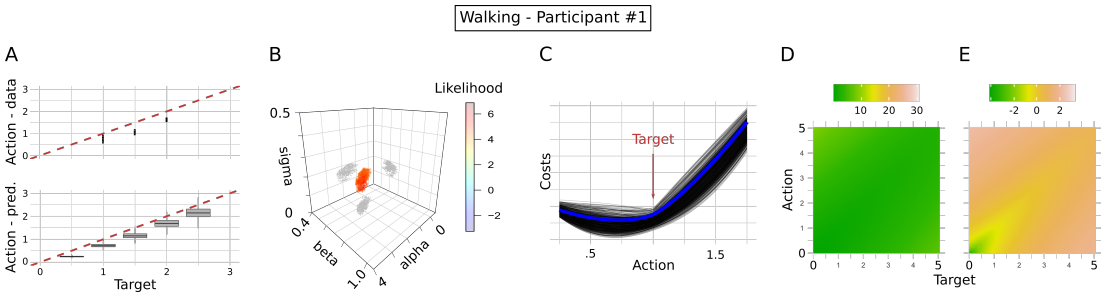

Figure 52: **Walking reproduction data (Sun et al., 2004).** Responses of one examplary participant from the distance walking experiment and the corresponding parameter inference. Note that target and response values are shown here as tenth of meters.

6.4 LOG-NORMAL VARIABILITY AND WEBERFRACTIONS

One of the most used concepts in the description of variability of subjects in psychophysic experiments is the concept of weberfractions. However, this concept is based on the assumption of normally distributed variables that are linearly scaled for larger deviations at higher magnitudes of stimuli. As discussed above, the use of log-normally distributed variables offers several advantages, not least the more realistic interpretation of strictly positive values, but leads to a lack of comparability with results from previous studies. Here we additionally postulate a possibility to transform inferred uncertainties σ_{log} of log-normal distributed variables into weberfractions. Following the transformation formula to calculate weberfractions from uncertainties in graphical models with log-norm distributed variables will be derived. Consider a random variable x in the linear space that is distributed log-normal, then by definition its logarithm X is normally distributed (see figure 53 A)):

$$X \sim \mathcal{N}(\log(x), \sigma) \tag{32}$$

In order to find a criterion to tell two signals apart we can use signal detection theory. In a first step we determine the probability distribution of difference between X_2 and X_1:

$$P(X_2 > X_1) = P(X_2 - X_1 > 0) = \mathcal{N}(\log(x+\Delta) - \log(x), \sqrt{2}\sigma) \tag{33}$$

Here we replace x_2 and x_1 with $x+\Delta$ and x as we are interested in the increment Δ, necessary to perceive a difference. The probability Θ that X_2 is perceived as bigger is then described by the cumulative distribution function $\Phi(x)$:

$$\Phi\left(\frac{\log(x+\Delta) - \log(x)}{\sqrt{2}\sigma}\right) = \Theta \tag{34}$$

We can now solve this equation for $\frac{\Delta}{x}$ and obtain the formula for calculating the weber-fraction based on the log-normal variability and Θ:

$$\frac{\Delta}{x} = e^{\sqrt{2}\sigma\Phi^{-1}(\Theta)} - 1 \tag{35}$$

Using this transformation direct comparisons of inferred posterior values of uncertainty coming from a log-normal distribution with old values for weberfractions from the literature are possible.

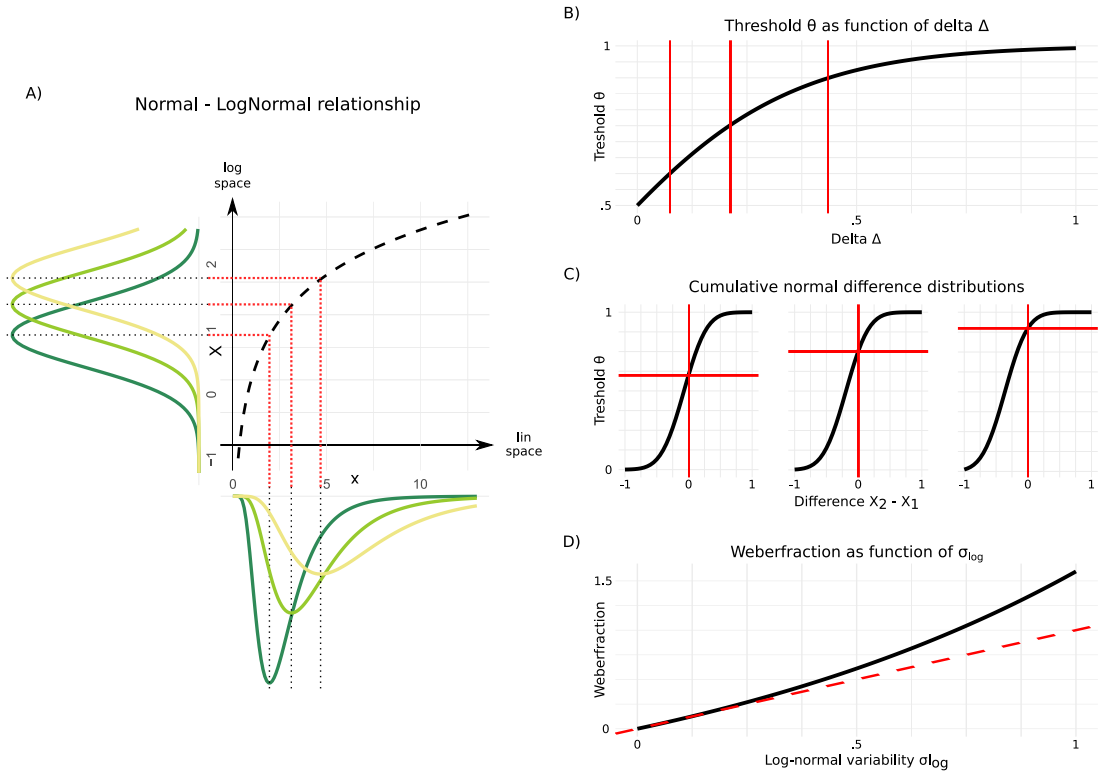

Figure 53: **Weberfraction derivation from log-normal distributions.** A) Relationship between the normal and log-normal distribution, enabling the use of classic signal detection theory for two normal distributions. Three exemplary log-normal distributions are shown on the x-axis in the linear space with their log-transformed counterparts on the X-axis in the log-space. Logarithmic function is shown as dotted black line. B) Visualization of equation 34. Detection threshold Θ as function of difference between two stimuli Δ for given stimulus at $x = 1$ and uncertainty $\sigma = .2$. Red lines mark values of Δ that lead to a threshold Θ at .6, .75 and .9. C) Three resulting cumulative normal difference distributions for three different stimulus differences Δ at .075, .212 and .435 leading to corresponding aforementioned threshold level Θ at .6, .75 and .9. D) Weberfraction as a function of log-normal variability σ as shown in equation 35 for the common threshold level Θ at .75 (Wichmann and Jäkel, 2018). Discrepancy between weberfractions and inferred log-normal variabilities σ diverges for higher values of uncertainty.

6.5 DISCUSSION

Variability and Weber-Fechner

If values can be assumed to be represented on a logarithmic scale is debatable (Cantlon et al., 2009; Dehaene et al., 2008; Lejeune and Wearden, 2006; Yi, 2009). However, direct implications of properties specific to the log-normal distribution like the natural integration of Weber-Fechner like scaling (Battaglia, Kersten, and Schrater, 2011; Neupärtl, Tatai, and Rothkopf, 2020) and the strictly positive values speak strongly in favor of using them for modeling instead of over-simplified Gaussians. Especially for perceived stimuli and responses positive values must be assumed. By choosing log-normal distributions negative values can be elegantly excluded. For resulting values of variability in these distributions we have proposed a transformation to further compare these values with weberfractions in the literature. It is noticeable that discrepancies between log-normal variability and weberfraction start to rise for higher levels of uncertainty. For uncertainties $\sigma < .1$ the difference is negligible.

Explanation of undershots

Our proposed MCMC framework deals with the interaction of uncertainty in perception and action with the costs of outcomes and the effort to generate them on the one hand and with an explanation for the pervasive phenomenon of undershots on the other hand. But what other concepts are there that try to explain undershots? In addition to experiments with pure undershots, overshots for shorter stimuli were also found in some experiments. In these experiments undershots and overshots have been explained as a result of a regression and range effect when learning statistics of an experiment while performing (Petzschner and Glasauer, 2011; Petzschner, Glasauer, and Stephan, 2015). More precisely, it has been argued that subjects gradually learn the a priori distributions of the stimulus variables in an experiment and are thus biased for smaller and bigger stimuli towards the mean. Such behavior was mainly observed in human navigation and path integration (Loomis et al., 1993; Petzschner and Glasauer, 2011), but also in time estimation (Sims and Gray, 2008). However learning a prior and thus develop a bias can not explain behavior when there is only an undershot or when participants can not learn these priors due to the experimental design or strong previously learnt prior beliefs. In the area of motor behavior, however, there were other explanations especially for the frequent occurrence of undershots: overshooting limb movements are more energy-costly (Elliott et al., 2004; Oliveira, Elliott, and Goodman, 2005) and limb movements show increased costs for second corrective movements, which have to change direction strongly or even diametrically (Elliott et al., 2010, 2004; Lyons et al., 2006). These second corrective movements with higher costs for inverted direction however can not explain undershots in non-sequential tasks and maximizing mechanical advantages only applies in the modest number of these explicit motor behavior experiments. Nevertheless the idea of introducing costs scaling continuously with the effort is useful, e.g. when making greater limb movements (Elliott et al., 2004), longer lasting gaze switches (Harris, 1995) or enduring longer without blinking (Hoppe, Helfmann, and Rothkopf, 2018), and is in accordance with our implementation of effort costs, which can be emphasized using more asymmetrical cost functions like in column 4 in figure 47.

In order for people to be able to optimally take uncertainties into account, they need

to be aware of them in the first place. How far such an endogenous knowledge goes is debated in meta cognition, however time-discrimination experiments with rats (Foote and Crystal, 2007), memory experiments with macaque monkeys (Hampton, 2001) and experiments about human movement planning and interval timing (Balcı et al., 2011; Hudson, Maloney, and Landy, 2008; Sims and Gray, 2008) deliver evidence that mammals are able to consider their own uncertainty, at least to some extent.

Taken together, our proposed framework is a further step towards understanding the complex interlocking of perception and action and provides a possible explanation for the recurrent and pervasive phenomenon of undershots in human and animal behavior throughout the literature.

7

NATURALISTIC INTERACTIONS ELICIT INTUITIVE PHYSICAL BEHAVIOR

7.1 INTRODUCTION

Common to probabilistic models of intuitive physical reasoning is a rather disembodied approach to cognition: inference about physical scenarios is based on probabilistic representations of physical quantities (Sanborn, Mansinghka, and Griffiths, 2013), symbolic representations of objects and relationships (Ullman et al., 2018), or geometric descriptions with physical properties (Battaglia, Hamrick, and Tenenbaum, 2013), which are thought to be extracted from two-dimensional computer rendered images of scenes. Reasoning unfolds in mental models akin to physics game engines (Ullman et al., 2017) or by generating programs through probabilistic programming (Ullman et al., 2018). In line with this view, participants' responses mostly consist of binary judgements (Kubricht et al., 2016; Sanborn, Mansinghka, and Griffiths, 2013) or estimation of a single parameter (Battaglia, Hamrick, and Tenenbaum, 2013). Very rarely subjects can interact with scenes at all, but then by simulating different manual interactions and tool use with a computer mouse (Smith, Battaglia, and Vul, 2013) or by simulating a touch by clicking with a computer mouse on simulated two-dimensional objects rendered on a computer screen (Bramley et al., 2018; Smith, Battaglia, and Vul, 2018) instead of through visuomotor actions, as in every-day situations. Given evidence that cognition is at least partly grounded in mechanisms for interaction with the environment, that is, mechanisms of sensory processing and motor control in specific situations (Anderson, 2003; Foglia and Wilson, 2013; Wilson, 2002), this raises the question, whether intuitive physical reasoning may take advantage of embodied representations. Accordingly, we hypothesized that the mode of visuomotor interaction in an intuitive physical reasoning scenario may affect the responses, whether it is a button press simulating an interaction or a multimodal visuomotor interaction with physical objects.

Here, we consider two variants of a visuomotor control task to investigate whether naturalistic, multimodal, embodied interactions elicit the same physical behavior as less representative, more abstract task designs. Subjects were asked to propel pucks into a target's bulls-eye positioned at different distances across trials. In a first condition, the scene was rendered on a monitor and the interaction was achieved through a button press on a keyboard, as in (Neupärtl, Tatai, and Rothkopf, 2020). In a second condition, subjects were immersed in a virtual environment viewed through a head-mounted display and interacted with a real hockey puck, sensed its weight, and slid it on a real table. The visual displays were adjusted in exploratory experiments to result in comparable uncertainties about the target's distance. The physical simulations were identical. In both conditions, subjects were not given any feedback about the puck's movement and final position to ensure that they could only rely on their a priori internal model and their beliefs about physical factors, such as the table's friction coefficient and the laws of motion.

7.2 METHOD

7.2.1 *Participants*

Sixteen subjects had performed the experiment using a keyboard and computer screen, as described in (Neupärtl, Tatai, and Rothkopf, 2020). Sixteen additional subjects were recorded in the Virtual Reality (VR) based experiment. All participants were undergraduate or graduate students recruited at the Technical University of Darmstadt, who were paid 10 € or received course credit for participation. All experimental procedures were carried out in accordance with the guidelines of the German Psychological Society and approved by the ethics committee of the Technical University of Darmstadt. Informed consent was obtained from all participants prior to carrying out the experiment. All subjects had normal or corrected to normal vision. One participant from the keyboard condition was excluded from further analysis, because variability of estimated mass beliefs was more than two standard deviations larger than those of the other participants.

7.2.2 *Apparatus*

In the keyboard condition participants saw the scene containing the puck and the target displayed on a computer monitor and responded through button presses on a keyboard. All trials were rendered using Unity. Participants were seated so that their eyes were approximately 40 cm away from the display and the monitor subtended approximately 66° of visual angle horizontally and 41° vertically. For more details see (Neupärtl, Tatai, and Rothkopf, 2020).

The haptic condition was also implemented in Unity but using the SteamVR plugin and the HTC Vive Pro Eye head-mounted display (HMD) with a resolution of 1440 x 1600 pixels per eye and a field of view of 110° horizontally and 110° vertically. For motion tracking purposes the Qualisys Motion Tracking system with six 6+ cameras was used. To easily change the weight of the object to be propelled we custom built a puck by drilling multiple holes into the puck and filling them with different metal weights, resulting in a mass of 0.25 kg or 0.35 kg. Drill holes were covered with a 3D printed plastic covering staffed with four passive markers. Elastic fabric was fixed on the table with bench vice to protect the motion tracking cameras and to facilitate trial resets. Thus, the puck was restricted to a smaller area, allowing the subject to grab it by themselves at the beginning of a trial.

7.2.3 *Experimental design*

In both experiments participants were instructed to slide pucks into the bulls eye of a target, see figure 54. The two experiments however differed in the way subjects were able to make the puck slide. In the keyboard condition the puck was a two-dimensional rendition on a computer screen. Subjects carried out 50 trials in which the target was placed at distances drawn uniformly at random between 1m and 5m, where the entire scene displayed on the monitor was 7.5m in the vertical dimension. The duration of the key press determined the duration of the impact of a constant force, i.e. the change in momentum. Participants were told that they were able to adjust this force, which initially was going to accelerate the puck and thus the initial velocity of the puck, by the duration of their press. However, they were not explicitly

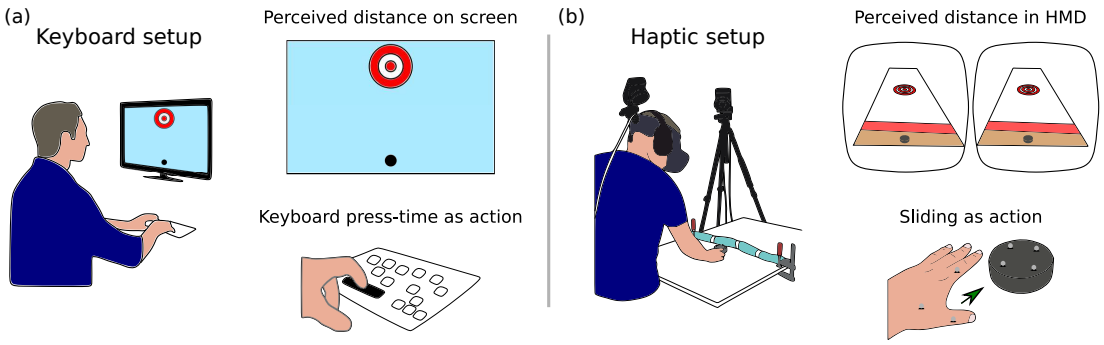

Figure 54: Comparison of both experimental setups. (a) In the keyboard condition participants saw the target and the puck on a computer screen and adjusted the momentum acting upon the puck via press-time of a keyboard button (Neupärtl, Tatai, and Rothkopf, 2020). (b) In the Virtual Reality setup participants viewed the scene including the distance to the target in a Head Mounted Display (HMD) and were able to grasp the actual puck and slide it naturally on a table.

told about the linear relationship between the press time and the initial velocity. In contrast, participants in the haptic condition were able to pick up the custom built hockey puck and pushed it in 100 trials on a table with their own hands. The objects in the VR scene were carefully designed to match their actual dimensions, the table on which the real pucks were slid and the puck itself. The target was placed at distances drawn uniformly at random between .3m and 2.5m. Subjects were randomly assigned a puck with a mass of either 0.25 kg or 0.35 kg. Here, the puck and the bulls eye were shown in VR using an HTC-Vive HMD.

In both setups, subjects did not obtain any feedback about their action by blanking out the resulting movement as well as the final position in which the puck came to a stop. For this purpose the screen turned dark for half a second in the keyboard condition after participants released the key and thus the puck. In the haptic condition, the field of view was not completely darkened for safety reasons. Instead, both the puck and the target were blanked out. Thus, the table was still visible to avoid dizziness. Explorative trials were carried out prior to obtaining the experimental data to ensure that the perceptual uncertainty about the targets' distances were comparable across the two experimental setups.

7.2.4 *Physical description of sliding task*

To be able to compare the actions propelling pucks between both experiments, it is necessary to find a single description of the physics governing the puck's motion. Besides the distance to the target, the impulse that subjects intend to use p_{int} to propel the puck to the target is the decisive physical quantity. When adjusting the necessary impulse to reach the target's bulls eye both participants' belief about the necessary speed v_{int} and their belief about the puck's mass m_B play a crucial role:

$$p_{int} = m_B \cdot v_{int} \tag{36}$$

Now, both experiments differ in the way how participants can propel the puck and control the resulting impulse. In the case of the haptic condition participants could directly interact with the puck and accelerate it to the intended velocity by controlling the release impulse with respect to the perceived mass, see eq.37(a). In the keyboard

condition, subjects could control the impulse via the duration of a key-press. Here the magnitude of the force F and the puck's mass m_B were abstract and hypothetical quantities, unknown to the participant, and can be summarized as a constant variable C_1, see eq.37(b):

$$v_{int} = \frac{p_{int}}{m_B} \tag{37a}$$

$$v_{int} = \frac{F}{m_B} \cdot t_{key} = C_1 \cdot t_{key} \tag{37b}$$

This means, that the use of haptic interaction in the haptic condition enabled a direct naturalistic control of the intended velocity compared to the indirect abstract control in the keyboard condition. The magnitude of the intended velocity v_{int} however needs to be chosen in both scenarios depending on the final distance to be covered x and on the influence of the decelerating friction, i.e. the product of the friction coefficient μ_{fr} and the gravitational acceleration g:

$$v_{int} = \sqrt{2 \cdot \mu_{fr} \cdot g \cdot x} = C_2 \cdot \sqrt{x} \tag{38}$$

The friction coefficients are unknown to participants in both conditions and their product with the gravitational accelerations can be summarized as constant variable C_2, since both variables do not change during the experiment. Because subjects never obtained feedback about the movement of the puck, they had no possibility to infer the values of these constants. This has the consequence, that even if subjects consistently acted under the belief of a specific gravitational acceleration, mass, and friction coefficient, these values are interdependent. To allow recovering subjects' beliefs, we therefore can set two of these values to constants. In the haptic condition we set the friction coefficient to the true value measured for the table and the true gravitational constant. Note that this does neither affect the physical relationship described by either Newtonian physics or the linear heuristic nor the variability observed in participants' actions, upon which our conclusions rest.

In the keyboard condition, subjects had no opportunity to infer either the initial force, nor the coefficient of friction or the puck's mass. Note however, that these constants all enter the computation of the intended velocity linearly. Thus, if subjects acted under a consistent belief for these quantities, we can set two of these values to constants an investigate the variability of the third quantity. To be able to compare the inferred values across both conditions we set the friction coefficient and initial force so as to result in puck masses with the same mean as the masses in the haptic condition. Note that this does not alter the conclusions that can be drawn from the inferred variables, as this constitutes only a linear scaling in the masses. Subjects' uncertainty about these environmental variables can still be captured by the spread of the posterior over the mass beliefs, which is then compared across subjects. The important point here is that these constraints do not affect the assumptions about the basic relationship between intended velocity and distance to the target and thus still allow the computational analysis of the two experiments based on probabilistic models.

Taken together, two experiments were set up to study human behavior in the physics-based task of sliding an object, in this case a puck, as accurately as possible across a given distance into a target under the effect of friction, without feedback. The experiments differed primarily in the form of the available action: via a button press in the keyboard condition and by pushing a real puck by hand in the haptic condition. In the following, the effects of this difference on the behavior of subjects

will be investigated based on participants' beliefs as estimated by a Bayesian model of the interaction task.

7.2.5 *Bayesian graphical model of physical interaction*

The Bayesian model depicted in figure 55(a) considers the subjects' actions from the experimenter's point of view. This means that variables that were experimentally measurable, such as the distance to the target in the display and the actual magnitude of the sliding action, are included as observed variables in the model. Variables that describe the physical assumptions and perceptual beliefs of the subjects are unknown to the experimenter, and therefore unknown in the model. Thus, this model constitutes a departure from an ideal observer model in that the subject's beliefs about task relevant quantities are explicitly modeled. This in turn requires using Bayesian inference to infer these latent beliefs of the subjects based on the model structure and the observed experimental data. In figure 55, known observed nodes are shown in gray and unknown latent ones are shown in white.

The perception of the actual distance x is naturally subject to sensory uncertainty. This sensory uncertainty is modeled by the parameter σ_x of the Log-Normal distribution of the perceived distance x_{per}. Given her perception, the subject internally decides about a velocity v_{int} required to let the puck slide to the target and stop there. However, the subject is now dependent on her internal model, which describes the relationship between target distance and initial velocity. Here we consider two candidates as possible internal models describing the relationship between the distance x and necessary speed v_{int}: a linear and a square root relationship:

$$v_{int} \sim x \tag{39}$$

$$v_{int} \sim \sqrt{x} \tag{40}$$

The linear relation in eq.39 corresponds to an approximate heuristic and the square root relation in eq.40 is the relationship prescribed by Newtonian physics.

Note that the other physical parameters of the environment such as the coefficient of friction, the gravitational constant, and the force in the keyboard condition were unknown to the participants throughout the experiment. Since subjects never saw the puck gliding, decelerating, and stopping after being propelled, they could not calibrate the impulse with which they push the puck nor the coefficient of friction describing the gliding properties of the surface. Thus, the aforementioned constant variables C_1 and C_2, used to summarize these environmental variables, are not included in the figure, as their values are fixed and they no longer functionally affect the inferences, of course apart from their influence on the magnitude of the estimates.

The velocity v_{int} estimated in this manner, together with their belief about the mass m_B of the puck to be accelerated, now guides the subject to produce the necessary impulse p_{int}. Her belief about the mass is relevant since heavier objects need larger impulses to reach the same velocity. The finally measured impulse p is the result of the intended impulse p_{int} and the action variability σ_p of the subject during the execution of the control action.

The basic Bayesian impulse model in figure 55(a) is based on these assumptions, with the linear and Newtonian models differing only in the calculation of the intended velocity v_{int}. While keeping in mind that variable p still denotes the puck's momentum whereas p(x) denotes the probability of a variable x, the joint posterior probability of the observed data d and all parameters Θ expressed by this model can be written as follows:

$$p(d, \Theta) = p(x)\, p(\sigma_x)\, p(x_{per}|x, \sigma_x)\, p(m_B)\, p(p_{int}|x_{per}, m_B)\, p(\sigma_p)\, p(p|p_{int}, \sigma_p)$$

and accordingly the posterior probability of the parameters $p(\Theta|d)$ given the model and the data d can be computed using Bayes' theorem:

$$p(\Theta|d) = \frac{p(\sigma_x)\, p(x_{per}|x, \sigma_x)\, p(m_B)\, p(p_{int}|x_{per}, m_B)\, p(\sigma_p)\, p(p|p_{int}, \sigma_p)}{p(p|x)}$$

For comparison of the two potential model candidates we used the *product space method* (Lodewyckx et al., 2011). For this purpose, a hierarchical model is used in which both models are included and an index variable determines which model is selected to explain the data. All inferences were carried out in R via Markov Chain Monte Carlo using the JAGS package (Plummer, 2003).

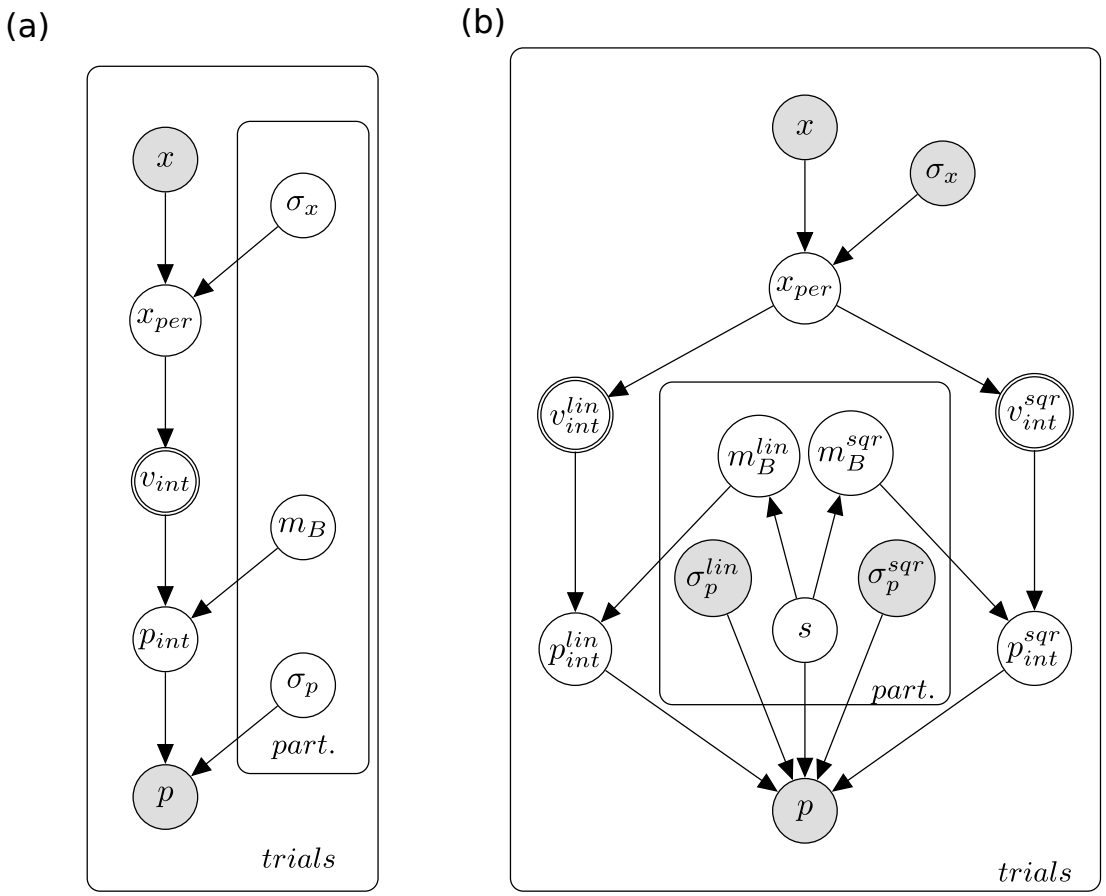

Figure 55: Basic Bayesian interaction model (a) and corresponding nested model (b) for the product space method. Shaded nodes, e.g. the actual distance x and impulse p in the basic impulse model, are observed and known to the experimenter. White nodes are latent and need to be inferred. Participants' observation of the actual distance x is inevitably subject to perceptual uncertainty σ_x and thus leads to a noisy percept x_{per}.

In figure 55(b) the index variable s selects which model is used to describe the data for each participant. Whenever one model is selected on an iteration, the parameters of this model are updated based on the experimental data. Because the selected model now describes the data better on the basis of the updated parameters, the alternate model would become less likely to be selected on subsequent iterations. To avoid this, we adopt the common technique of sampling the parameters of the unselected model by an already optimized pseudo-prior. This is also why there is not only an arrow from s to p, indicating the model selection process in each iteration, but also arrows to m_B^{lin} and m_B^{sqrt} describing the influence of the indicator variable s whether the mass is sampled from the prior or pseudo-prior. The perceptual uncertainties σ_x and action variabilities σ_p as well as the parameter of those pseudo-prior for the mass beliefs m_B for each participant were determined in advance by single model runs for both models. Based on the posterior odds of s one can calculate the Bayes factors supporting one or the other model. For a more detailed explanation of the method, see (Lodewyckx et al., 2011).

7.3 RESULTS

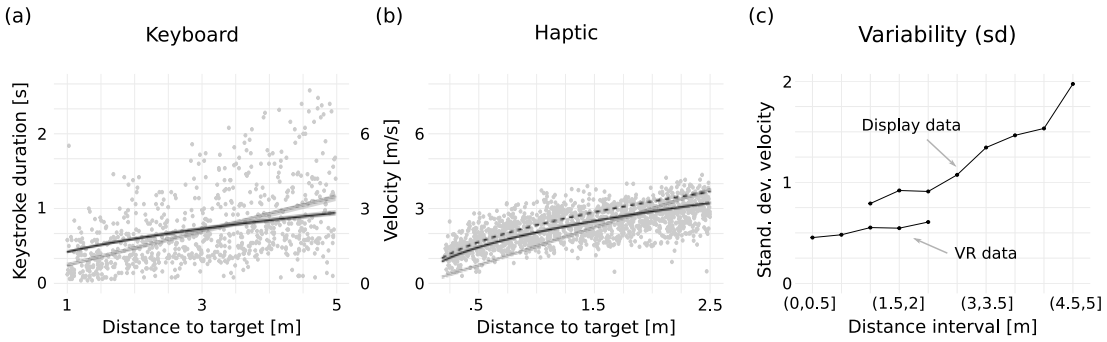

Figure 56: Actions as function of the initial distance to the target for the keyboard (a) and haptic (b) conditions across all participants. Best generalized additive model fits based on maximum likelihood are shown for a linear and a square-root relationship in light and dark grey, respectively. For the data from the haptic condition, the ideal curve based on the actual weight of the puck and friction coefficients is also drawn as dotted line. (c) Estimated variability of participants' actions as function of distance to target.

First, we can compare subjects' raw responses in the two conditions, i.e. the press times in the screen condition and the puck's release velocity in the haptic condition. These data are shown in figure 56 as function of the initial distance of the target aggregated across subjects and trials. In the keyboard condition, subjects were constrained to interact with the keyboard while having only very vague beliefs about the puck's mass and the friction coefficient. Subjects had additional uncertainty about how the duration of a key press translates to an initial velocity, i.e. the strength of the acting force. In the haptic condition, on the other hand, subjects were able to grasp and accelerate the puck with their own hands, giving them a sensory measurement of the puck's mass through haptic feedback and the necessary momentum. In both experiments, participants did not obtain any sensory feedback about the motion trajectories nor about the endpoint of the puck's motion. Therefore, participants could not update their beliefs about the friction coefficient.

To compare subjects' responses, we transformed subjects' press times in the keyboard condition to initial velocities according to equation $v = \frac{F \cdot t}{m}$, see right axis labeling in the first panel of figure 56. Because subjects were never able to update their beliefs about the initial force and the coefficient of friction and these quantities both enter the target velocity linearly, we can rescale the duration of button presses linearly according to equation $\frac{F}{m} \approx 3$, to be within a comparable range of velocities. Accordingly, the rescaling can be interpreted as setting specific values for force and mass. The values were chosen ($m = .3kg$, $F = .9N$) so that both graphs are in a comparable range, see first two panels in figure 56, and to allow a comparison of masses between the keyboard and haptic conditions, see first two panels in figure 58. The graph clearly illustrates the larger variability in subjects' actions in the keyboard condition compared to the haptic condition. To illustrate differences in variability, the third panel in figure 56 shows standard deviations for intervals binned over distance for both experiments, ranging from 0.79 to $1.97 \frac{m}{s}$ in the keyboard and 0.45 to $0.61 \frac{m}{s}$ in the haptic condition. The plots also demonstrate the in response variability with increased action magnitude, which was captured by the log-normal distribution in the Bayesian interaction model.

7.3.1 *Subjects' beliefs*

Based on the Bayesian generative model shown in figure 55(a) we are able to infer the perceptual uncertainty σ_x, the action variability σ_p and the mass m_B in the Newtonian model or the linear factor in the linear heuristics model for each individual subject. Modes of posterior distributions of perceptual uncertainty σ_x as well as action variability σ_p are plotted in figure 57 both under the assumption that participants employed a linear heuristic model or a Newtonian physics model. The plots distinguish the putative internal model by the color of data points and the two conditions by the shape of data points. Which model better accounted for an individual's data was decided based on the resulting Bayes-factors obtained through the nested Bayesian model in the product-space method, see below.

Figure 57(a) compares the perceptual uncertainties inferred by the linear heuristics model (x-axis) and the Newtonian model (y-axis) for each subject in both conditions. Through preliminary explorative trials, the experimental setup of the two conditions were adjusted to have comparable perceptual uncertainties about the target's distance. Indeed, inferred perceptual uncertainties do not differ significantly between the two conditions (paired Wilcoxon signed rank test, $V = 254$, $p = 0.8609$). We also tested, whether the perceptual uncertainties inferred from data under the two putative internal models differed. No significant difference in inferred perceptual uncertainties was found between the linear heuristics model and the Newtonian physics model (paired Wilcoxon signed rank test, $V = 253$, $p = 0.8465$).

By contrast, inferred action variability was clearly different when comparing the linear heuristics and the Newtonian models in both experimental conditions. Figure 57(b) shows the corresponding plot of inferred action variabilities, demonstrating the separation of the data of the two conditions. Modes of the inferred action variabilities significantly differ between both, the linear and the Newtonian model, when analyzing the keyboard condition's data (pairwise Wilcoxon signed rank test, $V = 112$, $p = .02567$) as well as for the haptic condition's data (pairwise Wilcoxon signed rank test, $V = 0$, $p < .001$, both p-value adjusted after (Benjamini and Hochberg, 1995)).

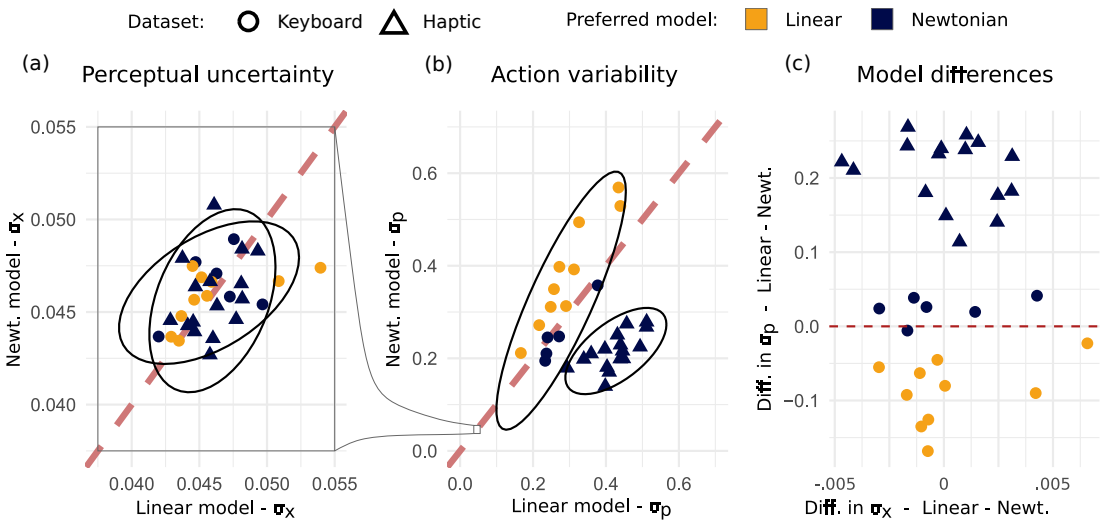

Figure 57: Comparison of inferred perceptual uncertainties and action variabilities for both conditions and models. (a) The x-axis shows the perceptual uncertainty σ_x inferred using the linear model and the y-axis the one inferred using the Newtonian model. (b) Inferred values for the action variability σ_p, again with values on the x-axis for the linear and on the y-axis for the Newtonian model. (c) Differences between linear and Newtonian model inferences for σ_x and σ_p.

In these plots, data points beneath the red dotted line, which indicates the equality of variability in both models, require less additive noise to be explained with the Newtonian model compared to the linear heuristics model. The results of both inferences of perceptual uncertainty and action variability are plotted together in figure 57(c). First, all our participants' behavior in the haptic condition was better accounted for by the Newtonian model while most of the participants' behavior was better accounted for by the linear heuristics model in the keyboard condition. Second, while perceptual uncertainties were comparable across the two putative internal models, the linear heuristics model required higher levels of additional noise to account for our subjects' actions in the haptic condition.

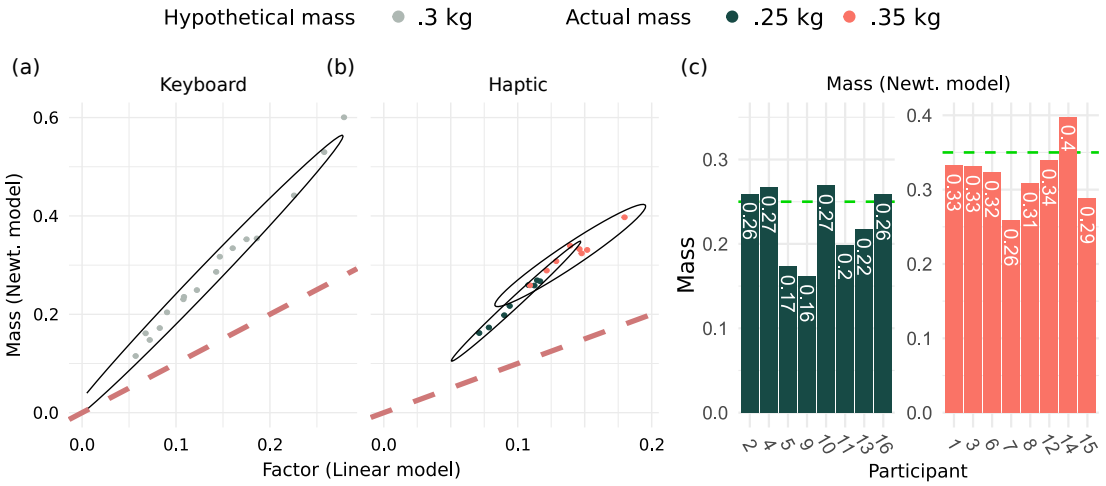

Figure 58: Comparison of inferred mass beliefs (Newtonian model) and linear factors (linear heuristic) for both conditions and models. (a),(b) The x-axis shows the linear factor inferred using the linear model and the y-axis the mass inferred using the Newtonian model for the two conditions, respectively. (c) Individually inferred modes of the mass posterior compared to the actual mass of the used puck in the haptic condition.

The Bayesian generative model also allows inferring individual participants' internal beliefs about the masses of the pucks. The inferred modes of the mass posteriors for each participant are plotted in figure 58. As subjects in the keyboard condition never had access to any sensory measurement about the puck's physical properties, they had to entirely rely on their prior belief of its mass. Because the puck's intended velocity depends on its mass, the initial force, and the duration of the key press, we can use an arbitrary values for the three factors entering the intended velocity linearly. We adjusted the arbitrary factors in such a way, that the masses of the pucks in the keyboard condition had the same mean as the masses in the haptic condition. The resulting inferred masses across participants accordingly have a mean of 0.296kg and standard deviation of 0.138kg. By contrast, in the haptic condition a real puck and its mass was haptically accessible to participants. They were able to grab and lift the puck, and thus to adjust their belief accordingly. In both conditions, inferred linear factors for the heuristic model were smaller than the inferred masses in the Newtonian model (keyboard condition: Wilcoxon signed rank test, $V = 0$, $p < 0.001$; haptic condition: Wilcoxon signed rank test, $V = 0$, $p < 0.001$), accommodating the undershoots that subjects showed with increasing distance of the target, see figure 56.

In the case of the mass inferences of the Newtonian model in the haptic condition we can furthermore investigate, how close participant's estimates of pucks' masses were based on the available haptic cues. Figure 58(c) shows the posterior modes of the inferred masses for all participants. Remarkably, the mass estimates are quite close to the true values of 0.25 and 0.35 kg, with overall mean values for each puck being slightly smaller at 0.226 and 0.323 kg, respectively. This difference was significant for the heavier puck (One sample t-test, $t = -1.9243$, $p = .04786$) but not for the lighter one (One sample t-test, $t = -1.5744$, $p = .0797$). Subjects' behavior was well calibrated to the mass of the puck, as modes of the inferred posterior distribution of masses for the lighter puck are significantly smaller than for the heavy one, as expected (Welch two sample t-test, $t = -4.5967$, $p < .001$).

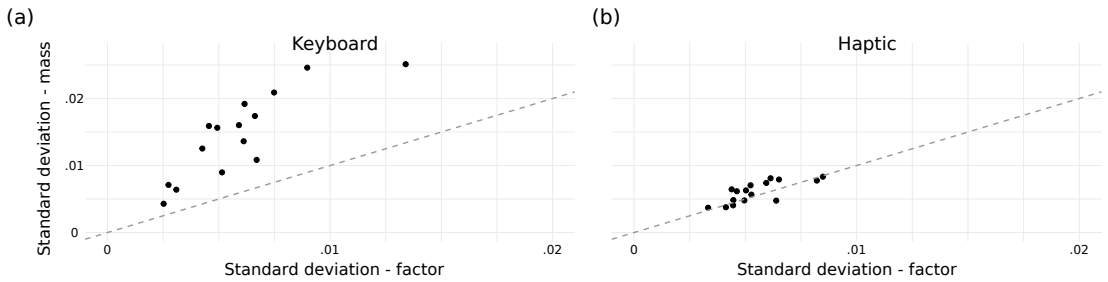

Figure 59: Standard deviation of posterior distributions over mass beliefs in the Newtonian model (y-axis) and linear factor (x-axis) in the linear model for the keyboard (a) and haptic conditions (b).

The Bayesian interaction model additionally allows investigating the variability in subjects' mass beliefs and linear factors across trials. The standard deviations of inferred posterior distributions for the masses in the Newtonian model and the linear factors in the linear model are plotted in figure 59. First, variability of standard deviations in mass beliefs is larger in the keyboard condition compared to the haptic condition (Levene's Test, $F = 29.833$, $p < 0.001$), reflecting the larger uncertainty about physical parameters in the keyboard condition. Secondly, standard deviations inferred with the Newtonian model are significantly higher in the keyboard condition than in haptic (Wilcoxon rank sum test, $W = 215$, $p < 0.001$), which is not true

for the linear model (Wilcoxon rank sum test, $W = 128$, $p = 0.3851$). This indicates a more precise computational description of participants' behavior with the Newtonian model and a higher consistency of subjects' decisions across the experiment in the haptic condition. However, note that in the keyboard condition variability for the linear factor according to the linear heuristic was on average only 1.08 times larger than in the haptic condition. Remarkably, for some subjects, this variability was even smaller in the keyboard condition compared to some subjects in the haptic condition. This clearly demonstrates, that subjects in the keyboard condition were pushing the key to propel the puck under a consistent belief about stable and lawful properties of the puck.

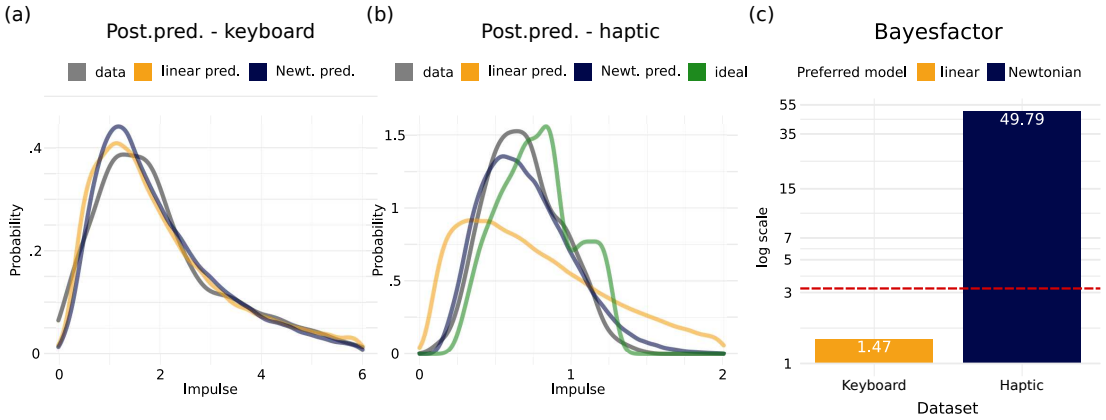

Figure 60: (a),(b) Posterior predictives for both models and data sets in comparison with the actual data and (c) Bayesfactors calculated based on the inferred posterior odds of the nested model. Ideal behavior shown as green distribution for the haptic condition. For a better overview, Bayes factors in (c) are plotted on a log scale. Red dotted line indicates threshold at 3.2 for substantial evidence that one model is superior to the other.

Finally, we evaluated the goodness of fit of the linear and Newtonian models to data from both experimental conditions. First, we obtained posterior predictive distributions of initial impulse for both conditions, as plotted in figure 60(a) and (b), respectively. While the linear heuristics model is slightly closer to the observed data in the keyboard condition, the Newtonian model is clearly closer to the data in the haptic condition. Note that the distribution of momentum based on the real weight of the pucks, the friction and the distance to the target, i.e. the ideal observer's distribution, is additionally shown in green. The two peaks of the ideal distribution are due to the two different masses used in both groups. One particular strength of probabilistic modeling via nested models lies in the possibility of model comparison. The Bayes factor favors the linear model in the keyboard condition, albeit with a value of 1.47 this is only anecdotal evidence. In stark contrast, the Bayes factor of 49.79 in the haptic condition shows very strong evidence for the Newtonian modes.

7.3.2 *Deviations from target based on subjects' beliefs*

Based on the inferred, best parameters for each subject we can calculate deviations from the target according to both models. Here we can compare the performance, i.e. the deviation from the target, as if the best fitting parameters would correspond to the actual environment. This allows investigating participants' consistency with regard to their own, possibly wrong, beliefs. As an example, for the Newtonian model we

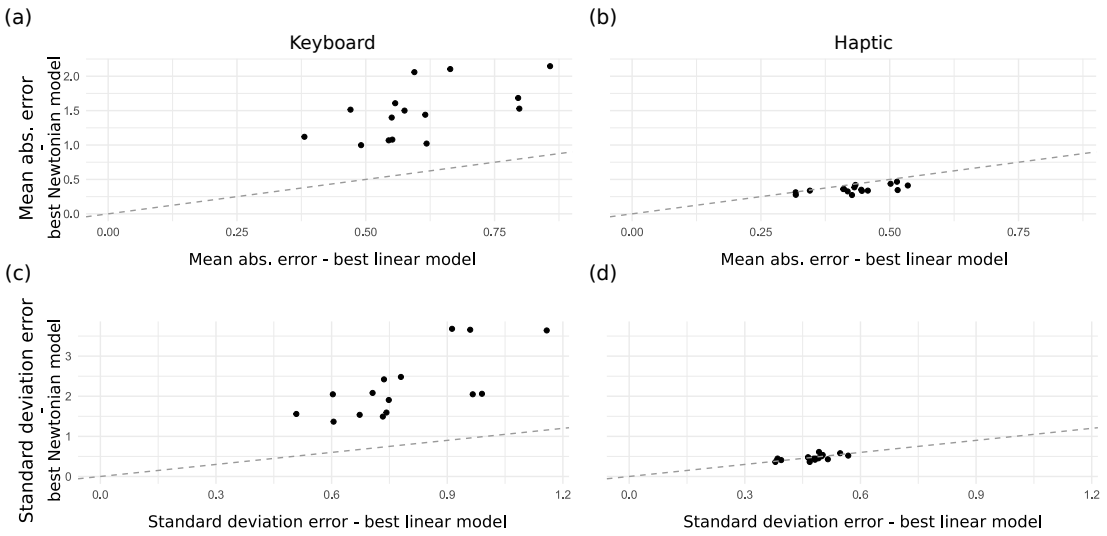

Figure 61: Mean absolute error and standard deviation of errors for each subject based on the best parameters for both models. Values for the best linear model are shown on the x- and for the best Newtonian model on the y-axis. Gray line marks equal values, above lie data of subjects with higher values for the Newtonian model and below with higher values for the linear model.

can compute how far the puck would have slid using their internal beliefs inferred from the Bayesian interaction model. Figure 61 (a) and (b) show the mean absolute error for the keyboard and haptic conditions, again in comparison for the Newtonian model and the linear heuristic. Comparing these errors between both models based on the keyboard condition shows significantly higher error values for the Newtonian model (Wilcoxon signed rank test, $V = 120$, $p < 0.001$; see figure 61(a)). Based on the haptic condition, however, mean absolute error values are significantly higher for the linear model (Paired t-test, $t = -5.8371$, $p < 0.001$; see figure 61(b)). Both results again emphasize the better fit of the linear and Newtonian model to the keyboard and haptic conditions data, respectively. Additionally, we can also compare these errors between both conditions for each model. As expected, the mean absolute errors in the keyboard condition are significantly larger than in the haptic condition, both for the linear model (Wilcoxon rank sum test, $W = 219$, $p < 0.001$) and for the Newtonian model (Wilcoxon rank sum test, $W = 240$, $p < 0.001$). This reflects the higher uncertainty about the pucks mass in the keyboard condition.

Similar to the mean absolute error, the standard deviation of the errors for the Newtonian model is significantly larger than for the linear model in the keyboard condition (Wilcoxon signed rank test, $V = 120$, $p < 0.001$; see figure 61(c)). However, for the haptic condition, there is no significant difference between both models (Paired t-test, $t = -0.6736$, $p = 0.5108$; see figure 61(d)). This suggests that the Newtonian model is not able to capture the complete range of participants' actions in the keyboard data, potentially caused by larger deviations at higher distances (see figure 56(a)). The fact that there is no difference for the haptic data set can also be well explained with reference to the data in figure 56(b). The systematic bias of the linear approximation with its undershots at near and overshots at far distances leads to the higher mean absolute error for the linear model in figure 61(b) but keeps the standard deviation at these lower values in figure 61(d). Taken together, these analyses further demonstrate not only the better fit of the linear model for the keyboard condition's data and the Newtonian model for the haptic condition's data, but also the increased consistency in subjects' actions within the more naturalistic haptic condition.

7.4 DISCUSSION

To investigate whether naturalistic, embodied, multimodal interactions influence visuomtor behavior involving the judgement of physical relationships between task relevant quantities, we designed an experiment in which subjects needed to propel pucks toward a target's bulls-eye, which was positioned at different distances across trials. While in the keyboard condition subjects saw the target displayed on a monitor and propelled a virtual puck with the duration of a key press, in the haptic condition the scene was seen through a head-mounted VR display and a real puck with one of two masses could be pushed on a tabletop. Importantly, subjects obtained no visual feedback about their actions in either condition. Therefore, subjects needed to rely on their prior beliefs about physical properties and their lawful relationships to accomplish either task. While in the keyboard condition the puck's mass, the force with which the duration of the key press was scaled, and the coefficient of friction were unknown, only the coefficient of friction was unknown in the in the haptic condition.

The task requires participants first to visually estimate the distance that the puck has to travel to reach the target's bulls-eye. Then, subjects need to propel the puck toward the target. For this, subjects need to choose the right impulse, which depends on the puck's mass, the coefficient of friction describing the surface on which the puck is sliding, and the gravitational constant. In the keyboard condition, the initial impulse was achieved through the length of a key press. Importantly, Newtonian physics prescribes a relationship that is linear in the puck's mass and grows with the square-root of the target's distance. Alternatively, subjects may employ a heuristic by which the momentum and therefore the initial velocity of the puck is scaled linearly with the distance to the target.

To be able to compare the behavior in the two conditions, a Bayesian model of the full interaction task including the perception of distance and the generation of a puck sliding action was devised involving perceptual uncertainty and action variability. The model was fit on an individual-by-individual and trial-by-trial basis under the hypothesis that subjects could either use a linear heuristic or the relationships prescribed by Newtonian physics. Results show very strong evidence that the multimodal naturalistic embodied condition elicited the square root scaling of initial velocity by the target's distance, which is consistent with Newtonian physics as demonstrated by a Bayes factor of 49.8. By contrast, the keyboard condition, in which subjects interacted with the puck through a key press on a keyboard, resulted in anecdotal evidence that the elicited behavior was better accounted for by the linear heuristic. Closer evaluation of Bayes factors at the individual subject level showed, that ten of the sixteen subjects in the keyboard condition were better accounted for by the linear heuristic while six were better accounted for by Newtonian physics. Analyses of the variability of actions and mass beliefs supported this conclusion additionally.

Further analyses of subjects' beliefs required constraining some of the constant parameters in the Bayesian interaction model. Because subjects never obtained feedback about the puck's dynamics, they were not able to infer the scaling of force in the keyboard condition or the coefficient of friction in both conditions. The gravitational constant, which also enters the computation of the initial velocity linearly, can be assumed to be known to subjects based on previous research (Hubbard, 2020;

Jörges and López-Moliner, 2017; McIntyre et al., 2001). The coefficient of friction in the haptic condition was set to the actual value of the table used. For the keyboard condition, the initial force and the friction coefficient were adjusted to result in estimated masses with approximately the same mean as in the haptic condition. Note that this does not alter the conclusions about the model used by participants but allows comparing the consistency and variability of participants beliefs. Indeed, subjects acted with remarkable consistency in the keyboard condition. Even though the keyboard condition elicited higher variability of beliefs about mass and linear factors ($\sigma_m = 0.138$kg, $\sigma_f = 0.065$kg) compared to the haptic condition ($\sigma_m = 0.068$kg, $\sigma_f = 0.029$kg), individual subjects showed highly consistent variability within their factor beliefs, being on average only 1.08 times larger than in the haptic condition, see figure 58,59.

A first potential concern might be that interacting with a keyboard could influence participants to use a particular non-linear function. That this is unlikely the case stems from the fact that ample research has employed button presses on keyboards to investigate human time perception and timing of actions, e.g. (Buhusi and Meck, 2005). The results of these studies show that people seem to be quite unbiased in controlling their button press duration and adhere to Weber's Law in that the standard deviation of press times scales linearly with duration. Some studies have reported anchoring effects leading to overshots at smaller durations and undershots at larger durations, but these effects are also described as linear (Jazayeri and Shadlen, 2010). This suggests, that the scaling of press times in the keyboard condition were not caused by an idiosyncratic mapping pertaining to the pressing of buttons on a keyboard, particularly, because some participants' press times were better explained by the linear and others' by the square-root relationship.

One may argue that the differences between the two conditions arise because of the difference in the mode of visual presentation of the scenes. Indeed, several previous studies have provided evidence, that uncertainty about physical parameters depends on the mode of presentation. Adding motion cues (Kaiser et al., 1992) or auditory cues (Gerstenberg, Siegel, and Tenenbaum, 2018) to stimuli used in probing intuitive physical reasoning has been shown to reduce uncertainty about physical parameters. While in the present experiments subjects saw the puck and the target displayed on a two-dimensional screen in the keyboard condition, they had access to depth cues present in the stereoscopic head-mounted display in the haptic condition. But, importantly, preliminary explorative trials were used to match the perceptual uncertainties across the two conditions. This was furthermore confirmed by the perceptual uncertainties estimated using the Bayesian interaction model. Indeed, no significant difference was found for the perceptual uncertainties between the two conditions. Thus, we do not find evidence that the mode of visual presentation was the cause for the difference in adopted strategies.

A further concern may be, that participants' uncertainty about the mass, the coefficient of friction, and the mapping from press times to initial velocities in the keyboard condition led them to use random press times that only in the aggregated data suggest a linear relationship with the initial target distance. Again, the analyses with the Bayesian interaction model suggest otherwise. By estimating subjects' implicit beliefs about the puck's mass or equivalently linear factor on a subject-by-subject basis, one can infer the variability in beliefs trial-by-trial. This analysis revealed, that in the key-

board condition, standard deviations of subjects mass beliefs were on average only about 2.4 times as large as in the haptic condition and for some subjects even comparable between the two conditions. This is a remarkable result, as it provides evidence, that subjects consistently used a mass belief to propel the puck towards the target in the haptic condition.

A very much related question is whether subjects may have selected the correct physical relationship only by virtue of touching a real puck and thereby sensing its mass. The ability to grasp and hold the real puck certainly reduced subjects' uncertainty about the pucks' weights in the haptic condition. This was confirmed by participants' inferred mass beliefs. Nevertheless, as state above, the variability in the factor equivalent to mass in the linear relationship in the keyboard condition was only 1.08 times larger than the value in the haptic condition, showing that subjects used a consistent mass belief in their actions in the keyboard condition, in which they could not sense a puck's mass. Thus, it seems rather unlikely, that this differences in terms of the uncertainty in belief about the pucks mass could be the sole reason for adopting a different functional relationship. Instead, this suggests that it was primarily the mode of interaction contributing to the difference in adopted physical relationship.

Taken together, the present study is in accordance with previous studies on intuitive physics within the noisy Newton framework (Kubricht, Holyoak, and Lu, 2017), which assumes that internal models based on physical laws interact probabilistically with inherently uncertain and ambiguous sensory measurements. The systematic deviations in our subjects' press-times from those prescribed by Newtonian physics under full knowledge of all parameters were explained quantitatively as stemming from perceptual uncertainties interacting with prior beliefs about physical relationships and motor variability. The results of the present study furthermore support the notion of structured internal causal models of physical relationships and shows the importance of using structured probabilistic generative models that contain interpretable variables to quantitatively reverse engineer human cognition (Griffiths et al., 2010). Although visual feedback was never given about the pucks' sliding dynamics and final position, subjects showed behavior that was consistent with the implicit assumption of a stable and lawful world. By employing a full generative model of the interaction task, it was possible to infer subjects' beliefs on an individual-by-individual and trial-by-trial basis.

The present study established that the availability of naturalistic multimodal sensorimotor interactions with physical pucks resulted in subjects adopting the functional relationship prescribed by Newtonian physics. Instead, when the same task was presented on a computer monitor lacking depth cues and the interaction was implemented through a button press on a keyboard, subjects' behavior was more in line with a linear heuristic. This result strongly suggests, that our subjects were able to take advantage of the motor planning and motor output generating the physically appropriate responses. This in turn suggests, that generating the actions involved in physical reasoning can take advantage of representations that are not independent of the motor control and the body but are thus "embodied". Previous research on physical reasoning has emphasized abstract internal physics models (Battaglia, Hamrick, and Tenenbaum, 2013; Bramley et al., 2018; Sanborn, Mansinghka, and Griffiths, 2013) and the few studies allowing subjects to interact with scenes implemented those

interactions through abstract mouse clicks in computer simulations (Bramley et al., 2018). Thus, the current results extend our understanding based on previous studies addressing differences in physical reasoning between tasks (Smith, Battaglia, and Vul, 2018) and quantifying different sources of uncertainty in physical reasoning (Smith and Vul, 2013) by adding the mode of physical interaction as an additional factor. This may also reconcile some previous result on intuitive physics, which reported strong deviations from Newtonian physics, but utilized very abstract depictions of scenes and no possibility for interaction (Caramazza, McCloskey, and Green, 1981; Todd and Warren Jr, 1982).

Overall, the present results contribute to our understanding of how the brain may implement physical reasoning. Indeed, in terms of a computational level account (Marr, 1982) of intuitive physical reasoning, it is not clear, why the output of a putative physical simulation engine should depend on the mode of interaction. But, at the implementational level of description there is evidence that different neuronal substrates are involved in physical reasoning, some of which are also implicated in motor planning and visuomotor control of actions involving the body. Previous studies have found evidence for the representation of abstract physical factors in parietal and frontal regions, when physics students thought about verbally presented physics terms (Mason and Just, 2016). Similarly, recent studies involving physical reasoning about objects' dynamics on the basis of short movies also identified frontal and parietal regions representing abstract physical quantities such as mass (Schwettmann, Tenenbaum, and Kanwisher, 2019) and involved in judging physical interactions (Fischer et al., 2016). These results give credence to the notion of causal generative models of physical objects and their interactions compared to model-free pattern recognition approaches, such as those based on deep neural networks. Nevertheless, the involvement of overlapping parietal regions in the representation of physical quantities such as mass when planning visuomotor interactions (Gallivan et al., 2014) and the additional involvement of motor related regions in such tasks (Chouinard, Leonard, and Paus, 2005) speak for a crucial role of representations tied to motor planning and motor output with the body (Anderson, 2003; Foglia and Wilson, 2013; Wilson, 2002), i.e. of embodied representations in physical reasoning at the implementational level.

8

GENERAL DISCUSSION

8.1 OVERVIEW OF RESULTS

In this thesis we examined human behavior in several experiments requiring interactions with the environment. Behavior was modeled by taking into account both task dependent, external as well as human internal constraints. Because the external world and access to its information, sensory systems, and consequences of actions are ambiguous, noisy, and uncertain, these factors are crucial elements requiring probabilistic modeling. While experiments may seem to keep the environment simple and the number of relevant factors small, we developed experiments with many structured sources of uncertainties and varying modes of interaction. Accordingly, we developed several algorithms to investigate people's behavior, all rooted in the Bayesian decision theory. This allowed investigating the rationality in decision making with respect to experimental designs and subjective beliefs.

8.2 HUMAN CONSISTENCY, GENERALIZATION AND TRANSFER

Humans show a stunning ability to learn and solve a broad range of differing and complex tasks throughout their lives. In the field of artificial intelligence, studies have attempted to mimic this evolutionary success story by building machines that are supposed to perform and learn like humans (Ellis et al., 2020; Lake et al., 2017) with the goal of tackling tasks for achieving human performance and generalization.

One of these approaches to come closer to this goal are neural networks. Especially, neural networks have been claimed to achieve and even exceed human performance e.g. in object detection (Cai et al., 2016; Viola and Jones, 2004) or classification (Ciresan, Meier, and Schmidhuber, 2012; Mundt et al., 2019). Nevertheless, they also usually suffer from the necessity of huge amounts of training data (Goodfellow, Bengio, and Courville, 2016; LeCun, Bengio, and Hinton, 2015), over-fitting and the bias-variance dilemma (Geman, Bienenstock, and Doursat, 1992) and lacking both the robustness to distortions and adversarial attacks and the ability to generalize well (Brown et al., 2017; Geirhos et al., 2018; Goodfellow, Shlens, and Szegedy, 2014; Nguyen, Yosinski, and Clune, 2015; Szegedy et al., 2013). By contrast, people are known to adapt, generalize well and even learn with very little information or few samples (Biederman, 1987) sometimes referred to as one shot learning (Landau, Smith, and Jones, 1988). This is particularly true for the rapid learning about concepts and categories in infants and children (Izard et al., 2009; Markman, 1989). This fact contradicts the necessity of abundant training data of most artificial neural network algorithms. On the other hand, Bayesian models get by with significantly less data describing human behavior with prior beliefs obtained through constant interactions with their environment while mimicking, among others, the human approach to classification in speech and visual perception (Lake et al., 2014, 2011; Xu and Tenenbaum, 2007). It is apparent that some prior beliefs should be highly consistent through our daily life and across various tasks that share a common influence. For instance, grav-

ity, or more precisely the gravitational constant, does not change noticeably in the course of our lives and forms a strong prior (Jörges and López-Moliner, 2017), which even persists when the environment changes (McIntyre et al., 2001). Likewise, our perception is influenced by the prior beliefs that light comes from above (Adams, Graf, and Ernst, 2004) or that cardinal orientations (Girshick, Landy, and Simoncelli, 2011) and slow velocities are more likely in our environment (Weiss, Simoncelli, and Adelson, 2002). Familiar objects in our environment can form such reliable prior as well as entities with stable properties like size (Kilpatrick and Ittelson, 1953; Konkle and Oliva, 2011) or surface texture and gloss (Adams et al., 2018; Fleming, Wiebel, and Gegenfurtner, 2013), and thereby influence our perception (Konkle and Oliva, 2012).

In order to investigate people's consistency across different tasks and with respect to beliefs about familiar size we implemented two tasks about distance perception, differing in the way decisions were made, and two methods, inferring subjective size beliefs, in chapter 3. Overall consistent deviations from optimal responses in both distance perception tasks indicate a general bias. With participants being restricted to two-dimensional projections in these tasks, it is reasonable to assume that these consistent deviations are driven by biased prior beliefs about object sizes (Gogel, 1963; Hochberg and Hochberg, 1952; Kilpatrick and Ittelson, 1953). Biases in inferred size beliefs also do not significantly differ across the two different methods utilized to measure them and thus seem to be general. Nevertheless, not all deviations in responses could be quantitatively well explained by biases in size beliefs, thereby still raising the question of potential causes, like misconceptions of the task or the use of a heuristic. So participants could rather just rely on heuristics based on the visual angle (Proffitt, 2006; Yilmaz and Warren, 1995), e.g. decide using constant ratios as decision thresholds , than make an accurate inference of distances. In chapter 4 we further tested whether participants were able to transfer information from perceiving a dynamical interaction , the collision of two pucks, to a continuous action control task of sliding pucks (Neupärtl, Tatai, and Rothkopf, 2020). Participants learned the functional relationship of their action and the resulting slide distances for two different pucks via visual feedback. After seeing several collisions of these pucks with an unknown one, participants were able to appropriately scale their actions without ever having received any feedback about the unknown pucks trajectories. Thus, participants learned not only the correct functional relationship but readily interpreted observed bounces of objects as being caussaly determined by their respective masses and transferred their mass beliefs from watching these collisions to a subsequent interaction task.

To summarize, we showed that in environments with control over relevant variables participants had previously learnt stable prior beliefs about familiar objects, acted consistently across tasks according to their uncertainties and biases and were able to learn functional relationships and prior beliefs via visual feedback and transfer them appropriately to a distinct interaction task.

8.3 OPTIMALITY IN HUMAN BEHAVIOR: HEURISTICS AND CONSTRAINED MODELS

It is undeniable that humans constantly deviate from ideal behavior in a vast field of interactions showing various degrees of variability and systematic biases. How-

ever, it is controversial whether these deviations are caused by people relying on fundamentally wrong assumptions about their environment and strongly simplified approximations that govern their behavior, often so called heuristics or heuristic decision making (Gigerenzer and Gaissmaier, 2011), or whether these deviations can be explained with probabilistic models that take natural physiological and task dependent constraints into account and can otherwise be seen as optimal (Kubricht, Holyoak, and Lu, 2017; Lieder and Griffiths, 2020).

Heuristics have been proposed among others for naive beliefs explaining misconceptions about trajectories of cut pendula (Caramazza, McCloskey, and Green, 1981), curvilinear trajectories (McCloskey and Kohl, 1983), judgments about mass in object collisions (Cohen, 2006; Gilden and Proffitt, 1994), probability judgments (Tversky and Kahneman, 1974) or optimal control policies in interception (Belousov et al., 2016; Zago et al., 2009). Constrained models, on the other hand, argue that humans behave optimally given their constraints. These models are known under different names, often in relation to their scope of application, e.g. as the noisy Newton framework in intuitive physics (Kubricht, Holyoak, and Lu, 2017) or resource rational models in neuroscience and economics (Lieder and Griffiths, 2020). Considered constraints can be physiological as the limited precision in sensory systems in visual (Hoppe and Rothkopf, 2016), haptic (Battaglia, Kersten, and Schrater, 2011; Ernst and Banks, 2002) or auditory perception (Birkenbusch, Ellermeier, and Kattner, 2015), and their combinations (Alais and Burr, 2004), or as the inevitable variability in executing continuous actions (Körding and Wolpert, 2004a; Trommershäuser et al., 2005). However, constraints can have their root in the availability of correct information, too, and arise due to the task design, e.g. when feedback is deprived (Körding and Wolpert, 2004a; Neupärtl, Tatai, and Rothkopf, 2020; Willey and Liu, 2018b), the environment's dynamics and statistics are unknown (Hoppe, Helfmann, and Rothkopf, 2018; Hoppe and Rothkopf, 2016; Neupärtl, Tatai, and Rothkopf, 2020), changes in accustomed dynamics like gravity (Clark et al., 2015; Jörges and López-Moliner, 2017; McIntyre et al., 2001) or after exposition to an altered environment (Zago et al., 2004). Probabilistic models considering these kind of limitations have been proven to be successful in a wide range of applications from describing mental simulations about stability of blocks (Battaglia, Hamrick, and Tenenbaum, 2013; Hamrick et al., 2016), pendula cutting and catching (Smith, Battaglia, and Vul, 2013) and object collisions (Gerstenberg et al., 2015; Sanborn, Mansinghka, and Griffiths, 2013; Ullman et al., 2018) to describing human understanding of liquid dynamics (Bates et al., 2019) or tool usage (Allen, Smith, and Tenenbaum, 2020).

We showed in chapter 4 that participants' behavior in a puck sliding task under realistic friction can be well described with the noisy Newton framework (Kubricht, Holyoak, and Lu, 2017) when feedback was available. When initially dynamics were unknown neither a linear heuristic nor the noisy Newton framework were clearly supported by the model comparison. This is not particularly surprising since no information about the puck's mass, the friction of the surface or the scaling of the acceleration was available. Yet with feedback about resulting trajectories present the Newton framework clearly outperforms the linear heuristic with a Bayes factor of 9.71 (Neupärtl, Tatai, and Rothkopf, 2020). Likewise the Newtonian model is able to infer meaningful parameters like the mass belief describing participants' high average accuracy. Based on findings that the way of participants' mode of interaction may influence their behavior (Dijkstra, Kaschak, and Zwaan, 2007; Foglia and Wilson,

2013; Smith, Battaglia, and Vul, 2018) we transferred the task design to enable visuo-haptic interaction, as described in chapter 7. Here, we showed that even without any feedback participants were not only able to adjust initial momentum appropriately resulting in near-optimal inferences for mass beliefs but that the Newton framework surpasses the linear heuristic by lengths with a Bayes factor of 49.79. This change in interaction seems to facilitate people's ability to recruit the (noisy) Newtonian model, trained by ubiquitous interactions in daily life. Furthermore, we examined participants' behavior in distance perception tasks in chapter 3. Here, individuals deviated both from optimal responses and also from actual size values. Deviations in their responses are overall consistent across both distance perception tasks and inferred size beliefs do not differ significantly between human MCMC and depth camera measurements. However, a probabilistic model using the inferred biases in the size beliefs does not explain all deviations well. This could be due to a consistent bias in both prior measurements or due to participants additionally relying on heuristics.

In summary, these three experiments yield evidence that considering their natural variability people are near-optimal or rational when being able to access all necessary information. Thus, the necessity arises to control the environment for relevant variables and assure their accessibility to the participants while making the interaction as realistic as possible to facilitate appropriate model recruitment. The results give insights about experimental designs and their influence on near-optimal responses and thus help to bridge the gap between people's partially deficient performance in some physical reasoning tasks and yet being well tuned to environmental dynamics of their daily lifes.

8.4 FROM INDIVIDUAL BELIEFS TO INDIVIDUAL COST FUNCTIONS

We know that prior beliefs can be extremely useful to describe and explain individual's perception and behavior (Adams, Graf, and Ernst, 2004; Mamassian and Goutcher, 2001; Weiss, Simoncelli, and Adelson, 2002). Yet, prior belief and likelihood are just means to describe perception and do not suffice to explain the complete process up to action selection. After all, when choosing an action one must take into account not only their posterior belief, but also the cost or reward associated with this action (Körding and Wolpert, 2004b; Wolpert and Landy, 2012). Costs are usually assumed to be implicitly stated through the task (Harris and Wolpert, 1998) but can be made explicit as well (Trommershäuser et al., 2005). This means, costs are judged based on the action's outcome alone. However, it is known that the effort to come up with an action itself affects behavior too as shown for when the urge to blink had to be suppressed (Hoppe, Helfmann, and Rothkopf, 2018) or even in perceptual 2AFC tasks with options differing in the required effort (Hagura, Haggard, and Diedrichsen, 2017). Thus, realistic cost functions, should consider both, the evaluation based on the task demand and the effort to produce it. While the inference of costs underlying behavior is classic problem both in economics (Kahneman, 1979) and psychology (Mosteller and Nogee, 1951), it has seen a renaissance in the field of artificial intelligence and machine learning (Boularias, Kober, and Peters, 2011; Finn, Levine, and Abbeel, 2016; Ng, Russell, et al., 2000; Ziebart et al., 2008). Specifically Inverse Reinforcement Learning strives to infer the cost function that is optimized (Boularias, Kober, and Peters, 2011; Ng, Russell, et al., 2000; Ziebart et al., 2008) or approximately optimized (Rothkopf and Dimitrakakis, 2011) by an agent. Some recent work has particularly looked at leveraging these methods for measuring the cost

functions underlying sensorimotor behavior (Mombaur, Truong, and Laumond, 2010; Muelling et al., 2014; Reddy, Dragan, and Levine, 2018; Rothkopf and Ballard, 2013; Schmitt et al., 2017; Zhang et al., 2018). Note however, that these methods assume perfect observability of the state of the world. By contrast, in this thesis human behavior always involves perceptual uncertainty. Thus, how to recover such a cost function quantitatively and yet take the influence of other e.g. physiological constraints and perceptual uncertainty into account?

In chapter 5 we proposed an algorithm that enables us to recover the individual cost functions that shaped people's responses in continuous estimation tasks like production and reproduction paradigms (Gescheider, 2013b; Wichmann and Jäkel, 2018). Besides considering physiological constraints in perception and action execution this algorithm further includes also an effort or action magnitude dependent term. The proposed algorithm is based on the following four basic building blocks: 1) perceptual uncertainty and 2) action variability implemented as log-normal distributions, since human precision in sensory systems and action execution is limited, as well as costs that depend on 3) the resulting distance to the perceived target or error and 4) the effort to produce this action. This allows asymmetric distributions and cost functions, which are able to explain deviations from optimal behavior and thus avoid simply attributing it to seeming misconceptions about the task or the environment. Using synthetic data for different cost functions we could show the algorithm's ability to successfully recover individual parameters. Based on this algorithm undershoots, pervasive in ubiquitous continuous action control tasks, were investigated in chapter 6. These undershoots occur among others in reproducing distances on bicycles (Sun, Campos, and Chan, 2004), sliding pucks to a target (Neupärtl, Tatai, and Rothkopf, 2020), throwing beanbags to a target (Willey and Liu, 2018a,b), reproducing forces (Onneweer, Mugge, and Schouten, 2015) and multiples of auditory perceived time-intervals (Birkenbusch, Ellermeier, and Kattner, 2015). Using this algorithm we are able to measure individual cost functions revealing similarities between individuals and tasks as well as showing the influence of task designs on behavior. Thus, one can assess how laborious people perceive tasks and explain the degree of expected deviations from optimal behavior.

Taken together, we introduced a new algorithmic approach to infer individual variability and cost functions for continuous action control tasks. Especially the individual cost functions can yield relevant insights about similarities between subjects and tasks and likewise about the effort people are facing when trying to meet the task demands. By using the algorithm's ability to recover more complex cost functions and realistic positively skewed distributions, describing the noisy perception and action variability, seemingly suboptimal deviations previously attributed to misconceptions can be explained as rational decisions.

8.5 THE MODE OF INTERACTION AND ITS INFLUENCE ON MODEL RECRUITMENT

When designing experiments, especially perceptual ones, controlling stimuli and their presentation is crucial as one need to consider phenomena like illusions (Weiss, Simoncelli, and Adelson, 2002), grouping (Wagemans et al., 2012; Wertheimer, 1912) or crowding (Levi, 2008; Whitney and Levi, 2011), just to name a few. Just as significant for right conclusions is to revise which information is available, useful and

distracting when conducting experiments (Alais and Burr, 2004; Ernst and Banks, 2002; Knill, 1998; Landy et al., 1995). However, besides the indisputable influence of these factors and despite the numerous experimental paradigms that have formed over the years (Gescheider, 2013b; Wichmann and Jäkel, 2018), an additional impact of the actual mode of action on behavior and internal model recruitment has been questioned (Fodor and Pylyshyn, 1988).

This shortcoming is in part being addressed within the field of embodied cognition arguing that our sensory and motor systems are not mere means as input and output devices but are interlinked with the cognitive process itself (Foglia and Wilson, 2013; Niedenthal, 2007; Wilson, 2002), see also (Smith, 2005) or grounded cognition (Barsalou, 2008). Indeed, in terms of Bayesian models of behavior at the computational level it might be unexpected, that the mode of interaction could influence the results in a physical reasoning experiment. But, at the implementational level this may be much less surprising. While speculative, with limited neuronal resources devoted to representing external states and mediating visuomotor actions, it may be resource rational to encode actions dependent on the dynamics of external objects.

Here, we utilized a continuous action control task of sliding objects on surfaces under influence of friction without visual feedback to test participants' a priori assumptions about physical dynamics of their environment and compared their behavior when being restricted to keyboard interactions and being able to grab and accelerate them with their hands (see chapter 7). When being able to interact with a real puck participants not only performed extraordinarily well given the missing feedback about their trajectories but also clearly relied on an internal model considering the non-linear nature of the task, whereas they mostly resorted to linear approximations in the keyboard condition. This provides evidence for the far-reaching effects of embodiment for designing experiments and explaining the discrepancy between humans mastering daily tasks and their deficient performance in abstract reasoning tasks. Similarly, Smith, Battaglia, and Vul (2018) came to a related conclusion using tasks with swinging pendula (Caramazza, McCloskey, and Green, 1981) to test participants' abilities in physical reasoning and continuous interaction or studies investigating effects of mental simulation on mechanical reasoning (Hegarty, 2004) like Schwartz and Black (1999) in a task about spill over when tilting glasses with and without the prompt to mentally simulate it.

In sum, we showed that utilizing a VR setup where people could naturally interact with haptically accessible objects enabled them to recruit internal models in accordance with Newtonian physics. Since people preferentially relied on rough approximations in the same task when interactions were restricted to keyboard inputs this indicates that even the choice of the interaction mode in an experiment can lead to more than just a change in precision but fundamentally shift results and biases conclusions, providing evidence in favor of an embodied view of cognition.

9 CONCLUSION

We as humans solve a variety of highly complex tasks on a daily basis, and we do so without having to ponder over individual processes for too long. However, when we start thinking about and describing many of these tasks, this ease seems to crumble away. But how can this discrepancy between routine acting and deficient reasoning be explained? Using the experiments, algorithms and models in this thesis we have investigated this issue showing that people are indeed well tuned to interact successfully and near-optimal given their perceptual uncertainty, action variability, individual cost functions and sometimes biased a priori expectations. Naturalistic interactions in tasks can facilitate correct recruitment of internal models and seem to prevent the occurrence of systematic misconceptions. Thus, we argue that we need to understand behavioral patterns as mixture of environmental factors, limiting precision and sometimes even depriving relevant information, and internal factors, like prior beliefs and individual cost functions.

BIBLIOGRAPHY

Acerbi, Luigi, Wei Ji Ma, and Sethu Vijayakumar (2014). "A Framework for Testing Identifiability of Bayesian Models of Perception." In: *NIPS*, pp. 1026–1034.

Adams, Wendy J, Erich W Graf, and Marc O Ernst (2004). "Experience can change the'light-from-above'prior." In: *Nature neuroscience* 7.10, p. 1057.

Adams, Wendy J, Iona S Kerrigan, and Erich W Graf (2010). "Efficient visual recalibration from either visual or haptic feedback: the importance of being wrong." In: *Journal of Neuroscience* 30.44, pp. 14745–14749.

Adams, Wendy J, Gizem Kucukoglu, Michael S Landy, and Rafał K Mantiuk (2018). "Naturally glossy: Gloss perception, illumination statistics, and tone mapping." In: *Journal of Vision* 18.13, pp. 4–4.

Akdoğan, Başak and Fuat Balcı (2017). "Are you early or late?: Temporal error monitoring." In: *Journal of Experimental Psychology: General* 146.3, p. 347.

Alais, David and David Burr (2004). "The ventriloquist effect results from near-optimal bimodal integration." In: *Current biology* 14.3, pp. 257–262.

Allen, Kelsey R, Kevin A Smith, and Joshua B Tenenbaum (2020). "Rapid trial-and-error learning with simulation supports flexible tool use and physical reasoning." In: *Proceedings of the National Academy of Sciences* 117.47, pp. 29302–29310.

Anderson, Michael L (2003). "Embodied cognition: A field guide." In: *Artificial intelligence* 149.1, pp. 91–130.

Balcı, Fuat, David Freestone, Patrick Simen, Laura Desouza, Jonathan D Cohen, and Philip Holmes (2011). "Optimal temporal risk assessment." In: *Frontiers in Integrative Neuroscience* 5, p. 56.

Barsalou, Lawrence W (2008). "Grounded cognition." In: *Annu. Rev. Psychol.* 59, pp. 617–645.

Bates, Christopher J, Ilker Yildirim, Joshua B Tenenbaum, and Peter Battaglia (2019). "Modeling human intuitions about liquid flow with particle-based simulation." In: *PLoS computational biology* 15.7, e1007210.

Battaglia, Peter W, Jessica B Hamrick, and Joshua B Tenenbaum (2013). "Simulation as an engine of physical scene understanding." In: *Proceedings of the National Academy of Sciences* 110.45, pp. 18327–18332.

Battaglia, Peter W, Daniel Kersten, and Paul R Schrater (2011). "How haptic size sensations improve distance perception." In: *PLoS computational biology* 7.6, e1002080.

Baugh, Lee A, Michelle Kao, Roland S Johansson, and J Randall Flanagan (2012). "Material evidence: Interaction of well-learned priors and sensorimotor memory when lifting objects." In: *Journal of neurophysiology* 108.5, pp. 1262–1269.

Beaumont, Mark A, Wenyang Zhang, and David J Balding (2002). "Approximate Bayesian computation in population genetics." In: *Genetics* 162.4, pp. 2025–2035.

Becker, Wolfgang and Albert F Fuchs (1969). "Further properties of the human saccadic system: eye movements and correction saccades with and without visual fixation points." In: *Vision research* 9.10, pp. 1247–1258.

Belousov, Boris, Gerhard Neumann, Constantin A Rothkopf, and Jan R Peters (2016). "Catching heuristics are optimal control policies." In: *Advances in neural information processing systems* 29, pp. 1426–1434.

Benjamini, Yoav and Yosef Hochberg (1995). "Controlling the false discovery rate: a practical and powerful approach to multiple testing." In: *Journal of the Royal statistical society: series B (Methodological)* 57.1, pp. 289–300.

Bergmann, Johanna, Elsa Krauß, Agnes Münch, Reiner Jungmann, Daniel Oberfeld, and Heiko Hecht (2011). "Locomotor and verbal distance judgments in action and vista space." In: *Experimental brain research* 210.1, pp. 13–23.

Berthoz, Alain, Isabelle Israel, Pierre Georges-Francois, Renato Grasso, and Toshihiro Tsuzuku (1995). "Spatial memory of body linear displacement: what is being stored?" In: *Science* 269.5220, pp. 95–98.

Biederman, Irving (1987). "Recognition-by-components: a theory of human image understanding." In: *Psychological review* 94.2, p. 115.

Birkenbusch, Jana, Wolfgang Ellermeier, and Florian Kattner (2015). "Octuplicate this interval! Axiomatic examination of the ratio properties of duration perception." In: *Attention, Perception, & Psychophysics* 77.5, pp. 1767–1780.

Bishop, Christopher M (2006). "Pattern recognition." In: *Machine learning* 128.9.

Boularias, Abdeslam, Jens Kober, and Jan Peters (2011). "Relative entropy inverse reinforcement learning." In: *Proceedings of the Fourteenth International Conference on Artificial Intelligence and Statistics*. JMLR Workshop and Conference Proceedings, pp. 182–189.

Bramley, Neil R, Tobias Gerstenberg, Joshua B Tenenbaum, and Todd M Gureckis (2018). "Intuitive experimentation in the physical world." In: *Cognitive psychology* 105, pp. 9–38.

Brannon, Elizabeth M, Courtney J Wusthoff, CR Gallistel, and John Gibbon (2001). "Numerical subtraction in the pigeon: Evidence for a linear subjective number scale." In: *Psychological Science* 12.3, pp. 238–243.

Britten, Kenneth H, Michael N Shadlen, William T Newsome, and J Anthony Movshon (1992). "The analysis of visual motion: a comparison of neuronal and psychophysical performance." In: *Journal of Neuroscience* 12.12, pp. 4745–4765.

Brown, Tom B, Dandelion Mané, Aurko Roy, Martín Abadi, and Justin Gilmer (2017). "Adversarial patch." In: *arXiv preprint arXiv:1712.09665*.

Buhusi, Catalin V and Warren H Meck (2005). "What makes us tick? Functional and neural mechanisms of interval timing." In: *Nature reviews neuroscience* 6.10, pp. 755–765.

Burwick, Thomas (2014). "The binding problem." In: *Wiley Interdisciplinary Reviews: Cognitive Science* 5.3, pp. 305–315.

Cai, Zhaowei, Quanfu Fan, Rogerio S Feris, and Nuno Vasconcelos (2016). "A unified multi-scale deep convolutional neural network for fast object detection." In: *European conference on computer vision*. Springer, pp. 354–370.

Cantlon, Jessica F, Sara Cordes, Melissa E Libertus, and Elizabeth M Brannon (2009). "Comment on" Log or Linear? Distinct Intuitions of the Number Scale in Western and Amazonian Indigene Cultures"." In: *science* 323.5910, pp. 38–38.

Caramazza, Alfonso, Michael McCloskey, and Bert Green (1981). "Naive beliefs in "sophisticated" subjects: Misconceptions about trajectories of objects." In: *Cognition* 9.2, pp. 117–123.

Chater, Nick, Joshua B Tenenbaum, and Alan Yuille (2006). "Probabilistic models of cognition: Conceptual foundations." In: *Trends in cognitive sciences* 10.7, pp. 287–291.

Chouinard, Philippe A, Gabriel Leonard, and Tomáš Paus (2005). "Role of the primary motor and dorsal premotor cortices in the anticipation of forces during object lifting." In: *Journal of Neuroscience* 25.9, pp. 2277–2284.

Ciresan, Dan, Ueli Meier, and Jürgen Schmidhuber (2012). "Multi-column deep neural networks for image classification." In: *2012 IEEE conference on computer vision and pattern recognition*. IEEE, pp. 3642–3649.

Clark, Torin K, Michael C Newman, Charles M Oman, Daniel M Merfeld, and Laurence R Young (2015). "Modeling human perception of orientation in altered gravity." In: *Frontiers in systems neuroscience* 9, p. 68.

Cochran, William G (1937). "Problems arising in the analysis of a series of similar experiments." In: *Supplement to the Journal of the Royal Statistical Society* 4.1, pp. 102–118.

Cohen, Andrew L (2006). "Contributions of invariants, heuristics, and exemplars to the visual perception of relative mass." In: *Journal of experimental psychology: human perception and performance* 32.3, p. 574.

Dayan, Peter and Nathaniel D Daw (2008). "Decision theory, reinforcement learning, and the brain." In: *Cognitive, Affective, & Behavioral Neuroscience* 8.4, pp. 429–453.

Dehaene, Stanislas (2003). "The neural basis of the Weber–Fechner law: a logarithmic mental number line." In: *Trends in cognitive sciences* 7.4, pp. 145–147.

Dehaene, Stanislas, Véronique Izard, Elizabeth Spelke, and Pierre Pica (2008). "Log or linear? Distinct intuitions of the number scale in Western and Amazonian indigene cultures." In: *science* 320.5880, pp. 1217–1220.

Dijkstra, Katinka, Michael P Kaschak, and Rolf A Zwaan (2007). "Body posture facilitates retrieval of autobiographical memories." In: *Cognition* 102.1, pp. 139–149.

Elliott, Digby, Steve Hansen, Lawrence EM Grierson, James Lyons, Simon J Bennett, and Spencer J Hayes (2010). "Goal-directed aiming: two components but multiple processes." In: *Psychological bulletin* 136.6, p. 1023.

Elliott, Digby, Steven Hansen, Jocelyn Mendoza, and Luc Tremblay (2004). "Learning to optimize speed, accuracy, and energy expenditure: A framework for understanding speed-accuracy relations in goal-directed aiming." In: *Journal of motor behavior* 36.3, pp. 339–351.

Ellis, Kevin, Catherine Wong, Maxwell Nye, Mathias Sable-Meyer, Luc Cary, Lucas Morales, Luke Hewitt, Armando Solar-Lezama, and Joshua B Tenenbaum (2020). "Dreamcoder: Growing generalizable, interpretable knowledge with wake-sleep bayesian program learning." In: *arXiv preprint arXiv:2006.08381*.

Engelbrecht, Sascha E, Neil E Berthier, and Laura P O'Sullivan (2003). "The undershoot bias: learning to act optimally under uncertainty." In: *Psychological Science* 14.3, pp. 257–261.

Ernst, Marc O and Martin S Banks (2002). "Humans integrate visual and haptic information in a statistically optimal fashion." In: *Nature* 415.6870, p. 429.

Fechner, Gustav Theodor (1860). *Elemente der psychophysik*. Vol. 2. Breitkopf u. Härtel.

Fengler, Alexander, Lakshmi N Govindarajan, Tony Chen, and Michael J Frank (2021). "Likelihood approximation networks (LANs) for fast inference of simulation models in cognitive neuroscience." In: *Elife* 10, e65074.

Finn, Chelsea, Sergey Levine, and Pieter Abbeel (2016). "Guided cost learning: Deep inverse optimal control via policy optimization." In: *International conference on machine learning*. PMLR, pp. 49–58.

Fischer, Jason, John G Mikhael, Joshua B Tenenbaum, and Nancy Kanwisher (2016). "Functional neuroanatomy of intuitive physical inference." In: *Proceedings of the national academy of sciences* 113.34, E5072–E5081.

Flanagan, J Randall, Jennifer P Bittner, and Roland S Johansson (2008). "Experience can change distinct size-weight priors engaged in lifting objects and judging their weights." In: *Current Biology* 18.22, pp. 1742–1747.

Fleming, Roland W, Christiane Wiebel, and Karl Gegenfurtner (2013). "Perceptual qualities and material classes." In: *Journal of vision* 13.8, pp. 9–9.

Fodor, Jerry A and Zenon W Pylyshyn (1988). "Connectionism and cognitive architecture: A critical analysis." In: *Cognition* 28.1-2, pp. 3–71.

Foglia, Lucia and Robert A Wilson (2013). "Embodied cognition." In: *Wiley Interdisciplinary Reviews: Cognitive Science* 4.3, pp. 319–325.

Foote, Allison L and Jonathon D Crystal (2007). "Metacognition in the rat." In: *Current Biology* 17.6, pp. 551–555.

Fraisse, Paul (1984). "Perception and estimation of time." In: *Annual review of psychology* 35.1, pp. 1–37.

Gallivan, Jason P, Jonathan S Cant, Melvyn A Goodale, and J Randall Flanagan (2014). "Representation of object weight in human ventral visual cortex." In: *Current Biology* 24.16, pp. 1866–1873.

Geirhos, Robert, Carlos R Medina Temme, Jonas Rauber, Heiko H Schütt, Matthias Bethge, and Felix A Wichmann (2018). "Generalisation in humans and deep neural networks." In: *arXiv preprint arXiv:1808.08750*.

Gellrich, Janine, Carolin Stetzler, Anna Oleszkiewicz, Thomas Hummel, and Valentin A Schriever (2017). "Olfactory threshold and odor discrimination ability in children–evaluation of a modified "Sniffin'Sticks" test." In: *Scientific reports* 7.1, pp. 1–6.

Gelman, Andrew, John B Carlin, Hal S Stern, David B Dunson, Aki Vehtari, and Donald B Rubin (2013). *Bayesian data analysis*. Chapman and Hall/CRC.

Geman, Stuart, Elie Bienenstock, and René Doursat (1992). "Neural networks and the bias/variance dilemma." In: *Neural computation* 4.1, pp. 1–58.

Gershman, Samuel J, Eric J Horvitz, and Joshua B Tenenbaum (2015). "Computational rationality: A converging paradigm for intelligence in brains, minds, and machines." In: *Science* 349.6245, pp. 273–278.

Gerstenberg, Tobias, Noah D Goodman, David A Lagnado, and Joshua B Tenenbaum (2015). "How, whether, why: Causal judgments as counterfactual contrasts." In: *Proceedings of the 37th Annual Conference of the Cognitive Science Society*, pp. 782–787.

Gerstenberg, Tobias, Matthew F Peterson, Noah D Goodman, David A Lagnado, and Joshua B Tenenbaum (2017). "Eye-tracking causality." In: *Psychological science* 28.12, pp. 1731–1744.

Gerstenberg, Tobias, Max Siegel, and Joshua Tenenbaum (2018). "What happened? Reconstructing the past through vision and sound." In: *Proceedings of the 40th Annual Conference of the Cognitive Science Society*.

Gescheider, George A (2013a). *Psychophysics: the fundamentals*. Psychology Press.

Gescheider, George A (2013b). "The Classical Psychophysical. Methods." In: *Psychophysics*. Psychology Press, pp. 55–82.

Gibbon, John and Russell M Church (1981). "Time left: linear versus logarithmic subjective time." In: *Journal of Experimental Psychology: Animal Behavior Processes* 7.2, p. 87.

Gigerenzer, Gerd and Wolfgang Gaissmaier (2011). "Heuristic decision making." In: *Annual review of psychology* 62, pp. 451–482.

Gilden, David L and Dennis R Proffitt (1994). "Heuristic judgment of mass ratio in two-body collisions." In: *Perception & Psychophysics* 56.6, pp. 708–720.

Girshick, Ahna R, Michael S Landy, and Eero P Simoncelli (2011). "Cardinal rules: visual orientation perception reflects knowledge of environmental statistics." In: *Nature neuroscience* 14.7, pp. 926–932.

Gogel, Walter C (1963). "The visual perception of size and distance." In: *Vision Research* 3.3-4, pp. 101–120.

Gold, Joshua I and Michael N Shadlen (2003). "The influence of behavioral context on the representation of a perceptual decision in developing oculomotor commands." In: *Journal of Neuroscience* 23.2, pp. 632–651.

Goodfellow, Ian J, Jonathon Shlens, and Christian Szegedy (2014). "Explaining and harnessing adversarial examples." In: *arXiv preprint arXiv:1412.6572*.

Goodfellow, Ian, Yoshua Bengio, and Aaron Courville (2016). *Deep learning*. MIT press.

Griffiths, Thomas L, Nick Chater, Charles Kemp, Amy Perfors, and Joshua B Tenenbaum (2010). "Probabilistic models of cognition: Exploring representations and inductive biases." In: *Trends in cognitive sciences* 14.8, pp. 357–364.

Griffiths, Thomas L, Falk Lieder, and Noah D Goodman (2015). "Rational use of cognitive resources: Levels of analysis between the computational and the algorithmic." In: *Topics in cognitive science* 7.2, pp. 217–229.

Hagura, Nobuhiro, Patrick Haggard, and Jörn Diedrichsen (2017). "Perceptual decisions are biased by the cost to act." In: *Elife* 6, e18422.

Hamilton, Antonia F de C, Kelvin E Jones, and Daniel M Wolpert (2004). "The scaling of motor noise with muscle strength and motor unit number in humans." In: *Experimental brain research* 157.4, pp. 417–430.

Hampton, Robert R (2001). "Rhesus monkeys know when they remember." In: *Proceedings of the National Academy of Sciences* 98.9, pp. 5359–5362.

Hamrick, Jessica B, Peter W Battaglia, Thomas L Griffiths, and Joshua B Tenenbaum (2016). "Inferring mass in complex scenes by mental simulation." In: *Cognition* 157, pp. 61–76.

Hamrick, Jessica B, Abram L Friesen, Feryal Behbahani, Arthur Guez, Fabio Viola, Sims Witherspoon, Thomas Anthony, Lars Buesing, Petar Veličković, and Théophane Weber (2020). "On the role of planning in model-based deep reinforcement learning." In: *arXiv preprint arXiv:2011.04021*.

Harris, Christopher M (1995). "Does saccadic undershoot minimize saccadic flight-time? A Monte-Carlo study." In: *Vision research* 35.5, pp. 691–701.

Harris, Christopher M and Daniel M Wolpert (1998). "Signal-dependent noise determines motor planning." In: *Nature* 394.6695, pp. 780–784.

Harris, Laurence R, Michael Jenkin, and Daniel C Zikovitz (2000). "Visual and non-visual cues in the perception of linear self motion." In: *Experimental brain research* 135.1, pp. 12–21.

Harrison, Peter, Raja Marjieh, Federico Adolfi, Pol van Rijn, Manuel Anglada-Tort, Ofer Tchernichovski, Pauline Larrouy-Maestri, and Nori Jacoby (2020). "Gibbs sampling with people." In: *Advances in Neural Information Processing Systems* 33.

Hawkins, Stephanie L (2011). "William James, Gustav Fechner, and early psychophysics." In: *Frontiers in Physiology* 2, p. 68.

Hegarty, Mary (2004). "Mechanical reasoning by mental simulation." In: *Trends in cognitive sciences* 8.6, pp. 280–285.

Hertwig, Ralph, Greg Barron, Elke U Weber, and Ido Erev (2004). "Decisions from experience and the effect of rare events in risky choice." In: *Psychological science* 15.8, pp. 534–539.

Hochberg, Carol Barnes and Julian E Hochberg (1952). "Familiar size and the perception of depth." In: *The Journal of Psychology* 34.1, pp. 107–114.

Hoppe, David, Stefan Helfmann, and Constantin A Rothkopf (2018). "Humans quickly learn to blink strategically in response to environmental task demands." In: *Proceedings of the National Academy of Sciences* 115.9, pp. 2246–2251.

Hoppe, David and Constantin A Rothkopf (2016). "Learning rational temporal eye movement strategies." In: *Proceedings of the National Academy of Sciences* 113.29, pp. 8332–8337.

Hoppe, David and Constantin A Rothkopf (2019). "Multi-step planning of eye movements in visual search." In: *Scientific reports* 9.1, pp. 1–12.

Hosking, Simon G and Boris Crassini (2010). "The effects of familiar size and object trajectories on time-to-contact judgements." In: *Experimental brain research* 203.3, pp. 541–552.

Houlsby, Neil MT, Ferenc Huszár, Mohammad M Ghassemi, Gergő Orbán, Daniel M Wolpert, and Máté Lengyel (2013). "Cognitive tomography reveals complex, task-independent mental representations." In: *Current Biology* 23.21, pp. 2169–2175.

Hubbard, Timothy L (2020). "Representational gravity: Empirical findings and theoretical implications." In: *Psychonomic bulletin & review* 27.1, pp. 36–55.

Hudson, Todd E, Laurence T Maloney, and Michael S Landy (2008). "Optimal compensation for temporal uncertainty in movement planning." In: *PLoS Comput Biol* 4.7, e1000130.

Izard, Véronique, Coralie Sann, Elizabeth S Spelke, and Arlette Streri (2009). "Newborn infants perceive abstract numbers." In: *Proceedings of the National Academy of Sciences* 106.25, pp. 10382–10385.

Jacobs, Robert A (2002). "What determines visual cue reliability?" In: *Trends in cognitive sciences* 6.8, pp. 345–350.

Jazayeri, Mehrdad and Michael N Shadlen (2010). "Temporal context calibrates interval timing." In: *Nature neuroscience* 13.8, pp. 1020–1026.

Jörges, Björn and Joan López-Moliner (2017). "Gravity as a strong prior: implications for perception and action." In: *Frontiers in Human Neuroscience* 11, p. 203.

Kahneman, Daniel (1979). "Prospect theory: An analysis of decisions under risk." In: *Econometrica* 47, p. 278.

Kaiser, Mary K, Dennis R Proffitt, Susan M Whelan, and Heiko Hecht (1992). "Influence of animation on dynamical judgments." In: *Journal of experimental Psychology: Human Perception and performance* 18.3, p. 669.

Kaiser, Mary Kister, Dennis R Proffitt, and Michael McCloskey (1985). "The development of beliefs about falling objects." In: *Perception & Psychophysics* 38.6, pp. 533–539.

Kersten, Daniel, Pascal Mamassian, and Alan Yuille (2004). "Object perception as Bayesian inference." In: *Annu. Rev. Psychol.* 55, pp. 271–304.

Kersten, Daniel and Alan Yuille (2003). "Bayesian models of object perception." In: *Current opinion in neurobiology* 13.2, pp. 150–158.

Kilpatrick, FP and WH Ittelson (1953). "The size-distance invariance hypothesis." In: *Psychological Review* 60.4, p. 223.

Kirkpatrick, Scott, C Daniel Gelatt, and Mario P Vecchi (1983). "Optimization by simulated annealing." In: *science* 220.4598, pp. 671–680.

Knill, David C (1998). "Ideal observer perturbation analysis reveals human strategies for inferring surface orientation from texture." In: *Vision research* 38.17, pp. 2635–2656.

Knill, David C and Whitman Richards (1996). *Perception as Bayesian inference*. Cambridge University Press.

Knill, David C and Jeffrey A Saunders (2003). "Do humans optimally integrate stereo and texture information for judgments of surface slant?" In: *Vision research* 43.24, pp. 2539–2558.

Konkle, Talia and Aude Oliva (2011). "Canonical visual size for real-world objects." In: *Journal of Experimental Psychology: human perception and performance* 37.1, p. 23.

Konkle, Talia and Aude Oliva (2012). "A familiar-size Stroop effect: real-world size is an automatic property of object representation." In: *Journal of Experimental Psychology: Human Perception and Performance* 38.3, p. 561.

Körding, Konrad P, Ulrik Beierholm, Wei Ji Ma, Steven Quartz, Joshua B Tenenbaum, and Ladan Shams (2007). "Causal inference in multisensory perception." In: *PLoS one* 2.9, e943.

Körding, Konrad P and Daniel M Wolpert (2004a). "Bayesian integration in sensorimotor learning." In: *Nature* 427.6971, p. 244.

Körding, Konrad P and Daniel M Wolpert (2006). "Bayesian decision theory in sensorimotor control." In: *Trends in cognitive sciences* 10.7, pp. 319–326.

Körding, Konrad Paul and Daniel M Wolpert (2004b). "The loss function of sensorimotor learning." In: *Proceedings of the National Academy of Sciences* 101.26, pp. 9839–9842.

Körding, Konrad (2007). "Decision theory: what" should" the nervous system do?" In: *Science* 318.5850, pp. 606–610.

Kubricht, James R, Keith J Holyoak, and Hongjing Lu (2017). "Intuitive physics: Current research and controversies." In: *Trends in cognitive sciences* 21.10, pp. 749–759.

Kubricht, James, Chenfanfu Jiang, Yixin Zhu, Song-Chun Zhu, Demetri Terzopoulos, and Hongjing Lu (2016). "Probabilistic Simulation Predicts Human Performance on Viscous Fluid-Pouring Problem." In: *Proceedings of the 38th annual conference of the cognitive science society*,

Lake, Brenden M, Tomer D Ullman, Joshua B Tenenbaum, and Samuel J Gershman (2017). "Building machines that learn and think like people." In: *Behavioral and brain sciences* 40.

Lake, Brenden, Chia-ying Lee, James Glass, and Josh Tenenbaum (2014). "One-shot learning of generative speech concepts." In: *Proceedings of the Annual Meeting of the Cognitive Science Society*. Vol. 36.

Lake, Brenden, Ruslan Salakhutdinov, Jason Gross, and Joshua Tenenbaum (2011). "One shot learning of simple visual concepts." In: *Proceedings of the Annual Meeting of the Cognitive Science Society*. Vol. 33.

Landau, Barbara, Linda B Smith, and Susan S Jones (1988). "The importance of shape in early lexical learning." In: *Cognitive development* 3.3, pp. 299–321.

Landy, Michael S, Martin S Banks, and David C Knill (2011). "Ideal-observer models of cue integration." In: *Sensory cue integration*, pp. 5–29.

Landy, Michael S and Haruyuki Kojima (2001). "Ideal cue combination for localizing texture-defined edges." In: *JOSA A* 18.9, pp. 2307–2320.

Landy, Michael S, Laurence T Maloney, Elizabeth B Johnston, and Mark Young (1995). "Measurement and modeling of depth cue combination: in defense of weak fusion." In: *Vision research* 35.3, pp. 389–412.

LeCun, Yann, Yoshua Bengio, and Geoffrey Hinton (2015). "Deep learning." In: *nature* 521.7553, pp. 436–444.

Lee, Michael D and Eric-Jan Wagenmakers (2014). *Bayesian cognitive modeling: A practical course*. Cambridge university press.

Lejeune, Helga and Pierre Jasselette (1986). "Accurate DRL performance in the pigeon: Comparison between perching and treadle pressing." In: *Animal Learning & Behavior* 14.2, pp. 205–211.

Lejeune, Helga and Marc Richelle (1982). "Differential reinforcement of perching duration in the pigeon: a comparison with differential-reinforcement-of-low-rate key-pecking." In: *Behaviour Analysis Letters* 2, pp. 49–57.

Lejeune, Helga and JH Wearden (2006). "Scalar properties in animal timing: Conformity and violations." In: *Quarterly Journal of Experimental Psychology* 59.11, pp. 1875–1908.

Levi, Dennis M (2008). "Crowding—An essential bottleneck for object recognition: A mini-review." In: *Vision research* 48.5, pp. 635–654.

Lieder, Falk and Thomas L Griffiths (2020). "Resource-rational analysis: Understanding human cognition as the optimal use of limited computational resources." In: *Behavioral and Brain Sciences* 43.

Lodewyckx, Tom, Woojae Kim, Michael D Lee, Francis Tuerlinckx, Peter Kuppens, and Eric-Jan Wagenmakers (2011). "A tutorial on Bayes factor estimation with the product space method." In: *Journal of Mathematical Psychology* 55.5, pp. 331–347.

Long, Bria and Talia Konkle (2017). "A familiar-size Stroop effect in the absence of basic-level recognition." In: *Cognition* 168, pp. 234–242.

Loomis, Jack M, Roberta L Klatzky, Reginald G Golledge, Joseph G Cicinelli, James W Pellegrino, and Phyllis A Fry (1993). "Nonvisual navigation by blind and sighted: assessment of path integration ability." In: *Journal of Experimental Psychology: General* 122.1, p. 73.

Lowe, C Fergus, Peter Harzem, and Peter T Spencer (1979). "Temporal control of behavior and the power law." In: *Journal of the Experimental Analysis of Behavior* 31.3, pp. 333–343.

Luna, Rogelio, Adrián Hernández, Carlos D Brody, and Ranulfo Romo (2005). "Neural codes for perceptual discrimination in primary somatosensory cortex." In: *Nature neuroscience* 8.9, pp. 1210–1219.

Lyons, James, Steve Hansen, Suzanne Hurding, and Digby Elliott (2006). "Optimizing rapid aiming behaviour: Movement kinematics depend on the cost of corrective modifications." In: *Experimental Brain Research* 174.1, pp. 95–100.

Maereg, Andualem Tadesse, Atulya Nagar, David Reid, and Emanuele L Secco (2017). "Wearable vibrotactile haptic device for stiffness discrimination during virtual interactions." In: *Frontiers in Robotics and AI* 4, p. 42.

Maloney, Laurence T and Pascal Mamassian (2009). "Bayesian decision theory as a model of human visual perception: Testing Bayesian transfer." In: *Visual neuroscience* 26.1, pp. 147–155.

Mamassian, Pascal and Ross Goutcher (2001). "Prior knowledge on the illumination position." In: *Cognition* 81.1, B1–B9.

Markman, Ellen M (1989). *Categorization and naming in children: Problems of induction*. MIT Press.

Marr, David (1982). *Vision: a computational investigation into the human representation and processing of visual information*. San Francisco: W. H. Freeman.

Mason, Robert A and Marcel Adam Just (2016). "Neural representations of physics concepts." In: *Psychological science* 27.6, pp. 904–913.

McCloskey, Michael, Alfonso Caramazza, and Bert Green (1980). "Curvilinear motion in the absence of external forces: Naive beliefs about the motion of objects." In: *Science* 210.4474, pp. 1139–1141.

McCloskey, Michael and Deborah Kohl (1983). "Naive physics: The curvilinear impetus principle and its role in interactions with moving objects." In: *Journal of Experimental Psychology: Learning, Memory, and Cognition* 9.1, p. 146.

McIntosh, Robert D and Gavin Lashley (2008). "Matching boxes: Familiar size influences action programming." In: *Neuropsychologia* 46.9, pp. 2441–2444.

McIntyre, Joseph, Myrka Zago, Alain Berthoz, and Francesco Lacquaniti (2001). "Does the brain model Newton's laws?" In: *Nature neuroscience* 4.7, p. 693.

McNaughton, Bruce L, Francesco P Battaglia, Ole Jensen, Edvard I Moser, and May-Britt Moser (2006). "Path integration and the neural basis of the'cognitive map'." In: *Nature Reviews Neuroscience* 7.8, pp. 663–678.

Miltner, Wolfgang HR, Christoph H Braun, and Michael GH Coles (1997). "Event-related brain potentials following incorrect feedback in a time-estimation task: evidence for a "generic" neural system for error detection." In: *Journal of cognitive neuroscience* 9.6, pp. 788–798.

Mittelstaedt, Marie-Luise and Horst Mittelstaedt (2001). "Idiothetic navigation in humans: estimation of path length." In: *Experimental Brain Research* 139.3, pp. 318–332.

Mombaur, Katja, Anh Truong, and Jean-Paul Laumond (2010). "From human to humanoid locomotion—an inverse optimal control approach." In: *Autonomous robots* 28.3, pp. 369–383.

Mosteller, Frederick and Philip Nogee (1951). "An experimental measurement of utility." In: *Journal of Political Economy* 59.5, pp. 371–404.

Muelling, Katharina, Abdeslam Boularias, Betty Mohler, Bernhard Schölkopf, and Jan Peters (2014). "Learning strategies in table tennis using inverse reinforcement learning." In: *Biological cybernetics* 108.5, pp. 603–619.

Mundt, Martin, Sagnik Majumder, Sreenivas Murali, Panagiotis Panetsos, and Visvanathan Ramesh (2019). "Meta-learning convolutional neural architectures for multi-target concrete defect classification with the concrete defect bridge image dataset." In: *Proceedings of the IEEE/CVF Conference on Computer Vision and Pattern Recognition*, pp. 11196–11205.

Munhall, Kevin G, P Gribble, L Sacco, and M Ward (1996). "Temporal constraints on the McGurk effect." In: *Perception & psychophysics* 58.3, pp. 351–362.

Murray, Scott O, Paul Schrater, and Daniel Kersten (2004). "Perceptual grouping and the interactions between visual cortical areas." In: *Neural Networks* 17.5-6, pp. 695–705.

Neupärtl, Nils and Constantin A Rothkopf (2021). "Inferring perceptual decision making parameters from behavior in production and reproduction tasks." In: *arXiv preprint arXiv:2112.15521*.

Neupärtl, Nils and Constantin Rothkopf (2018). "Perceptual explaining away in depth judgements." In: *Journal of Vision* 18.10, pp. 660–660.

Neupärtl, Nils, Fabian Tatai, and Constantin A Rothkopf (2021). "Naturalistic embodied interactions elicit intuitive physical behaviour in accordance with Newtonian physics." In: *Cognitive Neuropsychology*, pp. 1–15.

Neupärtl, Nils, Fabian Tatai, and Constantin A. Rothkopf (2020). "Intuitive physical reasoning about objects' masses transfers to a visuomotor decision task consistent with Newtonian physics." In: *PLoS Comput Biol* 16.10, e1007730.

Ng, Andrew Y, Stuart J Russell, et al. (2000). "Algorithms for inverse reinforcement learning." In: *Icml*. Vol. 1, p. 2.

Nguyen, Anh, Jason Yosinski, and Jeff Clune (2015). "Deep neural networks are easily fooled: High confidence predictions for unrecognizable images." In: *Proceedings of the IEEE conference on computer vision and pattern recognition*, pp. 427–436.

Niedenthal, Paula M (2007). "Embodying emotion." In: *science* 316.5827, pp. 1002–1005.

O'Sullivan, Ian, Etienne Burdet, and Jörn Diedrichsen (2009). "Dissociating variability and effort as determinants of coordination." In: *PLoS computational biology* 5.4, e1000345.

Oliveira, Flavio TP, Digby Elliott, and David Goodman (2005). "Energy-minimization bias: compensating for intrinsic influence of energy-minimization mechanisms." In: *Motor control* 9.1, pp. 101–114.

Onneweer, Bram, Winfred Mugge, and Alfred C Schouten (2015). "Force reproduction error depends on force level, whereas the position reproduction error does not." In: *IEEE transactions on haptics* 9.1, pp. 54–61.

Petzschner, Frederike H and Stefan Glasauer (2011). "Iterative Bayesian estimation as an explanation for range and regression effects: a study on human path integration." In: *Journal of Neuroscience* 31.47, pp. 17220–17229.

Petzschner, Frederike H, Stefan Glasauer, and Klaas E Stephan (2015). "A Bayesian perspective on magnitude estimation." In: *Trends in cognitive sciences* 19.5, pp. 285–293.

Plummer, Martyn (2003). "JAGS: A program for analysis of Bayesian graphical models using Gibbs sampling." In: *Proceedings of the 3rd international workshop on distributed statistical computing*. Vol. 124. 125.10. Vienna, Austria., pp. 1–10.

Pooley, CM and G Marion (2018). "Bayesian model evidence as a practical alternative to deviance information criterion." In: *Royal Society open science* 5.3, p. 171519.

Proffitt, Dennis R (2006). "Distance perception." In: *Current Directions in psychological science* 15.3, pp. 131–135.

Reddy, Siddharth, Anca D Dragan, and Sergey Levine (2018). "Where do you think you're going?: Inferring beliefs about dynamics from behavior." In: *arXiv preprint arXiv:1805.08010*.

Roberts, Gareth O, Andrew Gelman, Walter R Gilks, et al. (1997). "Weak convergence and optimal scaling of random walk Metropolis algorithms." In: *The annals of applied probability* 7.1, pp. 110–120.

Roberts, William A (2006). "Evidence that pigeons represent both time and number on a logarithmic scale." In: *Behavioural processes* 72.3, pp. 207–214.

Robertson, Lynn C (2003). "Binding, spatial attention and perceptual awareness." In: *Nature Reviews Neuroscience* 4.2, pp. 93–102.

Rothkopf, Constantin A and Dana H Ballard (2013). "Modular inverse reinforcement learning for visuomotor behavior." In: *Biological cybernetics* 107.4, pp. 477–490.

Rothkopf, Constantin A and Christos Dimitrakakis (2011). "Preference elicitation and inverse reinforcement learning." In: *Joint European conference on machine learning and knowledge discovery in databases*. Springer, pp. 34–48.

Sagiv, Noam and Lynn C Robertson (2005). "Synesthesia and the binding problem." In: *Synesthesia: Perspectives from cognitive neuroscience*, pp. 90–107.

Sanborn, Adam N, Vikash K Mansinghka, and Thomas L Griffiths (2013). "Reconciling intuitive physics and Newtonian mechanics for colliding objects." In: *Psychological review* 120.2, p. 411.

Sanborn, Adam and Thomas L Griffiths (2008). "Markov chain Monte Carlo with people." In: *Advances in neural information processing systems*, pp. 1265–1272.

Schmitt, Felix, Hans-Joachim Bieg, Michael Herman, and Constantin A Rothkopf (2017). "I see what you see: Inferring sensor and policy models of human real-world motor behavior." In: *Thirty-First AAAI Conference on Artificial Intelligence*.

Schwartz, Daniel L and Tamara Black (1999). "Inferences through imagined actions: Knowing by simulated doing." In: *Journal of Experimental Psychology: Learning, Memory, and Cognition* 25.1, p. 116.

Schwettmann, Sarah, Joshua B Tenenbaum, and Nancy Kanwisher (2019). "Invariant representations of mass in the human brain." In: *eLife* 8, e46619.

Searle, CL, LD Braida, MF Davis, and HS Colburn (1976). "Model for auditory localization." In: *The Journal of the Acoustical Society of America* 60.5, pp. 1164–1175.

Seitz, Aaron R, Dongho Kim, and Takeo Watanabe (2009). "Rewards evoke learning of unconsciously processed visual stimuli in adult humans." In: *Neuron* 61.5, pp. 700–707.

Shergill, Sukhwinder S, Paul M Bays, Chris D Frith, Daniel M Wolpert, et al. (2003). "Two eyes for an eye: the neuroscience of force escalation." In: *Science* 301.5630, pp. 187–187.

Siegler, Robert S and John E Opfer (2003). "The development of numerical estimation: Evidence for multiple representations of numerical quantity." In: *Psychological science* 14.3, pp. 237–250.

Simon, Herbert A (1955). "A behavioral model of rational choice." In: *The quarterly journal of economics* 69.1, pp. 99–118.

Sims, Chris R and Wayne D Gray (2008). "Adaptation to embodied dynamics: Evidence from Bayes' ball." In: *Proceedings of the Annual Meeting of the Cognitive Science Society*. Vol. 30.

Slutsky, Daniel A and Gregg H Recanzone (2001). "Temporal and spatial dependency of the ventriloquism effect." In: *Neuroreport* 12.1, pp. 7–10.

Smilek, Daniel, Mike J Dixon, Cera Cudahy, and Philip M Merikle (2001). "Synaesthetic photisms influence visual perception." In: *Journal of cognitive neuroscience* 13.7, pp. 930–936.

Smith, Kevin A, Peter W Battaglia, and Edward Vul (2018). "Different physical intuitions exist between tasks, not domains." In: *Computational Brain & Behavior* 1.2, pp. 101–118.

Smith, Kevin A, Peter Battaglia, and Edward Vul (2013). "Consistent physics underlying ballistic motion prediction." In: *Proceedings of the 35th annual meeting of the cognitive science society*. Vol. 35, 3426–3431.

Smith, Kevin A, Eyal Dechter, Joshua B Tenenbaum, and Edward Vul (2013). "Physical predictions over time." In: *Proceedings of the 35th annual meeting of the cognitive science society*. Vol. 35.

Smith, Kevin A, Filipe Peres, Edward Vul, and Joshua Tenebaum (2017). "Thinking inside the box: Motion prediction in contained spaces uses simulation." In: *Proceedings of the 39th annual meeting of the cognitive science society*.

Smith, Kevin A and Edward Vul (2013). "Sources of uncertainty in intuitive physics." In: *Topics in cognitive science* 5.1, pp. 185–199.

Smith, Linda B (2005). "Cognition as a dynamic system: Principles from embodiment." In: *Developmental Review* 25.3-4, pp. 278–298.

Stevens, Stanley S (1957). "On the psychophysical law." In: *Psychological review* 64.3, p. 153.

Stevens, Stanley Smith (1958). "Problems and methods of psychophysics." In: *Psychological Bulletin* 55.4, p. 177.

Stocker, Alan A and Eero P Simoncelli (2006). "Noise characteristics and prior expectations in human visual speed perception." In: *Nature neuroscience* 9.4, pp. 578–585.

Stüttgen, Maik Christopher, Cornelius Schwarz, and Frank Jäkel (2011). "Mapping spikes to sensations." In: *Frontiers in Neuroscience* 5, p. 125.

Sun, Hong-Jin, Jennifer L Campos, and George SW Chan (2004). "Multisensory integration in the estimation of relative path length." In: *Experimental brain research* 154.2, pp. 246–254.

Sun, Hong-Jin, Jennifer L Campos, Meredith Young, George SW Chan, and Colin G Ellard (2004). "The contributions of static visual cues, nonvisual cues, and optic flow in distance estimation." In: *Perception* 33.1, pp. 49–65.

Szegedy, Christian, Wojciech Zaremba, Ilya Sutskever, Joan Bruna, Dumitru Erhan, Ian Goodfellow, and Rob Fergus (2013). "Intriguing properties of neural networks." In: *arXiv preprint arXiv:1312.6199*.

Todd, James T and William H Warren Jr (1982). "Visual perception of relative mass in dynamic events." In: *Perception* 11.3, pp. 325–335.

Todorov, Emanuel (2004). "Optimality principles in sensorimotor control." In: *Nature neuroscience* 7.9, pp. 907–915.

Todorov, Emanuel and Michael I Jordan (1998). "Smoothness maximization along a predefined path accurately predicts the speed profiles of complex arm movements." In: *Journal of Neurophysiology* 80.2, pp. 696–714.

Todorov, Emanuel and Michael I Jordan (2002). "Optimal feedback control as a theory of motor coordination." In: *Nature neuroscience* 5.11, pp. 1226–1235.

Todorov, Emanuel, Reza Shadmehr, and Emilio Bizzi (1997). "Augmented feedback presented in a virtual environment accelerates learning of a difficult motor task." In: *Journal of motor behavior* 29.2, pp. 147–158.

Treisman, Anne M and Garry Gelade (1980). "A feature-integration theory of attention." In: *Cognitive psychology* 12.1, pp. 97–136.

Trommershäuser, Julia, Sergei Gepshtein, Laurence T Maloney, Michael S Landy, and Martin S Banks (2005). "Optimal compensation for changes in task-relevant movement variability." In: *Journal of Neuroscience* 25.31, pp. 7169–7178.

Trommershäuser, Julia, Laurence T Maloney, and Michael S Landy (2003). "Statistical decision theory and the selection of rapid, goal-directed movements." In: *JOSA A* 20.7, pp. 1419–1433.

Trommershäuser, Julia, Laurence T Maloney, and Michael S Landy (2008). "Decision making, movement planning and statistical decision theory." In: *Trends in cognitive sciences* 12.8, pp. 291–297.

Tversky, Amos and Daniel Kahneman (1974). "Judgment under uncertainty: Heuristics and biases." In: *science* 185.4157, pp. 1124–1131.

Ullman, Tomer D, Elizabeth Spelke, Peter Battaglia, and Joshua B Tenenbaum (2017). "Mind games: Game engines as an architecture for intuitive physics." In: *Trends in cognitive sciences* 21.9, pp. 649–665.

Ullman, Tomer D, Andreas Stuhlmüller, Noah D Goodman, and Joshua B Tenenbaum (2018). "Learning physical parameters from dynamic scenes." In: *Cognitive psychology* 104, pp. 57–82.

Van Beers, Robert J, Patrick Haggard, and Daniel M Wolpert (2004). "The role of execution noise in movement variability." In: *Journal of neurophysiology* 91.2, pp. 1050–1063.

Viola, Paul and Michael J Jones (2004). "Robust real-time face detection." In: *International journal of computer vision* 57.2, pp. 137–154.

Von Der Malsburg, Christoph (1994). "The correlation theory of brain function." In: *Models of neural networks*. Springer, pp. 95–119.

Von Der Malsburg, Christoph (1999). "The what and why of binding: the modeler's perspective." In: *Neuron* 24.1, pp. 95–104.

Von Helmholtz, Hermann (1867). *Handbuch der physiologischen Optik: mit 213 in den Text eingedruckten Holzschnitten und 11 Tafeln*. Vol. 9. Voss.

Wagemans, Johan, James H Elder, Michael Kubovy, Stephen E Palmer, Mary A Peterson, Manish Singh, and Rüdiger von der Heydt (2012). "A century of Gestalt psychology in visual perception: I. Perceptual grouping and figure–ground organization." In: *Psychological bulletin* 138.6, p. 1172.

Wallace, Mark T, GE Roberson, W David Hairston, Barry E Stein, J William Vaughan, and Jim A Schirillo (2004). "Unifying multisensory signals across time and space." In: *Experimental brain research* 158.2, pp. 252–258.

Walsh, Lee D, Janet L Taylor, and Simon C Gandevia (2011). "Overestimation of force during matching of externally generated forces." In: *The Journal of physiology* 589.3, pp. 547–557.

Ward, Jamie and Jason B Mattingley (2006). "Synaesthesia: an overview of contemporary findings and controversies." In: *Cortex* 42.2, pp. 129–136.

Weber, Elke U, Sharoni Shafir, and Ann-Renee Blais (2004). "Predicting risk sensitivity in humans and lower animals: risk as variance or coefficient of variation." In: *Psychological review* 111.2, p. 430.

Weber, Ernst Heinrich (1834). *De Pulsu, resorptione, auditu et tactu: Annotationes anatomicae et physiologicae.* Leipzig, Germany: CF Koehler.

Weber, Ronald B and Robert B Daroff (1971). "The metrics of horizontal saccadic eye movements in normal humans." In: *Vision research* 11.9, 921–IN2.

Weiss, Yair, Eero P Simoncelli, and Edward H Adelson (2002). "Motion illusions as optimal percepts." In: *Nature neuroscience* 5.6, p. 598.

Wertheimer, Max (1912). "Experimentelle studien uber das sehen von bewegung." In: *Zeitschrift fur psychologie* 61.

Whitney, David and Dennis M Levi (2011). "Visual crowding: A fundamental limit on conscious perception and object recognition." In: *Trends in cognitive sciences* 15.4, pp. 160–168.

Wichmann, Felix A and Frank Jäkel (2018). "Methods in psychophysics." In: *Stevens' Handbook of Experimental Psychology and Cognitive Neuroscience* 5, pp. 1–42.

Wild-Wall, Nele, Rita Willemssen, and Michael Falkenstein (2009). "Feedback-related processes during a time-production task in young and older adults." In: *Clinical Neurophysiology* 120.2, pp. 407–413.

Willey, Chéla R and Zili Liu (2018a). "Limited generalization with varied, as compared to specific, practice in short-term motor learning." In: *Acta Psychologica* 182, pp. 39–45.

Willey, Chéla R and Zili Liu (2018b). "Long-term motor learning: Effects of varied and specific practice." In: *Vision research* 152, pp. 10–16.

Wilson, Margaret (2002). "Six views of embodied cognition." In: *Psychonomic bulletin & review* 9.4, pp. 625–636.

Wolpert, Daniel M and Michael S Landy (2012). "Motor control is decision-making." In: *Current opinion in neurobiology* 22.6, pp. 996–1003.

Wulfmeier, Markus, Peter Ondruska, and Ingmar Posner (2015). "Maximum entropy deep inverse reinforcement learning." In: *arXiv preprint arXiv:1507.04888*.

Xu, Fei and Joshua B Tenenbaum (2007). "Word learning as Bayesian inference." In: *Psychological review* 114.2, p. 245.

Yi, Linlin (2009). "Do rats represent time logarithmically or linearly?" In: *Behavioural processes* 81.2, pp. 274–279.

Yilmaz, Emre H and William H Warren (1995). "Visual control of braking: A test of the tau-dot hypothesis." In: *Journal of Experimental Psychology: Human Perception and Performance* 21.5, p. 996.

Yuille, Alan and Daniel Kersten (2006). "Vision as Bayesian inference: analysis by synthesis?" In: *Trends in cognitive sciences* 10.7, pp. 301–308.

Zago, Myrka, Gianfranco Bosco, Vincenzo Maffei, Marco Iosa, Yuri P Ivanenko, and Francesco Lacquaniti (2004). "Internal models of target motion: expected dynamics overrides measured kinematics in timing manual interceptions." In: *Journal of neurophysiology* 91.4, pp. 1620–1634.

Zago, Myrka, Joseph McIntyre, Patrice Senot, and Francesco Lacquaniti (2009). "Visuomotor coordination and internal models for object interception." In: *Experimental Brain Research* 192.4, pp. 571–604.

Zednik, Carlos and Frank Jäkel (2016). "Bayesian reverse-engineering considered as a research strategy for cognitive science." In: *Synthese* 193.12, pp. 3951–3985.

Zeiler, Michael D and Mark S Hoyert (1989). "Temporal reproduction." In: *Journal of the Experimental Analysis of Behavior* 52.2, pp. 81–95.

Zhang, Ruohan, Shun Zhang, Matthew H Tong, Yuchen Cui, Constantin A Rothkopf, Dana H Ballard, and Mary M Hayhoe (2018). "Modeling sensory-motor decisions in natural behavior." In: *PLoS computational biology* 14.10, e1006518.

Ziebart, Brian D, Andrew L Maas, J Andrew Bagnell, Anind K Dey, et al. (2008). "Maximum entropy inverse reinforcement learning." In: *Aaai*. Vol. 8. Chicago, IL, USA, pp. 1433–1438.

DECLARATION

I declare that I have developed and written the enclosed doctoral thesis entitled *Interacting with an uncertain physical world: probabilistic models of human perception and action* completely by myself, and have not used sources or means without declaration in the text. Any thoughts from others or literal quotations are clearly marked. This thesis was not used in the same or in a similar version to achieve an academic grading or is being published elsewhere.

Darmstadt, 08.08.2022

Nils Neupärtl